

Portland State University

PDXScholar

Dissertations and Theses


Dissertations and Theses

Summer 7-19-2013

Developing Thyronamine Analog Pharmaceuticals Targeting TAAR1 to Treat Methamphetamine Addiction

Troy Andrew Wahl
Portland State University

Follow this and additional works at: https://pdxscholar.library.pdx.edu/open_access_etds

 Part of the [Chemicals and Drugs Commons](#), and the [Medicinal-Pharmaceutical Chemistry Commons](#)
Let us know how access to this document benefits you.

Recommended Citation

Wahl, Troy Andrew, "Developing Thyronamine Analog Pharmaceuticals Targeting TAAR1 to Treat Methamphetamine Addiction" (2013). *Dissertations and Theses*. Paper 1109.
<https://doi.org/10.15760/etd.1109>

This Dissertation is brought to you for free and open access. It has been accepted for inclusion in Dissertations and Theses by an authorized administrator of PDXScholar. Please contact us if we can make this document more accessible: pdxscholar@pdx.edu.

Developing Thyronamine Analog Pharmaceuticals Targeting TAAR1 to Treat
Methamphetamine Addiction

by

Troy Andrew Wahl

A dissertation submitted in partial fulfillment of the
requirements for the degree of

Doctor of Philosophy
in
Chemistry

Dissertation Committee:
David H. Peyton, Chair
Suzanne Estes
David Grandy
Dirk Iwata-Reuyl
Robert Strongin

Portland State University
2013

© 2013 Troy Andrew Wahl

Abstract

As a part of the overall program in the Grandy laboratory at Oregon Health & Science University (OHSU), studying the underlying chemical biology of methamphetamine (Meth) addiction, this dissertation reports on the development of six new thyronamine analogs which were synthesized and assayed against trace amine associated receptor 1 (TAAR1), giving preliminary results consistent with the analogs being inverse agonists. Due to highly variable TAAR1 expression levels in the assays, based on inter-assay response to control Meth stimulation as well as other possible factors, kinetic models were developed to qualitatively explain the assay results. The models set approximate limits on the analogs' binding and disassociation rates relative to those of Meth. Analysis of the assays also provides more evidence of TAAR1's basal activity. Based on the models, the conversion rate of ligand-free inactive TAAR1 to ligand-free active TAAR1 is less than 6% of the binding rate of Meth to TAAR1. The models also suggest that the inverse agonists bind to the inactive ligand-free form of TAAR1 between 10 and 100 times faster than Meth binds to the inactive ligand-free form of TAAR1. Three of the new analogs, **G5-110s8**, **G5-112s5**, and **G5-114s5**, bind to the ligand-free active form of TAAR1 faster than they bind to the inactive ligand-free form of TAAR1. The models do not suggest an upper limit on the binding rate of those 3 analogs to the ligand-free active form of TAAR1. A control assay lacking TAAR1 revealed an electrophysiological off-target effect caused by **G5-109s8**. Also, a novel synthetic

route was developed for **ET-92**, the lead compound for this project, which reduced the number of synthetic steps from 14 to 5 and improved the overall yield from 15.3% to 18.3% (77.4 mg) with the hope that further improvements in yield are possible.

Acknowledgments

Working with Dr. Grandy, a renowned expert on TAAR1 and who laid the foundation for this work by proposing the connection between TAAR1 and Meth addiction, was greatly appreciated. It is also appreciated that Oregon Health & Sciences University hosted this research.

The following people provided additional support in the form of materials, and advice:

- Dr. Niles Lehman
- Dr. Dirk Iwata-Reuyl
- Dr. David Peyton
- Dr. Rolf Winter
- Dr. Michael Cohen
- Dr. David Dawson
- Dr. Thomas Scanlan
- Dr. Yohei Norimatsu

With special thanks to my volunteer “editorial staff:”

- Cheryl Hodson
- Rob Jensen
- Katherine Liebman
- Kelsie Kendrick
- Natasja Swartz
- Kimberly Wahl
- Sheila Wahl

Emma Florence Martin Holt and Sheila Wahl provided personal financial aid which is greatly appreciated.

This research was made possible, in part, by funding from the National Institute on Drug Abuse, The Portland Oregon Methamphetamine Research Center, The Medical Research Foundation of Oregon, The Steinberg Fund and the Department of Physiology & Pharmacology, School of Medicine, Oregon Health & Science University.

The following people have my gratitude for their help and mentoring over the years independent of their involvement in the project:

PhD Committee Members

Dr. Suzanne Estes
Dr. David Grandy
Dr. Dirk Iwata-Reuyl
Dr. David H. Peyton
Dr. Robert Strongin

Grandy Research Group at OHSU

Dr. David Grandy
Anthony Beers
Madeline Grandy
Ashley Kimbel
Katie Tallman

Others at OHSU

Dr. Michael Cohen
Dr. David Dawson
Dr. Jeffrey Karpen
Dr. Yohei Norimatsu
Dr. Thomas Scanlan

Peyton Research Group at PSU

Dr. David Peyton
Cheryl Hodson
Rob Jensen
Katherine Liebmann
Kelsie Kendrick

Simoyi Research Group at PSU

Dr. Rueben Simoyi
Wilbes Mbiya

Goforth Research Group at PSU

Dr. Andrea Goforth
William DeBenedetti
Beth Manhat

Others at PSU

Kirk Fisher
Keith James
Dr. Niles Lehman
Dr. David McClure
Nicolas Meier
Dr. Keith Schwartz
Dr. Eric Sheagley
Dr. Carl Wamser
Dr. Rolf Winter

Celera Genomics

Dr. Dan Dickman
Dr. Paul Grothaus
Dr. Orion Jankowski
Dr. John Link
Dr. Ellen Leah
Colin O'Bryan
Dr. Jennifer Riggs
Dr. William Shrader
Dr. Kieron Wesson
Dr. Wendy Young
Sheila Zipfel, MS

Cellgate

Dr. Tad Jessop
Dr. Thorsten Kirschberg
Dr. Paul McGrane
Dr. Sriram Naganathan
Dr. Jonathan Rothbard

Peninsula Laboratories/Bachem

Dr. Alfred Chen
Dr. Ruoheng Zhang

Others

Raymond King - AboutUs
Brian Lundquist - Nanotechnology Now

Table of Contents

<i>Abstract</i>	i
<i>Acknowledgments</i>	iii
<i>List of Tables</i>	x
<i>List of Figures</i>	xi
CHAPTER 1 <i>A New Approach for Treating Methamphetamine Addiction</i>	1
1.1 Background on Trace Amine Associated Receptor 1 (TAAR1)	1
1.2 Methamphetamine	5
1.3 Justification for targeting TAAR1	7
1.4 Overview of Current TAAR1 Medicinal Chemistry	11
CHAPTER 2 <i>New ET-92 Synthesis</i>	14
2.1 Cost-effective synthetic route to ET-92 and its analogs	14
CHAPTER 3 <i>New ET- 92 Analogs</i>	23
3.1 Initial attempts to synthesize new analogs	23
3.2 Change in strategy and targets	24
3.3 Another strategy change	27
3.4 Final attempt to synthesize 6 - 14	29
CHAPTER 4 <i>Biological Results</i>	32
4.1 The experiments	33
4.2 Results	37
4.2.1 Testing G5-109s8	37
4.2.2 Testing the other compounds	45
4.3 Concluding remarks about the assays	49

Table of Contents

CHAPTER 5	<i>Kinetic Modeling</i>	51
5.1	Quick Review of Kinetics	51
5.2	TAAR1 Kinetics	52
5.3	Model B: Modeling TAAR1 equilibria	55
5.4	Model C: Modeling the oocyte data	60
5.5	Stop Flow Model; a hybrid approach	68
5.6	Concluding remarks	70
CHAPTER 6	<i>Conclusions</i>	72
CHAPTER 7	<i>Methodology</i>	75
7.1	Synthetic Methods	75
7.1.1	Equipment and Chemicals	75
7.1.2	Compounds	75
7.1.2.1	5-bromo-2-(hexyloxy)benzaldehyde: G4-12s16	76
7.1.2.2	Hexyl 2-(hexyloxy)-5-nitrobenzoate: G5-047s10	77
7.1.2.3	(2-(hexyloxy)-5-nitrophenyl)(pyrrolidin-1-yl)methanone: G5-090s11	78
7.1.2.4	2-(hexyloxy)-5-nitrobenzaldehyde: G5-120s11	79
7.1.2.5	(5-bromo-2-(hexyloxy)phenyl)(phenyl)-methanol: G4-19s13	80
7.1.2.6	(5-(4-fluorophenoxy)-2-(hexyloxy)phenyl)-	
7.1.2.7	-(phenyl)methanol: G4-74s14	83
7.1.2.8	(2-(hexyloxy)-5-(phenylamino)phenyl)-	
	-(phenyl)methanol: G2-100s9	86
7.1.2.9	(5-((4-fluorophenyl)amino)-2-(hexyloxy)-	
	-phenyl)(phenyl)methanol: G2-101s9	88
7.1.2.10	(5-((3-fluorophenyl)amino)-2-(hexyloxy)-	
	-phenyl)(phenyl)methanol: G2-102s9	90
7.1.2.11	Hexyl 2-(hexyloxy)-5-(phenylamino)-	
	-benzoate: G5-059s9	92
7.1.2.12	Hexyl 5-((4-fluorophenyl)amino)-2-	
	-(hexyloxy)benzoate: G5-060s9	95
7.1.2.13	Hexyl 5-((3-fluorophenyl)amino)-2-	
	-(hexyloxy)benzoate: G5-061s9	98
7.1.2.14	(2-(hexyloxy)-5-(phenylamino)phenyl)-	
	-(pyrrolidin-1-yl)methanone: G5-112s5	101

Table of Contents

7.1.2.15	(5-((4-fluorophenyl)amino)-2-(hexyloxy)-phenyl)(pyrrolidin-1-yl)methanone: G5-113s5	104
7.1.2.16	(5-((3-fluorophenyl)amino)-2-(hexyloxy)-phenyl)(pyrrolidin-1-yl)methanone: G5-114s5	106
7.1.2.17	3-(1,3-dioxolan-2-yl)-4-(hexyloxy)-N-phenylaniline: G5-125s6	108
7.1.2.18	3-(1,3-dioxolan-2-yl)-N-(4-fluorophenyl)-4-(hexyloxy)aniline: G5-126s6	111
7.1.2.19	3-(1,3-dioxolan-2-yl)-N-(3-fluorophenyl)-4-(hexyloxy)aniline: G5-127s6	113
7.1.2.20	Hexyl 5-(benzylamino)-2-(hexyloxy)benzoate: G5-049s10	115
7.1.2.21	Hexyl 2-(hexyloxy)-5-((4-fluorobenzyl)-amino)benzoate: G5-050s10	117
7.1.2.22	Hexyl 2-(hexyloxy)-5-((pyridin-2-ylmethyl)-amino)benzoate: G5-051s10	119
7.1.2.23	Hexyl 5-((2-fluorobenzyl)amino)-2-(hexyloxy)benzoate: G5-052s10	121
7.1.2.24	Hexyl 5-((3-fluorobenzyl)amino)-2-(hexyloxy)benzoate: G5-053s10	124
7.1.2.25	(5-(benzylamino)-2-(hexyloxy)phenyl)-(pyrrolidin-1-yl)methanone: G5-103s10	127
7.1.2.26	(5-((4-fluorobenzyl)amino)-2-(hexyloxy)-phenyl)(pyrrolidin-1-yl)methanone: G5-108s10	129
7.1.2.27	(5-((3-fluorobenzyl)amino)-2-(hexyloxy)-phenyl)(pyrrolidin-1-yl)methanone: G5-109s8	131
7.1.2.28	(5-((2-fluorobenzyl)amino)-2-(hexyloxy)-phenyl)(pyrrolidin-1-yl)methanone: G5-110s8	133
7.1.2.29	(2-(hexyloxy)-5-((pyridin-2-ylmethyl)-amino)phenyl)(pyrrolidin-1-yl)methanone: G5-111s8	135
7.1.2.30	Hexyl 5-amino-2-(hexyloxy)benzoate: G5-048s10	137
7.1.2.31	(5-amino-2-(hexyloxy)phenyl)(pyrrolidin-1-yl)methanone: G5-106s7	138
7.1.2.32	3-(1,3-dioxolan-2-yl)-4-(hexyloxy)aniline: G5-124s5	138
7.1.2.33	2-(5-bromo-2-(hexyloxy)phenyl)-2-phenylacetonitrile: G4-026s10	139
7.1.2.34	2-(5-(4-fluorophenoxy)-2-(hexyloxy)-phenyl)-2-phenylacetonitrile: G4-079s9	142

Table of Contents

7.1.2.35	2-(5-bromo-2-(hexyloxy)phenyl)-1,3-dioxolane: G1-130s5	145
7.1.2.36	2-(2-(hexyloxy)-5-nitrophenyl)-1,3-dioxolane: G5-122s6	145
7.1.2.37	2-(5-(4-fluorophenoxy)-2-(hexyloxy)- -phenyl)-2-phenylethanamine hydrochloride: ET-92 (G4-091s14 and G5-002s12)	148
7.1.2.38	(2-hydroxy-5-nitrophenyl)(pyrrolidin-1- -yl)methanone: G5-098s6 and G5-088s8	149
7.1.2.39	5-(4-fluorophenoxy)-2-(hexyloxy)- -benzaldehyde: G4-068s20 and G4-70s6	150
7.2	Biological Assays: TEVC Methods	154
7.2.1	In Vitro Transcription	154
7.2.2	Preparation and Microinjection of Oocytes	155
7.2.3	Whole Cell Recordings	156
7.2.3.1	Compound Assays	156
<i>References & Notes</i>		159
Appendix A	<i>NMR Spectra</i>	166
A.1	5-bromo-2-(hexyloxy)benzaldehyde: G4-012s16	166
A.2	5-(4-fluorophenoxy)-2-(hexyloxy)benzaldehyde: G4-068s20 & G4-070s6	173
A.3	(5-(4-fluorophenoxy)-2-(hexyloxy)phenyl)- -(phenyl)methanol: G4-074s14	181
A.4	2-(5-(4-fluorophenoxy)-2-(hexyloxy)phenyl)- -2-phenylacetonitrile: G4-079s9	189
A.5	ET-92 : 2-(5-(4-fluorophenoxy)-2- -(hexyloxy)phenyl)-2-phenylethanamine hydrochloride: G4-091s14	197
A.6	(2-hydroxy-5-nitrophenyl)(pyrrolidin- -1-yl)methone: G5-088s8	205
A.7	(2-(hexyloxy)-5-nitrophenyl)(pyrrolidin- -1-yl)methone: G5-090s10	212
A.8	(5-amino-2-(hexyloxy)phenyl)(pyrrolidin- -1-yl)methone: G5-106s7	219
A.9	(5-((3-fluorobenzyl)amino)-2-(hexyloxy)- -phenyl)(pyrrolidin-1-yl)methone: G5-109s8	222

Table of Contents

Appendix B	<i>High Resolution Mass Spectra</i>	226
B.1	5-bromo-2-(hexyloxy)benzaldehyde: G4-012s16	226
B.2	5-(4-fluorophenoxy)-2-(hexyloxy)benzaldehyde: G4-068s20 & G4-070s6	228
B.3	(5-(4-fluorophenoxy)-2-(hexyloxy)phenyl)- -(phenyl)methanol: G4-074s14	230
B.4	2-(5-(4-fluorophenoxy)-2-(hexyloxy)- -phenyl)-2-phenylacetonitrile: G4-079s9	232
B.5	ET-92 : 2-(5-(4-fluorophenoxy)- -2-(hexyloxy)phenyl)-2-phenylethanamine hydrochloride: G4-091s14	234

List of Tables

Table 7.1	High resolution mass spectrum (ESI) of 5-bromo-2-(hexyloxy)benzaldehyde (G4-012s16)	77
Table 7.2	High resolution mass spectrum (ESI) of (5-bromo-2-(hexyloxy)(phenyl))(phenyl)methanol (G4-019s13)	81
Table 7.3	High resolution mass spectrum (ESI) of 5-(4-fluorophenoxy)-2-(hexyloxy)(phenyl)-methanol (G4-074s14)	84
Table 7.4	HPLC Conditions used to purify G4-068s16	153
Table 7.5	High resolution mass spectrum (ESI) of 5-(4-fluorophenoxy)-2-(hexyloxy)benzaldehyde (G4-068s20)	154

List of Figures

FIGURE 1.1	TAAR1 agonists.	2
FIGURE 1.2	The known signaling pathway of TAAR1.	4
FIGURE 1.3	Structures of ATP, cAMP, GTP and GDP.	5
FIGURE 1.4	<i>In vitro</i> methamphetamine stimulated TAAR1 dose response	8
FIGURE 1.5	Structures of EPPTB and ET-92 (racemic)	9
FIGURE 1.6	Mouse <i>in vivo</i> studies of the effects of ET-92 or EPPTB in reducing Meth stimulated locomotion.	10
FIGURE 1.7	Racemic mixtures of some phenethylamine (PEA) analogs that bind to TAAR1.	11
FIGURE 1.8	Racemic mixtures of some cathinone analogs.	11
FIGURE 1.9	Structure of Guanabenz	12
FIGURE 1.10	Analogues of thyronamine.	12
FIGURE 1.11	TAAR1-specific compounds from Hoffmann-LaRoche.	12
FIGURE 2.1	The original ET-92 synthetic route.	15
FIGURE 2.2	The new synthetic route to ET-92 .	16
FIGURE 2.3	The Miyaura boration reaction did not work with this substrate.	16
FIGURE 2.4	A boronic acid synthesis followed by a Chan-Lam reaction to make 15 .	18
FIGURE 2.5	A possible route to chiral ET-92 .	20
FIGURE 2.6	Nitrilation reaction confirmed the feasibility of the new ET-92 route.	21
FIGURE 3.1	First new analog targets to be synthesized.	23
FIGURE 3.2	The first step in synthesizing compounds 1 and 2 .	24
FIGURE 3.3	New targets and ET-92	25
FIGURE 3.4	The first steps towards the new analogs.	26
FIGURE 3.5	Reduction of ester to aldehyde.	26
FIGURE 3.6	Synthesis of a key intermediate.	27
FIGURE 3.7	Functionalizing the amine.	28
FIGURE 3.8	A failed Grignard reaction.	28

List of Figures		
FIGURE 3.9	The final synthesizes of thyronamine analogs.	29
FIGURE 3.10	SAR comparison between (S)-sulpiride, ET-10, ET-92 , and G5-109s8 through G5-114s5 .	31
FIGURE 4.1	Compounds tested	32
FIGURE 4.2	<i>In vitro</i> methamphetamine stimulated TAAR1 concentration response	34
FIGURE 4.3	Structure of Forskolin.	36
FIGURE 4.4	Pretreatment with 20 μ M G5-109s8 followed by 100 μ M Meth.	38
FIGURE 4.5	Heads up competition between Meth and G5-109s8 .	39
FIGURE 4.6	CFTR only control experiments to detect off-target effects.	41
FIGURE 4.7	Heads up competition between Meth and G5-110s8 .	47
FIGURE 4.8	Heads up competition between Meth and G5-111s8 .	47
FIGURE 4.9	Heads up competition between Meth and G5-112s5 .	48
FIGURE 4.10	Heads up competition between Meth and G5-113s5 .	48
FIGURE 4.11	Heads up competition between Meth and G5-114s5 .	49
FIGURE 5.1	Kinetic Schemes for TAAR1.	54
FIGURE 5.2	The model is very sensitive to rate of equilibrium between R_i and R_a .	57
FIGURE 5.3	Simulation of competition between Meth and Inhibitor.	58
FIGURE 5.4	Receptor overexpression can lead to counter-intuitive results.	60
FIGURE 5.5	Oocyte response to various stimuli.	65
FIGURE 5.6	Slow inhibitor off-rate results in a total sub-basal response.	67
FIGURE 5.7	Very fast inhibitor on-rate deepens the trough.	67
FIGURE 5.8	Slow inhibitor on-rate prevents the complete inhibition of Meth.	68
FIGURE 5.9	Hybrid model allows trough-peak-trough response pattern.	70
FIGURE 7.1	Chromatographic purification of G4-019s9.	82
FIGURE 7.2	Chromatographic purification of G4-074s12.	85
FIGURE 7.3	Chromatographic purification of G2-100s8.	87
FIGURE 7.4	Chromatographic purification of G2-101s8.	89
FIGURE 7.5	Chromatographic purification of G2-102s8.	91
FIGURE 7.6	Chromatographic purification of G5-059s7.	93
FIGURE 7.7	Chromatographic purification of G5-060s7.	97

FIGURE 7.8 Chromatographic
purification of G5-061s7.

	100	
FIGURE 7.9	Chromatographic purification of G5-112s4.	103
FIGURE 7.10	Chromatographic purification of G5-113s4.	105
FIGURE 7.11	Chromatographic purification of G5-114s4.	107
FIGURE 7.12	Chromatographic purification of G5-125s5.	110
FIGURE 7.13	Chromatographic purification of G5-126s5.	112
FIGURE 7.14	Chromatographic purification of G5-127s5.	114
FIGURE 7.15	Chromatographic purification of G5-049s7.	116
FIGURE 7.16	Chromatographic purification of G5-050s7.	118
FIGURE 7.17	Chromatographic purification of G5-051s7.	120
FIGURE 7.18	Chromatographic purification of G5-052s7.	123
FIGURE 7.19	Chromatographic purification of G5-053s7.	126
FIGURE 7.20	Chromatographic purification of G5-103s8.	128
FIGURE 7.21	Chromatographic purification of G5-108s7.	130
FIGURE 7.22	Chromatographic purification of G5-109s7.	132
FIGURE 7.23	Chromatographic purification of G5-110s7.	134
FIGURE 7.24	Chromatographic purification of G5-111s7.	136
FIGURE 7.25	Chromatographic purification of G4-026s8.	141
FIGURE 7.26	Chromatographic purification of G4-079s8.	144
FIGURE 7.27	Chromatographic purification of G5-122s5.	147
FIGURE 7.28	Chromatographic purification of G4-068s14.	152

For the past 30⁺ years, the paradigm of methamphetamine's (Meth) mechanism of action (MOA)¹ has been that it blocks the uptake of extracellular dopamine (DA) and interferes with the vesicular monoamine transporters (VMAT) causing an increase in intracellular (cytosol) DA. Once intracellular levels of DA are high enough, the DA gradient-dependent dopamine transporter (DAT) allows the DA to move out of the neuron. Meth effects the release of serotonin and norepinephrin in similar ways. Due to dopamine's^{2,3} association with pleasure, particularly the anticipation of pleasure, the dopamine hypothesis of addiction has been the basis for trying to develop treatments for Meth addiction. There is a membrane-bounded receptor, the Trace Amine Associated Receptor 1 (TAAR1), which is activated by Meth, that is a new potential target for treating Meth addiction.^{4,5}

1.1 *Background on Trace Amine Associated Receptor 1 (TAAR1)*

A good review of the current TAAR1 literature was written by Gregory Miller.⁶ TAAR1 was discovered in 2001^{4,7} and is a G-protein coupled receptor (GPCR) widely distributed throughout the body and is activated by a variety of substrates (**FIGURE 1.1**) including the neurotransmitter dopamine (DA); the biogenic trace amines: β -phenylethylamine (PEA), p-tyramine, octopamine, synephrine, and

Background on Trace Amine Associated Receptor 1 (TAAR1)

thyronamines. TAAR1 is also affected by exogenous drugs of abuse (**FIGURE 1.1**), such as: amphetamine, N-methamphetamine (Meth) and methylenedioxymethamphetamine (MDMA, AKA: Ecstasy).⁴ Of particular importance for this work, TAAR1 is co-expressed with the dopamine transporter (DAT) and the dopamine receptors as part of the dopaminergic system in the ventral tegmental area (VTA), which is a major part of the brain's reward circuitry. As part of the dopaminergic system, TAAR1 is suspected to be involved in depression, addiction attention-deficit/hyperactivity disorder, Parkinson's disease, schizophrenia,⁸ and anxiety.⁹⁻¹¹ There is also evidence that links TAAR1 to fibromyalgia¹² and B-cell pathologies (lymphomas).¹³ TAAR1 is largely expressed on intracellular membranes.^{4,6,8-11,14}

FIGURE 1.1: TAAR1 agonists.

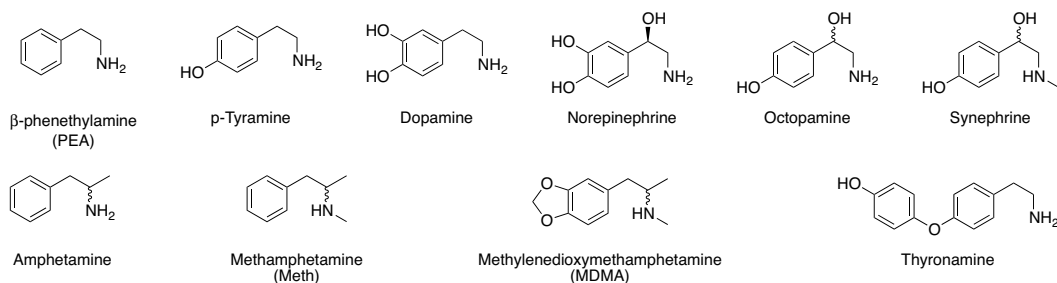


FIGURE 1.2 shows the sequence of the TAAR1 signaling pathway starting with Meth binding to the TAAR1- $G_{\alpha s}/G_{\beta/\gamma}$ complex (1). Once activated by Meth, TAAR1 stimulates $G_{\alpha s}$ to exchange GDP^{15,16} for GTP (2). The TAAR1- $G_{\alpha s}/G_{\beta/\gamma}$ complex disassociates, and $G_{\alpha s}$ binds to adenylyl cyclase (3). At this stage, the $G_{\beta/\gamma}$ subunit could modulate the activity of effectors (enzymes, ion channels, etc).

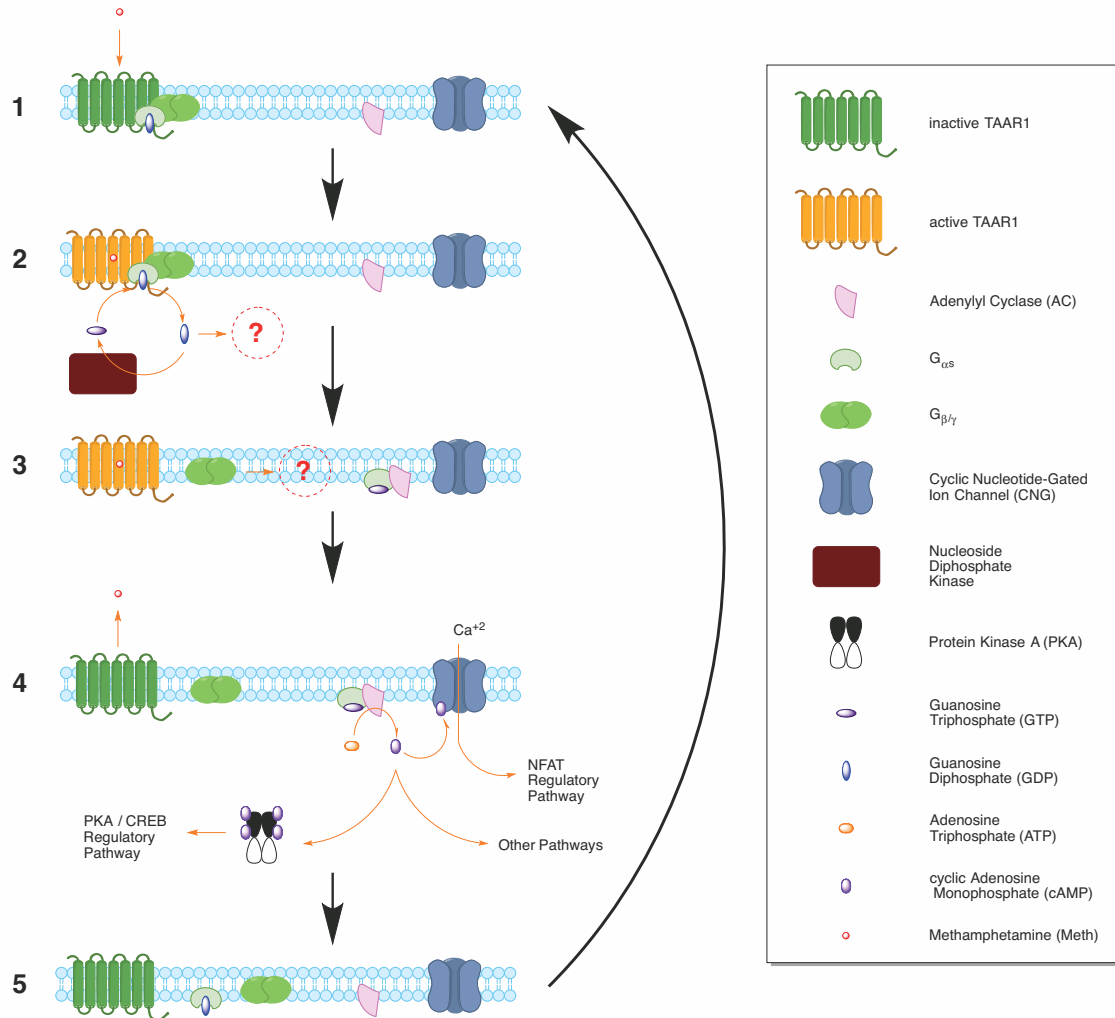
Background on Trace Amine Associated Receptor 1 (TAAR1)

In step 4, adenylyl cyclase converts ATP to cAMP. From that point, signaling proceeds through the cAMP/ protein kinase A (PKA)/cAMP response element binding protein (CREB) pathway.¹⁰ Also, activated TAAR1 signals through the protein kinase C (PKC)/Ca⁺²/nuclear factor of activated T-cells (NFAT) pathway.¹⁰ The literature clearly indicates a connection between TAAR1 and the NFAT pathway, however the precise mechanism by which they are connected was not proposed. One possible way for them to be connected is through a Ca⁺² cyclic nucleotide-gated ion channel (CNG). Both the CREB and NFAT pathways lead to the blocking of monoamine uptake.

There is evidence that TAAR1 tonically activates inwardly rectifying K⁺ channels, presumably by Kir3-type K⁺ channels via activated G_{β/γ}. TAAR1 inhibition increases affinity of dopamine to the D₂-receptor (D₂R) and reduces the desensitization rate of D₂R.¹¹ Furthermore, TAAR1-D₂R heterodimers have been observed.¹⁴ Early work with the thyronamine family of compounds, including their analogs developed by Dr. Edwin Tan,^{17,18} implicated TAAR1 in the thermoregulatory processes, but that has since been challenged.^{10,19} Basal (constitutive) or tonic activity of TAAR1 has been hypothesized^{9,11} and research in this area is on going.

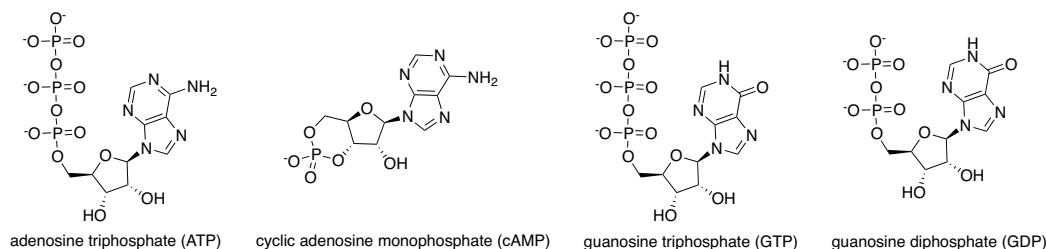
Background on Trace Amine Associated Receptor 1 (TAAR1)

FIGURE 1.2: The known signaling pathway of TAAR1. (1) System at rest until Meth binds to TAAR1. (2) Activated TAAR1 stimulates $G_{\alpha s}$ to exchange GDP for GTP. GDP is then recycled into GTP by nucleoside diphosphate kinase. The literature has little information about other effects this GDP might have. (3) The TAAR1- $G_{\alpha s}$ / $G_{\beta/\gamma}$ complex disassociates and $G_{\alpha s}$ binds to adenylyl cyclase (AC). (4) AC converts ATP to cAMP. It is then possible that cAMP activates the PKC/NFAT regulatory pathway via a calcium ion cyclic nucleotide-gated ion channel. cAMP also activates the CREB regulatory pathway via PKA. Additionally, the cAMP produced by the TAAR1 pathway may affect other pathways. Also, TAAR1 releases the Meth (shown in step 4 but could happen in step 3). (5) $G_{\alpha s}$ disassociates from AC, and GTP is hydrolyzed to GDP. The system is now ready to reset. Original artwork by Troy Wahl.



Methamphetamine

FIGURE 1.3: Structures of ATP, cAMP, GTP and GDP.



1.2 Methamphetamine

Methamphetamine (Meth), **FIGURE 1.1**, is a psychostimulant that effects the Dopamine Transporter (DAT), Norepinephrine Transporter (NET), Serotonin Transporter (SERT), Vesicular Monoamine Transporters (VMAT)^{20,21} and TAAR1.⁴ By inhibiting VMAT, Meth causes DA to accumulate in the cytosol until the concentration of DA is high enough that gradient dependent DAT allows a net flow of DA out of the neuron and into the synaptic cleft. In the parlance of chemical biology, Meth blocks the re-uptake of neurotransmitters and thus elevates signaling. Meth affects norepinephrine and serotonin in a similar manner as DA.

Dopamine³ is part of the reward system and is associated with pleasant or excited feelings, which in part, is why it is implicated in addiction. DA is considered to modulate *prediction error*,² which is the difference between an expected outcome and the actual outcome of an event. When an expectation is met, dopamine levels increase, reinforcing the expectation/lesson, otherwise dopamine levels drop. DA, also, is associated with *seeking* behaviors.²²⁻²⁷ In general, medications that increase DA in the synaptic cleft, such as amphetamine and meth-

Methamphetamine

ylphenidate,²⁸ are effective attention deficit hyperactive disorder (ADHD) medications. Finally, DA is associated with agitation and anxiety (worry/anxiety can be described, in part, as the expectation of negative or undesirable outcomes).²⁹

Norepinephrine³⁰ is part of the fight-or-flight response (adrenergic system) and increases heart rate, blood pressure and the release of glucose into the blood. Norepinephrine is also involved in attention, wakefulness (arousal) and alertness. Atomoxetine (Strattera)³¹ is a selective norepinephrine reuptake inhibitor (4 nM K_i) prescribed to treat ADHD, it is also weak serotonin reuptake inhibitor (77 nM K_i). Both epinephrine (adrenaline) and norepinephrine are associated with the panic symptoms of anxiety.

Serotonin³² is involved in mood regulation with low levels being associated with depression. Extremely high levels of serotonin results in serotonin syndrome,³³ which is potentially fatal.

Overall Meth, like all the amphetamines, increases alertness, wakefulness, and attention (particularly to repetitive tasks) but decreases appetite and is a euphoric. Side-effects include addiction, high blood pressure, irritability, aggression, hyperthermia and anxiety-like symptoms (especially paranoia and obsessive-compulsive disorder). Due to its benefits, Meth might appeal to those seeking to reduce stress due to fatigue, those with excessive time demands (long work hours or multiple

Justification for targeting TAAR1

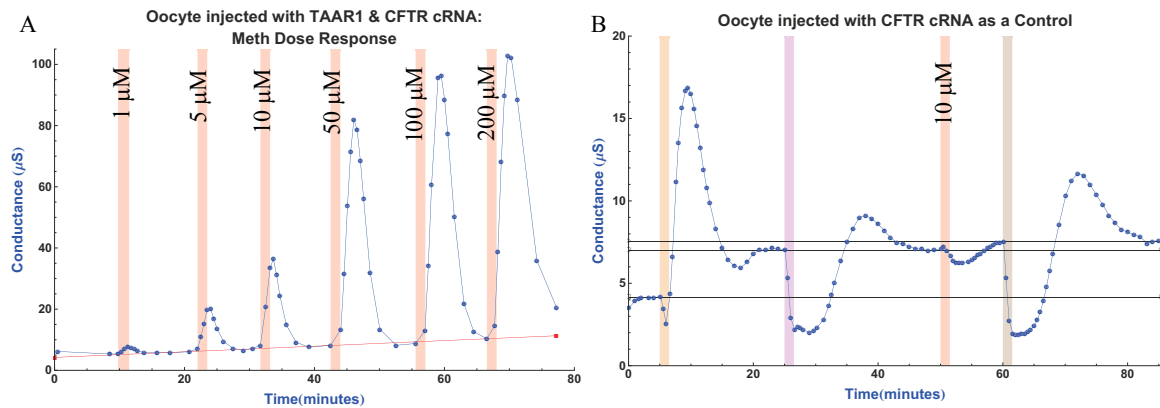
jobs or overbooked social commitments), excessive deadlines, who need to focus on highly repetitive tasks, who are bored, depression or who perceive the needed to get a competitive edge over others.

1.3 *Justification for targeting TAAR1*

TAAR1 was chosen as the target receptor for treating methamphetamine (Meth) addiction because TAAR1 is activated by Meth in a dose (concentration * 1.5 minutes * 4 ± 1 mL/minute) dependent manner (**FIGURE 1.4A**). In an experiment with an oocyte that was not injected with hTAAR1 encoding RNA, Meth caused a drop in transmembrane conductance (**FIGURE 1.4B**, red shaded region). While this small drop in transmembrane conductance, which has been observed only once, needs to be verified before considered as solid evidence for an new Meth target, it is clearly different than the response to Meth when TAAR1 is present. Also, *in vivo* mouse studies, **FIGURE 1.6**, show how the dose-dependent inhibition of TAAR1 by **ET-92**¹⁷ and EPPTB³⁴ (**FIGURE 1.5**) reduces Meth stimulated locomotion. These results represent the strongest type of justification for a medicinal chemistry project, namely a desired phenotypical response (blocking the effects of Meth) due to the action of a known molecular target (TAAR1).

Justification for targeting TAAR1

FIGURE 1.4: A) Two electrode voltage clamp (TEVC) methamphetamine dose (concentration * 1.5 minutes * 4 ± 1 mL/minute) response from *Xenopus Laevis* frog oocyte injected with hTAAR1 and hCFTR encoding RNA (n=1). The doses, indicated on the graph, of Meth in Frog Ringer's solution (red bars) were pulsed for 1.5 minutes. At all other times the oocyte was washed with Frog Ringer's solution. The experiment (n=1) was done by Dr. Yohei Noramatsu, OHSU. The red line is an approximate baseline. B) TEVC Meth response in an oocyte injected with hCFTR encoding RNA. Meth (10 μ M, red region) in Frog Ringer's solution was pulsed for 1.5 minutes followed by washing with Frog Ringer's solution (n=1). The horizontal lines are visual aids.

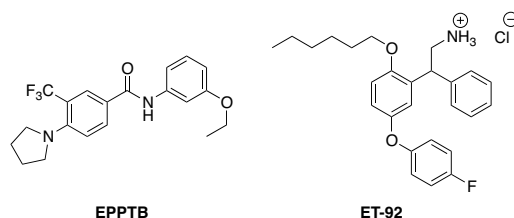


In **FIGURE 1.4**, the two electrode voltage clamp (TEVC) results are shown from dosing frog oocytes injected with hTAAR1 and hCFTR encoding RNA (**FIGURE 1.4A**) or just hCFTR encoding RNA (**FIGURE 1.4B**) with Meth, both with n=1. CFTR (cystic fibrosis transmembrane conductance regulator)³⁵ is a chloride channel that is activated by cAMP. By pairing TAAR1, whose activation results in increased cAMP production, and CFTR in an oocyte, a biological circuit is made for assaying the activity of TAAR1 via monitoring the oocytes transmembrane conductance. An oocyte just injected with hCFTR encoding RNA served as the control experiment. In the absence of TAAR1, Meth caused a drop in transmembrane conductance in this single run. It is unlikely that the drop was caused by the effects of Meth on any of the dopamine, norepinephrine, serotonin receptors or transporters as the oocytes do not express them. The drop in transmembrane con-

Justification for targeting TAAR1

ductance might involve a hitherto unknown target of Meth as a literature survey has not revealed any such reports. Confirmation of this result will be needed.

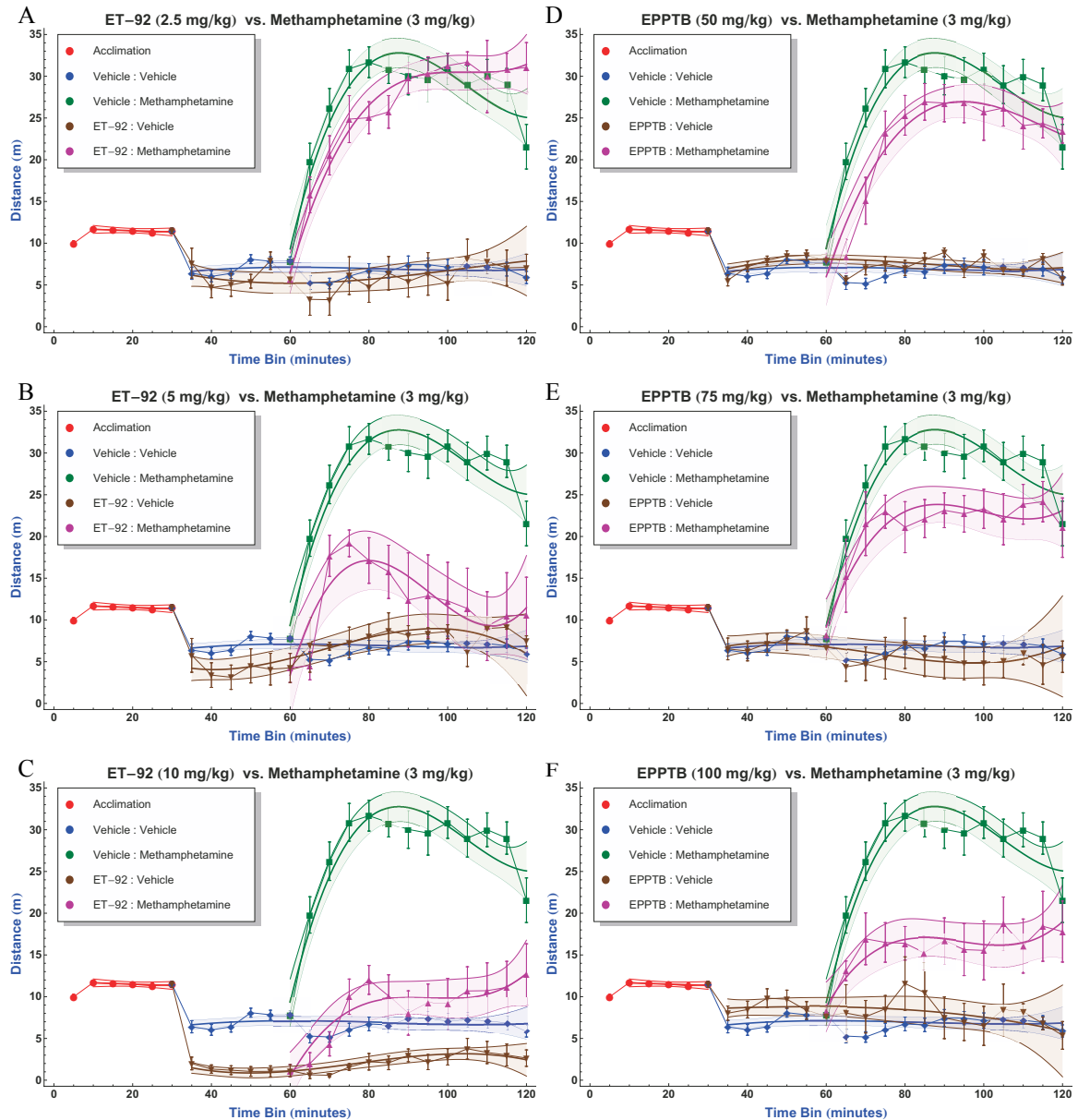
FIGURE 1.5: Structures of EPPTB and ET-92 (racemic)



The *in vivo* results for ET-92, **FIGURE 1.6A-C**, were known at the start of the project but those of EPPTB, **FIGURE 1.7D-F**, were not as EPPTB was still fairly new.¹¹ Both of these compounds, which were designed to be TAAR1 antagonists, reduce Meth stimulated locomotion in mice in a dose-dependent manner thus validating that TAAR1 plays a significant role in Meth signaling and potentially a target for treating Meth addiction. Meth self-administration experiments with EPPTB or ET-92 treatments have yet to be done. Such experiments would demonstrate whether or not TAAR1 antagonists modulate the motivation to acquire or self-administer Meth. However, their lack does not diminish the potential of treating Meth addiction by targeting TAAR1 as self-administration experiments, and other animal model testing, are usually done fairly late in pre-clinical development. Animal efficacy testing late in the project development may seem counter-intuitive but the expense of animal testing is great enough that a viable drug-candidate (potent, bioavailable, low toxicity, etc.) is desired before proceeding to test efficacy.

Justification for targeting TAAR1

FIGURE 1.6: Mouse *in vivo* studies of the effects of ET-92 (A-C) or EPPTB (D-F) in reducing Meth stimulated locomotion. From these studies it is clear that both ET-92 and EPPTB inhibit Meth stimulated locomotion in a dose-dependent manner. The thick lines are cubic polynomial least-squares models of the data, with the exception of the model for the acclimation data which is a linear least-squares model. The shaded regions are the model lines' 95% confidence intervals for their respected model. The modeling provides a very quick check for statistical difference - the less overlap between the confidence intervals, the greater the probability that the data sets are statistically different. In all cases, the vehicle was DMSO. Data was provided by Madeline Grandy, Ashley Kimbell, and Katie Tallman and the statistical modeling was done by Troy Wahl.³⁶



Overview of Current TAAR1 Medicinal Chemistry

1.4 Overview of Current TAAR1 Medicinal Chemistry

TAAR1 binds a variety of biogenic trace amines, as have been previously listed (**FIGURE 1.1**),^{5,6} it also binds a wide range of synthetic analogs of phenethylamine (PEA), some of which are shown in **FIGURE 1.7**. However Simmler²⁰ reported that cathinones (β -keto amphetamines, **FIGURE 1.8**) have poor binding affinities to TAAR1. Guanabenz, **FIGURE 1.9**, an antihypertensive α_2 -adrenergic agonist is also a highly potent TAAR1 agonist.¹⁴ The first synthetic TAAR1 ligands were those of Tan¹⁷ and are analogs of thyronamine, **FIGURE 1.10**. The problem with all of these compounds, as indicated in the above citations, is that they lack TAAR1 specificity, except perhaps the thyronamines. The lack of specificity is not necessarily a problem for a drug so long as side-effects are minimal. However, the lack of specificity becomes a major problem for the development of tool kits to study TAAR1 *in vivo* because side-effects can confound the interpretation of experimental results.

FIGURE 1.7: Racemic mixtures of some phenethylamine (PEA) analogs that bind to TAAR1.

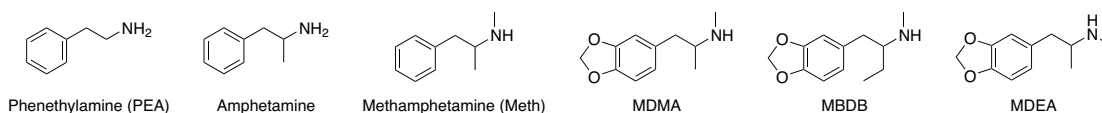
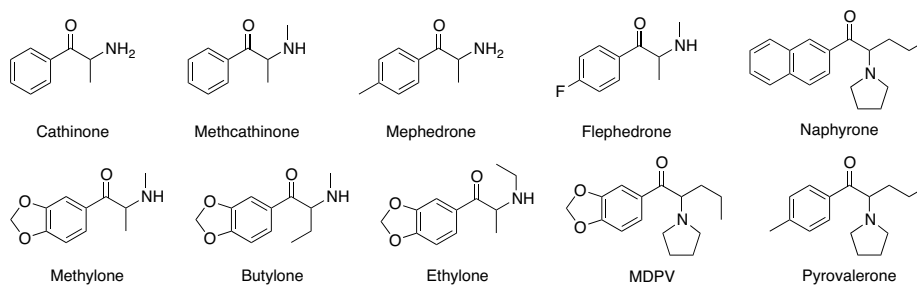


FIGURE 1.8: Racemic mixtures of some cathinone analogs.



Overview of Current TAAR1 Medicinal Chemistry

FIGURE 1.9: Guanabenz

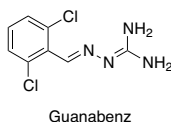
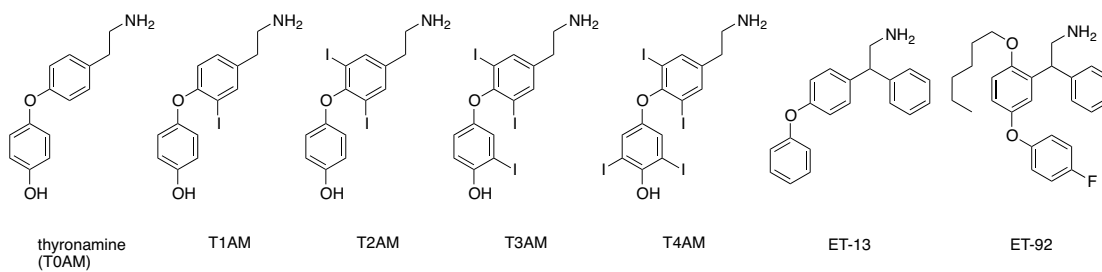
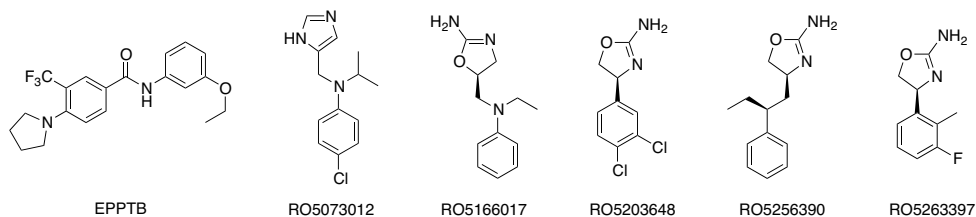


FIGURE 1.10: Analogs of thyronamine. ET-13 is a TAAR1 agonist, while ET-92 is an antagonist. ET-13 and ET-92 are racemic mixtures.



Currently, the only documented TAAR1 specific compounds are from Hoffmann-LaRoche, **FIGURE 1.11**. These compounds range from antagonist, EPPTB, to partial agonists, RO5203648, and full agonists, RO5073012 and RO5166017.^{9,10,34,37} Selectivity of these compounds were determined by screening against over 100 receptors, ion channels, transporters and enzymes, with the most problematic off-target being the α_2 -adrenergic receptor. In the course of developing these compounds Hoffmann-LaRoche created an extensive patent library,^{8,34,38-56} which greatly restricts the development of new compounds targeting TAAR1.

FIGURE 1.11: TAAR1-specific compounds from Hoffmann-LaRoche.



Overview of Current TAAR1 Medicinal Chemistry

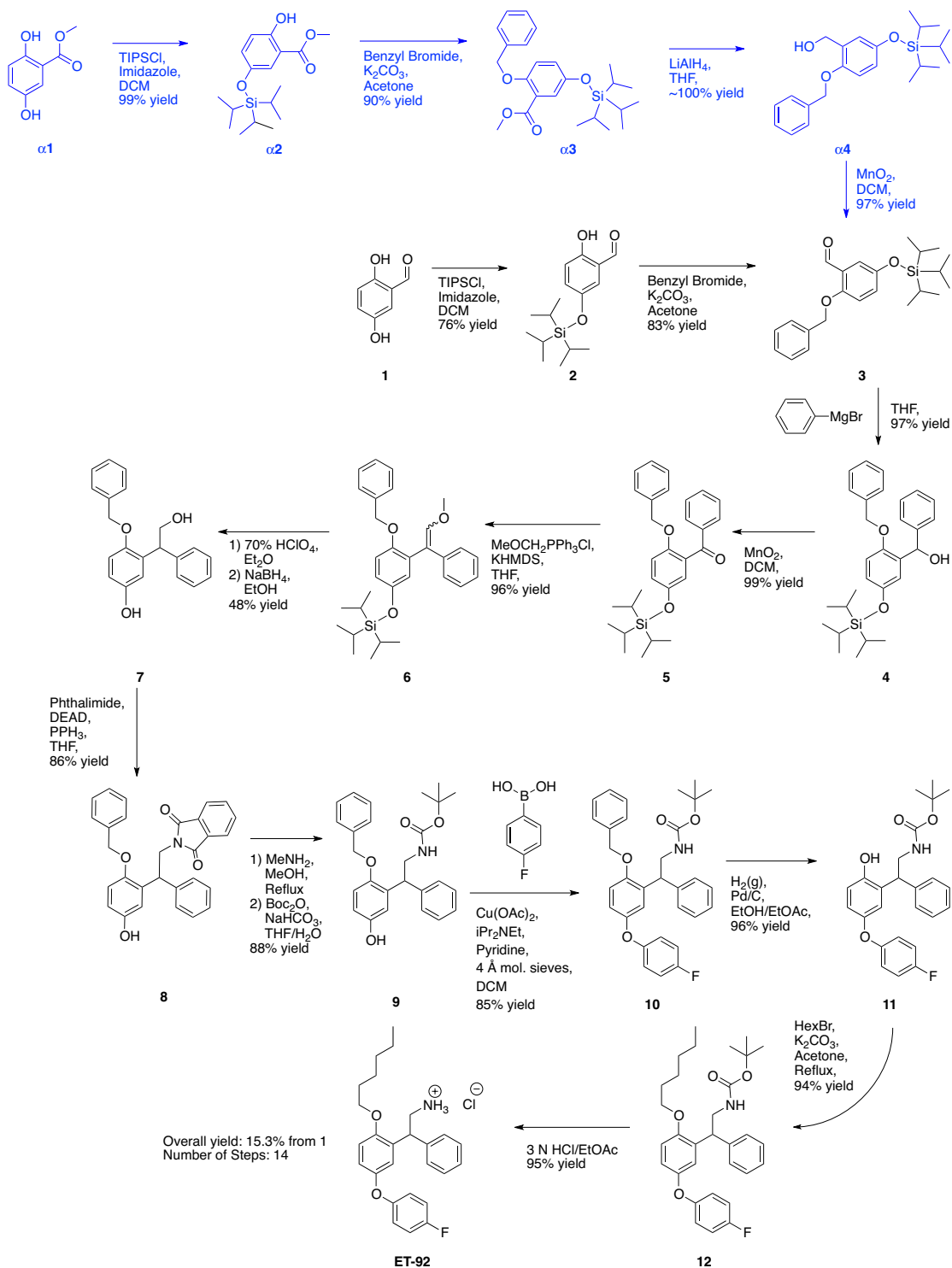
As seen in **FIGURE 4.6**, **ET-92** is more efficacious *in vivo* in mice than EPPTB by a molar ratio greater than 10.7:1, which made it an attractive lead for further development. Furthermore, Oregon Health & Science University (OHSU) owns the patent on the thyronamine family,⁵⁷ and there is substantial room for further SAR (structure-activity-relationship) development in Tan's work.¹⁷ At the outset of the project, the thyronamines, **ET-92** in particular, had 3 liabilities: poor drug-like properties (high lipophilicity, poor solubility and a hydroquinone core, which has known toxicity issues), thermoregulatory side-effects and a lengthy synthetic route.

2.1 *Cost-effective synthetic route to ET-92 and its analogs*

The original synthesis of ET-92,¹⁷ **FIGURE 2.1**, is fourteen steps starting from 2,5-dihydroxybenzaldehyde with an overall yield of 15.3%, and involves multiple protecting groups with steps **4** → **5** and **9** → **10** taking up to 7 days each to complete. In order to develop **ET-92**, or closely related analogs, into an FDA approved drug, large batches of cGMP grade material would need to be produced. Based on an old estimate of \$10,000 per day⁵⁸ in a process plant for facility charges, that might not include the costs of setting-up or clean-up, original **ET-92** synthesis would be expensive (minimum facility charges: \$150K - \$410K) even before the cost of reagents and waste disposal are considered. Finally, the length of the synthesis would make rapid develop of **ET-92** analogs difficult. For these reasons, a new cost-effective synthetic route was developed, **FIGURE 2.2**.

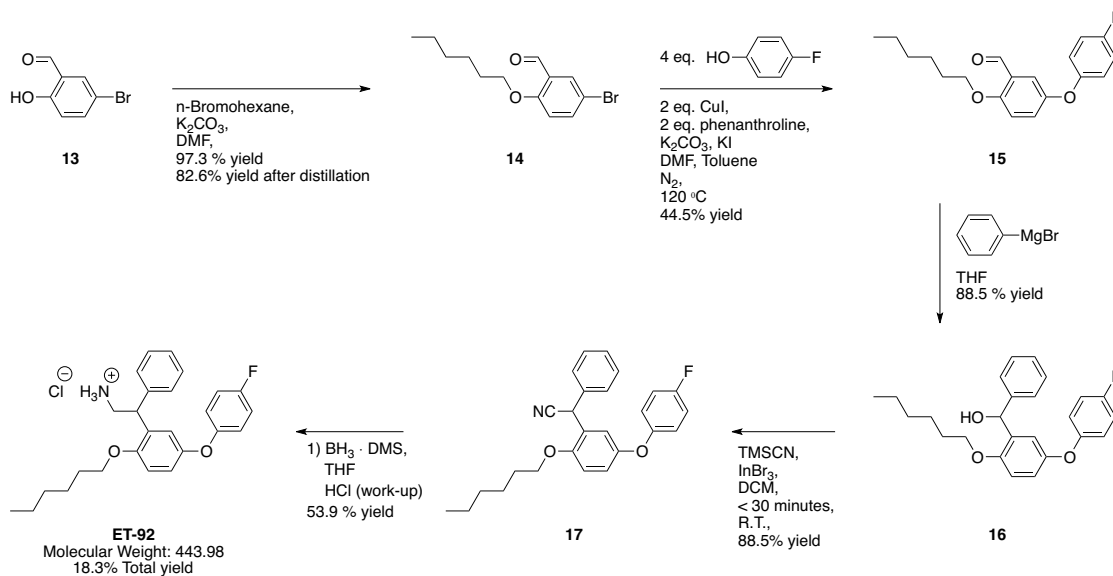
Cost-effective synthetic route to ET-92 and its analogs

FIGURE 2.1: The original ET-92 synthetic route¹⁷ starting with 2,5-dihydroxybenzaldehyde (**1**) or with the alternative starting material, methyl 2,5-dihydroxybenzoate (**α_1**), involves fourteen steps from **1** with an overall yield of 15.3%.



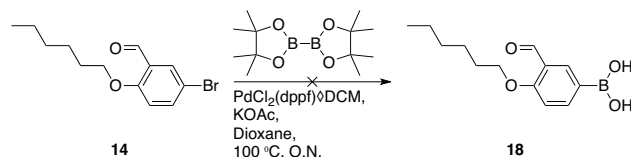
Cost-effective synthetic route to ET-92 and its analogs

FIGURE 2.2: The new synthetic route to **ET-92**. Most steps are complete in less than 4 hours and are in high yield. Further optimization of **14** → **15** and **17** → **ET-92** is needed as well as improved purification (likely via distillation).



A new 5 step synthetic route was developed for **ET-92** starting with the alkylation of 5-bromosalicylaldehyde, **13** → **14**, which is quantitatively complete within 4 hours and resulting in a 97.3% isolated yield. In order to produce a publication quality NMR, **14** was vacuum distilled (46 mTorr, bp 104-130 °C at 46 mTorr, 85.6% total yield). However, distillation at this step is not necessary as the crude product is pure enough to use in the next reaction.

FIGURE 2.3: The Miyaura boration reaction did not work with this substrate.



To convert **14** into **15**, several different reaction types were tried: Miyaura boration (**FIGURE 2.3**)⁵⁹⁻⁶⁶ followed by Chan-Lam reaction (**20** → **15** in **FIGURE**

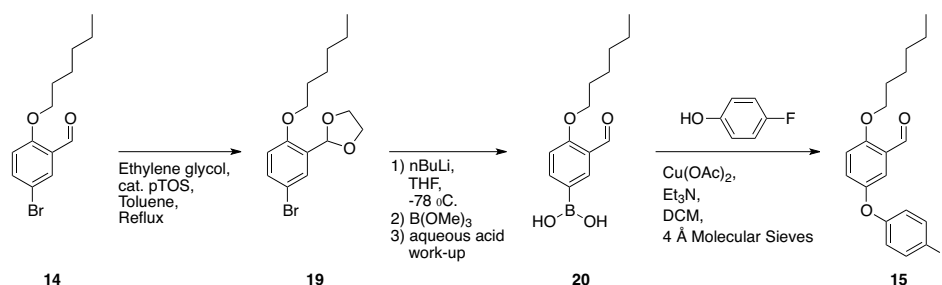
Cost-effective synthetic route to ET-92 and its analogs

2.4), a traditional boronic acid synthesis followed by Chan-Lam reaction (**FIGURE 2.4**) and finally the modified Ullmann reaction (**14** → **15** in **FIGURE 2.2**). The use of copper catalyzed reactions (Chan-Lam and Ullmann) was preferred to palladium catalyzed reactions (Miyaura and Buchwald-Hartwig) for economic reasons, copper catalysts being much less expensive than palladium ones. If the Miyaura boration had worked, then there was the possibility of immediately following it with a Buchwald-Hartwig reaction to synthesis **15** in a one-pot reaction. It was for that reason that the Miyaura boration reaction was tried first. The Miyaura boration also served as an indicator for other palladium catalyzed reactions, failure of this reaction lead to the conclusion not to pursue other palladium catalyzed reactions. Although the Miyauara boration is known to work with 5-bromo-2-(methoxymethoxy)benzoic acid,⁶³ 5-bromo-2-(methoxymethoxy)benzaldehyde⁶⁷ and 5-bromosalicylaldehyde under microwave reaction conditions,⁶⁸ it produced no detectable product using **14** and PdCl₂(dppf)·DCM as the catalyst.

In the more traditional boronic acid synthesis (**19** → **20** in **FIGURE 2.4**) two issues were encountered: the acetal (**19**) appears to coordinate water, which in turn hydrolyzes the acetal over time; also, the boronic acid tended to form mixed anhydrides which did not react well in the Chan-Lam step. This is a stark contrast to the results achieved in previous work at Celera Genomics with 2-benzyloxy-3-bromobenzaldehyde.

Cost-effective synthetic route to ET-92 and its analogs

FIGURE 2.4: A traditional boronic acid synthesis followed by a Chan-Lam reaction to make **15**. Although this route did work, yields of the boronic acid, **20**, were very inconsistent.



With poor results through the Chan-Lam route, it was decided to try the modified Ullmann ether synthesis (**14** → **15** in **FIGURE 2.2**).^{69,70} Although the Ullmann ether synthesis is air sensitive like the Buchwald-Hartwig reaction, the reagents are less expensive and are easy to remove during the work-up. After an initial screen of ligands (2,2'-bipyridine, phenanthroline, N,N-dimethylglycine, N,N,N',N'-tetramethylethane-1,2-diamine, and tributylphosphine) and anhydrous solvents (DMF, DMSO, and dioxane), qualitatively TLC spot intensity indicated that phenanthroline in either DMF or DMSO worked best. It was also found that all combinations of solvent and ligands worked to some extent except for tributylphosphine and N,N-dimethylglycine in dioxane. Further screening found that a 1:1 ratio of phenanthroline to CuI produced the same result as the literature standard ratio of 2:1. Also, the use K₃PO₄ instead of K₂CO₃ decreased reaction yields. Among the conditions tested the highest yield occurred with two equivalents of CuI and phenanthroline and 4 equivalents of phenol slowly added to the reaction. The addition of KI to the reaction results in a modest improvement of the yield. In the final reaction toluene, about 10% total volume, was added to azeotrope off any

Cost-effective synthetic route to ET-92 and its analogs

water present. That addition clearly does not reduce the reaction yield, but it is unclear whether or not it improves. As phenanthroline monohydrate was initially used successfully, this reaction is tolerant of some water. The major side-product of this reaction is 2-(hexyloxy)benzaldehyde, which co-elutes with **15** on silica and must be removed before continuing the synthesis. As **15** is a liquid, vacuum distillation would be an inexpensive purification method. Due to the high viscosity and expected boiling point of **15**, multistage vacuum falling film distillation⁷¹ would be a good technique to use as it would reduce the hold-up. Since **15** was prepared on a small and micro-scale vacuum distillation equipment was not available, **15** was purified by C-18 rpHPLC.

While working on the reaction of **14** to **15**, several experiments lead to notable observations. Acetonitrile does work as a reaction solvent, though poorly (<25% yield), and yields large amounts of an orange powder that could be nano-copper particles, since the powder dissolved in aqueous HCl producing a blue-green solution that was visually similar to solutions of CuCl₂. Also, Cu(OAc)₂, instead of CuI works, but very poorly (<10% yield); however the addition of KI greatly improves the reaction yield. Conventional wisdom holds that the Ullmann reaction proceeds by oxidative addition of Cu⁺¹ to the arylhalide resulting in a Cu⁺³ species or by transmetallization with Cu⁺², however neither of these explain why Cu(OAc)₂ works (Cu⁺⁴ is unknown and there were no other metal species present

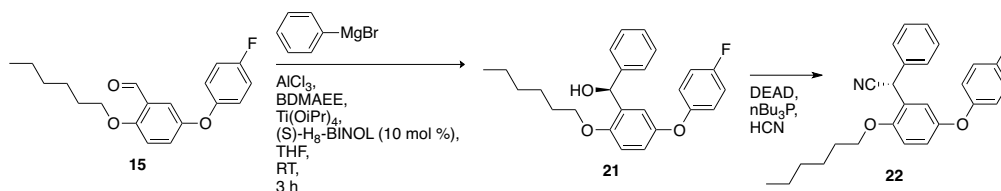
Cost-effective synthetic route to ET-92 and its analogs

for Cu^{+2} to transmetalate with). One possible explanation is σ -bond metathesis,⁷² which was an unknown reaction when most of the mechanistic research was done on the Ullmann reaction. The improved yield upon addition of KI to $\text{Cu}(\text{OAc})_2$ reaction mixture, is most probably due to a redox reaction:



The Grignard reaction, **15** \rightarrow **16**, **FIGURE 2.2**, is very clean and straight forward. A chiral variation has been reported by Fan⁷³ which if followed by a Mitsunobu with HCN could produce chiral **ET-92** (**FIGURE 2.5**). However, these reactions were not pursued due to a desire to first develop an achiral **ET-92** synthesis then use that route to develop new thyronamine analogs.

FIGURE 2.5: A possible route to chiral **ET-92**.

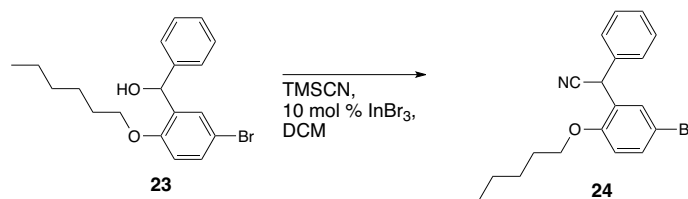


The nitration of **16**, **FIGURE 2.2**, has been attempted with pTosCl and thionyl chloride followed by KCN before settling on the $\text{TMSCN}/\text{InBr}_3$ catalyzed reaction.⁷⁴ When the test reaction **23** \rightarrow **24** (**FIGURE 2.6**) was purified by basic alumina chromatography eluting with hexanes and EtOAc , which removed the sole major by-product, 4-bromo-2-((hexyloxy)-(phenyl)methyl)phenol, $^1\text{H-NMR}$ of **24** in DMSO-d_6 revealed that the proton next to the nitrile has a chemical shift of 5.78

Cost-effective synthetic route to ET-92 and its analogs

ppm which previously had been mistaken as residual DCM (5.76 ppm) due the use of house vacuum and the inability to completely remove solvents from samples. Armed with that information, samples of **17** made with pTosCl and thionyl chloride were repurified on basic alumina, confirming that those reactions had also worked but were not as pure nor as high yielding as the TMSCN/ InBr_3 catalyzed reaction. Another advantage of the TMSCN/ InBr_3 reaction is that it is so fast that it might be complete within seconds of mixing the reagents, thus allowing for the reaction to be done in a continuous flow reactor with an inline basic alumina plug filtration, and significant cost savings.

FIGURE 2.6: Nitration reaction confirmed the feasibility of the new ET-92 route. This reaction is complete in less than 30 minutes, possibly seconds, with only one major side product: 4-bromo-2-((hexyloxy)-(phenyl)methyl)phenol at 16%.



The reduction of **17** to **ET-92** proved to be problematic, with the highest yield to date being 53.9% using $\text{BH}_3 \cdot \text{DMS}$ in refluxing THF overnight.⁷⁵ When the hard reducing agents (LiAlH_4 and Dibal-H) were used, the yields are very low (~10%) with large amounts of side-products. Reduction with Pd/C had no effect.

In summery, a novel synthetic route was developed for **ET-92**, the lead compound for this project, which reduced the number of synthetic steps from 14 to 5

Cost-effective synthetic route to ET-92 and its analogs

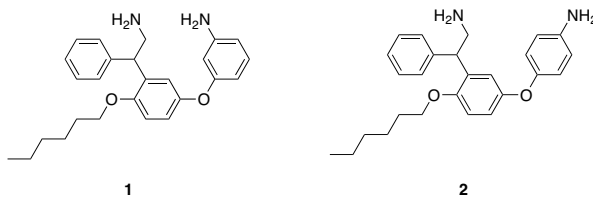
and improved the overall yield from 15.3% to 18.3% (77.4 mg). Although this was not a production this sets the table for future scale-up work.

With the working hypothesis that TAAR1 activation by Meth is significantly responsible for desirable characteristics of Meth intoxication, the development of TAAR1 inverse agonists (basal inhibitors) as treatments for Meth addiction may not be possible, since they could push the Meth user further away from how they want to feel. However, the development of selective TAAR1 antagonists are needed to pharmacologically determine the role of TAAR1-mediated signaling *in vitro* and *in vivo*. In future work, the development of partial or fully agonists could provide effective treatments.

3.1 Initial attempts to synthesize new analogs

Once the new ET-92 synthetic route had been developed, ET-92 analogs were postulated that had greater water solubility and further explored the structure-activity-relationships (SAR) of the thyronamine family. Thus, the synthesis of compounds **1-2** (**FIGURE 3.1**) was begun.

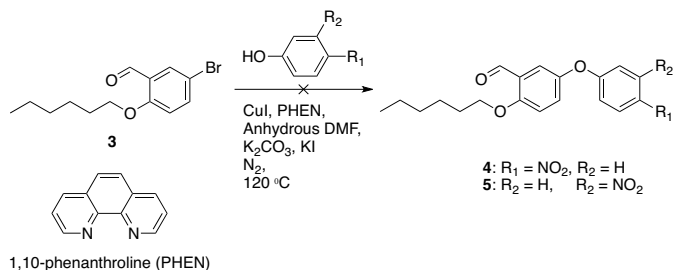
FIGURE 3.1: First new analog targets to be synthesized.



Change in strategy and targets

To make compounds **1** and **2**, the Ullmann reaction between **3** and either *meta*- or *para*-nitrophenol was attempted, **FIGURE 3.2**. Unfortunately, the reactions did not produce a detected amounts of product, probably due to increased acidity of *para*- and *meta*-nitrophenol (pka 7.12 and 8.36 respectfully) compared to 4-fluorophenol (pka 9.81) and phenol (pka 10.02). Ullmann reaction works best with amines, then amides and finally alcohols but not at all with carboxylic acids.⁶⁹ In other words, reaction yields decrease as acidity of the nucleophile increases. After several attempts with no evidence of the desired products, compounds **1** and **2** were triaged to low priority.

FIGURE 3.2: The first step in synthesizing compounds **1** and **2**.

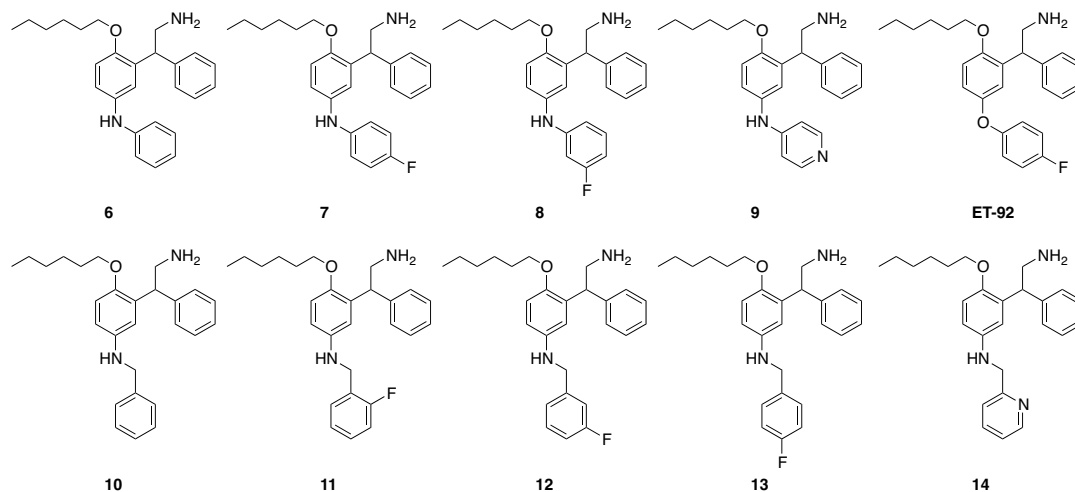


3.2 Change in strategy and targets

Due to the synthetic difficulties outlined above, and the desire to have target compounds with improved water solubility, syntheses of the molecules depicted in **FIGURE 3.3** were pursued next. Although the 4-aminophenol⁷⁶ core of **6** - **14** may have similar toxicity issues to the hydroquinone⁷⁷ core of **1**, **2**, and **ET-92**, it allows one to develop different chemistries to explore the SAR.

Change in strategy and targets

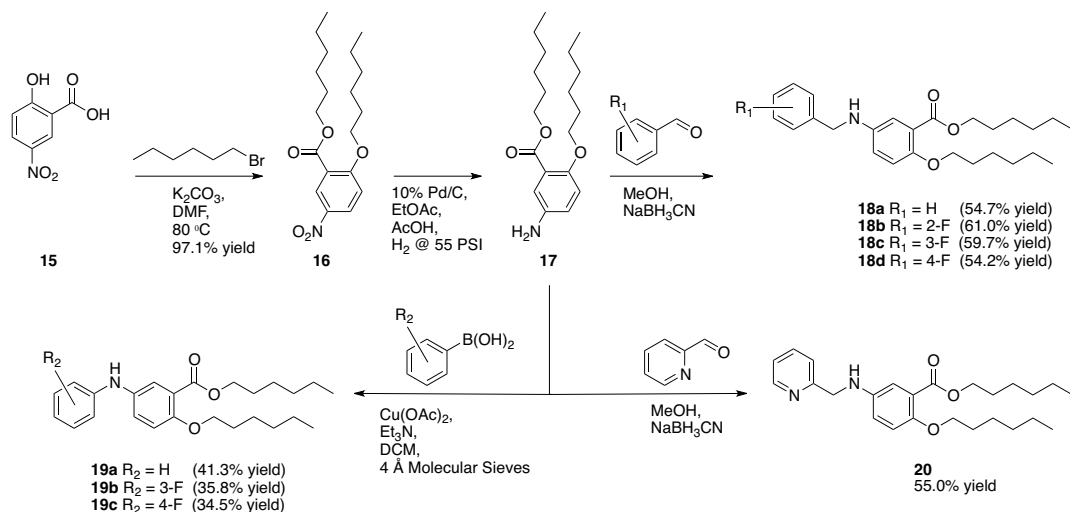
FIGURE 3.3: New targets and ET-92



Starting with 5-nitrosalicylic acid, **15**, the synthesis proceeded smoothly through three steps, **FIGURE 3.4**. An attempt to couple 4-pyridylboronic acid and **17** under Chan-Lam conditions did not work, but that was not especially surprising as pyridylboronic acids are known to be difficult coupling partners. Yields on the Chan-Lam reactions, **19a-c**, were ~35-42% while the reductive aminations, **18a-d** and **32**, were ~53 - 61%. In going from **16** to **17**, acetic acid was added to the reaction mixture to promote hydrogen transfer in the aprotic ethyl acetate and to prevent the amine from chelating the palladium, which can be an issue. Later work demonstrated that addition of acid was not needed during the hydrogenation.

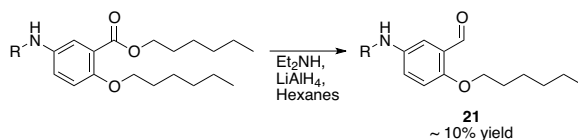
Change in strategy and targets

FIGURE 3.4: The first steps towards the new analogs.



Reduction of the esters to aldehydes followed, and, although showing promise, only resulted in ~10% yields by ¹H-NMR, **FIGURE 3.5**. The Et₂NH, LiAlH₄ and hexanes were premixed, then the ester was added.⁷⁸ Since no benzyl alcohols nor carboxylic acids were detected by ¹H-NMR, there was simply not enough reducing agent present to drive the reaction to completion. The aniline amine may have also reacted with some of the reducing agent, limiting the effectiveness of the reaction. With more development this reaction could prove useful, however further development was set aside.

FIGURE 3.5: Reduction of ester to aldehyde.



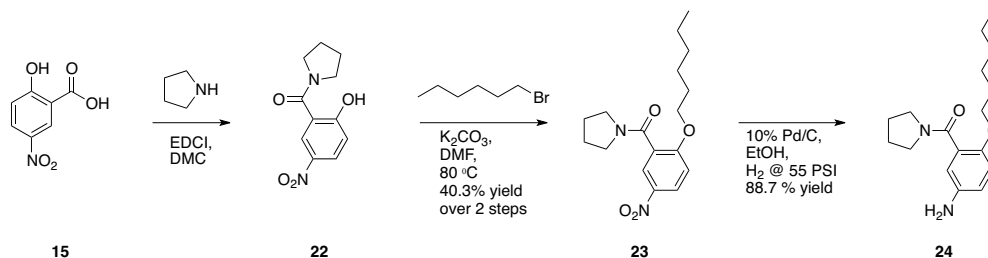
Another strategy change

3.3 *Another strategy change*

Since the reduction of the esters did not immediately result in high yields of the corresponding aldehydes, the synthetic route was once again changed. The plan became to form a tertiary amide then convert the amide to a ketone by reacting it with a Grignard reagent.

Starting with 5-nitrosalicylic acid and pyrrolidine, the amide (**22**) was formed with the use of either EDCI, DCC, or DCC and HOBT·H₂O, **FIGURE 3.6**. In all cases, the yields were highly variable (~20 - 91% by mass) with no obvious reason for the differences. A survey of SciFinder results for amide formation with various salicylic acids revealed a similar range of yields. Although the use of HOBT produced the highest yield, the product contained impurities that were difficult to remove. The rest of the sequence to **24** is straightforward.

FIGURE 3.6: Synthesis of a key intermediate.



As before, the amine of **24** was functionalized through either reductive amination or the Chan-Lam reaction, **FIGURE 3.7**. When the Grignard reaction of **25a**, **FIGURE 3.8**, was attempted, nothing happened despite using 5 equivalents of phenylmagnesiumbromide. The large amount of Grignard reagent was sufficient to

Another strategy change

react with the residual water in the THF, deprotonate the amine, and yet leave enough to react with the amide. The amide's lack of reactivity maybe the result of steric hindrance, as $^1\text{H-NMR}$ reveals that the pyrrolidinamide exists as a rotamer with the pyrrolidine ring askew, but not perpendicular, to the central phenyl as evidenced by the ~ 0.32 ppm $^1\text{H-NMR}$ shift difference between the methylene protons on either side of the pyrrolidine's nitrogen. However, one might think that with the amide being co-planar with the adjacent phenyl ring that the Grignard reagent would have a clear path for a facial attack on the amide.

FIGURE 3.7: Functionalizing the amine.

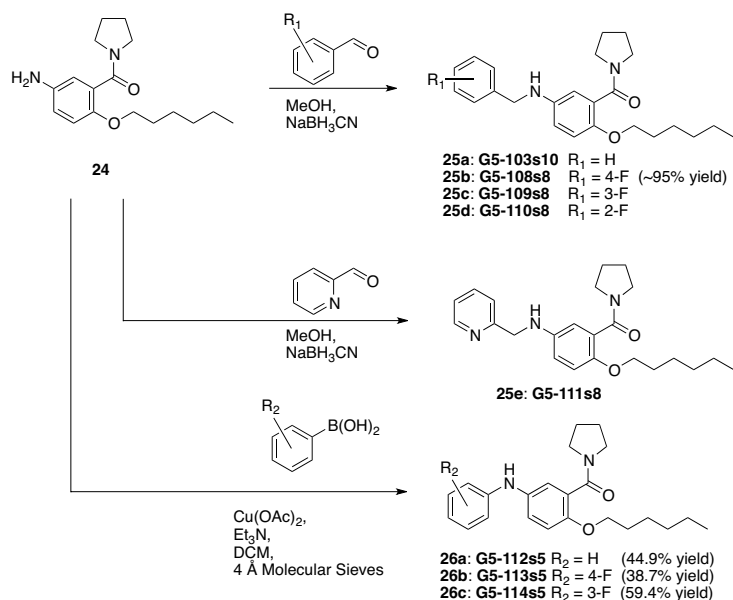
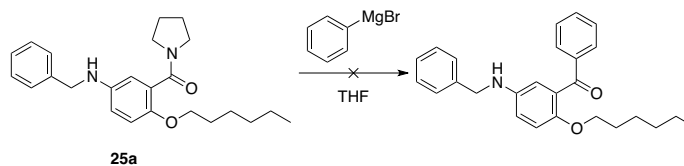


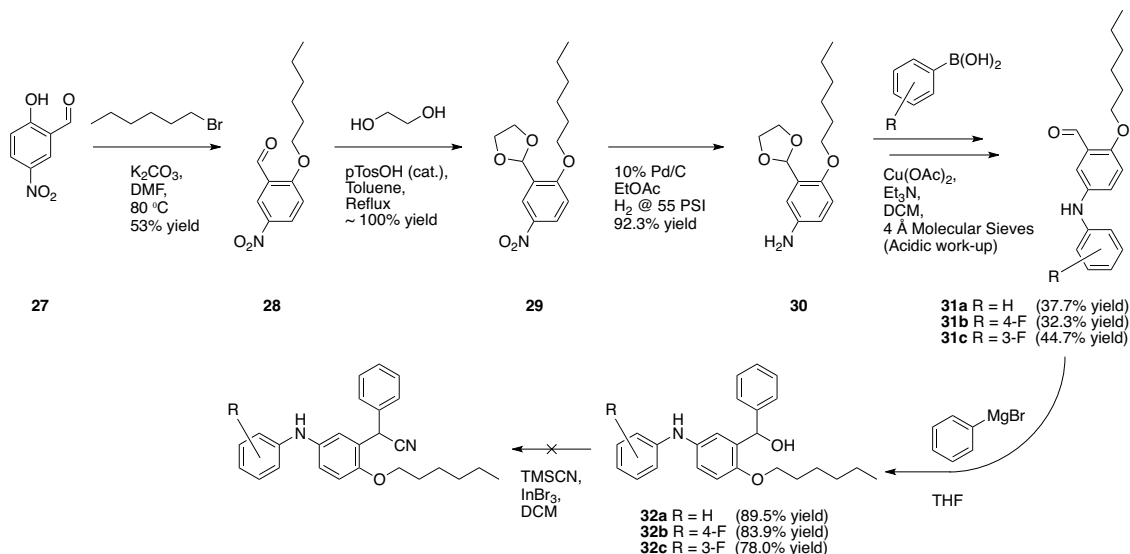
FIGURE 3.8: A failed Grignard reaction.



Final attempt to synthesize 6 - 14

3.4 Final attempt to synthesize 6 - 14

FIGURE 3.9: The final syntheses of thyronamine analogs.



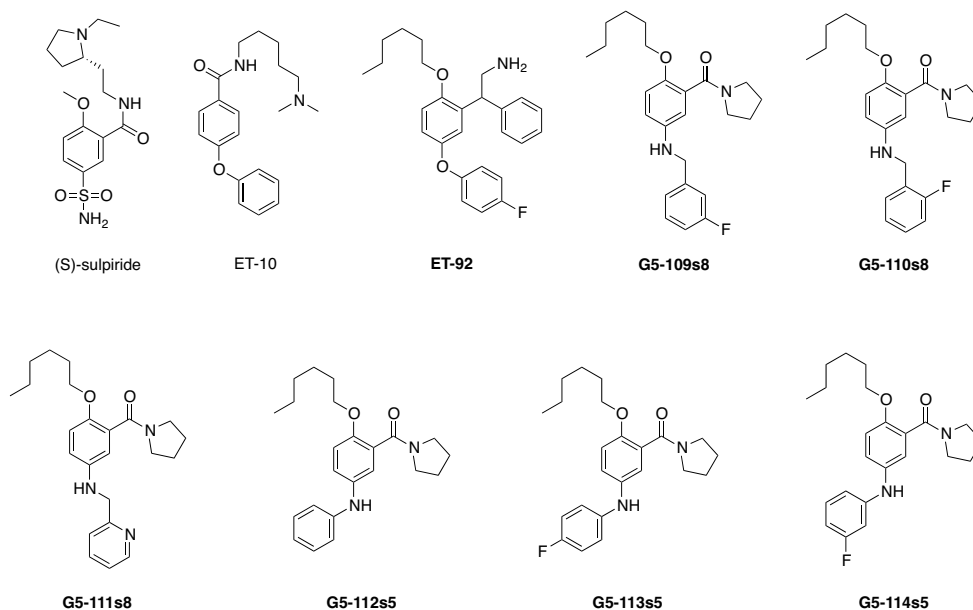
Upon acquiring 5-nitrosalicylaldehyde, **15**, the final synthesis, shown in **FIGURE 3.9**, was started. The reaction sequence worked well except for the last step. The nitrilation reaction might not have worked well due to the amine in **32a-c** forming a salt with cyanide or the amine forming a complex with indium. There was 1H -NMR evidence that some TMS ether of **32a-c** formed, indicating that extraneous water was probably not the cause of the poor yield. In the future, one might attempt to form the nitrile by reacting **32a-c** with either p-tosyl chloride or thionyl chloride followed by displacement with KCN. An attempt to methylate the amine had been made after the Chan-Lam reaction, **31**, but was unsuccessful. Not shown in **FIGURE 3.9**, was the unsuccessful attempt to reductively aminate **30** with various aldehydes, which was not considered significant since the equivalent products could be made in the future with the appropriate benzyl halides.

Final attempt to synthesize 6 - 14

At this point, it was decided to assay **G5-109s8** through **G5-114s5** in oocytes injected with hTAAR1 and hCFTR encoding RNA. Although these compounds were synthesized as intermediates to **6**, **7**, **8**, **12**, **13**, and **14**, they comprise interesting SAR in their own right. (S)-sulpiride (**FIGURE 3.10**, a D₂ and D₃ receptor antagonist approved in several countries outside the USA for use as an antipsychotic) was considered a template molecule during the original TAAR1 ligand development project,¹⁷ however the only compounds synthesized in that project that contained an amide group were analogs of ET-10, so **G5-109s8** through **G5-114s5** explore a gap in the TAAR1 SAR. Also, **G5-109s8** through **G5-114s5** contain similar peripheral SAR as **ET-92**: the consistent 2-hexyl ether; and the variable SAR aromatic group at the 5 position, as well as a rigid cyclic functional group one carbon off the 1 position of the core phenyl ring.

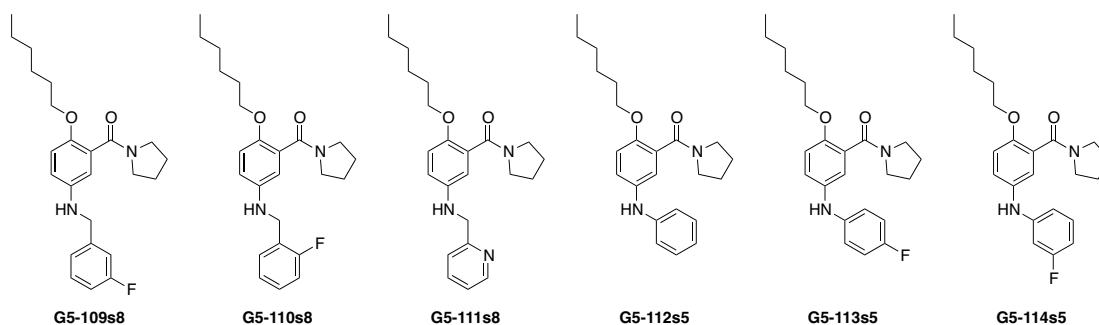
Final attempt to synthesize 6 - 14

FIGURE 3.10: SAR comparison between (S)-sulpiride (a D₂ and D₃ receptor antagonist), ET-10 (a TAAR1 agonist), **ET-92** and **G5-109s8** through **G5-114s5**. Although (S)-sulpiride was considered a template molecule during the original TAAR1 ligand development project,¹⁷ analogs of ET-10 were the only one made that contained amides. **G5-109s8** has the same 1, 2, 5 substitution pattern as (S)-sulpiride and **ET-92**. It also similar peripheral SAR as **ET-92**: the hexyl ether; fluorinated aromatic; and rigid third cyclic functional group, pyrrolidine instead of the phenyl ring of **ET-92**. Thus, even though **G5-109s8** was synthesized as an intermediate to **24**, it has SAR worth testing in its own right.



The compounds shown in **FIGURE 4.1** were evaluated for TAAR1 activity by monitoring the transmembrane conductance of *Xenopus Laevis* (frog) oocytes injected with hTAAR1 and hCFTR³⁵ encoding RNA or just hCFTR encoding RNA as the control via two electrode voltage clamp (TEVC). The oocytes were harvested and prepared by Dr. Yohei Norimatsu according to the procedure in Chapter 7.2. As stated in Chapter 1.1, a downstream effect of TAAR1 activation is increased production of cAMP, where as CFTR is activated by cAMP and upon activation increases the transmembrane conductance by allowing chloride ions to cross the cell's plasma membrane. Thus an oocyte expressing both TAAR1 and CFTR acts as a biological circuit for measuring the activity of TAAR1.

FIGURE 4.1: Compounds tested



These compounds could be evaluated by fluorescent cellular assays sensitive to cAMP levels using HEK cells transfected with mouse TAAR1 (mTAAR1). The

The experiments

quality of results from this type of cellular assay depend on the accuracy and consistency of one's pipetting, and the stability of the cell line. Other draw backs of this technique are that it only provides one type of data (cAMP concentrations) and the fact that the project is to treat human Meth addiction not mouse Meth addiction. The fluorescent assays have the advantage of being well suited for high-through-put screening, especially if one has access to robotic pipetting systems.

Although highly automated TEVC systems exist, including machines that inject oocytes, the system used for this work was manual with computerized data collection, please see Chapter 7.2.3 for more details. Also, the oocytes were manually injected, Chapter 7.2.2. The advantages of TEVC are that the oocytes are prepared weekly, eliminating potential cell-line stability problems though expression levels can still be an issue; both transmembrane conductance and potential can be monitored independent of what causes the changes. Finally, TEVC allows one to conduct many different variations of steady-state or time-dependent response experiments. Also, by monitoring transmembrane conductance and potential, TEVC allows one to detect off-target effects mechanistically unrelated to cAMP levels, a significant advantage over cAMP fluorescent assays, which only assay cAMP concentrations.

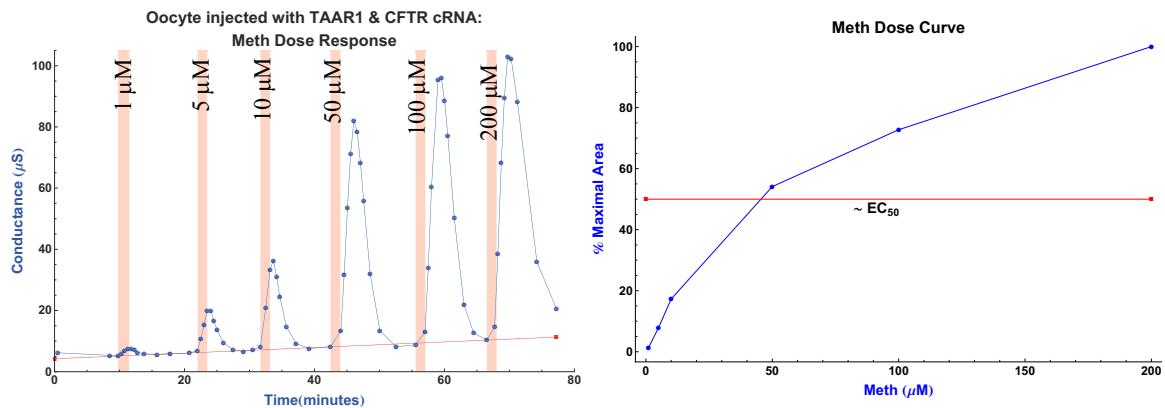
4.1 *The experiments*

All assays were preformed once as first pass activity screens.

The experiments

For all oocytes injected with both hTAAR1 and hCFTR encoding RNA, 10 times more hTAAR1 cRNA, by mass, was injected into the oocytes than hCFTR cRNA. This was a deliberate attempt to observe basal activity of TAAR1, as the unperturbed transmembrane conductance of the oocyte would increase as the expression of TAAR1 increased if TAAR1 had basal activity.

FIGURE 4.2: (A) Dose (concentration * 1.5 minutes * 4 ± 1 mL/minute) response testing of Meth in oocytes injected with hTAAR and hCFTR cRNA. The dose, indicated by the labeled red regions, was perfused for 1.5 minutes followed by perfusing with Frog Ringer's solution until the next dose ($n=1$). The red line is an approximate baseline. (B) Dose response curve for (A). The experiment was performed by Dr. Yohei Norimatsu, who provided the data to the author.



The Meth dose (concentration * 1.5 minutes * 4 ± 1 mL/minute) response experiment in **FIGURE 4.2** was performed by Dr. Yohei Norimatsu, using an oocyte injected with hTAAR1 and hCFTR encoding RNA, and using 1 μM, 5 μM, 10 μM, 50 μM, 100 μM and 200 μM Meth in FR pulses (red shaded regions) followed by washing with FR. Integration of the area under the curves show that the 10 μM Meth peak has an area of ~18% of the 200 μM Meth peak and the 100 μM Meth peak is about equal to the 200 μM Meth peak. The EC₅₀ for Meth in this experiment is ~50 μM Meth. The choice to go with Dr. Norimatsu's recommenda-

The experiments

tion of using 10 μ M Meth for the compound assays was made prior to analyzing this data.

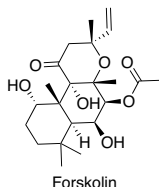
A 100 mM stock solution of each test compound, in DMSO, was made, and then used to make the test solutions.

With the exception of the first and last compound assay (**FIGURE 4.4** and **4.6(1)**, respectfully), all assays followed a head-to-head competition assay paradigm where a 1.5 minute pulse of 10 μ M Meth in Frog Ringer's solution (FR) was perfused over an oocyte, injected with hTAAR1 and hCFTR encoding RNA, followed by a wash-out period with FR. After the initial Meth pulse and wash-out, a series of 1.5 minute pulse of 10 μ M Meth and test compound (1 nM to 10 μ M) in FR was followed by FR wash-out cycles were preformed. At the end of each experiment, a 1.5 minute pulse of 10 μ M forskolin⁷⁹ and 10 μ M of the test compound in FR followed by a FR wash-out period. The wash-out periods lasted between 15 and 25 minutes (long enough for the conductance to stabilize). The application of forskolin and test compound at the end of the experiments served as a control to demonstrate that the test compound was not blocking either CFTR or adenylyl cyclase. Although some may criticize these experiments because they did not follow the common practice of pretreating with the test compound followed by agonist, the shape of the response curves provide kinetic information. These head-

The experiments

to-head competition experiments were designed by analogy to stopped-flow chemical kinetics experiments.⁸⁰

FIGURE 4.3: Structure of Forskolin.



In the first assay, **FIGURE 4.4**, an oocyte injected with hTAAR1 and hCFTR encoding RNA was used. The Meth pulses were 1.5 minutes long and at 100 μM concentration in FR. Each Meth pulse was followed by a 15 minute FR wash-out period. After the second pulse of Meth, 20 μM **G5-109s8** in FR was applied immediately followed by a Meth pulse. No forskolin control was done in this experiment.

For the last assay, **FIGURE 4.6(1)**, an oocyte injected with hCFTR encoding RNA was used. Between each pulse of testing solution, the oocyte was washed with FR. The 1.5 minute pulses used were: 5 μM forskolin, 10 μM **G5-109s8**, 10 μM Meth, and a combination of 5 μM forskolin and 10 μM **G5-109s8**. All of these solutions were made using FR.

The TEVC used in these experiments required that the siphon from the solution reservoirs to the recording chamber to be manually pinched closed before it was transferred between reservoirs. The manual transfer had the potential to create

Results

air bubbles in the siphon (uncertainty in the volume of solution applied) and timing uncertainty leading to errors estimated at $\pm 10\%$. Both of those issues could be reduced or eliminated through the use of an automated multi-valved perfusion system, such as the Octaflow IITM from ALA Scientific Instruments.⁸¹ Another source of error in the analysis of these experiments was the need to estimate the observed peaks' baselines before integrating their areas, which is a subjective process. The final concern with these assays was the variability of expression levels of hTAAR1 and hCFTR in the oocytes. The variability could be due to variance in cRNA injection volumes. Since these experiments were intended to be initial compound activity screens and concerns of measurement uncertainties, the results will be discussed qualitatively.

4.2 Results

4.2.1 Testing G5-109s8

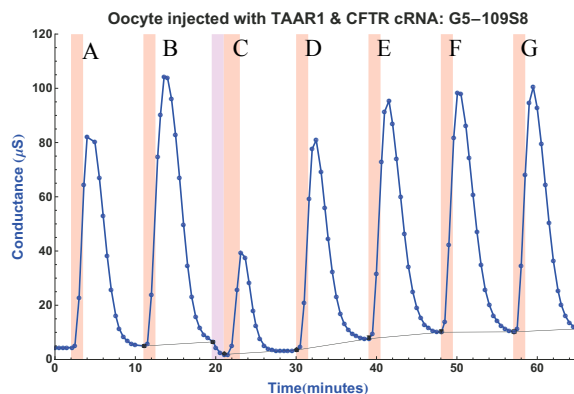
Of the compounds to be tested, **G5-109s8** was the purest by ¹H-NMR, which is why it was the most heavily tested in the limited time available. Also, being an oil, it dissolved into DMSO faster than the other test compounds, and thus it was the first tested.

In the first experiment, **FIGURE 4.4**, 20 μ M **G5-109s8** (green shaded region) caused the rapid drop in transmembrane conductance. The pulse of Meth (peak C) immediately following the pulse of **G5-109s8** is visibly smaller than all other

Results

peaks, including peak A, which was the result of a fumbled siphon transfer resulting in less than the full 1.5 minute pulse of Meth. Although peak F is smaller than E-G, the difference is not large enough for a single trial to be confident that it is not the result of some error. The small size of peak C is strong evidence that **G5-109s8** is blocking the TAAR1 pathway, if not TAAR1 itself. This experiment was originally envisioned as part of a series of experiments to determine the K_d and IC_{50} of each test compound, however upon realizing how time consuming that was going to be a head-to-head competition assay was designed for the rest of the testing.

FIGURE 4.4: Pretreatment with 20 μ M **G5-109s8** (magenta region) for 1.5 minutes followed by 1.5 minute pulses of 100 μ M Meth (red regions). Although the original intent was to measure the off-rate of **G5-109s8**, peak C is visibly smaller than all others indicating that **G5-109s8** inhibited Meth binding to TAAR1. The gray line segments are the approximate baseline. It is worth noting that **G5-109s8** caused a drop in the baseline. Peak A represents a fumbled siphon transfer, so a second Meth control stimulation, B, was preformed. This experiment was performed once.

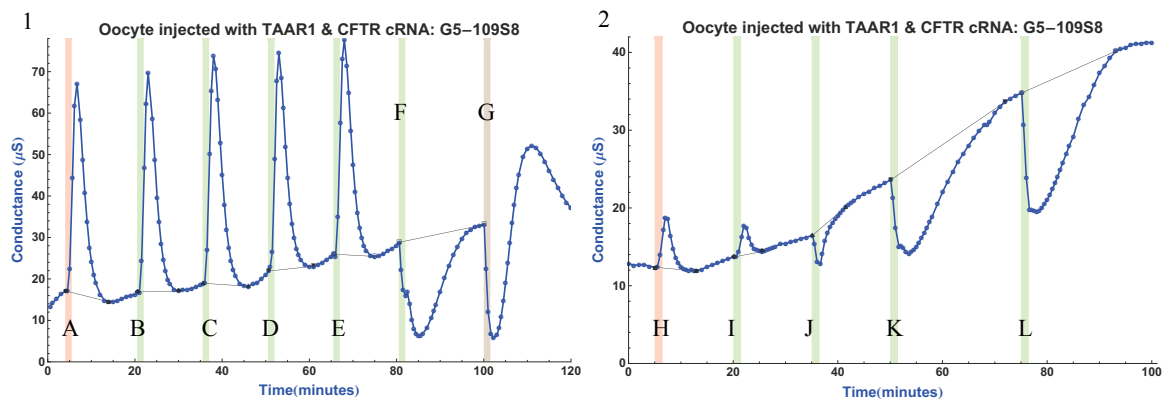


In **FIGURE 4.5**, one sees the dose response curves for the head-to-head competition assay between **G5-109s8** and 10 μ M Meth (each pulse, B-F and I-L, was a mixture of both compounds). In **FIGURE 4.5** the doses of **G5-109s8** were B: 1 nM, C: 10 nM, D: 100 nM, E: 1 μ M, F: 10 μ M, I: 1 μ M, J: 3 μ M, K: 5 μ M and L: 7 μ M. The weak response to Meth, peak H, in the experiment shown in **FIGURE 4.5(2)**

Results

indicates that the oocyte was not expressing a lot of TAAR1 but there was enough to establish that **G5-109s8** inhibits Meth stimulation of the TAAR1 pathway in a dose dependent manner. Since **G5-109s8** caused a maximal depression of transmembrane conductance ~4.5 minutes after the end of pulse F, and the transmembrane conductance took ~17 minutes to return to basal levels after pulse F but only ~10 minutes after pulse A (just Meth), then **G5-109s8** must have a slower off-rate than Meth.

FIGURE 4.5: Heads up competition between Meth and **G5-109s8** (n=1 for both assays). Pulses were 1.5 minutes in duration. Grey line segments are the approximate baseline. (1) A) 10 μ M Meth, B) 10 μ M Meth & 1 nM **G5-109s8**, C) 10 μ M Meth & 10 nM **G5-109s8**, D) 10 μ M Meth & 100 nM **G5-109s8**, E) 10 μ M Meth & 1 μ M **G5-109s8**, F) 10 μ M Meth & 10 μ M **G5-109s8**, G) 10 mM **G5-109s8** & 10 mM forskolin. (2) H) 10 mM Meth, I) 10 mM Meth & 1 mM **G5-109s8**, J) 10 mM Meth & 3 mM **G5-109s8**, K) 10 mM Meth & 5 mM **G5-109s8**, L) 10 mM Meth & 7 mM **G5-109s8**.



For **G5-109s8** to cause sub-basal transmembrane conductance as in **FIGURE 4.5(G, J, K, and L)** the TAAR1 pathway must have basal activity, and **G5-109s8** must be bound to nearly all free binding sites of whatever it is binding to in the pathway. If **G5-109s8** only prevented Meth from reaching TAAR1 (by inhibiting DAT, for example), then **G5-109s8** would have no effect on the TAAR1 pathway's

Results

basal activity. Therefore **G5-109s8** must be binding to either TAAR1, $G_{\alpha s}$, $G_{\beta/\gamma}$, adenylyl cyclase or CFTR.

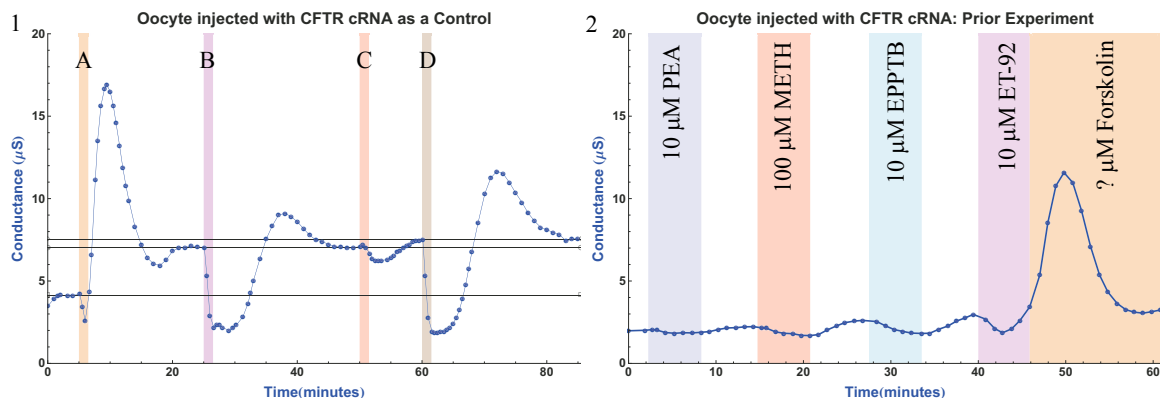
From the response to forskolin and **G5-109s8** (10 μ M each) in **FIGURE 4.5G**, it can be concluded that neither adenylyl cyclase nor CFTR were blocked by **G5-109s8**. Although there is initially a large drop in conductance for pulse G, the trough is considerably narrower than the one in F and appears to be the independent sum of fast TAAR1 inhibition by **G5-109s8** followed by a slower but strong activation of adenylyl cyclase by forskolin. This conclusion is consistent with Occam's razor (explanations with the fewest assumptions are preferred), since **G5-109s8** is an analog of a family known to inhibit TAAR1. If **G5-109s8** was inhibiting adenylyl cyclase or even one of the G-protein subunits instead of TAAR1, then **G5-109s8** would have unacceptable off-target effects as a treatment for addiction - both adenylyl cyclase and the G-proteins are involved in too many other regulatory pathways to be safely inhibited for this application. However, inhibiting adenylyl cyclase or the G-proteins might be acceptable for something like chemotherapy. Similarly, an argument that **G5-109s8** is inhibiting CFTR is an argument for an unacceptable off-target effect (in this case, one that would resemble cystic fibrosis). Before one spends more time developing analogs like **G5-109s8**, experiments that definitely rule out the inhibition of adenylyl cyclase, the G-proteins and CFTR by **G5-109s8** should be done. One possible experiment could be a TEVC experiment with a hTAAR1 and hCFTR expressing oocyte where one perfused 10 μ M

Results

G5-109s8 until the transmembrane conductance was constant, then perfused with a 1.5 minute pulse of 10 μ M **G5-109s8** and 10 μ M forskolin solution followed by washing with 10 μ M **G5-109s8**. If that experiment had a forskolin response equal to a TAAR1 and CFTR expressing oocyte assayed with a 1.5 minute pulse of 10 μ M forskolin, then neither adenylyl cyclase nor CFTR can be inhibited.

In **FIGURE 4.5**, one begins to see a general trend followed by the rest of the assays, namely the increase in transmembrane conductance as the experiments proceed. Not shown, but observed, was the time-dependent, and possibly dose-dependent, drop of the transmembrane potential, typically about 50% by the end of the experiment. Currently, it is not clear how much of the long-term changes in the conductance and potential are the result of the oocytes response to stress or some auxiliary effect of the compounds being tested.

FIGURE 4.6: (1) CFTR only control experiment to detect off-target effects. Pulses were 1.5 minutes in duration. A) 5 μ M forskolin, B) 10 μ M **G5-109s8**, C) 10 μ M Meth, D) 10 μ M **G5-109s8** & 5 μ M forskolin. Grey lines are visual aids. (2) CFTR only control experiment to detect off-target effects. This experiment was a prior result from the Grandy lab (n=1). Unfortunately, the notes about it how it was performed were a bit ambiguous, but it appears from them that the compounds were perfused over the oocyte for the entire period of the compound's shaded region. However, the response to ET-92 looks like the response one would expect from a minute or so application. The concentration of the forskolin used was not recorded.



Results

FIGURE 4.6(1) shows a control experiment done with an oocyte injected with hCFTR encoding RNA alone. Here 5 μ M forskolin was applied (A) then 10 μ M **G5-109s8** (B). Upon seeing the drop in conductance after applying **G5-109s8**, 10 μ M Meth was applied to demonstrate that a TAAR1/CFTR expressing oocyte had not been used by mistake. Finally a combination of **G5-109s8** and forskolin was applied (D) resulting in a response between A and B. Overall, this oocyte had an unexpectedly weak response to forskolin and Meth depressed the conductance (maximum change in conductance $\approx -1 \mu$ S), which may signal a hitherto unknown target of Meth. The response to pulse D is difficult to explain as it does not look like a simple sum of response to A and B. The response to D could indicate that **G5-109s8** weakly inhibits $G_{\alpha s}$ or adenylyl cyclase. It could also indicate that **G5-109s8** affects a pathway involving CFTR.

Although the off-target drop in transmembrane conductance caused by **G5-109s8** (**FIGURE 4.6(1)**) needs to be confirmed, it is very troubling, as it is the result of unknown electrophysiological changes. Those changes could be detrimental to many systems, such as: the central nervous system, cardiovascular system and mucus membranes. Thus this off-target effect could be evidence for major or even fatal toxic side-effects such as: psychosis, heart failure and ulcers. The criteria of the FDA, and organizations like it around the world, to approve a new pharmaceutical agent is that the agent must be both efficacious and reasonably safe. In order to prove that **G5-109s8** is reasonably safe and continue developing

Results

the thyronamine family of compounds as pharmaceuticals, the cause of this off-target effect needs to be identified, evaluated for toxicity, and then new compounds in the thyronamine family would need to be screened against it. The identification of the mechanism for the electrophysiological off-target effect of **G5-109s8** is a major biochemistry or chemical biology project and is beyond the scope of this drug discovery project.

With $n=1$ for the control assay, it is reasonable for one to ask whether or not the off-target effect is experimentally reproducible, and whether or not the off-target effect is experimentally valid (or real, if one prefers). Reproducibility is an issue of how frequent a result occurs, whereas validity is an issue of experimental accuracy. Strictly as a point of logic, a valid result maybe difficult to reproduce due to low frequency of occurrence. If the off-target effect seen in **FIGURE 4.6(1)** is sufficiently infrequent, then **G5-109s8** can be used in chemical biology studies of TAAR1 with few complications. However, for the purpose of drug discovery a compound's safety is a function of how frequently the compound causes adverse effects and their severity. Validating the off-target effect (again, off-target because TAAR1 was not present in the assay) could be complicated by the possibility that the oocytes have a heterogeneous (*i.e.*: poly-modal) response to **G5-109s8** due to genetic variability of the oocytes where some of the modes are rare.

Assuming the off-target effect in **FIGURE 4.6(1)** is valid, it can not account for the depressed conductance seen in **FIGURE 4.5F** unless the off-target effect is the

Results

result of inhibiting adenylyl cyclase, the G-proteins, or CFTR. If **G5-109s8**'s only mode of action was through this off-target effect, and was completely independent of the TAAR1 pathway, then one would add the 10 μ M Meth response curve in **FIGURE 4.5A** (maximum change in conductance $\approx 70 \mu$ S) to the off-target effect (maximum change in conductance $\approx -5 \mu$ S) in order to get the response to a combination of 10 μ M Meth and 10 μ M **G5-109s8**. When that is done, the result is not **FIGURE 4.5F**. Therefore **G5-109s8** must effect the TAAR1 pathway.

Upon seeing the **G5-109s8** off-target effect, evidence was sought for a similar effect from **ET-92**. **FIGURE 4.6(2)** shows an experiment, done previously by the Grandy lab, dosing an oocyte injected with hCFTR encoding RNA alone. In the experiment, 10 μ M PEA, 100 μ M Meth, 10 μ M EPPTB, 10 μ M **ET-92** and an unidentified concentration of forskolin were applied to the oocyte. In this experiment there appears to be a weak response to **ET-92**, maximum change in conductance $\approx -1 \mu$ S , and the possibility of very weak response to Meth and **EPPTB**. If this is not convincing, a comparison between the mouse *in vivo* data for **ET-92**/vehicle and **EPPTB**/vehicle trials, **FIGURE 1.6**, clearly shows a dose-dependent drop in locomotion for **ET-92**/vehicle, especially from 5 mg/kg to 10 mg/kg, but no such effect for the selective **EPPTB**. In addition to the **ET-92** effect on locomotion, when **ET-92** was first studied *in vivo* (mice) a 20 mg/kg dose of **ET-92** caused the mice to be hypothermic for 4 days after injection, thus requiring the mice to be euthanized.⁸² Taken together, the possible electrophysiological observation (**FIG-**

Results

URE 4.6(1)), thermoregulatory loss, and locomotion effects of the thyronamine family of analogs renders them a potentially risky class of compounds for further pharmaceutical development without first evaluating the actual risk posed by these effects.

4.2.2 Testing the other compounds

Since the original intent of making these compounds, **G5-110s8** through **G5-114s5**, was for use as intermediates in the synthesis of other compounds, not all of them were as pure as **G5-109s8**, but they were deemed sufficiently pure (>95% by $^1\text{H-NMR}$ excluding residual solvents) for a first pass activity screen. The testing for **G5-110s8** through **G5-114s5** followed the procedure outlined in Chapter 7.2. **FIGURE 4.8**, and **4.11** do not all show the full forskolin response range because it is off the scale in comparison to the other peaks. **FIGURE 4.10**, a repeat of an earlier experiment, omitted repeating the 10 μM forskolin and 10 μM **G5-113s5** pulse. None of the assayed compounds blocked forskolin activity.

All of the compounds show sub-basal transmembrane conductance for at least part of the response curve F. Only **G5-114s5** (**FIGURE 4.11**) showed any reliable effect at $\leq 1 \mu\text{M}$. **G5-111s8** (**FIGURE 4.8F**) shows complete sub-basal conductance. **G5-113s5** (**FIGURE 4.10F**) shows a peak followed by a sub-basal trough with the possibility of a brief sub-basal trough before the peak (this observed dip in conductance is small enough that it might be the result of an air bubble). **G5-110s8**, **G5-112s5** and **G5-114s5** (**FIGURE 4.7F**, **4.9F**, and **4.11E-F** respectfully)

Results

show a sub-basal trough then peak followed by another sub-basal trough. The only way to produce a trough-peak-trough pattern in this system is if TAAR1 has basal activity, the compounds bind to TAAR1, and the compounds bind the ligand-free active form of TAAR1 faster than they bind the ligand-free inactive form of TAAR1 (this claim will be fully justified by kinetic analysis in Chapter 5). The peaks are the result of Meth stimulation, since Meth does not stimulate the G-proteins, adenylyl cyclase nor CFTR (**FIGURE 4.6**). If **G5-110s8**, **G5-112s5** and **G5-114s5** inhibited the G-proteins, adenylyl cyclase or CFTR sufficiently to block the basal signal of TAAR1 then the TAAR1 Meth stimulated signal would also be blocked; therefore by elimination TAAR1 must be inhibited. Since all of the tested compounds are structurally very similar to **G5-110s8**, **G5-112s5** and **G5-114s5**, it is logical to conclude *by reason of similarity*⁸³ that their primary method of action is the inhibition of TAAR1 and not the inhibition of the G-proteins, adenylyl cyclase or CFTR. Since the compounds suppress TAAR1 activity to sub-basal levels, the compounds are inverse agonists.⁸⁴ Going back to **FIGURE 4.3**, one might estimate that TAAR1 basal activity is about 5% of its total possible activity (determined by dividing the basal level by the maximum Meth response). Using that estimation all the compounds are around IC₉₀ at 10 μ M, otherwise there would be enough TAAR1 available for Meth to bind for the total activity to remain above the baseline. More justification for this claim will be provided in the next chapter.

Results

FIGURE 4.7: Heads up competition between Meth and **G5-110s8** (n=1). Pulses were 1.5 minutes in duration. A) 10 μ M Meth, B) 10 μ M Meth & 1 nM **G5-110s8**, C) 10 μ M Meth & 10 nM **G5-110s8**, D) 10 μ M Meth & 100 nM **G5-110s8**, E) 10 μ M Meth & 1 μ M **G5-110s8**, F) 10 μ M Meth & 10 μ M **G5-110s8**, G) 10 μ M **G5-110s8** & 10 μ M forskolin. Grey line segments are the approximate baseline.

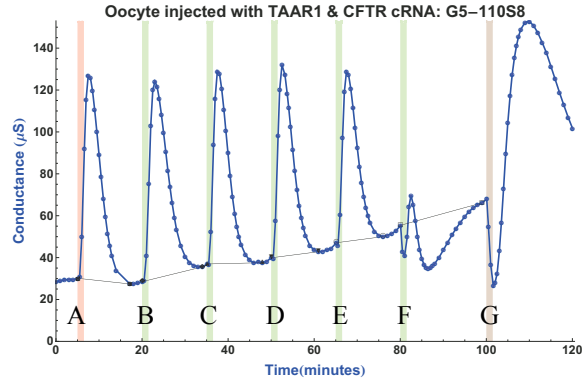
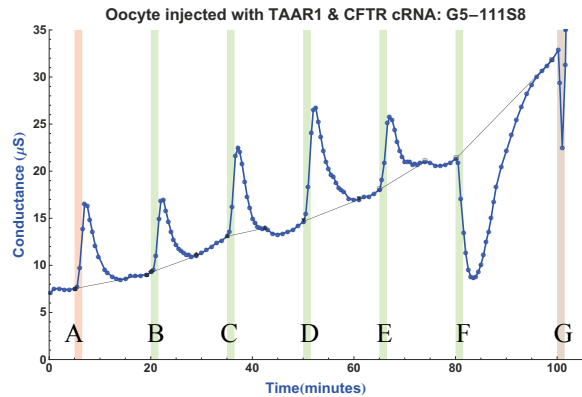


FIGURE 4.8: Heads up competition between Meth and **G5-111s8** (n=1). Pulses were 1.5 minutes in duration. A) 10 μ M Meth, B) 10 μ M Meth & 1 nM **G5-111s8**, C) 10 μ M Meth & 10 nM **G5-111s8**, D) 10 μ M Meth & 100 nM **G5-111s8**, E) 10 μ M Meth & 1 μ M **G5-111s8**, F) 10 μ M Meth & 10 μ M **G5-111s8**, G) 10 μ M **G5-111s8** & 10 μ M forskolin (off-scale). Grey line segments are the approximate baseline.



Results

FIGURE 4.9: Heads up competition between Meth and **G5-112s5** (n=1). Pulses were 1.5 minutes in duration. A) 10 μ M Meth, B) 10 μ M Meth & 1 nM **G5-112s5**, C) 10 μ M Meth & 10 nM **G5-112s5**, D) 10 μ M Meth & 100 nM **G5-112s5**, E) 10 μ M Meth & 1 μ M **G5-112s5**, F) 10 μ M Meth & 10 μ M **G5-112s5**, G) 10 μ M **G5-112s5** & 10 μ M forskolin. Grey line segments are the approximate baseline.

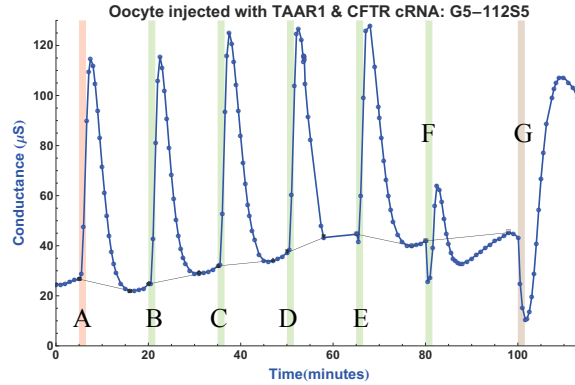
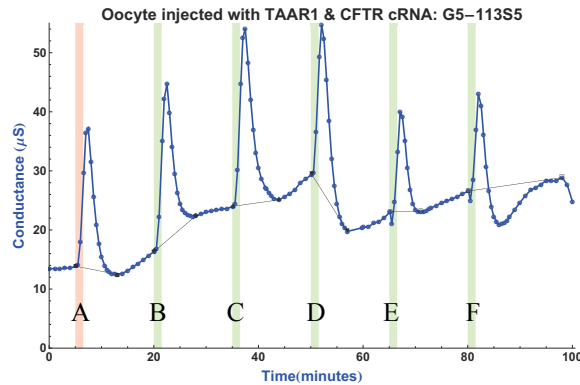
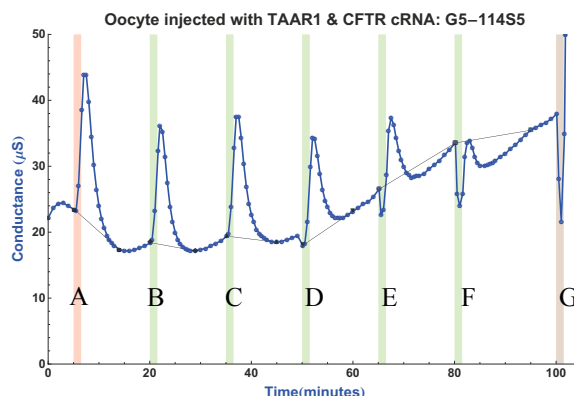


FIGURE 4.10: Heads up competition between Meth and **G5-113s5** (n=1). Pulses were 1.5 minutes in duration. A) 10 μ M Meth, B) 10 μ M Meth & 1 nM **G5-113s5**, C) 10 μ M Meth & 10 nM **G5-113s5**, D) 10 μ M Meth & 100 nM **G5-113s5**, E) 10 μ M Meth & 1 μ M **G5-113s5**, F) 10 μ M Meth & 10 μ M **G5-113s5**. Grey line segments are the approximate baseline.



Concluding remarks about the assays

FIGURE 4.11: Heads up competition between Meth and **G5-114s5** (n=1). Pulses were 1.5 minutes in duration. A) 10 μ M Meth, B) 10 μ M Meth & 1 nM **G5-114s5**, C) 10 μ M Meth & 10 nM **G5-114s5**, D) 10 μ M Meth & 100 nM **G5-114s5**, E) 10 μ M Meth & 1 μ M **G5-114s5**, F) 10 μ M Meth & 10 μ M **G5-114s5**, G) 10 μ M **G5-114s5** & 10 μ M forskolin (off-scale). Grey line segments are the approximate baseline.



4.3 Concluding remarks about the assays

Although one can draw conclusions from these assay results, it would be best to repeat the experiment at least 3 times with oocytes that express hTAAR1 and hCFTR more consistently than the ones used here. Doing so would both verify the results and allow quantification. Having to make decisions based on minimal, poor quality or incomplete data is not uncommon in industrial research, where the focus is on following up on promising leads and quickly moving away from unfavorable ones. That said, one tries to be as thorough as possible. The industrial research model is not perfect; false leads get followed and promising ones accidentally get discarded. Also, industrial research can seldom afford to treat every lead as thoroughly as is often done in academic research. In the end, industrial research must produce a marketable product. Although done in an academic setting, the assaying and subsequent analysis follow the industrial research model. At this time, the thy-

Concluding remarks about the assays

ronamine family of compounds appear to be high risk for further pharmaceutical development.

Starting from first principles,⁸⁵ a series of kinetic models were developed to explain the observed biological data in Chapter 4.

5.1 *Quick review of kinetics*

Unimolecular kinetics ($A \rightarrow B$, intramolecular conformation changes, disassociations, radioactive decay, etc.) are modeled by equations in the form of

$$\frac{d}{dt}[\chi] = k[\chi] \quad (\text{EQ 5.1})$$

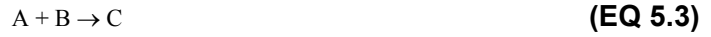
and bimolecular kinetics ($A + B \rightarrow C$, reactions between two chemicals, etc.) are modeled by equations in the form of

$$\frac{d}{dt}[\chi] = k[\chi][\Psi] \quad (\text{EQ 5.2})$$

In **EQ 5.1 - 5.2**, $[\chi]$ is the concentration or activity of χ (similarly for Ψ), and k is the rate constant (positive when creating a chemical species and negative when destroying a chemical species). To model more complex systems, one builds rate equations by adding terms for each reaction that occurs in the system. Each chemical species involved in the system requires its own rate equation. Also, mass balance equations and initial conditions are needed, both of which serve as constraints on the system. For example, **EQ 5.4 - 5.7** are the complete set of equations needed

TAAR1 Kinetics

to model a simple irreversible bimolecular reaction (**EQ 5.3**) with initial concentrations given by A_0 , B_0 , and C_0 .



$$[A] = A_0 - [C] \quad (\text{EQ 5.4})$$

$$[B] = B_0 - [C] \quad (\text{EQ 5.5})$$

$$C_0 = 0 \quad (\text{EQ 5.6})$$

$$-\frac{d}{dt}[A] = -\frac{d}{dt}[B] = \frac{d}{dt}[C] = k[A][B] = k[A_0 - C][B_0 - C] \quad (\text{EQ 5.7})$$

Since this example is a simple single step reaction, one only needs to solve for $[C]$ and then plug-in $[C]$ into **EQ 5.4 - 5.5** to get $[A]$, and $[B]$.

5.2 TAAR1 Kinetics

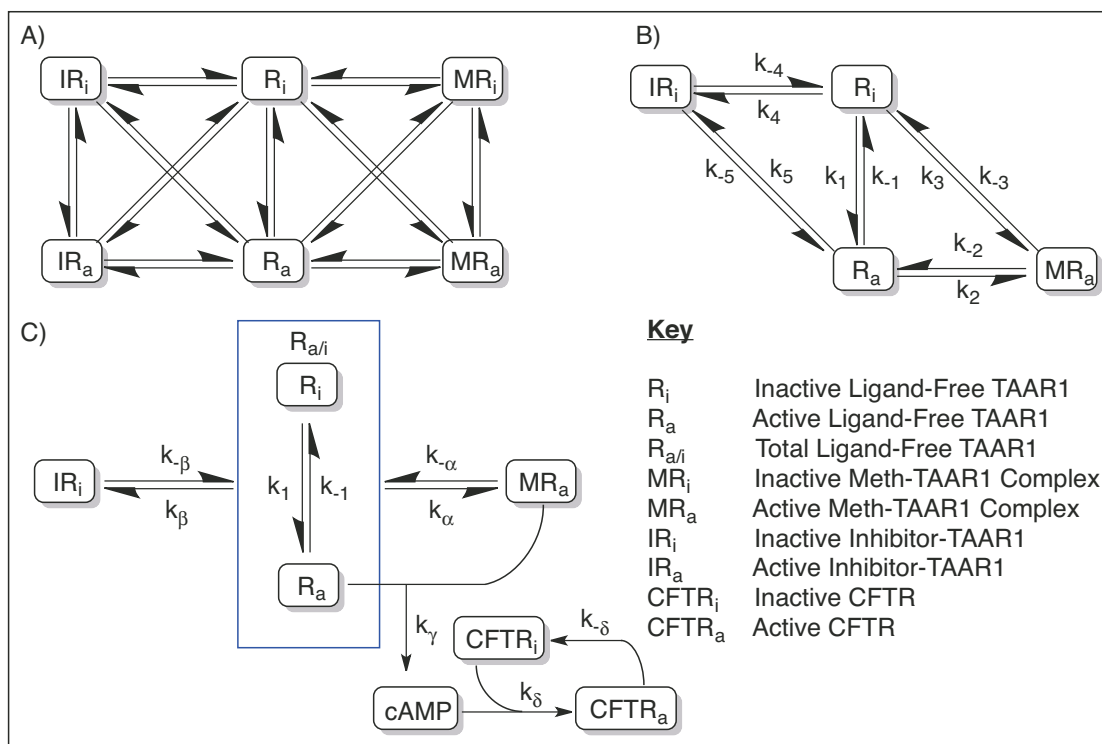
Receptors with basal activity, such as TAAR1, exist in an equilibrium between a ligand-free active form and a ligand-free inactive form. The interconversion between the two forms is a unimolecular process. Once ligands are introduced to the receptor, the ligands could potentially bind to either ligand-free form of the receptor creating either an active ligand-receptor complex or an inactive ligand-receptor complex. The ligand and the receptor bind in a bimolecular process. Interconversion between the active ligand-receptor complex and the inactive ligand-receptor complex is possible (a unimolecular process). Lastly, both forms of the ligand-receptor complex can disassociate in a unimolecular process.

TAAR1 Kinetics

FIGURE 5.1A shows all possible pathways for TAAR1 to interact with Meth (an agonist) and an inhibitor [as short-hand, inhibitor = inverse agonist]. Such a model has 22 rate constants, and with enough work one probably could make such a model fit most data. **FIGURE 5.1B** shows a simplified kinetic scheme where the inhibitor-TAAR1 complex can only exist in an inactive state (IR_i) and Meth only forms an active Meth-TAAR1 complex (MR_a). In **FIGURE 5.1C**, the equilibrium between the ligand-free inactive receptor (R_i) and its active form (R_a) is extremely fast compared to all other rate constants. Model C is also equivalent to Model B when $k_3 = k_2$, $k_{-3} = k_{-2}$, $k_4 = k_5$, $k_{-4} = k_{-5}$ and the equilibrium between R_i and R_a is very slow compared to all other processes in the model. Included in Model C is a gross simplification leading to the production of cAMP followed by the activation of CFTR. In all three models, arrows indicating either agonist/inhibitor binding or disassociation have been omitted for clarity.

TAAR1 Kinetics

FIGURE 5.1: Kinetic Schemes for TAAR1: A) All possible pathways for the basally active TAAR1 to interact with Methamphetamine (Meth) and an Inhibitor. The 22 rate constants have been omitted for clarity as have the arrows for binding and unbinding of both Meth and the Inhibitor. B) Simplified scheme assuming the Meth-TAAR1 complex is always active and the Inhibitor-TAAR1 complex is always inactive. C) When k_1 and k_{-1} are much faster than any of the other rate constants, then the total ligand-free TAAR1 can be treated as a single pool with active and inactive forms held at a fixed ratio. A step for the formation of cAMP and another for the CFTR cycle were added to model the oocyte data. Original artwork by Troy Wahl.



When one is trying to fit a reaction kinetic model to data, it is vital to have either accurate concentration or activity data for all chemical species in the model. Since neither the TAAR1 nor the CFTR expression levels were available nor were they consistent, qualitative agreement between the models and the data was sought. If the oocytes had had consistent hTAAR1 and hCFTR expression levels, then the total concentration of each could have been set to 1, allowing the rate constants to act as scaling factors, and the data fit. Once the data was fit, the rate constants could have been used to calculate IC_{50} values for each assayed compound.

Model B: Modeling TAAR1 equilibria

In all the simulations, the rate constants k_1 and k_{-1} were chosen to produce an $R_a:R_i$ ratio of 1:19 at equilibrium. Also, the concentrations for TAAR1, Meth and inhibitor used in the models are arbitrary. As long as the rate constant are scaled inversely, the concentrations can be changed without changing the results.

5.3 Model B: Modeling TAAR1 equilibria

Due to the kinetic complexity of basally active systems, the kinetic models were used to explore how TAAR1 might behave by varying rate constants and receptor concentration. The later variation could reveal some potential complications in interpreting *in vivo* overexpression studies. For the purpose of modeling the binding kinetics of Meth to TAAR1, *in vivo* experiments where Meth is administered to mice, the mice can be approximated as a closed system since the biological half-life (metabolism and excretion) of Meth is approximately 13 hours yet the effects of Meth on mice are noticeable within minutes. Chemical reactions in closed systems result in equilibria and are simpler to model than ones in open systems, so a TAAR1 equilibrium model will be the first one examined.

Using the kinetic scheme shown in **FIGURE 5.1B**, the mass balance equations for a closed system are given by **EQ 5.8 - 5.10**, and the rate equations are listed in **EQ 5.11 - 5.13**.

$$[R_T] = [R_i] + [R_a] + [MR_a] + [IR_i] \quad \text{(EQ 5.8)}$$

$$[M_T] = [M] + [MR_a] \quad \text{(EQ 5.9)}$$

Model B: Modeling TAAR1 equilibria

$$[Inh_T] = [Inh] + [IR_i] \quad (\text{EQ 5.10})$$

$$\begin{aligned} \frac{d}{dt}[R_a] &= k_1[R_i] - (k_{-1} + k_2[M] + k_5[Inh])[R_a] + k_{-2}[MR_a] + k_{-5}[IR_i] \\ &= k_1([R_T] - [R_a] - [MR_a] - [IR_i]) - (k_{-1} + k_2([M_T] - [MR_a]) + k_5([Inh_T] - [IR_i]))[R_a] \\ &\quad + k_{-2}[MR_a] + k_{-5}[IR_i] \end{aligned} \quad (\text{EQ 5.11})$$

$$\begin{aligned} \frac{d}{dt}[MR_a] &= (k_3[R_i] + k_2[R_a])[M] - (k_{-2} + k_{-3})[MR_a] \\ &= (k_3([R_T] - [R_a] - [MR_a] - [IR_i]) + k_2[R_a])([M_T] - [MR_a]) - (k_{-2} + k_{-3})[MR_a] \end{aligned} \quad (\text{EQ 5.12})$$

$$\begin{aligned} \frac{d}{dt}[IR_i] &= (k_4[R_i] + k_5[R_a])[Inh] - (k_{-4} + k_{-5})[IR_i] \\ &= (k_4([R_T] - [R_a] - [MR_a] - [IR_i]) + k_5[R_a])([Inh_T] - [IR_i]) - (k_{-4} + k_{-5})[IR_i] \end{aligned} \quad (\text{EQ 5.13})$$

The equations form a non-linear system of differential equations that does not have a closed form analytical solution, so numerical integration is needed to solve them. The equations were programed into Mathematica using the Runge-Kutta numerical method (this is not a built in function) with a step size, h , of 10^{-4} minutes. Runge-Kutta has an error in calculation on the order of h^5 , so at that step size the calculations had an error on the order of 10^{-20} , which was smaller then the precision of the calculations (~ 16 digits). Thus round-off error was the largest source of error in the simulations, being on the order of 10^{-16} times the number of steps need to get to a particular time point in the simulation. Since the simulations used a maximum of 200,000 steps, the maximum error in the simulations was on the order of 10^{-10} .

Model B: Modeling TAAR1 equilibria

FIGURE 5.2: The model is very sensitive to rate of equilibrium between R_i and R_a . The only difference between A and B are the values of k_1 and k_{-1} , with the values in A 5 times those in B. These simulations show the expected effects of Meth, an agonist, in that total TAAR1 activity increases above the basal activity. Due to the slow equilibrium between R_i and R_a , the disassociation of the Meth-TAAR1 complex leads to an increase in active ligand-free TAAR1 (R_a), which is the opposite of effect seen in A.

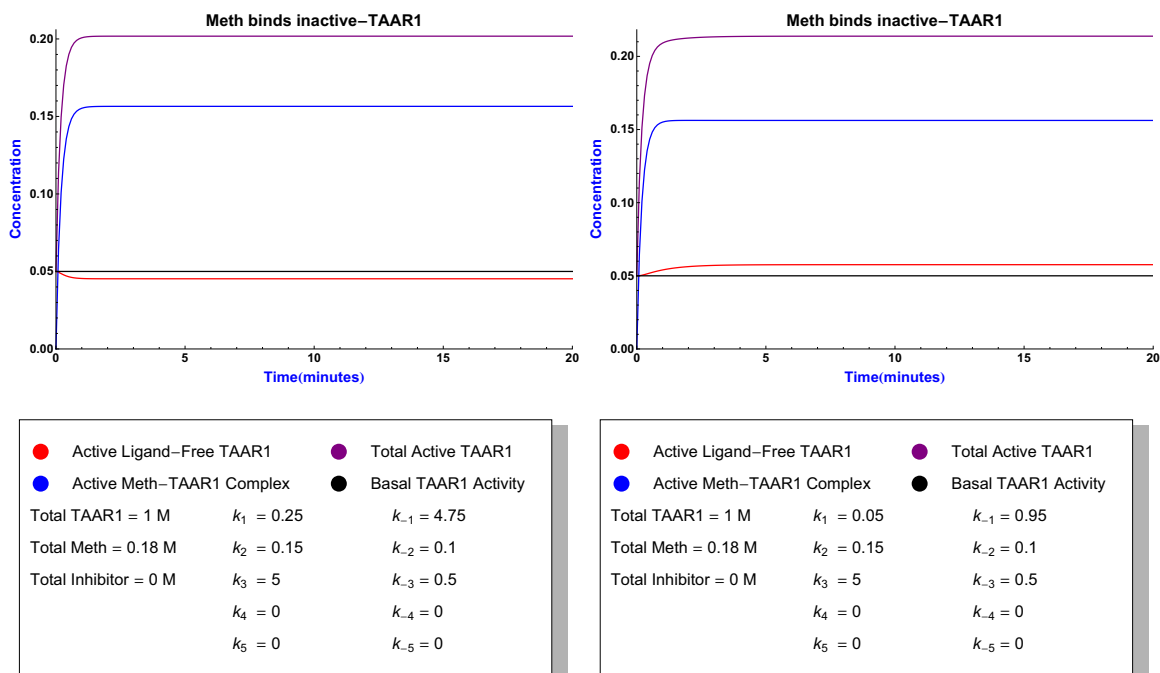


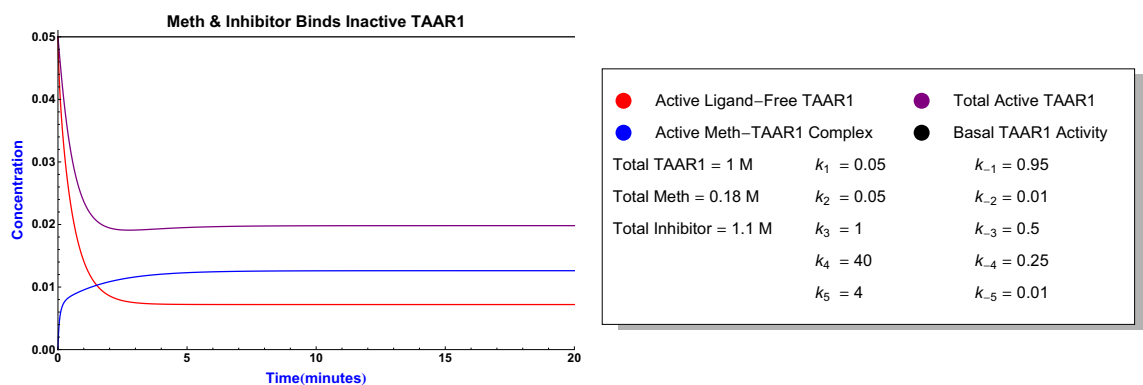
FIGURE 5.2 shows the simulation of Meth binding to TAAR1. The only difference between simulation A and B is that K_1 and K_{-1} are 5 times faster in **FIGURE 5.2A** than in **FIGURE 5.2B**. By slowing the rate at which R_a and R_i reach equilibrium, the concentrations active ligand-free TAAR1 (R_a), and total active TAAR1 increase compared to the faster equilibrium in **FIGURE 5.2A**. This is the result of the Meth-TAAR1 complex (MR_a) disassociation rate into R_a , determined by k_{-2} , causing R_a to accumulate faster than R_a can be converted into the inactive form of TAAR1, R_i .

Model B: Modeling TAAR1 equilibria

When Meth and Inhibitor are added to TAAR1, it is not difficult to suppress total TAAR1 activity below its basal level, **FIGURE 5.3**. In order to do so, k_4 and k_5 (the inhibitor rate binding constants) must be much faster than the rate binding constants for Meth, k_2 and k_3 . This should not be surprising as it only takes a little Meth activation to increase the total activity of TAAR1 above the basal level, but the inhibitor must block nearly all of TAAR1 to suppress the activity of the basal level. Also, in the case of a slow equilibrium between R_i and R_a , the inhibitor must rapidly bind R_a to produce a rapid drop in total activity below the basal level.

When the R_i and R_a equilibrium is fast, a drop in $[R_i]$ is quickly matched by a drop in $[R_a]$.

FIGURE 5.3: Simulation of competition between Meth and Inhibitor. It is fairly easy to suppress TAAR1 below its basal activity, but to do so the inhibitor must bind to both inactive TAAR1 (R_i) and active TAAR1 (R_a) much faster than Meth.



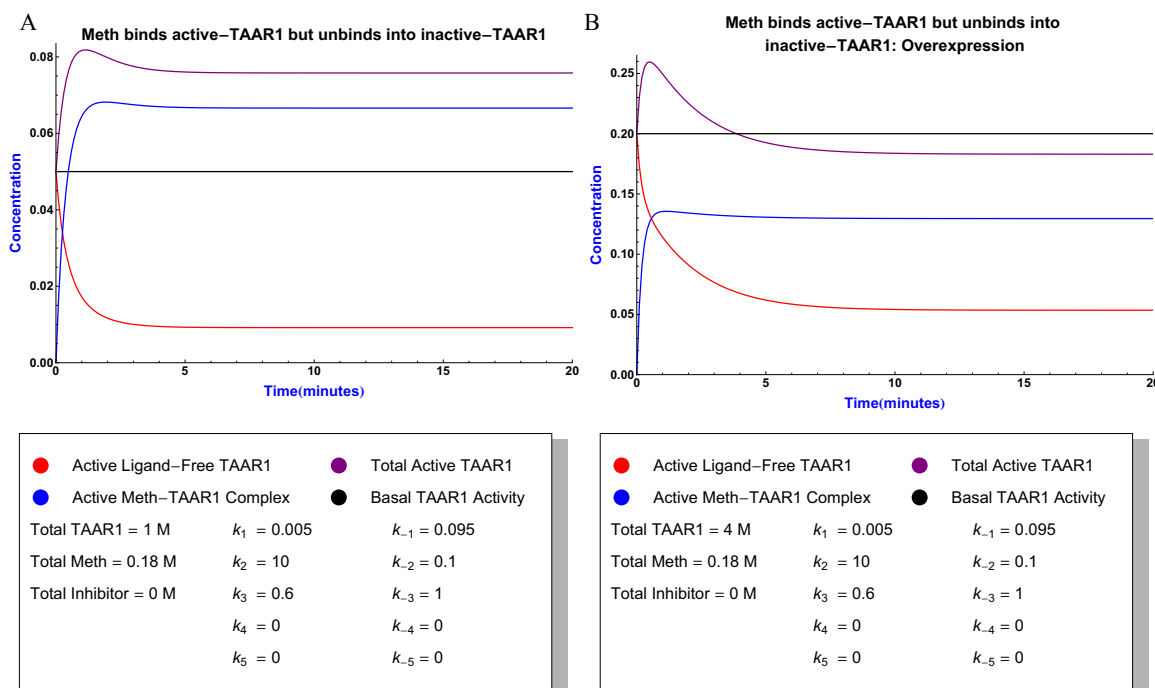
A counter-intuitive result is shown in **FIGURE 5.4B**, where an “overexpression” of TAAR1, simulated by the use of 4 M TAAR1 instead of the 1 M used in **FIGURE 5.4A**, results in Meth causing a drop in total activity. For the simulations

Model B: Modeling TAAR1 equilibria

in **FIGURE 5.4**, the rate constants have been set so that the fastest reactions proceeds from Meth binding the active form of TAAR1 (R_a), to the Meth-TAAR1 complex disassociating into the inactive form of TAAR1 (R_i), resulting in the accumulation of R_i due of the slow equilibrium between R_i and R_a . In the non-overexpression case, **FIGURE 5.4A**, despite the fact R_a is depleted, there is enough unbound Meth to create an equilibrium between Meth and MR_a that results in a net increase of TAAR1 activity. That is not the case with the TAAR1 overexpression, **FIGURE 5.4B**. In Revel's *in vivo* study of TAAR1 overexpressing mice,⁸⁶ conclusions are drawn based on the fact that Meth does not produce much stimulation in the overexpressing mice, however the result shown in **FIGURE 5.4B** requires extra caution when considering those conclusions.

Model C: Modeling the oocyte data

FIGURE 5.4: Receptor overexpression can lead to counter-intuitive results when the receptor has basal activity. The only difference between **A** and **B** is the concentration of TAAR1. In this example, the fastest path is Meth binding to active TAAR1 (R_a) to form the active Meth-TAAR1 complex (MR_a) which in turn releases Meth and inactive TAAR1 (R_i). (A) Although R_a is depleted, there is enough unbound Meth to create an equilibrium between Meth and MR_a that results in a net increase of TAAR1 activity. That is not the case with the TAAR1 overexpression, B.



5.4 Model C: Modeling the oocyte data

In order to model the oocyte data, one must address the fact that the experiments were not closed systems as the solutions with the test compounds flowed to the oocytes, where the oocytes respond to some of the molecules while the remainder flows past, never to interact with the oocyte again. Likewise, when the oocyte releases a molecule into the solution, that molecule is washed away. Model B could be used, but the mass balance equations for both Meth and the inhibitor would have to keep track of how many molecules of each compound flowed past the oocyte, and how much was bound to TAAR1, otherwise model would lack suf-

Model C: Modeling the oocyte data

efficient constraints to work properly. To do that, one would have to accurately know the quantities, in moles, of each chemical species present in the model, which was not the case. Fortunately, there is a work-around. While the test compounds are being applied, the incoming stream has a constant concentration and one can treat the oocyte as a point or infinitely thin membrane in the flow. This approximation allows one to disregard the molecules that either flowed past or were released by the oocyte. With this approximation, the mass balance equations are

$$1 = [R_{a/i}] + [MR_a] + [IR_i] \quad (\text{EQ 5.14})$$

$$[M] = \begin{cases} 0 & t < 0 \\ 1 & 0 \leq t < 1.5 \\ 0 & 1.5 \leq t \end{cases} \quad (\text{EQ 5.15})$$

$$[Inh] = \begin{cases} 0 & t < 0 \\ 1 & 0 \leq t < 1.5 \\ 0 & 1.5 \leq t \end{cases} \quad (\text{EQ 5.16})$$

Before the model can be constructed, the rate of equilibrium between R_i and R_a must be set either much faster or much slower (with $k_3 = k_2$, $k_{-3} = k_{-2}$, $k_4 = k_5$, and $k_{-4} = k_{-5}$) than any other process in the model. Doing this converts Model B into the TAAR1 portion of Model C. A very rapid equilibrium between R_i and R_a means that no matter what the other rate constants are, the ratio between $[R_i]$ and $[R_a]$ will be constant. With the other extreme, the system decouples into two linearly independent systems. With the equilibrium between R_i and R_a set to be very fast, one only need keep track of the total amount of ligand-free TAAR1, $R_{a/i}$,

Model C: Modeling the oocyte data

during the simulation then, afterwards, partition out R_i and R_a according to **EQ**

5.17 - 5.18.

$$[R_a] = \frac{k_1[R_{a/i}]}{k_1 + k_{-1}} \quad (\text{EQ 5.17})$$

$$[R_i] = \frac{k_{-1}[R_{a/i}]}{k_1 + k_{-1}} \quad (\text{EQ 5.18})$$

$$[MR_a]_{t=0} = [IR_i]_{t=0} = 0 \quad (\text{EQ 5.19})$$

$$[cAMP]_{t=0} = \frac{k_1 k_\gamma k_{-\delta}}{k_{-\delta}(k_1 + k_{-1}) - k_1 k_\gamma k_{-\delta}} \quad (\text{EQ 5.20})$$

$$[CFTR]_{t=0} = \frac{k_1 k_\gamma k_{-\delta}}{k_{-\delta}(k_1 + k_{-1})} \quad (\text{EQ 5.21})$$

In order to couple TAAR1 to CFTR, the model must produce cAMP which in turn activates CFTR. Model C (**FIGURE 5.1C**) treats cAMP production as an unimolecular process dependent on the concentration of all active TAAR1 species. In reality, the production of cAMP is the result of a sequence of reactions; however, for a crude qualitative model, the treatment is sufficient. Although it might be tempting to eliminate cAMP from the model by having active TAAR1 directly drive CFTR, doing so would be a mistake as cAMP serves as a capacitor, both creating a time delay and smoothing out sharp transitions. Putting this all together with the initial conditions, **EQ 5.19 - 5.21**, the rate equations for Model C are

$$\begin{aligned} \frac{d}{dt}[MR_a] &= k_\alpha[M][R_{a/i}] - k_{-\alpha}[MR_a] \\ &= k_\alpha[M](1 - [MR_a] - [IR_i]) - k_{-\alpha}[MR_a] \end{aligned} \quad (\text{EQ 5.22})$$

$$\begin{aligned} \frac{d}{dt}[IR_i] &= k_\beta[Inh][R_{a/i}] - k_{-\beta}[IR_i] \\ &= k_\beta[Inh](1 - [MR_a] - [IR_i]) - k_{-\beta}[IR_i] \end{aligned} \quad (\text{EQ 5.23})$$

Model C: Modeling the oocyte data

$$\begin{aligned}\frac{d}{dt}[cAMP] &= k_{\gamma}([MR_a] + [R_a]) - k_{\delta}[cAMP][CFTR_i] \\ &= k_{\gamma}\left([MR_a] + \frac{k_1[R_{a/i}]}{k_1 + k_{-1}}\right) - k_{\delta}[cAMP](1 - [CFTR_a]) \\ &= k_{\gamma}\left([MR_a] + \frac{k_1(1 - [MR_a] - [IR_i])}{k_1 + k_{-1}}\right) - k_{\delta}[cAMP](1 - [CFTR_a]) \\ &= k_{\gamma}(k_{-1}[MR_a] + k_1(1 - [IR_i])) - k_{\delta}[cAMP](1 - [CFTR_a])\end{aligned}\tag{EQ 5.24}$$

$$\begin{aligned}\frac{d}{dt}[CFTR_a] &= k_{\delta}[cAMP][CFTR_i] - k_{-\delta}[CFTR_a] \\ &= k_{\delta}[cAMP](1 - [CFTR_a]) - k_{-\delta}[CFTR_a]\end{aligned}\tag{EQ 5.25}$$

Instead of using concentrations in this model, the relative activities of the compounds will be used thus forcing the rate constants to contain information about the maximum concentration of the compounds. A convenient feature of Model C is that the rate equations for the TAAR1 portion, **EQ 5.22 - 5.23**, have exact solutions, though they are very long. In order to calculate the values for cAMP and CFTR, **EQ 5.24 - 5.25**, one takes the exact solutions for MR_a and IR_i from **EQ 5.22 - 5.23** as input for a Runge-Kutta numerical calculation with step size, h , equal to 10^{-4} minutes.

After setting the basal activity, $R_a = 0.05$, k_{α} and $k_{-\alpha}$ were adjusted until Meth produced a maximum total TAAR activity peak intensity of 0.2 and a profile similar to the oocytes response to $10 \mu\text{M}$ Meth, **FIGURE 5.5A**. Once these values for k_{α} and $k_{-\alpha}$ were found they were used for all the remaining Model C simulations. An interesting result is that in order to get the peak profile to match that in the biological data, $k_{\alpha} < k_{-\alpha}$ and $k_{\alpha} \approx k_{-\alpha}$ must be true. This makes sense from a biologi-

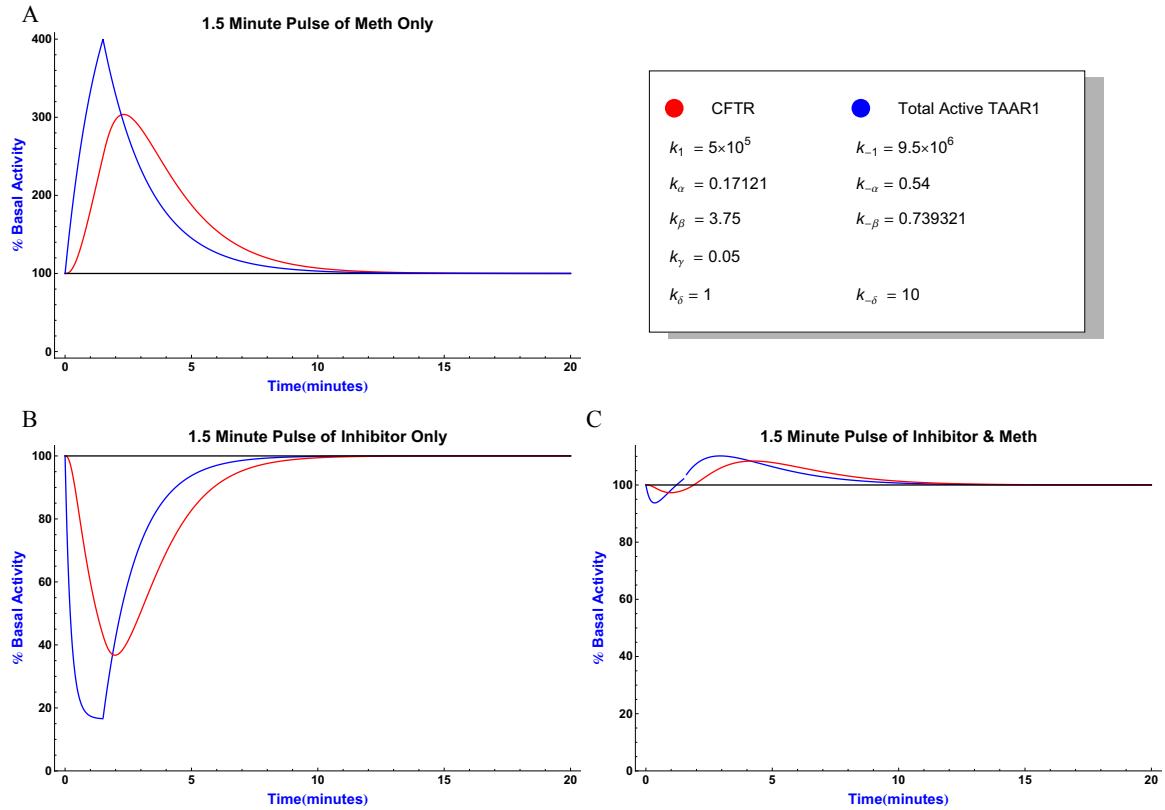
Model C: Modeling the oocyte data

cal perspective as receptors controlling neural activity must respond quickly to signals then reset, ready for the next signal.

Next came adjusting the values for k_β and $k_{-\beta}$. In **FIGURE 5.5B - C**, k_β was chosen to give strong TAAR1 inhibition, $k_\beta/k_\alpha = 21.9$, and $k_{-\beta}$ chosen to producing a rapid disassociation of the inhibitor, $k_{-\beta}/k_{-\alpha} = 1.37$. The k_β/k_α and $k_{-\beta}/k_{-\alpha}$ ratios determine the shape of the response curves when both Meth and inhibitor are applied. The ratios in **FIGURE 5.5C** yield weak initial sub-basal response followed by a weak stimulation. Essentially nearly all TAAR1 was inhibited but due to the inhibitor's fast off-rate enough Meth-TAAR1 complex remained to give some stimulatory effect before it too disassociated. If one were to drop k_β/k_α much lower than ~ 20 while holding $k_{-\beta}/k_{-\alpha}$ constant, one would only see a stimulatory response (a peak).

Model C: Modeling the oocyte data

FIGURE 5.5: Oocyte response to various stimuli: A) Meth only, B) Inhibitor only with a fast off-rate, $k_{-\beta}$, C) a combination of both Meth and Inhibitor. All the response curves been have normalized to their respective basal activities. The gap seen in C for the Total Active TAAR1 is a graphing artifact.



In moving to **FIGURE 5.6**, the only change made was to slow the inhibitor off-rate ($k_{\beta}/k_{\alpha} = 21.9$). With $k_{\beta}/k_{\alpha} = 0.60$, the inhibitor completely suppressed Meth stimulation. At this ratio, the response curve recovers to the basal level at about the same rate as seen in the biological data when the Meth response is completely suppressed. Increasing $k_{\beta}/k_{\alpha} = 29.2$, **FIGURE 5.7**, just deepens the trough. However, decreasing $k_{\beta}/k_{\alpha} = 11.68$, **FIGURE 5.8**, results in an initial Meth stimulation followed by a shallow sub-basal trough; not enough TAAR1 was inhibited. If k_{β}/k_{α} was reduced below ~ 10 , then the sub-basal trough disappeared.

Model C: Modeling the oocyte data

In the biological data there was little evidence that the 1 μ M test compounds inhibited 10 μ M Meth stimulation of TAAR1 and this model starts to reveal the reason. Since

$$\frac{k_{\beta}[Inh]}{k_{\alpha}[Meth]} \approx 10 \quad (\text{EQ 5.26})$$

appears to be the lower limit at which a trough forms, except for possibly **G5-114s5**, the upper limit on $k_{\beta}/k_{\alpha} < 100$ or the 1 μ M test compounds would produced a trough. Furthermore, limiting the estimate of $k_{\beta}/k_{\alpha} < 30$ is reasonable or the 1 μ M test compounds would produced obvious inhibition of the Meth stimulated peak. Since all 10 μ M test compounds produced a sub-basal trough, a estimate on the lower limit of $k_{\beta}/k_{\alpha} > 15$ is also reasonable.

Model C: Modeling the oocyte data

FIGURE 5.6: Slowing the inhibitor off-rate results in a total sub-basal response when both Meth and inhibitor are applied.

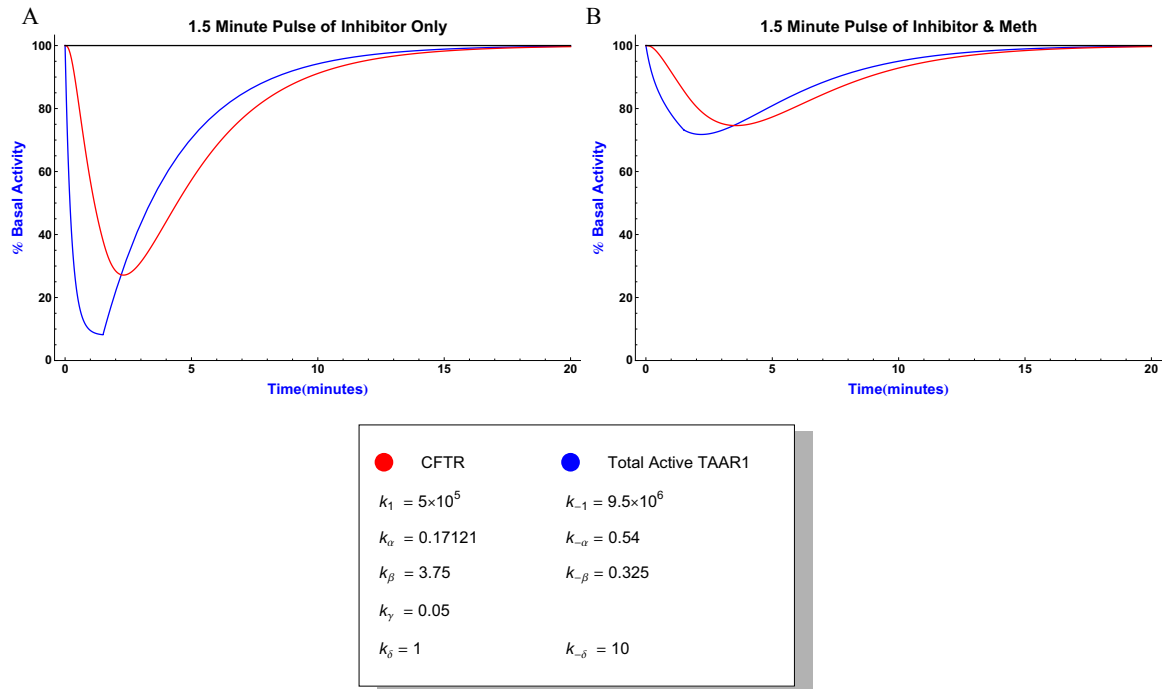
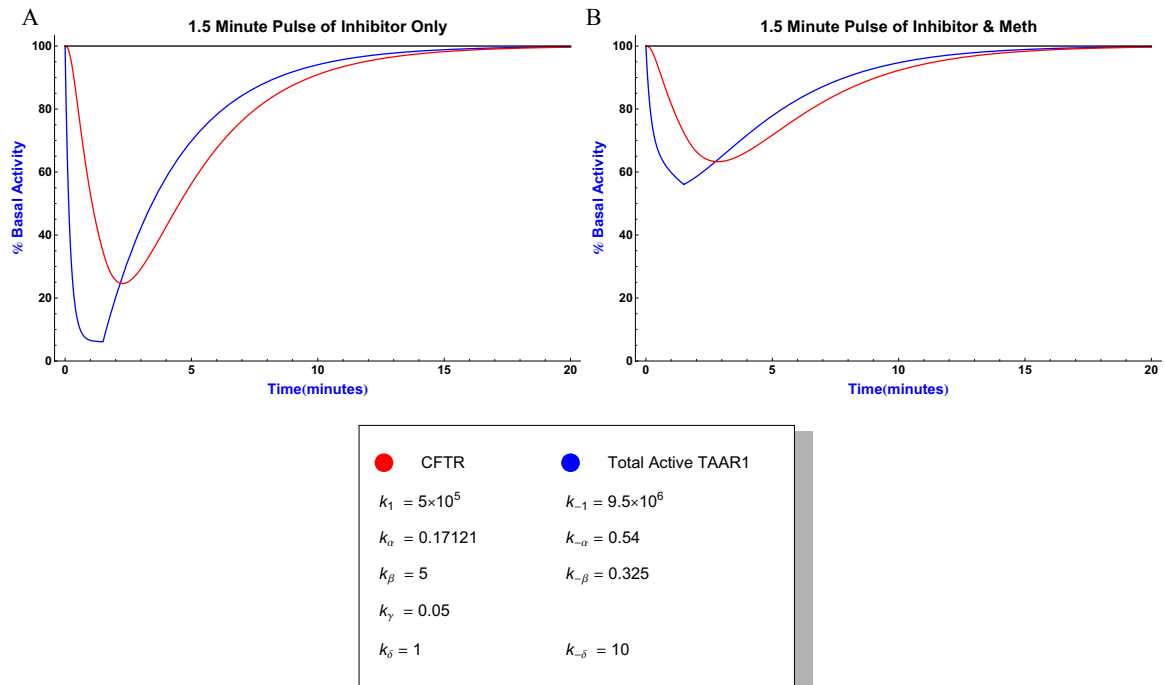
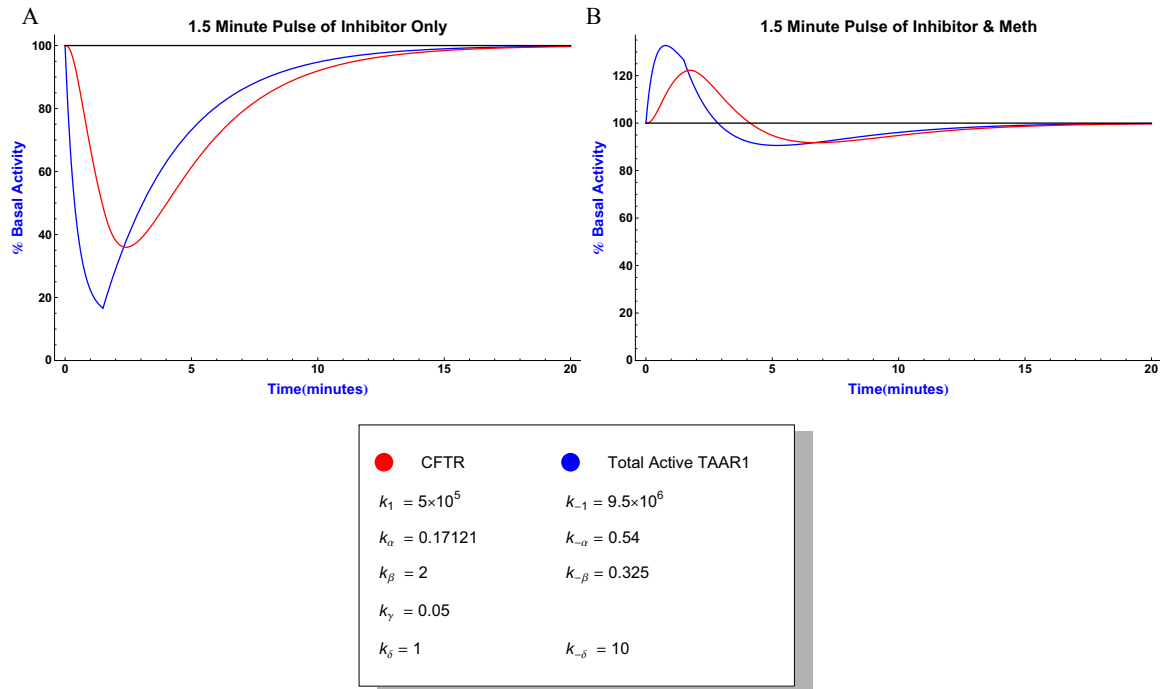


FIGURE 5.7: Increasing the inhibitor on-rate results just deepens the trough when both Meth and inhibitor are applied.



Stop Flow Model; a hybrid approach

FIGURE 5.8: Decreasing the inhibitor on-rate too much prevents the complete inhibition of Meth stimulation when both Meth and inhibitor are applied.



5.5 Stop Flow Model; a hybrid approach

The only response curve profile that proved elusive using Model C was the trough-peak-trough pattern. Considering how basic Model C was, it is not surprising that Model C can not produce the full range of data observed. After pondering the situation for awhile, it was realized that a hybrid model combining the TAAR1 kinetics of Model B, **EQ 5.8 - 5.13**, and cAMP/CFTR kinetics of Model C, **EQ 5.24 - 5.25**, would work to produce this last profile, if the oocyte was immersed in a closed system for the duration of the compound application and then washed for the remaining duration of the simulation. This is not an accurate model for the experiments performed, but by having a more limited supply of Meth and inhibitor than the actual experiments, it serves as a conservative model. The closed system

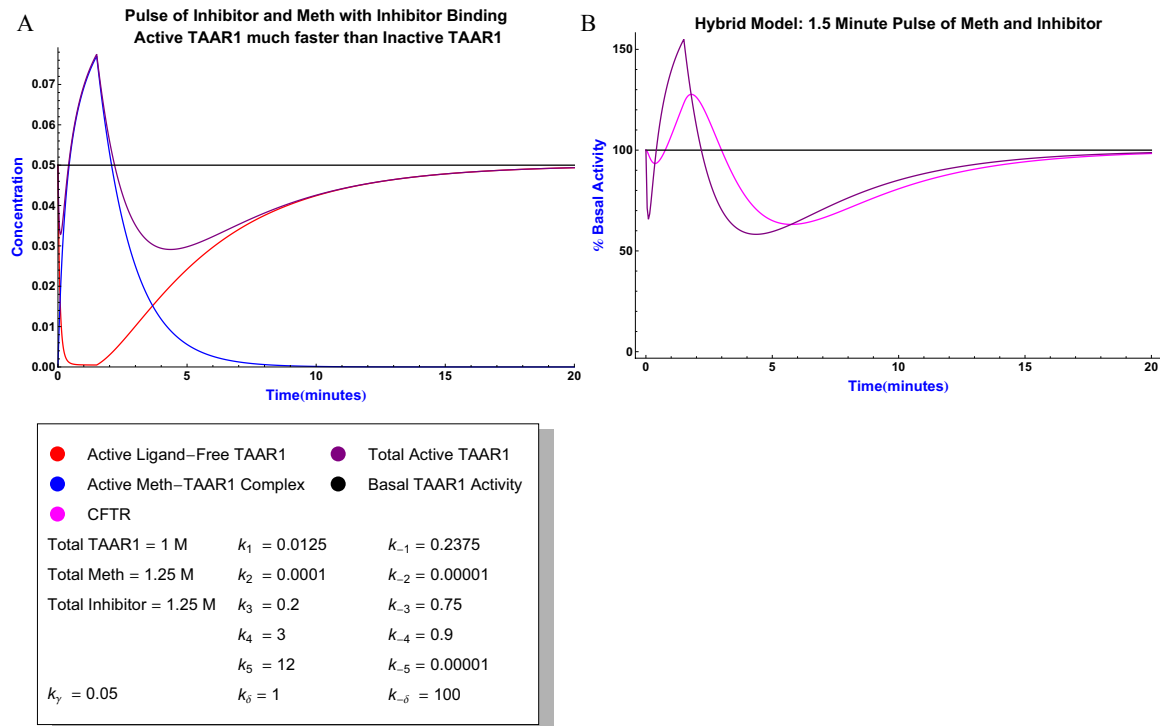
Stop Flow Model; a hybrid approach

makes the equilibrium equations valid. Once washing begins the Meth and Inhibitor concentrations are set to zero, and at that point the TAAR1 kinetics have an exact solution.

In order to produce the trough-peak-trough pattern seen in the response curves of **G5-110s8**, **G5-112s5** and **G5-114s5**, the inhibitor must rapidly bind to R_a , $k_5/k_3 > \sim 60$, with a slower binding to R_i , $k_4/k_3 \approx 15$. If k_4/k_3 is much above 15, the Meth response will be completely inhibited. The other requirement for this response profile is that the equilibrium between R_i and R_a must be slow, $k_1/k_3 < \sim 0.06$. The first trough in **FIGURE 5.9B** can be deepened by either increasing k_5/k_3 (not vary effective) or increasing k_4/k_3 , which also reduces the size of the peak.

Concluding remarks

FIGURE 5.9: By combining the TAAR1 components from Model B with the cAMP/CFTR components from Model C and using a stop-flow paradigm it is possible to produce the trough-peak-trough response profile seen from **G5-110s8**, **G5-112s5** and **G5-114s5**.



5.6 Concluding remarks

By modeling TAAR1 as a basally active receptor it was possible to qualitatively reproduce all the oocyte response curve profiles produced by the inhibitors tested. If TAAR1 was not basally active, it would not have been possible for an inhibitor to sub-basally suppress activity. Since a trough-peak-trough profile was observed with some of the tested inhibitors, the hybrid model suggests that the conversion rate of inactive to active TAAR1 is less than 6% of the binding rate of Meth to inactive-TAAR1. The models also suggest that the tested inhibitors are binding inactive TAAR1 at rates between 10 and 100 times faster than Meth binds.

Concluding remarks

The models do not suggest upper limits on the inhibitor binding rate to active TAAR1.

It is possible to fit the oocyte data with these models, but would require a special non-linear regression program to be written. Writing such a program can be done but it would not be a trivial task. Also, the resulting program would be slow. The simulations presented here took up to 20 minutes to run, although with optimization the code could run much faster. To find the best fit with a non-linear regression, one might have to run up to a thousand simulations. So even at 1.5 minutes per simulation, it could take a day to fit this type of data. A different experimental design, perhaps a steady-state one, could produce data that was easier to fit and use commercial software to do so.

As more research is done on TAAR1, it is becoming increasingly clear that it is an important player in many neurological disorders, including addiction. The approval of any pharmaceutical targeting TAAR1 is years away, with the closest candidates (from Hoffmann-LaRoche) just entering phase 1 clinical trials. Since TAAR1 is activated by Meth and inhibiting it blocks Meth signaling, there is reason to hope that a pharmaceutical will be developed to help in the treatment of Meth addiction.

During an assay of **G5-109s8** with an oocyte injected only with CFTR encoding RNA, **G5-109s8** caused a drop in transmembrane conductance. Since TAAR1 was not present in the oocyte (10 μ M Meth produced an $\sim 1\mu$ S drop in transmembrane conductance during this assay instead of the normal increase in conductance when TAAR1 is present), **G5-109s8** produced an electrophysiological off-target effect. In order to further develop the thyronamine family of analogs the cause of the electrophysiological off-target effect observed in the oocyte, if confirmed by replicate experiments, will have to be identified. This off-target effect is particularly troubling as it may indicate potential adverse central nervous system, cardiovascular or mucus membrane (ulcers, diarrhea, cystic fibrosis, etc.) events *in vivo*. At a minimum, the identification project will require using **G5-109s8** in a selectiv-

ity and toxicity screen against ion channels, neurotransmitter receptors and transporters, hERG, and the superfamily of cytochrome P450 (CYP P450). A good list to start from would be the CEREP panel used by Revel, *et al.*, consisting of 149 target proteins, transporters, ion channels, and receptors.⁹ The afore mentioned selectivity and toxicology screen can serve as a further test for any potential off-target effects. Furthermore, as part of due diligence in a medicinal chemistry project, a screen needs to be done.

Since the ultimate goal is to develop a TAAR1 ligand for the treatment of Meth addiction and not to develop a member of the thyronamine family into such a pharmaceutical, one could start a new hit generation program under the assumption that a random hit will have a different selectivity profile. As was done here, a TEVC oocyte control experiment can be used to detect electrophysiological off-target effects associated with the new TAAR1 hits. Under this approach, one would keep developing new hits until one was found that did not have electrophysiological off-target effects. Another option is to bust Hoffmann-LaRoche's TAAR1 patents (*i.e.*: develop analogs of their compounds that exploit loopholes in their patents).

Although the oocyte assays were performed only once as first pass activity screens, more evidence was found that TAAR1 has basal activity (constitutively active, for those who prefer that term) and 6 new TAAR1 inhibitors (inverse agonists) were developed. Also, although **32a-c** (**FIGURE 6.9**) would have to be re-

synthesized, they would also be interesting compounds to assay as they would explore the SAR necessity of the terminal amine found in **ET-92**. By testing the compounds in oocytes injected with hTAAR1 and hCFTR encoding RNA and qualitatively comparing the response curves to the results of kinetic simulations based on three models, estimates of several kinetic parameters were found relative to the binding rate of Meth to inactive TAAR1. By approximating the basal activity of TAAR1 to be 5% of the total ligand-free TAAR1, the conversion rate of inactive TAAR1 to active TAAR1 is less than 6% of the binding rate of Meth to inactive TAAR1. It is also estimated that the inhibitors bind to inactive TAAR1 between 10 and 100 times faster than Meth. Based on this work there is no upper rate limit for the inhibitors binding to active TAAR1.



7.1 Synthetic Methods

7.1.1 Equipment and Chemicals

NMR spectroscopy was performed on either a Bruker Avance II+ 400 MHz NMR Spectrometer or a Bruker Avance III 600 MHz NMR Spectrometer, both equipped with Bruker 5mm BBO probes, running Topspin software.

HPLC performed on Agilent (Varian) prep HPLC with 25 mL pumpheads, running Galaxy Star software. Flash chromatography used a Teledyne Isco Combi-Flash Rf-200 psi, model 68-5230-008.

Chemicals were bought from Sigma-Aldrich, TCI America, Fisher Scientific or EMD and used as is.

7.1.2 Compounds

IUPAC compound names were generated by ChemDraw Ultra 11.0.

GX-YsZ refers to laboratory notebook, first page number of the procedure and step number of the final product. The **G** is shorthand Grandy, **X** is 1-5, **Y** is 001-150 and **Z** is 1-50. For example, G4-120s5 is the 5th step of the procedure beginning on page 120 in the laboratory notebook Grandy4.

Synthetic Methods

7.1.2.1 5-bromo-2-(hexyloxy)benzaldehyde: G4-12s16

5-bromo-2-hydroxybenzaldehyde (26.69 g, 132.77 mmol), K_2CO_3 (20.179 g, 146 mmol) and anhydrous dimethylformamide (200 mL) were combined in a round bottom flask. While stirring, 1-bromohexane (24.108 g, 20.5 mL, 146 mmol) was added, then the reaction was stirred for 18 hours. The reaction was worked-up by adding water (500 mL), then extracting with hexanes (4 x 250 mL). The combined hexane phases were extracted with 0.05 M NaOH (2 x 500 mL), then dried with $MgSO_4$. After filtering off the $MgSO_4$, the filtrate was concentrated via rotary evaporation to a yellow oil (36.8359 g, 97.3% yield).

Optional: The oil was then distilled under vacuum (46 mTorr, bp 104-130 °C) using an unjacketed shortpath distillation head with Vigreux indentations. Colorless oil (31.2881 g, 82.6% yield).

Note: The product tends to exist as a supercooled liquid but under just the right conditions, it will crystallize (mp >23 °C) however it will melt if disturbed (for example by the applied pressure of a spatula attempting to remove the solid). Also, as the product ages it tends to slowly turn yellow.

1H -NMR δ (ppm)(DMSO- d_6): 10.286 (s, 1H), 7.790 (dd, J = 9.0 Hz, 3.0 Hz, 1H), 7.724 (d, J = 3.0 Hz, 1H), 7.225 (d, J = 9.0 Hz, 1H), 4.126 (t, J = 6.6 Hz, 2H), 1.73-1.79 (m, 2H), 1.41-1.46 (m, 2H), 1.26-1.34 (m, 4H), 0.870 (t, J = 6.9 Hz, 3H).

Synthetic Methods

^{13}C -NMR δ (ppm)(DMSO- d_6): 187.99, 160.08, 138.45, 129.69, 125.7, 116.33, 112.23, 68.82, 30.87, 28.28, 25.02, 21.98, 13.84.

TABLE 7.1: High resolution mass spectrum (ESI) of 5-bromo-2-(hexyloxy)benzaldehyde (**G4-012s16**)

Species	Chemical Formula	Calculated m/z	Observed m/z
$[\text{M} + \text{H}]^+$	$\text{C}_{13}\text{H}_{18}\text{BrO}_2^+$	285.04847	285.04869
$[\text{M} + \text{Na}]^+$	$\text{C}_{13}\text{H}_{17}\text{BrNaO}_2^+$	307.03041	307.03115
$[\text{M} + \text{CH}_3]^+$	$\text{C}_{14}\text{H}_{20}\text{BrO}_2^+$	299.06412	299.06453
$[\text{M} + \text{CH}_3 + \text{H} + \text{Na}]^+$	$\text{C}_{14}\text{H}_{21}\text{BrNaO}_2^+$	323.06171	323.02624
$[\text{M} + \text{MeOH} + \text{Na}]^{+a}$	$\text{C}_{14}\text{H}_{21}\text{BrNaO}_3^+$	339.05663	339.05742

a. This is the sodium cation form of the hemiacetal with MeOH.

7.1.2.2 Hexyl 2-(hexyloxy)-5-nitrobenzoate: **G5-047s10**

2-hydroxy-5-nitrobenzoic acid (30 mmol, 5.4963 g), K_2CO_3 (12.4389 g, 90 mmol) and anhydrous dimethylformamide (50 mL) were combined in a round bottom flask. While stirring, 1-bromohexane (14.8563 g, 12.63 mL, 90 mmol) was added, then the reaction was stirred for 25 hours at 80 °C. The reaction was worked-up by adding water (250 mL), then adjusting the pH =2 with 12 M HCl (~6 mL). The mixture was extracted with hexanes (2 x 100 mL). The combined hexane phases were washed with water (2 x 100 mL), and dried with MgSO_4 . After filtering off the MgSO_4 , the solution was concentrated by rotatory evaporation (10.23 g, 97.1% yield).

^1H -NMR δ (ppm)(DMSO- d_6): 8.45 (1 H, d, $J = 2.95$ Hz), 8.39 (1 H, dd, $J = 9.24, 2.98$ Hz), 7.38 (1 H, d, $J = 9.29$ Hz), 4.27 (2 H, t, $J = 6.54$ Hz), 4.20 (2 H, t, J

Synthetic Methods

= 6.28 Hz), 1.64-1.80 (4 H, m), 1.35-1.50 (4 H, m), 1.25-1.35 (6 H, m), 0.84-0.92 (6 H, m).

7.1.2.3 (2-(hexyloxy)-5-nitrophenyl)(pyrrolidin-1-yl)methanone: G5-090s11

(2-hydroxy-5-nitrophenyl)(pyrrolidin-1-yl)methanone (**G5-088s8**, 0.897 g, 2.8 mmol), K₂CO₃ (0.580 g, 4.2 mmol) and anhydrous dimethylformamide (5 mL) were combined in a round bottom flask. While stirring, 1-bromohexane (0.693 g, 0.590 mL, 4.2 mmol) was added, then the reaction was stirred for 10 hours at 80 °C. The reaction was worked-up by adding 2 M HCl (6 mL), then extracting with hexanes (3 x 5 mL). The combined hexane phases were washed with water (2 x 5 mL), then filtered through a fine sintered glass funnel, and the filtrate dried with MgSO₄. After filtering off the MgSO₄, the solution was concentrated by rotatory evaporation to an oil.

¹H-NMR δ (ppm)(DMSO-d₆): 8.28 (1 H, dd, J = 9.19, 2.90 Hz), 8.06 (1 H, d, J = 2.89 Hz), 7.31 (1 H, d, J = 9.24 Hz), 5.76 (0 H, s), 4.18 (2 H, t, J = 6.27 Hz), 3.46 (2 H, t, J = 6.55 Hz), 3.13 (2 H, t, J = 6.55 Hz), 1.76-1.92 (4 H, m), 1.67-1.76 (2 H, m), 1.35-1.45 (2 H, m), 1.26-1.35 (4 H, m), 0.88 (3 H, t, J = 6.83 Hz).

¹³C-NMR δ (ppm)(DMSO-d₆): 163.9, 159.4, 140.4, 128.1, 126.3, 123.3, 112.8, 69.0, 46.9, 45.3, 30.8, 28.2, 25.4, 24.9, 24.1, 22.0, 13.8.

Synthetic Methods

7.1.2.4 2-(hexyloxy)-5-nitrobenzaldehyde: G5-120s11

2-hydroxy-5-nitrobenzaldehyde (30 mmol, 5.0136 g), K_2CO_3 (60 mmol, 8.2926 g) and anhydrous dimethylformamide (100 mL) were combined in a round bottom flask. While stirring, 1-bromohexane (60 mmol, 9.9042 g, 8.422 mL) was added, then the reaction was stirred for 18 hours at 80 °C. The reaction was worked-up by adding water (250 mL), then extracting with ethyl acetate (50 mL). The aqueous phase was extracted with ethyl acetate (EtOAc, 3 x 100 mL). The ethyl acetate phases were combined then extracted with 0.6 M HCl (100 mL), then brine (50 mL). The organic phase was dried with $MgSO_4$. After filtering off the $MgSO_4$, the solution was concentrated by rotatory evaporation to an oil. The oil was purified by plug filtration through silica in a 150 mL sintered glass funnel, eluting with hexanes (150 mL) followed by dichloromethane (DCM, 500 mL), and collecting the hexanes and DCM eluants as separate fractions. The DCM fraction was concentrated by rotatory evaporation to a tan solid. The solid was dissolved in hexanes (100 mL) and DCM (10 mL), and the resulting solution was concentrated by rotatory evaporation at 40 °C until the DCM was removed. As the mixture cooled, crystals formed, which were filtered off using a medium sinter glass funnel and washed with hexanes (8.00 g, 53% yield).

1H -NMR δ (ppm)(DMSO- d_6): 10.35 (1 H, s), 8.49 (1 H, dd, J = 9.23, 2.99 Hz), 8.42 (1 H, d, J = 2.97 Hz), 7.48 (1 H, d, J = 9.27 Hz), 4.30 (2 H, t, J = 6.43 Hz),

Synthetic Methods

1.78-1.87 (2 H, m), 1.42-1.52 (2 H, m), 1.30-1.36 (4 H, m), 0.89 (3 H, t, $J = 6.84$ Hz).

^{13}C -NMR δ (ppm)(DMSO- d_6): 187.9, 165.0, 140.6, 130.9, 123.9, 123.5, 114.7, 69.8, 30.8, 28.2, 24.9, 22.0, 13.8.

7.1.2.5 (5-bromo-2-(hexyloxy)phenyl)(phenyl)methanol: G4-19s13

In a 20 mL vial with a septum cap, **5-bromo-2-(hexyloxy)benzaldehyde (G4-012s16**, 0.5 g, 1.75 mmol) was dissolved in anhydrous tetrahydrofuran (THF, 10 mL), and the resulting solution cooled to 0 °C. To the solution, phenylmagnesium-bromide (1.0 M in THF, 2.6 mL, 2.6 mmol) was added dropwise, and the reaction was allowed to warm to room temperature over 4 hours. The reaction was acidified to pH 6 with 0.1 M HCl (~50 mL), then extracted with ethyl acetate (EtOAc, 3 x 20 mL). The combined EtOAc phases were washed with water (2 x 25 mL), dried over MgSO_4 . After filtration, silica gel (~ 1 g) was added to the filtrate, then concentrated by rotatory evaporation to a powder. The powder was used as a dry-load for silica chromatography (**FIGURE 7.1**). Fractions 15-18 were combined and concentrated by rotatory evaporation to a white solid (0.4333 g, 68.2% yield).

^1H -NMR δ (ppm)(DMSO- d_6): 7.6384 (d, $J = 2.5$ Hz, 1H), 7.3478 (dd, $J = 8.7$ Hz, 2.5 Hz, 1H), 7.24 - 7.33 (m, 4H), 7.16 - 7.22 (m, 1H), 6.8906 (d, $J = 8.7$ Hz),

Synthetic Methods

5.902 (d, J = 4.4 Hz, 1H), 5.835 (d, J = 4.4 Hz, 1H), 3.87-3.94 (m, 2H), 1.60-1.71 (m, 2H), 1.30-1.38 (m, 2H), 1.23-1.30 (m, 4H), 0.874 (t, J = 6.76 Hz, 3H).

TABLE 7.2: High resolution MS (ESI) of (5-bromo-2-(hexyloxy)(phenyl))(phenyl)methanol (**G4-019s13**)

Species	Chemical Formula	Calculated m/z	Observed m/z
[M - OH] ⁺	C ₁₉ H ₂₂ BrO ⁺	345.08485	345.08485
[M + Na] ⁺	C ₁₉ H ₂₃ BrNaO ₂ ⁺	345.08485	345.08485

Synthetic Methods

FIGURE 7.1: Chromatographic purification of **G4-019s9**.

Sample: grandy4-017s9

Rf 200 : Isco Demo

Thursday 09 February 2012 01:14PM

RediSep Column: Silica 40g

Peak Tube Volume: Max.

SN: E041039E8B947 Lot: 1920177010W

Non-Peak Tube Volume: Max.

Flow Rate: 40 ml/min

Loading Type: Liquid

Equilibration Volume: 5.0 CV

Wavelength 1 (red): 254nm

Initial Waste: 0.0 CV

Peak Width: 2 min

Air Purge: 1.0 min

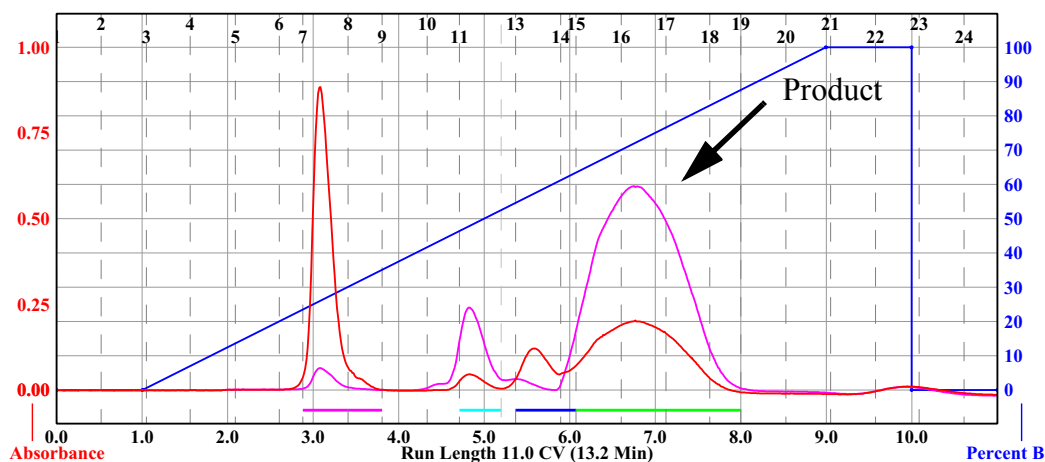
Threshold: 0.05 AU

Solvent: A1 hexane

Wavelength 2 (purple): 280nm

Solvent: B1 ethyl acetate

Run Notes:



Rack A				
(70)	(69)	(68)	(67)	(66)
(61)	(62)	(63)	(64)	(65)
(60)	(59)	(58)	(57)	(56)
(51)	(52)	(53)	(54)	(55)
(50)	(49)	(48)	(47)	(46)
(41)	(42)	(43)	(44)	(45)
(40)	(39)	(38)	(37)	(36)
(31)	(32)	(33)	(34)	(35)
(30)	(29)	(28)	(27)	(26)
(21)	(22)	(23)	(24)	(25)
(20)	(19)	(18)	(17)	(16)
(11)	(12)	(13)	(14)	(15)
(10)	(9)	(8)	(7)	(6)
(1)	(2)	(3)	(4)	(5)

18 mm x 150 mm Tubes

Peak #	Start Tube	End Tube
1	A:7	A:8
2	A:11	A:11
3	A:13	A:14
4	A:15	A:18

Duration	%B	Solvent A	Solvent B
0.0	0.0	A1 hexane	B1 ethyl acetate
1.0	0.0	A1 hexane	B1 ethyl acetate
8.0	100.0	A1 hexane	B1 ethyl acetate
1.0	100.0	A1 hexane	B1 ethyl acetate
0.0	0.0	A1 hexane	B1 ethyl acetate
1.0	0.0	A1 hexane	B1 ethyl acetate

Synthetic Methods

7.1.2.6 (5-(4-fluorophenoxy)-2-(hexyloxy)phenyl)(phenyl)methanol: G4-74s14

Under an N₂ atmosphere and in a round bottom flask, **5-(4-fluorophenoxy)-2-(hexyloxy)benzaldehyde** (1.5150 g, 4.79 mmol) was dissolved in anhydrous tetrahydrofuran (THF, 50 mL), then cooled to 0 °C. Phenylmagnesiumbromide (1.0 M in THF, 9.5 mL, 9.5 mmol, 2 eq) was added dropwise to the reaction. The reaction was allowed to warm to room temperature over at least 4 hours. The reaction was added to 2.4 M HCl (100 mL), then extracted with ethyl acetate (EtOAc, 3 x 25 mL). The combined EtOAc phases were washed with water (2 x 100 mL), brine (1 x 25 mL), and then dried over MgSO₄. After filtration, silica gel (~5 g) was added to the filtrate, and then concentrated by rotatory evaporation to a powder. The powder was used as a dry-load for silica chromatography (see **FIGURE 7.2**). Fractions 24-40 combined and concentrated by rotatory evaporation to a pale yellow oil (1.6727 g, 88.5% yield).

¹H-NMR δ (ppm)(DMSO-d₆): 7.24 - 7.31 (m, 4H), 7.228 (d, J = 3.0 Hz, 1H), 7.16 - 7.22 (m, 3H), 6.95 - 7.00 (m, 2H), 6.922 (d, J = 9.0 Hz, 1H), 6.848 (dd, J = 9.0 Hz, 3.0 Hz, 1H), 5.912 (d, J = 9.3 Hz, 1H), 5.730 (d, J = 9.3 Hz, 1H), 3.85-3.93 (m, 2H), 1.62-1.70 (m, 2H), 1.32-1.39 (m, 2H), 1.26-1.32 (m, 4H), 0.881 (t, J = 6.9 Hz, 3H).

¹³C-NMR δ (ppm)(DMSO-d₆): 157.64 (d, J = 239.9 Hz), 153.94, 151.09, 149.73, 144.80, 135.38, 127.82, 126.65, 126.54, 119.20 (d, J = 7.5 Hz), 117.92,

Synthetic Methods

117.16, 116.33 (d, $J = 22.6$ Hz), 112.58, 68.22, 67.90, 30.93, 28.69, 25.22, 22.03, 13.8.

^{19}F -NMR δ (ppm)(DMSO- d_6 , with C_6F_6 as reference at -164.9 ppm): -123.37 to -123.47.

TABLE 7.3: High resolution MS (ESI) of 5-(4-fluorophenoxy)-2-(hexyloxy)(phenyl)methanol (**G4-074s14**)

Species	Chemical Formula	Calculated m/z	Observed m/z
$[\text{M} + \text{H}]^+$	$\text{C}_{19}\text{H}_{22}\text{FO}_3^+$	317.15475	371.16291
$[\text{M} + \text{Na}]^+$	$\text{C}_{19}\text{H}_{21}\text{FNaO}_3^+$	339.13669	339.13728
$[\text{M} + \text{MeOH} + \text{Na}]^{+a}$	$\text{C}_{20}\text{H}_{25}\text{FNaO}_4^+$	371.16291	371.16289

a. This is the sodium cation form of the hemiacetal with MeOH.

Synthetic Methods

FIGURE 7.2: Chromatographic purification of G4-074s12.

Sample: grandy4-074s12

Rf 200 : OHSU COHEN RF200#1

Thursday 12 April 2012 09:36AM

RediSep Column: Silica 40g

Peak Tube Volume: Max.

SN: E04103BAEBBF Lot: 1922189010X

Non-Peak Tube Volume: Max.

Flow Rate: 40 ml/min

Loading Type: Solid

Equilibration Volume: 5.0 CV

Wavelength 1 (red): 254nm

Initial Waste: 0.0 CV

Peak Width: 2 min

Air Purge: 1.0 min

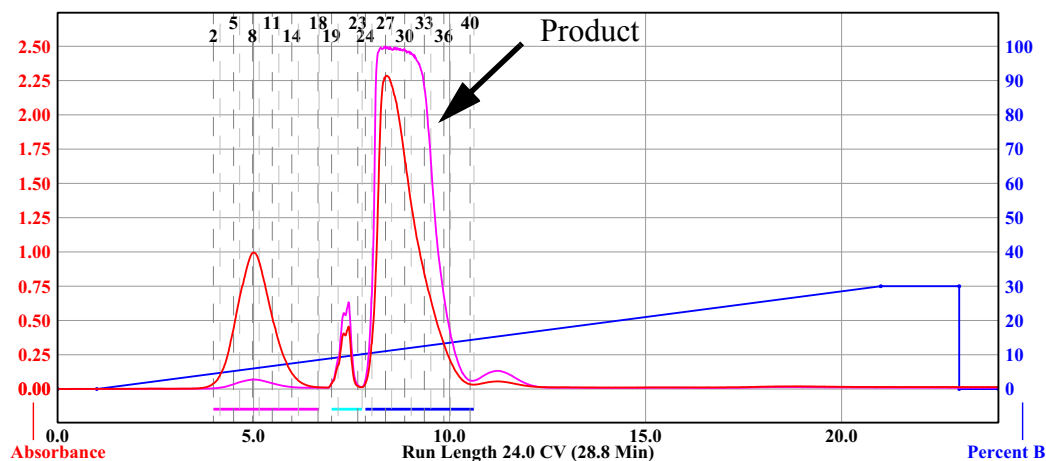
Threshold: 0.05 AU

Solvent: A1 hexane

Wavelength 2 (purple): 280nm

Solvent: B1 ethyl acetate

Run Notes:



Rack A

108	107	106	105	104	103
97	98	99	100	101	102
96	95	94	93	92	91
85	86	87	88	89	90
84	83	82	81	80	79
73	74	75	76	77	78
72	71	70	69	68	67
61	62	63	64	65	66
60	59	58	57	56	55
49	50	51	52	53	54
48	47	46	45	44	43
42	41	40	39	38	37
36	35	34	33	32	31
30	29	28	27	26	25
24	23	22	21	20	19
18	17	16	15	14	13
12	11	10	9	8	7
6	5	4	3	2	1

13 mm x 100 mm Tubes

Peak

Start Tube

End Tube

1	A:2	A:18
2	A:19	A:23
3	A:24	A:40

Duration	%B	Solvent A	Solvent B
0.0	0.0	A1 hexane	B1 ethyl acetate
1.0	0.0	A1 hexane	B1 ethyl acetate
20.0	30.0	A1 hexane	B1 ethyl acetate
2.0	30.0	A1 hexane	B1 ethyl acetate
0.0	0.0	A1 hexane	B1 ethyl acetate
1.0	0.0	A1 hexane	B1 ethyl acetate

Synthetic Methods

7.1.2.7 (2-(hexyloxy)-5-(phenylamino)phenyl)(phenyl)methanol: G2-100s9

In a 20 mL vial, **2-(hexyloxy)-5-(phenylamino)benzaldehyde (G5-135s7**, 0.309 g, 0.90 mmol) was dissolved in anhydrous tetrahydrofuran (THF, 5 mL). To the solution, phenylmagnesiumbromide (1.0 M in THF, 5 mL, 5 mmol) was added, and the reaction was stirred for an hour. Celite (~1 g) and 1 M NaOH (5 mL) was added to the reaction. The mixture was thoroughly mixed, filtered through a sintered glass funnel, and washed with ethyl acetate (EtOAc, 15 mL). The filtrate was extracted with brine (50 mL). The brine phase was extracted with EtOAc (30 mL). The combined EtOAc phases were dried with MgSO₄, and after filtering silica gel (~1 g) was added to the filtrate. This mixture was concentrated by rotatory evaporation to a powder, which was used as a dry-load for silica chromatography (**FIGURE 7.3**). Fractions 17-49 were combined and concentrated by rotatory evaporation (0.2880 g, 89.5% yield).

¹H-NMR δ (ppm)(DMSO-d₆): 7.85 (1 H, s), 7.29-7.35 (3 H, m), 7.23-7.29 (2 H, m), 7.11-7.17 (3 H, m), 6.88-6.94 (3 H, m), 6.83 (1 H, d, J = 8.71 Hz), 6.66-6.72 (1 H, m), 5.95 (1 H, d, J = 4.10 Hz), 5.64 (1 H, d, J = 4.08 Hz), 3.87 (2 H, td, J = 6.28, 2.99 Hz), 1.62-1.72 (2 H, m), 1.34-1.42 (2 H, m), 1.26-1.34 (4 H, m), 0.88 (4 H, t, J = 7.08 Hz).

Synthetic Methods

FIGURE 7.3: Chromatographic purification of G2-100s8.

Sample: grandy2-100

RediSep Column: Silica 40g

Flow Rate: 40 ml/min

Equilibration Volume: 5.0 CV

Initial Waste: 0.0 CV

Air Purge: 1.0 min

Solvent: A2 hexane

Solvent: B2 ethyl acetate

Rf 200 : OHSU COHEN RF200#1

Peak Tube Volume: Max.

Non-Peak Tube Volume: Max.

Loading Type: Solid

Wavelength 1 (red): 254nm

Peak Width: 2 min

Threshold: 0.05 AU

Wavelength 2 (purple): 280nm

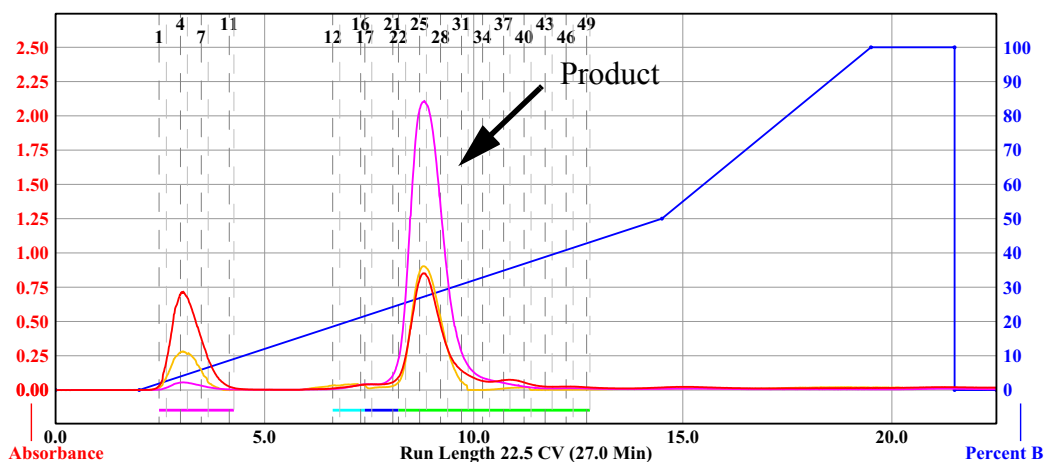
Wednesday 31 October 2012 07:39PM

All Wavelength (orange): 200nm - 360nm

Peak Width: 2 min

Threshold: 0.20 AU

Run Notes:



Rack A						Peak #	Start Tube	End Tube	
108	107	106	105	104	103	1	A:1	A:11	
97	98	99	100	101	102	2	A:12	A:16	
96	95	94	93	92	91	3	A:17	A:21	
85	86	87	88	89	90	4	A:22	A:49	
84	83	82	81	80	79				
73	74	75	76	77	78				
72	71	70	69	68	67				
61	62	63	64	65	66				
60	59	58	57	56	55				
49	50	51	52	53	54				
48	47	46	45	44	43				
37	38	39	40	41	42				
36	35	34	33	32	31				
25	26	27	28	29	30				
24	23	22	21	20	19				
13	14	15	16	17	18				
12	11	10	9	8	7				
1	2	3	4	5	6				
13 mm x 100 mm Tubes						Duration	%B	Solvent A	Solvent B
						0.0	0.0	A2 hexane	B2 ethyl acetate
						2.0	0.0	A2 hexane	B2 ethyl acetate
						12.5	50.0	A2 hexane	B2 ethyl acetate
						5.0	100.0	A2 hexane	B2 ethyl acetate
						2.0	100.0	A2 hexane	B2 ethyl acetate
						0.0	0.0	A2 hexane	B2 ethyl acetate
						1.0	0.0	A2 hexane	B2 ethyl acetate

Page 1 of 1

Synthetic Methods

7.1.2.8 5-((4-fluorophenyl)amino)-2-(hexyloxy)phenyl(phenyl)methanol: G2-101s9

In a 20 mL vial with a septum cap, **5-((4-fluorophenyl)amino)-2-(hexyloxy)benzaldehyde (G5-136s7)**, 0.228 g, 0.72 mmol) was dissolved in anhydrous tetrahydrofuran (THF, 5 mL). To the solution, phenylmagnesiumbromide (1.0 M in THF, 5 mL, 5 mmol) was added, and the reaction was stirred for an hour. Celite (~1 g) and 1 M NaOH (5 mL) was added to the reaction. The mixture was thoroughly mixed, filtered through a sintered glass funnel, and washed with ethyl acetate (EtOAc, 15 mL). The filtrate was extracted with brine (50 mL). The brine phase was extracted with EtOAc (30 mL). The combined EtOAc phases were dried with MgSO₄, and after filtering silica gel (~1 g) was added to the filtrate. This mixture was concentrated by rotatory evaporation to a powder, which was used as a dry-load for silica chromatography (**FIGURE 7.4**). Fractions 17-36 were combined and concentrated by rotatory evaporation (0.2377 g, 83.9% yield).

¹H-NMR δ (ppm)(DMSO-d₆): 7.81 (1 H, s), 7.30-7.34 (2 H, m), 7.23-7.29 (3 H, m), 7.14-7.19 (1 H, m), 7.00 (2 H, t, J = 8.81 Hz), 6.85-6.93 (3 H, m), 6.81 (1 H, d, J = 8.76 Hz), 5.94 (1 H, d, J = 4.09 Hz), 5.64 (1 H, d, J = 4.09 Hz), 3.86 (2 H, td, J = 6.32, 3.30 Hz), 1.62-1.71 (2 H, m), 1.33-1.42 (2 H, s), 1.26-1.33 (4 H, m), 0.88 (3 H, t, J = 6.58 Hz).

Synthetic Methods

FIGURE 7.4: Chromatographic purification of G2-101s8.

Sample: grandy2-101

RediSep Column: Silica 40g

Flow Rate: 40 ml/min

Equilibration Volume: 5.0 CV

Initial Waste: 0.0 CV

Air Purge: 1.0 min

Solvent: A2 hexane

Solvent: B2 ethyl acetate

Rf 200 : OHSU COHEN RF200#1

Peak Tube Volume: Max.

Non-Peak Tube Volume: Max.

Loading Type: Solid

Wavelength 1 (red): 254nm

Peak Width: 2 min

Threshold: 0.05 AU

Wavelength 2 (purple): 280nm

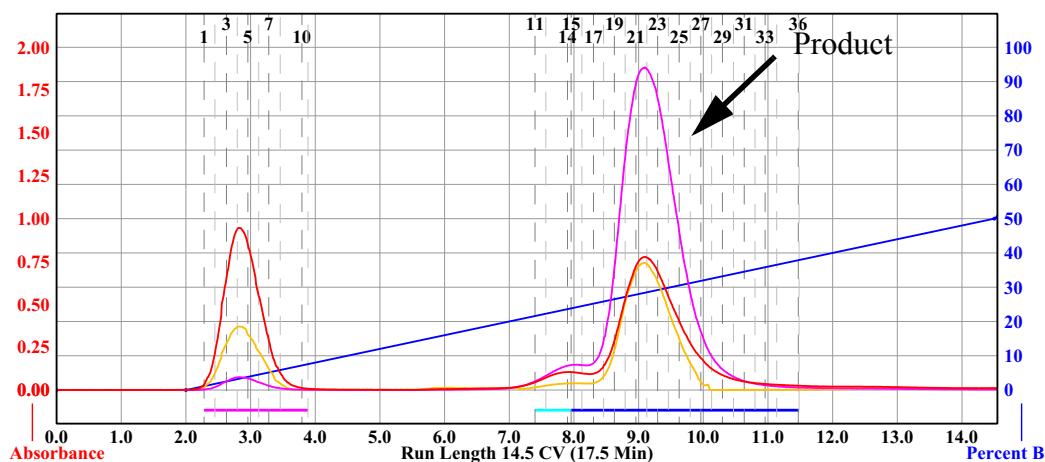
Wednesday 31 October 2012 08:24PM

All Wavelength (orange): 200nm - 360nm

Peak Width: 2 min

Threshold: 0.20 AU

Run Notes:



Rack A							Peak #	Start Tube	End Tube
108	107	106	105	104	103		1	A:1	A:10
97	98	99	100	101	102		2	A:11	A:14
96	95	94	93	92	91		3	A:15	A:36
85	86	87	88	89	90				
84	83	82	81	80	79				
73	74	75	76	77	78				
72	71	70	69	68	67				
61	62	63	64	65	66				
60	59	58	57	56	55				
49	50	51	52	53	54				
48	47	46	45	44	43				
37	38	39	40	41	42				
26	27	28	29	30	31				
25	24	23	22	21	20				
14	15	16	17	18	19				
3	4	5	6	7	8				
1	2	3	4	5	6				

13 mm x 100 mm Tubes

Page 1 of 1

Synthetic Methods

**7.1.2.9 5-((3-fluorophenyl)amino)-2-(hexyloxy)phenyl(phenyl)methanol:
G2-102s9**

In a 20 mL vial with a septum cap, **5-((3-fluorophenyl)amino)-2-(hexyloxy)benzaldehyde (G5-137s7**, 0.3480 g, 1.10 mmol) was dissolved in anhydrous tetrahydrofuran (THF, 5 mL). To the solution, phenylmagnesiumbromide (1.0 M in THF, 5 mL, 5 mmol) was added, and the reaction was stirred for an hour. Celite (~1 g) and 1 M NaOH (5 mL) was added to the reaction. The mixture was thoroughly mixed, filtered through a sintered glass funnel, and washed with ethyl acetate (EtOAc, 15 mL). The filtrate was extracted with brine (50 mL). The brine phase was extracted with EtOAc (30 mL). The combined EtOAc phases were dried with MgSO₄, and after filtering, silica gel (~1 g) was added to the filtrate. This mixture was concentrated by rotatory evaporation to a powder, which was used as a dry-load for silica chromatography (**FIGURE 7.5**). Fractions 17-28 were combined and concentrated by rotatory evaporation (0.3374 g, 78.0% yield).

¹H-NMR δ (ppm)(DMSO-d₆): 8.14 (1 H, s), 7.39-7.41(2 H, m), 7.31-7.36 (4 H, m), 7.13-7.15 (1 H, m), 6.95 (1 H, dd, J = 8.68, 2.80 Hz), 6.86 (1 H, d, J = 8.76 Hz), 6.66-6.71 (1 H, m), 6.60 (1 H, dt, J = 12.24, 2.31 Hz), 6.45 (1 H, td, J = 8.20, 2.48 Hz), 5.95 (1 H, d, J = 4.17 Hz), 5.68 (1 H, J = 4.16 Hz), 3.89 (2 H, td, J = 6.39, 2.78 Hz), 1.64-1.72 (2 H, m), 1.33-1.42 (2 H, m), 1.27-1.33 (4 H, m), 0.88 (3 H, t, J = 6.64 Hz).

Synthetic Methods

FIGURE 7.5: Chromatographic purification of G2-102s8.

Sample: grandy2-102s8

RediSep Column: Silica 40g

Flow Rate: 40 ml/min

Equilibration Volume: 5.0 CV

Initial Waste: 0.0 CV

Air Purge: 1.0 min

Solvent: A2 hexane

Solvent: B2 ethyl acetate

Rf 200 : OHSU COHEN RF200#1

Peak Tube Volume: Max.

Non-Peak Tube Volume: Max.

Loading Type: Solid

Wavelength 1 (red): 254nm

Peak Width: 2 min

Threshold: 0.05 AU

Wavelength 2 (purple): 280nm

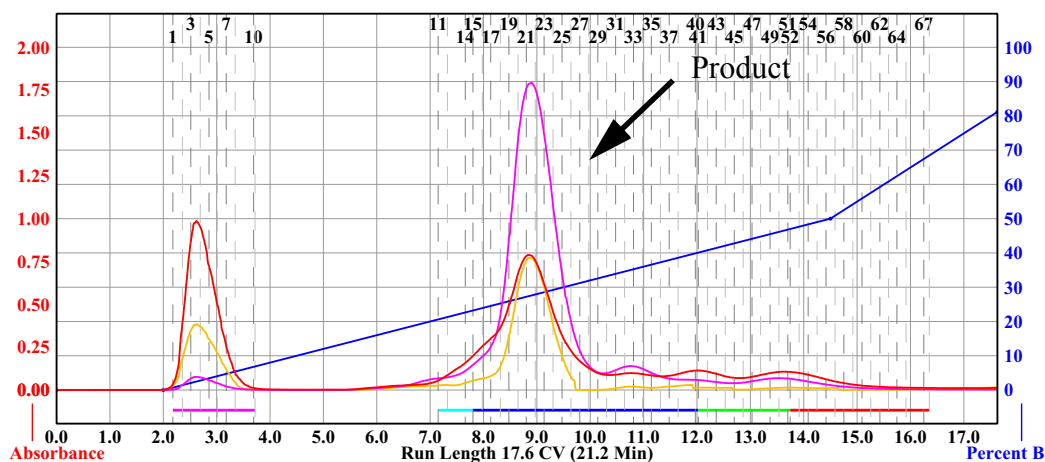
Wednesday 31 October 2012 08:55PM

All Wavelength (orange): 200nm - 360nm

Peak Width: 2 min

Threshold: 0.20 AU

Run Notes:



Rack A						Peak #	Start Tube	End Tube	
108	107	106	105	104	103	1	A:1	A:10	
97	98	99	100	101	102	2	A:11	A:14	
96	95	94	93	92	91	3	A:15	A:40	
85	86	87	88	89	90	4	A:41	A:51	
84	83	82	81	80	79	5	A:52	A:67	
73	72	75	76	77	78				
72	71	70	69	68	67				
61	60	59	58	57	56				
51	50	49	48	47	46				
41	40	39	38	37	36				
31	30	29	28	27	26				
21	20	19	18	17	16				
11	10	9	8	7	6				
1	2	3	4	5	6				
13 mm x 100 mm Tubes						Duration	%B	Solvent A	Solvent B
						0.0	0.0	A2 hexane	B2 ethyl acetate
						2.0	0.0	A2 hexane	B2 ethyl acetate
						12.5	50.0	A2 hexane	B2 ethyl acetate
						3.1	81.1	A2 hexane	B2 ethyl acetate

Synthetic Methods

7.1.2.10 Hexyl 2-(hexyloxy)-5-(phenylamino)benzoate: G5-059s9

In a round bottom flask equipped with a drying tube open to the air, **hexyl 5-amino-2-(hexyloxy)benzoate (G5-047s9)**, 82.95 mass% w/EtOAc, 3 mmol, 1.163 g), phenylboronic acid (12 mmol, 1.4692 g), Cu(OAc)₂ (6.9 mmol, 1.253 g), triethylamine (22.5 mmol, 2.277 g, 3.136 mL), powdered vacuum oven dried 4 Å molecular sieves (3 g) and anhydrous dichloromethane (DCM, 30 mL) were combined. After stirring for 2 days, the reaction mixture was filtered through packed celite (~2 cm in a 60 mL sintered glass funnel), and washed with DCM. The filtrate was extracted with 5 M NH₄OH (2 x 75 mL) followed by an extraction with water (50 mL). The DCM phase was dried with MgSO₄, and after filtering, silica gel (~5 g) was added to the filtrate. This mixture was concentrated by rotatory evaporation to a powder, which was used as a dry-load for silica chromatography (**FIGURE 7.6**). Fractions 15-24 were combined and concentrated by rotatory evaporation (0.492 g, 41.3% yield).

Notes: In climates drier than Portland, Oregon, 1 g of powdered molecular sieves should suffice. Also, if one were to repeat this experiment at the same scale and using 3 g of powdered molecular sieves, increasing the amount of DCM used would improve the stirrability of the reaction.

¹H-NMR δ (ppm)(DMSO-d₆): 8.01 (1 H, s), 7.36 (1 H, d, J = 2.90 Hz), 7.16-7.24 (3 H, m), 7.05 (1 H, d, J = 8.92 Hz), 6.95 (2 H, dt, J = 7.96, 1.12 Hz), 6.77 (1

Synthetic Methods

H, tt, J = 7.30, 1.00 Hz), 4.20 (2 H, t, J = 6.47 Hz), 3.96 (2 H, t, J = 6.32 Hz), 1.60-1.74 (4 H, m), 1.36-1.49 (4 H, m), 1.23-1.36 (8 H, m), 0.82-0.93 (6 H, m).

¹³C-NMR δ (ppm)(DMSO-d₆): 166.1, 151.8, 144.2, 136.1, 129.2, 123.1, 121.2, 120.1, 119.0, 115.5, 115.1, 68.8, 64.4, 31.0, 30.9, 28.8, 28.2, 25.2 (2 C), 22.1, 22.0, 14.1, 13.9.

Synthetic Methods

FIGURE 7.6: Chromatographic purification of G5-059s7.

Sample: grandy5-059s7

Rf 200 : OHSU COHEN RF200#1

Wednesday 22 August 2012 03:08PM

RediSep Column: Silica 24g

Peak Tube Volume: Max.

Flow Rate: 35 ml/min

Non-Peak Tube Volume: Max.

Equilibration Volume: 5.0 CV

Loading Type: Solid (Pause)

Initial Waste: 0.0 CV

Wavelength 1 (red): 254nm

Air Purge: 1.0 min

Peak Width: 1 min

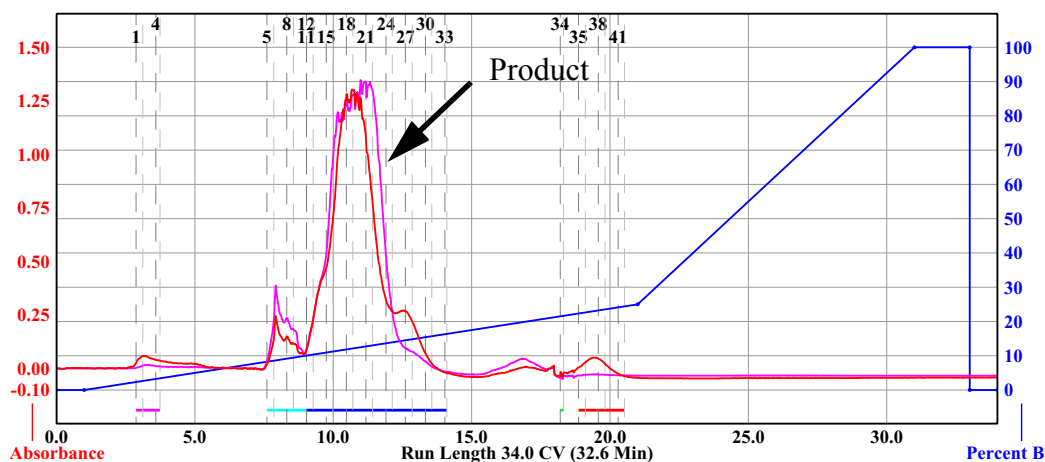
Solvent: A2 hexane

Threshold: 0.05 AU

Solvent: B2 ethyl acetate

Wavelength 2 (purple): 280nm

Run Notes: self-packed column, 50g



Rack A						Peak #	Start Tube	End Tube	
108	107	106	105	104	103	1	A:1	A:4	
97	98	99	100	101	102	2	A:5	A:11	
96	95	94	93	92	91	3	A:12	A:33	
85	86	87	88	89	90	4	A:34	A:34	
84	83	82	81	80	79	5	A:35	A:41	
73	72	71	70	69	68				
72	71	70	69	68	67				
61	62	63	64	65	66				
60	59	58	57	56	55				
49	50	51	52	53	54				
48	47	46	45	44	43				
37	36	35	34	33	32				
36	35	34	33	32	31				
25	26	27	28	29	30				
24	23	22	21	20	19				
13	14	15	16	17	18				
12	11	10	9	8	7				
1	2	3	4	5	6				
13 mm x 100 mm Tubes						Duration	%B	Solvent A	Solvent B
						0.0	0.0	A2 hexane	B2 ethyl acetate
						1.0	0.0	A2 hexane	B2 ethyl acetate
						20.0	25.0	A2 hexane	B2 ethyl acetate
						10.0	100.0	A2 hexane	B2 ethyl acetate
						2.0	100.0	A2 hexane	B2 ethyl acetate
						0.0	0.0	A2 hexane	B2 ethyl acetate
						1.0	0.0	A2 hexane	B2 ethyl acetate

Synthetic Methods

7.1.2.11 Hexyl 5-((4-fluorophenyl)amino)-2-(hexyloxy)benzoate: G5-060s9

In a 20 mL vial with a septum cap and equipped with a drying tube open to the air, **hexyl 5-amino-2-(hexyloxy)benzoate (G5-047s9)**, 82.95 mass% w/EtOAc, 1 mmol, 0.3960 g), 4-fluorophenylboronic acid (4 mmol, 0.5629 g), Cu(OAc)₂ (2.3 mmol, 0.313 g), triethylamine (7.5 mmol, 0.759 g, 1.045 mL), powdered vacuum oven dried 4 Å molecular sieves (1 g) and anhydrous dichloromethane (DCM, 10 mL) were combined. After stirring for 2 days, the reaction mixture was filtered through packed celite (~2 cm in a 60 mL sintered glass funnel), and washed with DCM. The filtrate was extracted with 5 M NH₄OH (2 x 75 mL) followed by an extraction with water (50 mL). The DCM phase was dried with MgSO₄, and after filtering, silica gel (~5 g) was added to the filtrate. This mixture was concentrated by rotatory evaporation to a powder, which was used as a dry-load for silica chromatography (**FIGURE 7.7**). Fractions 7-20 were combined and concentrated by rotatory evaporation (0.1435 g, 34.5% yield).

Notes: In climates drier than Portland, Oregon, 0.3 g of powdered molecular sieves should suffice. Also, if one were to repeat this experiment using 1 g of powdered molecular sieves, increasing the amount of DCM used would improve the stirrability of the reaction.

¹H-NMR δ (ppm)(DMSO-d₆): 7.96 (1 H, s), 7.30 (1 H, d, J = 2.91 Hz), 7.18 (1 H, dd, J = 8.88, 2.93 Hz), 7.01-7.09 (3 H, m), 6.93-6.99 (2 H, m), 4.19 (2 H, t, J =

Synthetic Methods

6.53 Hz), 3.95 (2 H, t, J = 6.33 Hz), 1.60-1.74 (4 H, m), 1.35-1.48 (4 H,m), 1.26-1.34 (8 H, m), 0.83-0.91 (6 H, m).

^{13}C -NMR δ (ppm)(DMSO- d_6): 166.1, (157.2 & 154.8 (1 C, d, J = 235.40 Hz), 151.6, 140.6, 136.6, 122.4, 121.3, 119.4, 117.45 (1 C, d, J = 7.58 Hz), 115.7 (1 C, d, J = 22.33 Hz), 115.3, 68.9, 64.4, 31.0, 30.9, 28.8, 28.2, 25.2, 22.4, 22.1, 22.0, 13.9 (2 C).

Synthetic Methods

FIGURE 7.7: Chromatographic purification of G5-060s7.

Sample: grandy5-060s7

Rf 200 : OHSU COHEN RF200#1

Wednesday 22 August 2012 04:10PM

RediSep Column: Silica 40g

Peak Tube Volume: Max.

Flow Rate: 40 ml/min

Non-Peak Tube Volume: Max.

Equilibration Volume: 5.0 CV

Loading Type: Solid (Pause)

Initial Waste: 0.0 CV

Wavelength 1 (red): 254nm

Air Purge: 1.0 min

Peak Width: 2 min

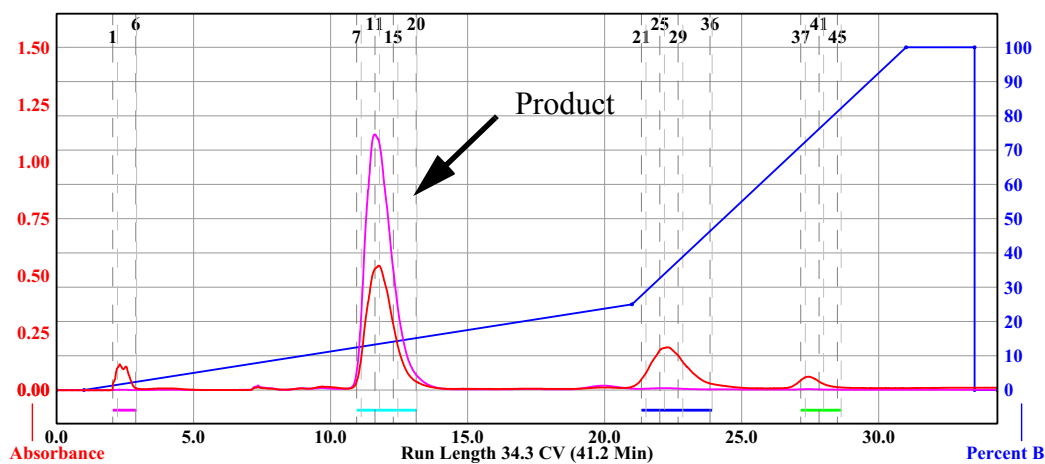
Solvent: A2 hexane

Threshold: 0.05 AU

Solvent: B2 ethyl acetate

Wavelength 2 (purple): 280nm

Run Notes: self-packed column, 50g



Rack A													Peak #	Start Tube	End Tube
108	107	106	105	104	103								1	A:1	A:6
97	98	99	100	101	102								2	A:7	A:20
96	95	94	93	92	91								3	A:21	A:36
85	86	87	88	89	90								4	A:37	A:45
84	83	82	81	80	79										
73	72	71	70	69	68										
72	71	70	69	68	67										
61	62	63	64	65	66										
60	59	58	57	56	55										
49	50	51	52	53	54										
48	47	46	45	44	43										
37	38	39	40	41	42										
36	35	34	33	32	31										
25	26	27	28	29	30										
14	15	16	17	18	19										
13	12	11	10	9	8										
2	3	4	5	6											

Duration	%B	Solvent A	Solvent B
0.0	0.0	A2 hexane	B2 ethyl acetate
1.0	0.0	A2 hexane	B2 ethyl acetate
20.0	25.0	A2 hexane	B2 ethyl acetate
10.0	100.0	A2 hexane	B2 ethyl acetate
2.5	100.0	A2 hexane	B2 ethyl acetate
0.0	0.0	A2 hexane	B2 ethyl acetate
0.8	0.0	A2 hexane	B2 ethyl acetate

13 mm x 100 mm Tubes

Page 1 of 1

Synthetic Methods

7.1.2.12 Hexyl 5-((3-fluorophenyl)amino)-2-(hexyloxy)benzoate: G5-061s9

In a 20 mL vial with a septum cap and equipped with a drying tube open to the air, **hexyl 5-amino-2-(hexyloxy)benzoate (G5-047s9)**, 82.95 mass% w/EtOAc, 1 mmol, 0.3909 g), 3-fluorophenylboronic acid (4 mmol, 0.5549 g), Cu(OAc)₂ (2.3 mmol, 0.313 g), triethylamine (7.5 mmol, 0.759 g, 1.045 mL), powdered vacuum oven dried 4 Å molecular sieves (1 g) and anhydrous dichloromethane (DCM, 10 mL) were combined. After stirring for 2 days, the reaction mixture was filtered through packed celite (~2 cm in a 60 mL sintered glass funnel), and washed with DCM. The filtrate was extracted with 5 M NH₄OH (2 x 75 mL) followed by an extraction with water (50 mL). The DCM phase was dried with MgSO₄, and after filtering, silica gel (~5 g) was added to the filtrate. This mixture was concentrated by rotatory evaporation to a powder, which was used as a dry-load for silica chromatography (**FIGURE 7.8**). Fractions 7-21 were combined and concentrated by rotatory evaporation (0.1487 g, 35.8% yield).

Notes: In climates drier than Portland, Oregon, 0.3 g of powdered molecular sieves should suffice. Also, if one were to repeat this experiment using 1 g of powdered molecular sieves, increasing the amount of DCM used would improve the stirrability of the reaction.

¹H-NMR δ (ppm)(DMSO-d₆): 8.27 (1 H, s), 7.38 (1 H, d, J = 2.88 Hz), 7.28 (1 H, dd, J = 8.88, 2.88 Hz), 7.16-7.23 (1 H, m), 7.09 (1 H, d, J = 8.96 Hz), 6.71-6.75 (1 H, m), 6.64 (1 H, dt, J = 11.92, 2.24 Hz), 6.49-6.55 (1 H, m), 4.20 (2 H, t, J =

Synthetic Methods

6.44 Hz), 3.98 (2 H, t, J = 6.32 Hz), 1.61-1.75 (4 H, m), 1.35-1.49 (4 H, m), 1.26-1.35 (8 H, m), 0.83-0.93 (6 H, m).

^{13}C -NMR δ (ppm)(DMSO- d_6): 166.0, 163.2 (1 C, d, J = 240.83 Hz), 152.6, 146.7 (1 C, d, J = 10.86 Hz), 134.8, 130.7 (1 C, d, J = 9.87 Hz), 124.5, 121.6, 121.2, 115.0, 110.7, 104.7 (1 C, d, J = 21.35 Hz), 100.9 (1 C, d, J = 24.99 Hz), 68.7, 64.5, 31.0, 30.9, 28.8, 28.2, 25.2 (2 C), 22.1, 22.0, 13.9 (2 C).

Synthetic Methods

FIGURE 7.8: Chromatographic purification of **G5-061s7**.

Sample: grandy5-061s7

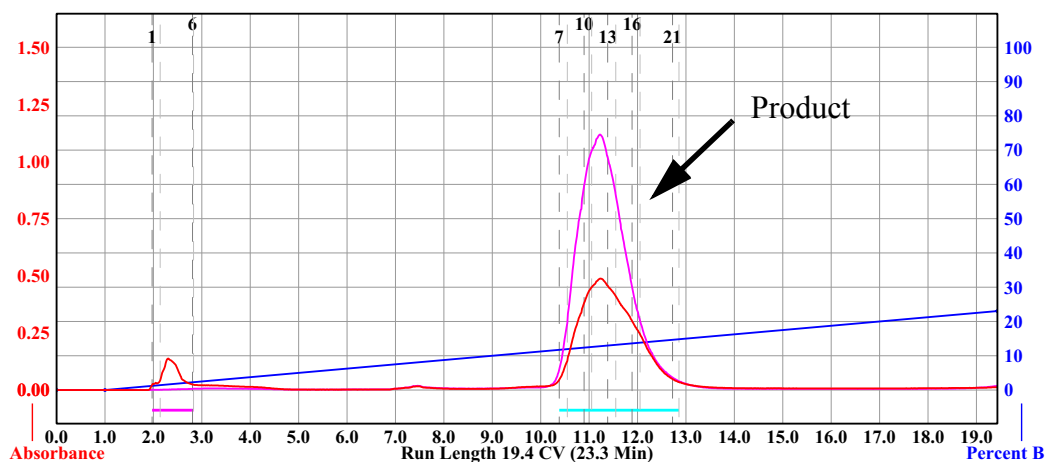
Rf 200 : OHSU COHEN RF200#1

Wednesday 22 August 2012 05:13PM

RediSep Column: Silica 40g
Flow Rate: 40 ml/min
Equilibration Volume: 5.0 CV
Initial Waste: 0.0 CV
Air Purge: 1.0 min
Solvent: A2 hexane
Solvent: B2 ethyl acetate

Peak Tube Volume: Max.
Non-Peak Tube Volume: Max.
Loading Type: Solid
Wavelength 1 (red): 254nm
Peak Width: 2 min
Threshold: 0.05 AU
Wavelength 2 (purple): 280nm

Run Notes: self-packed column, 50g



Rack A						Peak #	Start Tube	End Tube	
108	107	106	105	104	103	1	A:1	A:6	
97	98	99	100	101	102	2	A:7	A:21	
96	95	94	93	92	91				
85	86	87	88	89	90				
84	83	82	81	80	79				
73	74	75	76	77	78				
72	71	70	69	68	67				
61	62	63	64	65	66				
60	59	58	57	56	55				
49	50	51	52	53	54				
48	47	46	45	44	43				
37	38	39	40	41	42				
36	35	34	33	32	31				
25	26	27	28	29	30				
24	23	22	21	20	19				
13	14	15	16	17	18				
12	11	10	9	8	7				
1	2	3	4	5	6				
13 mm x 100 mm Tubes						Duration	%B	Solvent A	Solvent B
						0.0	0.0	A2 hexane	B2 ethyl acetate
						1.0	0.0	A2 hexane	B2 ethyl acetate
						18.4	23.0	A2 hexane	B2 ethyl acetate

Synthetic Methods

7.1.2.13 (2-(hexyloxy)-5-(phenylamino)phenyl)(pyrrolidin-1-yl)methanone: G5-112s5

In a 20 mL vial with a septum cap and equipped with a drying tube open to the air, **(5-amino-2-(hexyloxy)phenyl)(pyrrolidin-1-yl)methanone (G5-106s7**, 0.99 mmol, 0.2880 g), phenylboronic acid (1.5 mmol, 0.1859 g), Cu(OAc)₂ (2.3 mmol, 0.313 g), triethylamine (7.5 mmol, 0.759 g, 1.045 mL), powdered vacuum oven dried 4 Å molecular sieves (1 g) and anhydrous dichloromethane (DCM, 10 mL) were combined. After stirring for 4 days, the reaction mixture was filtered through a cotton ball packed into a 10 mL syringe body, and washed with DCM. Silica gel (~5 g) was added to the filtrate, and the resulting mixture was concentrated by rotatory evaporation to a powder, which was used as a dry-load for silica chromatography (**FIGURE 7.9**). Fractions 1-19 were combined and concentrated by rotatory evaporation to an oil that later crystallized (0.1646 g, 44.9% yield).

Notes: In climates drier than Portland, Oregon, 0.3 g of powdered molecular sieves should suffice. Also, if one were to repeat this experiment using 1 g of powdered molecular sieves, increasing the amount of DCM used would improve the stirrability of the reaction.

¹H-NMR δ (ppm)(DMSO-d₆): 7.92 (1 H, s), 7.16-7.22 (2 H, m), 7.07 (1 H, dd, J = 8.82, 2.78 Hz), 6.92-7.00 (3 H, m), 6.87 (1 H, d, J = 2.76 Hz), 6.72-6.78 (1 H, m), 3.94 (2 H, t, J = 6.23 Hz), 3.42 (2 H, t, J = 6.68 Hz), 3.11-3.21 (2 H, m), 1.74-

Synthetic Methods

1.89 (4 H, m), 1.60-1.69 (2 H, m), 1.35-1.44 (2 H, s), 1.24-1.35 (4 H, m), 0.88 (3 H, t, $J = 6.62$ Hz).

Synthetic Methods

FIGURE 7.9: Chromatographic purification of G5-112s4.

Sample: grandy5-112s4

Rf 200 : OHSU COHEN RF200#1

Monday 08 October 2012 02:32PM

RediSep Column: Silica 40g

Peak Tube Volume: Max.

Flow Rate: 40 ml/min

Non-Peak Tube Volume: Max.

Equilibration Volume: 240.0 ml

Loading Type: Solid

Initial Waste: 0.0 ml

Wavelength 1 (red): 254nm

Air Purge: 1.0 min

Peak Width: 2 min

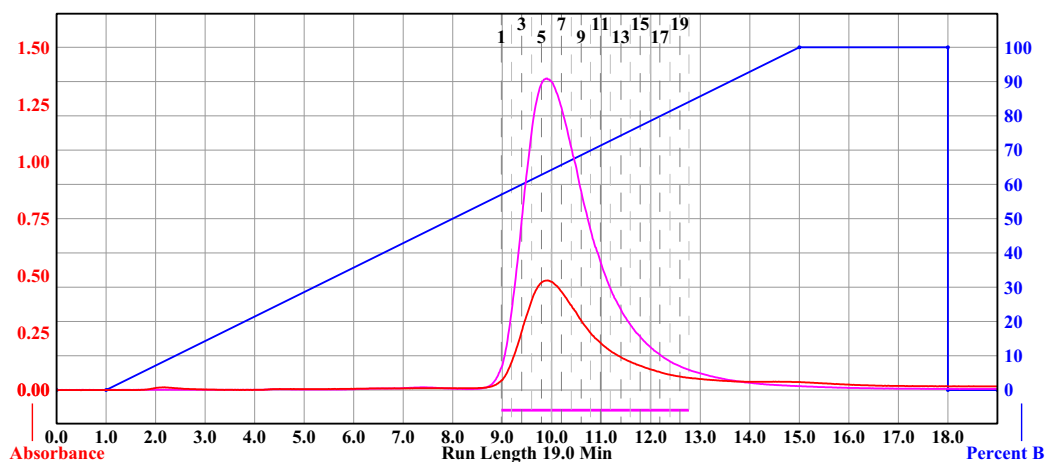
Solvent: A2 hexane

Threshold: 0.05 AU

Solvent: B2 ethyl acetate

Wavelength 2 (purple): 280nm

Run Notes: self-packed column



Rack A						Peak #	Start Tube	End Tube	
108	107	106	105	104	103	1	A:1	A:19	
97	98	99	100	101	102				
96	95	94	93	92	91				
85	86	87	88	89	90				
84	83	82	81	80	79				
73	74	75	76	77	78				
72	71	70	69	68	67				
61	62	63	64	65	66				
60	59	58	57	56	55				
49	50	51	52	53	54				
48	47	46	45	44	43				
37	38	39	40	41	42				
36	35	34	33	32	31				
25	26	27	28	29	30				
24	23	22	21	20	19				
13	14	15	16	17	18				
12	11	10	9	8	7				
1	2	3	4	5	6				
13 mm x 100 mm Tubes						Duration	%B	Solvent A	Solvent B
						0.0	0.0	A2 hexane	B2 ethyl acetate
						1.0	0.0	A2 hexane	B2 ethyl acetate
						14.0	100.0	A2 hexane	B2 ethyl acetate
						3.0	100.0	A2 hexane	B2 ethyl acetate
						0.0	0.0	A2 hexane	B2 ethyl acetate
						1.0	0.0	A2 hexane	B2 ethyl acetate

Synthetic Methods

7.1.2.14 (5-((4-fluorophenyl)amino)-2-(hexyloxy)phenyl)(pyrrolidin-1-yl)methanone: G5-113s5

In a 20 mL vial with a septum cap and equipped with a drying tube open to the air, **(5-amino-2-(hexyloxy)phenyl)(pyrrolidin-1-yl)methanone (G5-106s7**, 1.06 mmol, 0.3065 g), 4-fluorophenylboronic acid (1.5 mmol, 0.2128 g), Cu(OAc)₂ (2.3 mmol, 0.313 g), triethylamine (7.5 mmol, 0.759 g, 1.045 mL), powdered vacuum oven dried 4 Å molecular sieves (1 g) and anhydrous dichloromethane (DCM, 10 mL) were combined. After stirring for 4 days, the reaction mixture was filtered through a cotton ball packed into a 10 mL syringe body, and washed with DCM. Silica gel (~5 g) was added to the filtrate, and the resulting mixture was concentrated by rotatory evaporation to a powder, which was used as a dry-load for silica chromatography (**FIGURE 7.10**). Fractions 23-28 were combined and concentrated by rotatory evaporation to an oil that later crystallized (0.1578 g, 38.7% yield).

Notes: In climates drier than Portland, Oregon, 0.3 g of powdered molecular sieves should suffice. Also, if one were to repeat this experiment using 1 g of powdered molecular sieves, increasing the amount of DCM used would improve the stirrability of the reaction.

¹H-NMR δ (ppm)(DMSO-d₆): 7.87 (1 H, s), 6.92-7.08 (6 H, m), 6.81 (1 H, d, J = 2.69 Hz), 3.93 (2 H, t, J = 6.22 Hz), 3.41 (2 H, t, J = 6.80 Hz), 3.12-3.19 (2 H, m), 1.74-1.90 (4 H, m), 1.60-1.69 (2 H, m), 1.33-1.44 (2 H, m), 1.26-1.33 (4 H, m), 0.88 (3 H, t, J = 6.52 Hz).

Synthetic Methods

FIGURE 7.10: Chromatographic purification of **G5-113s4**.

Sample: grandy5-113s4

Rf 200 : OHSU COHEN RF200#1

Monday 08 October 2012 01:45PM

RediSep Column: Silica 40g

Peak Tube Volume: Max.

Flow Rate: 40 ml/min

Non-Peak Tube Volume: Max.

Equilibration Volume: 240.0 ml

Loading Type: Solid

Initial Waste: 0.0 ml

Wavelength 1 (red): 254nm

Air Purge: 1.0 min

Peak Width: 2 min

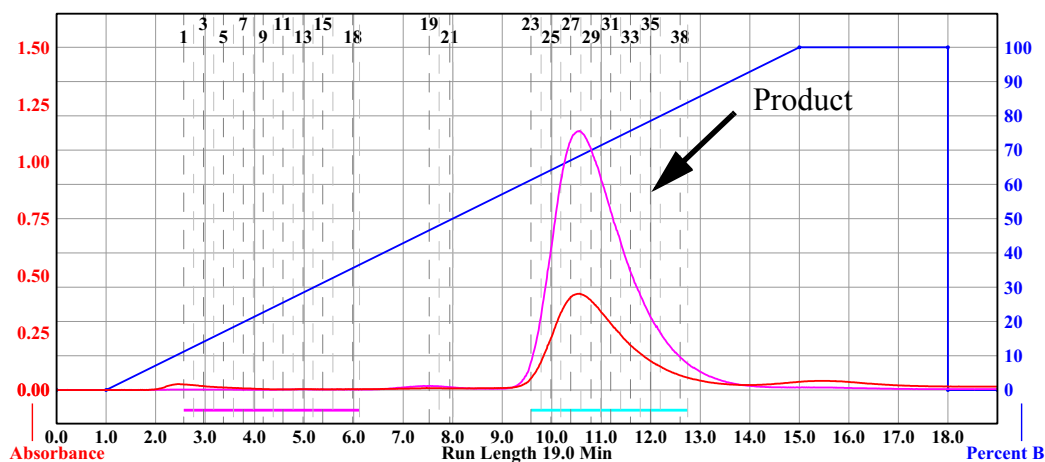
Solvent: A2 hexane

Threshold: 0.05 AU

Solvent: B2 ethyl acetate

Wavelength 2 (purple): 280nm

Run Notes: self-packed column



Rack A							Peak #	Start Tube	End Tube
108	107	106	105	104	103		1	A:1	A:18
97	98	99	100	101	102		2	A:23	A:38
96	95	94	93	92	91				
85	86	87	88	89	90				
84	83	82	81	80	79				
73	74	75	76	77	78				
72	71	70	69	68	67				
61	62	63	64	65	66				
60	59	58	57	56	55				
49	50	51	52	53	54				
48	47	46	45	44	43				
37	38	39	40	41	42				
26	25	24	23	22	21				
25	24	23	22	21	20				
14	15	16	17	18	19				
3	4	5	6	7	8				
2	1	0	9	8	7				
1	2	3	4	5	6				

13 mm x 100 mm Tubes

Page 1 of 1

Synthetic Methods

7.1.2.15 (5-((3-fluorophenyl)amino)-2-(hexyloxy)phenyl)(pyrrolidin-1-yl)methanone: G5-114s5

In a 20 mL vial with a septum cap and equipped with a drying tube open to the air, **(5-amino-2-(hexyloxy)phenyl)(pyrrolidin-1-yl)methanone (G5-106s7**, 0.83 mmol, 0.2406 g), 3-fluorophenylboronic acid (1.5 mmol, 0.1396 g), Cu(OAc)₂ (2.3 mmol, 0.313 g), triethylamine (7.5 mmol, 0.759 g, 1.045 mL), powdered vacuum oven dried 4 Å molecular sieves (1 g) and anhydrous dichloromethane (DCM, 10 mL) were combined. After stirring for 4 days, the reaction mixture was filtered through a cotton ball packed into a 10 mL syringe body, and washed with DCM. Silica gel (~5 g) was added to the filtrate, and the resulting mixture was concentrated by rotatory evaporation to a powder, which was used as a dry-load for silica chromatography (**FIGURE 7.11**). Fractions 1-15 were combined and concentrated by rotatory evaporation to an oil that later crystallized (0.1897 g, 59.4% yield).

Notes: In climates drier than Portland, Oregon, 0.3 g of powdered molecular sieves should suffice. Also, if one were to repeat this experiment using 1 g of powdered molecular sieves, increasing the amount of DCM used would improve the stirrability of the reaction.

¹H-NMR δ (ppm)(DMSO-d₆): 8.19 (1 H, s), 7.15-7.23 (1 H, m), 7.12 (1 H, dd, J = 8.80, 2.72 Hz), 7.02 (1 H, d, J = 8.83 Hz), 6.90 (1 H, d, J = 2.74 Hz), 6.70-6.74 (1 H, m), 6.63 (1 H, dt, J = 12.01, 2.29 Hz), 6.46-6.54 (1 H, m), 3.96 (2 H, t, J = 6.23 Hz), 3.42 (2 H, t, J = 6.67 Hz), 3.12-3.20 (2 H, m), 1.75-1.89 (4 H, m), 1.61-1.71 (2 H, m), 1.34-1.44 (2 H, m), 1.26-1.34 (4 H, m), 0.88 (3 H, t, J = 6.68 Hz).

Synthetic Methods

FIGURE 7.11: Chromatographic purification of **G5-114s4**.

Sample: grandy5-114s4

Rf 200 : OHSU COHEN RF200#1

Tuesday 09 October 2012 02:37PM

RediSep Column: Silica 40g

Peak Tube Volume: Max.

Flow Rate: 40 ml/min

Non-Peak Tube Volume: Max.

Equilibration Volume: 240.0 ml

Loading Type: Solid (Pause)

Initial Waste: 0.0 ml

Wavelength 1 (red): 254nm

Air Purge: 1.0 min

Peak Width: 2 min

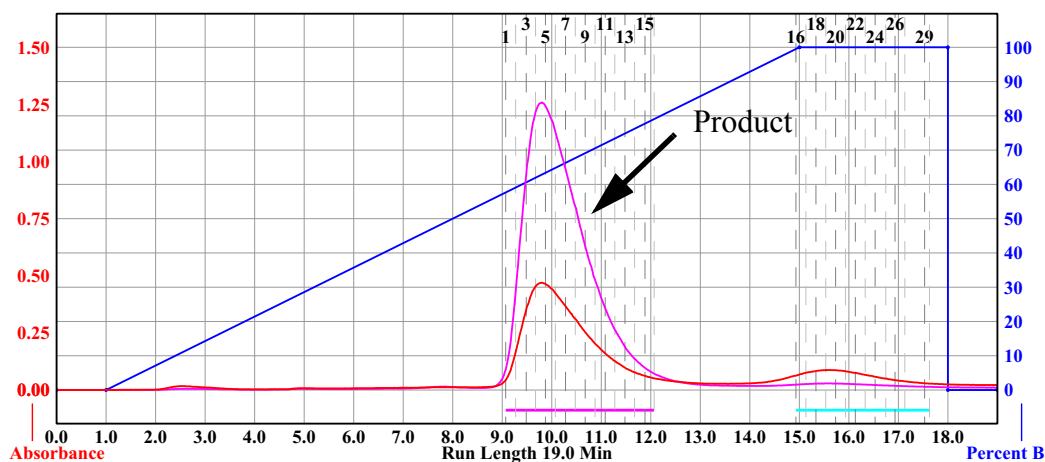
Solvent: A2 hexane

Threshold: 0.05 AU

Solvent: B2 ethyl acetate

Wavelength 2 (purple): 280nm

Run Notes:



Rack A							Peak #	Start Tube	End Tube
108	107	106	105	104	103		1	A:1	A:15
97	98	99	100	101	102		2	A:16	A:29
96	95	94	93	92	91				
85	86	87	88	89	90				
84	83	82	81	80	79				
73	74	75	76	77	78				
72	71	70	69	68	67				
61	62	63	64	65	66				
60	59	58	57	56	55				
49	50	51	52	53	54				
48	47	46	45	44	43				
37	38	39	40	41	42				
36	35	34	33	32	31				
25	26	27	28	29	30				
24	23	22	21	20	19				
13	14	15	16	17	18				
12	11	10	9	8	7				
1	2	3	4	5	6				

13 mm x 100 mm Tubes

Page 1 of 1

Synthetic Methods

7.1.2.16 3-(1,3-dioxolan-2-yl)-4-(hexyloxy)-*N*-phenylaniline: G5-125s6

In a 20 mL vial with a septum cap and equipped with a drying tube open to the air, **3-(1,3-dioxolan-2-yl)-4-(hexyloxy)aniline (G5-124s5)**, 2.2 mmol, 0.582 g), phenylboronic acid (3.3 mmol, 0.4024 g), Cu(OAc)₂ (4.8 mmol, 0.8718 g), triethylamine (16.5 mmol, 1.670 g, 2.3 mL), powdered vacuum oven dried 4 Å molecular sieves (1 g) and anhydrous dichloromethane (DCM, 10 mL) were combined. After stirring for 3 days, the reaction mixture was slurried with 1:3 mixture of silica gel and celite (~5 g total), and DCM. The slurry was filtered through a sintered glass funnel, and washed with DCM. Silica gel (~5 g) was added to the filtrate, and the resulting mixture was concentrated by rotatory evaporation to a powder, which was used as a dry-load for silica chromatography (**FIGURE 7.12**). Fractions 17-37 were combined and concentrated by rotatory evaporation to an oil that later crystallized (0.3039 g, 37.7% yield).

Notes: In climates drier than Portland, Oregon, 0.3 g of powdered molecular sieves should suffice. Also, if one were to repeat this experiment using 1 g of powdered molecular sieves, increasing the amount of DCM used would improve the stirrability of the reaction.

¹H-NMR δ (ppm)(DMSO-d₆): 7.89 (1 H, s), 7.13-7.21 (3 H, m), 7.08 (1 H, dd, J = 8.74, 2.86 Hz), 6.94 (1 H, d, J = 8.80 Hz), 6.88-6.93 (2 H, m), 6.69-6.75 (1 H, m), 5.96 (1 H, s), 4.00-4.04 (2 H, m), 3.88-3.99 (4 H, m), 1.65-1.75 (2 H, m), 1.38-1.48 (2 H, m), 1.28-1.35 (4 H, m), 0.89 (3 H, t, J = 6.77 Hz).

Synthetic Methods

^{13}C -NMR δ (ppm)(DMSO- d_6): 151.3, 144.9, 135.9, 129.1, 126.6, 120.4,
118.4, 117.9, 114.9, 113.5, 98.1, 68.5, 64.6, 30.9, 28.7, 25.1, 22.1, 13.9.

Synthetic Methods

7.1.2.17 3-(1,3-dioxolan-2-yl)-N-(4-fluorophenyl)-4-(hexyloxy)aniline: G5-126s6

In a 20 mL vial with a septum cap and equipped with a drying tube open to the air, **3-(1,3-dioxolan-2-yl)-4-(hexyloxy)aniline (G5-124s5)**, 2.66 mmol, 0.7052 g), 4-fluorophenylboronic acid (4.05 mmol, 0.5667 g), Cu(OAc)₂ (6 mmol, 1.090 g), triethylamine (20.25 mmol, 2.049 g, 2.822 mL), powdered vacuum oven dried 4 Å molecular sieves (1 g) and anhydrous dichloromethane (DCM, 10 mL) were combined. After stirring for 3 days, the reaction mixture was slurried with 1:3 mixture of silica gel and celite (~5 g total), and DCM. The slurry was filtered through a sintered glass funnel, and washed with DCM. Silica gel (~5 g) was added to the filtrate, and the resulting mixture was concentrated by rotatory evaporation to a powder, which was used as a dry-load for silica chromatography (**FIGURE 7.13**). Fractions 22-37 were combined and concentrated by rotatory evaporation to an oil that later crystallized (0.3211 g, 32.3% yield).

Notes: In climates drier than Portland, Oregon, 0.3 g of powdered molecular sieves should suffice. Also, if one were to repeat this experiment using 1 g of powdered molecular sieves, increasing the amount of DCM used would improve the stirrability of the reaction.

¹H-NMR δ (ppm)(DMSO-d₆): 7.84 (1 H, s), 7.12 (1 H, d, J = 2.84 Hz), 6.99-7.06 (3 H, m), 6.88-6.95 (3 H, m), 5.95 (1 H, s), 4.00-4.04 (2 H, m), 3.90-3.96 (4 H, m), 1.65-1.73 (2 H, m), 1.37-1.48 (2 H, m), 1.28-1.35 (4 H, m), 0.85-0.92 (3 H, m).

Synthetic Methods

FIGURE 7.13: Chromatographic purification of **G5-126s5**.

Sample: grandy5-126s

RediSep Column: Silica 40g

Flow Rate: 40 ml/min

Equilibration Volume: 5.0 CV

Initial Waste: 0.0 CV

Air Purge: 1.0 min

Solvent: A2 hexane

Solvent: B2 ethyl acetate

Rf 200 : OHSU COHEN RF200#1

Peak Tube Volume: Max.

Non-Peak Tube Volume: Max.

Loading Type: Solid

Wavelength 1 (red): 254nm

Peak Width: 2 min

Threshold: 0.05 AU

Wavelength 2 (purple): 280nm

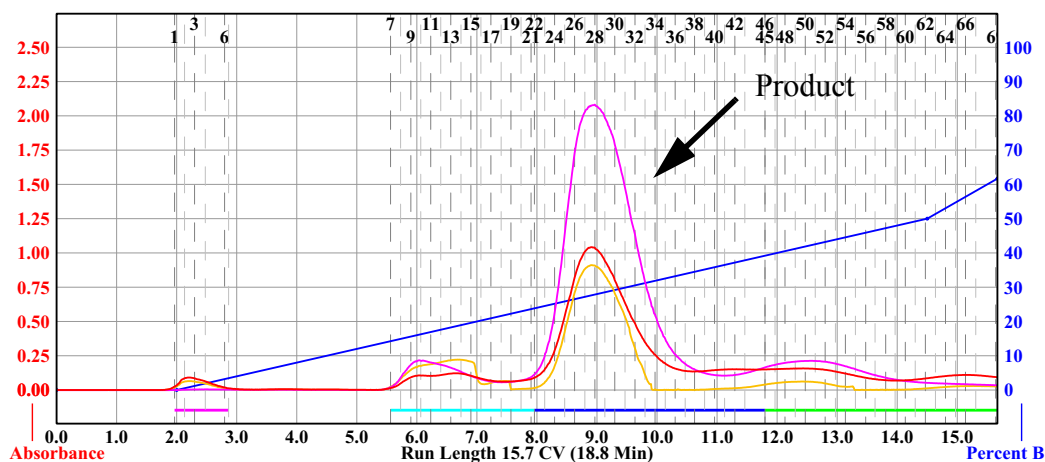
Wednesday 24 October 2012 01:21PM

All Wavelength (orange): 200nm - 360nm

Peak Width: 2 min

Threshold: 0.20 AU

Run Notes:



Rack A						Peak #	Start Tube	End Tube
108	107	106	105	104	103	1	A:1	A:6
97	98	99	100	101	102	2	A:7	A:21
96	95	94	93	92	91	3	A:22	A:45
85	86	87	88	89	90	4	A:46	A:69
84	83	82	81	80	79			
73	74	75	76	77	78			
72	71	70	69	68	67			
56	55	54	53	52	51			
40	39	38	37	36	35			
24	23	22	21	20	19			
8	7	6	5	4	3			
1	2	3	4	5	6			

Duration	%B	Solvent A	Solvent B
0.0	0.0	A2 hexane	B2 ethyl acetate
2.0	0.0	A2 hexane	B2 ethyl acetate
12.5	50.0	A2 hexane	B2 ethyl acetate
1.2	61.7	A2 hexane	B2 ethyl acetate

13 mm x 100 mm Tubes

Page 1 of 1

Synthetic Methods

7.1.2.18 3-(1,3-dioxolan-2-yl)-N-(3-fluorophenyl)-4-(hexyloxy)aniline: G5-127s6

In a 20 mL vial with a septum cap and equipped with a drying tube open to the air, **3-(1,3-dioxolan-2-yl)-4-(hexyloxy)aniline (G5-124s5)**, 2.64 mmol, 0.7011 g), 3-fluorophenylboronic acid (4.05 mmol, 0.5667 g), Cu(OAc)₂ (6 mmol, 1.090 g), triethylamine (20.25 mmol, 2.049 g, 2.822 mL), powdered vacuum oven dried 4 Å molecular sieves (1 g) and anhydrous dichloromethane (DCM, 10 mL) were combined. After stirring for 3 days, the reaction mixture was slurried with 1:3 mixture of silica gel and celite (~5 g total), and DCM. The slurry was filtered through a sintered glass funnel, and washed with DCM. Silica gel (~5 g) was added to the filtrate, and the resulting mixture was concentrated by rotatory evaporation to a powder, which was used as a dry-load for silica chromatography (**FIGURE 7.14**). Fractions 22-37 were combined and concentrated by rotatory evaporation to an oil that later crystallized (0.4405 g, 44.7% yield).

Notes: In climates drier than Portland, Oregon, 0.3 g of powdered molecular sieves should suffice. Also, if one were to repeat this experiment using 1 g of powdered molecular sieves, increasing the amount of DCM used would improve the stirrability of the reaction.

¹H-NMR δ (ppm)(DMSO-d₆): 8.17 (1 H, s), 7.10-7.21 (3 H, m), 6.98 (1 H, d, J = 8.75 Hz), 6.66-6.71 (1 H, m), 6.59 (1 H, dt, J = 12.09, 2.30 Hz), 6.44-6.51 (1 H, m), 5.97 (1 H, s), 3.89-4.04 (6 H, m), 1.66-1.75 (2 H, m), 1.38-1.49 (2 H, m), 1.31-1.32 (4 H, m), 0.89 (3 H, t, J = 6.74 Hz).

Synthetic Methods

FIGURE 7.14: Chromatographic purification of **G5-127s5**.

Sample: grandy5-127s5

RediSep Column: Silica 40g

Flow Rate: 40 ml/min

Equilibration Volume: 5.0 CV

Initial Waste: 0.0 CV

Air Purge: 1.0 min

Solvent: A2 hexane

Solvent: B2 ethyl acetate

Rf 200 : OHSU COHEN RF200#1

Peak Tube Volume: Max.

Non-Peak Tube Volume: Max.

Loading Type: Solid

Wavelength 1 (red): 254nm

Peak Width: 2 min

Threshold: 0.05 AU

Wavelength 2 (purple): 280nm

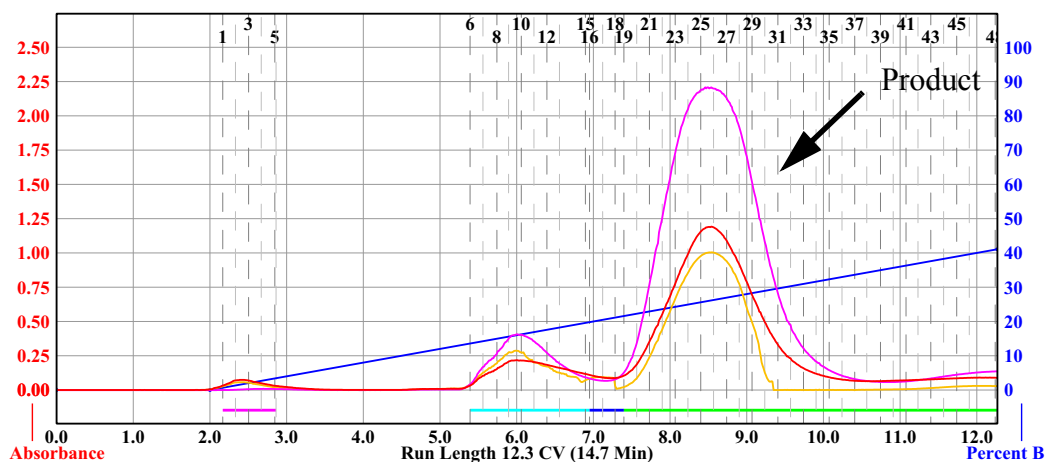
Wednesday 24 October 2012 01:52PM

All Wavelength (orange): 200nm - 360nm

Peak Width: 2 min

Threshold: 0.20 AU

Run Notes:



Rack A						Peak #	Start Tube	End Tube	
108	107	106	105	104	103	1	A:1	A:5	
97	98	99	100	101	102	2	A:6	A:15	
96	95	94	93	92	91	3	A:16	A:18	
85	86	87	88	89	90	4	A:19	A:48	
84	83	82	81	80	79				
73	72	71	70	69	68				
72	71	70	69	68	67				
61	62	63	64	65	66				
60	59	58	57	56	55				
49	50	51	52	53	54				
48	47	46	45	44	43				
37	38	39	40	41	42				
36	35	34	33	32	31				
25	26	27	28	29	30				
24	23	22	21	20	19				
13	14	15	16	17	18				
12	11	10	9	8	7				
1	2	3	4	5	6				
13 mm x 100 mm Tubes						Duration	%B	Solvent A	Solvent B
						0.0	0.0	A2 hexane	B2 ethyl acetate
						2.0	0.0	A2 hexane	B2 ethyl acetate
						10.3	41.1	A2 hexane	B2 ethyl acetate

Synthetic Methods

7.1.2.19 Hexyl 5-(benzylamino)-2-(hexyloxy)benzoate: G5-049s10

In a 20 mL vial, **hexyl 5-amino-2-(hexyloxy)benzoate (G5-047s9**, 82.95 mass% w/EtOAc, 3 mmol, 1.1669 g), and benzaldehyde (3 mmol, 0.3184 g, 0.305 mL) were dissolved in methanol (10 mL). The solution was stirred for 15 minutes, then NaBH₃CN (3.3 mmol, 0.2135 g) was slowly added, and the reaction stirred for another 18 hours. The reaction was worked-up by adding 1 M NaOH (3 mL), then extracting with hexanes (2 x 3 mL). The combined hexane phases were washed with water (3 mL), then dried with MgSO₄. After filtering, basic alumina (~2 g) was added to the filtrate. The mixture was concentrated by rotatory evaporation to a powder, which was used as a dry-load for silica chromatography (**FIGURE 7.15**). Fractions 3-8 were combined and concentrated by rotatory evaporation (0.6768 g, 54.7% yield).

¹H-NMR δ (ppm)(DMSO-d₆): 7.28-7.37 (4 H, m), 7.19-7.25 (1 H, m), 6.82-6.89 (2 H, m), 6.71 (1 H, dd, J = 8.83, 3.08 Hz), 6.10 (1 H, t, J = 6.10 Hz), 4.23 (2 H, d, J = 6.09 Hz), 4.15 (2 H, t, J = 6.48 Hz), 3.84 (2 H, t, J = 6.42 Hz), 1.58-1.68 (4 H, m), 1.34-1.43 (4 H, m), 1.25-1.34 (8 H, m), 0.84-0.91 (6 H, m).

¹³C-NMR δ (ppm)(DMSO-d₆): 166.6, 148.7, 142.5, 140.1, 128.2, 127.1, 126.6, 121.6, 116.7, 115.9, 113.8, 69.4, 64.2, 46.9, 31.0, 30.9, 28.9, 28.2, 25.2 (2 C), 22.1, 22.0, 13.9 (2 C).

Synthetic Methods

FIGURE 7.15: Chromatographic purification of **G5-049s7**.

Sample: grandy5-049s7

Rf 200 : OHSU COHEN RF200#1

Thursday 16 August 2012 02:04PM

RediSep Column: Silica 24g

Peak Tube Volume: Max.

Flow Rate: 35 ml/min

Non-Peak Tube Volume: Max.

Equilibration Volume: 5.0 CV

Loading Type: Solid (Pause)

Initial Waste: 0.0 CV

Wavelength 1 (red): 254nm

Air Purge: 1.0 min

Peak Width: 1 min

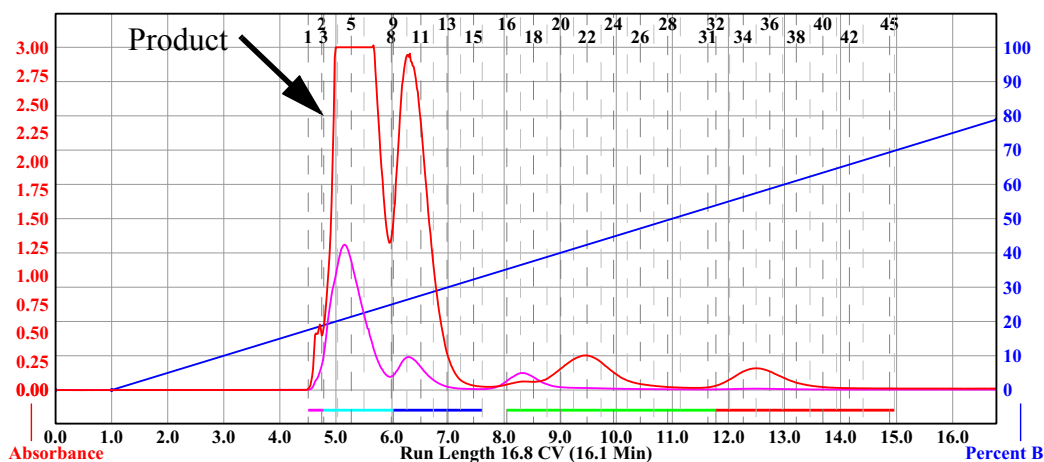
Solvent: A2 hexane

Threshold: 0.05 AU

Solvent: B2 ethyl acetate

Wavelength 2 (purple): 280nm

Run Notes:



Rack A						Peak #	Start Tube	End Tube
108	107	106	105	104	103	1	A:1	A:2
97	98	99	100	101	102	2	A:3	A:8
96	95	94	93	92	91	3	A:9	A:15
85	86	87	88	89	90	4	A:16	A:31
84	83	82	81	80	79	5	A:32	A:45
73	72	75	76	77	78			
72	71	70	69	68	67			
61	62	63	64	65	66			
60	59	58	57	56	55			
49	50	51	52	53	54			
48	47	46	45	44	43			
37	38	39	40	41	42			
36	35	34	33	32	31			
25	26	27	28	29	30			
24	23	22	21	20	19			
13	14	15	16	17	18			
12	11	10	9	8	7			
1	2	3	4	5	6			

Duration	%B	Solvent A	Solvent B
0.0	0.0	A2 hexane	B2 ethyl acetate
1.0	0.0	A2 hexane	B2 ethyl acetate
15.8	78.9	A2 hexane	B2 ethyl acetate

13 mm x 100 mm Tubes

Page 1 of 1

Synthetic Methods

7.1.2.20 Hexyl 2-(hexyloxy)-5-((4-fluorobenzyl)amino)benzoate: G5-050s10

In a 20 mL vial, **hexyl 5-amino-2-(hexyloxy)benzoate (G5-047s9**, 82.95 mass% w/EtOAc, 3 mmol, 1.1674 g), and 4-fluorobenzaldehyde (3 mmol, 0.3723 g, 0.3218 mL) were dissolved in methanol (10 mL). The solution was stirred for 15 minutes, then NaBH₃CN (3.3 mmol, 0.2101 g) was slowly added, and the reaction stirred for another 18 hours. The reaction was worked-up by adding 1 M NaOH (3 mL), then extracting with hexanes (2 x 3 mL). The combined hexane phases were washed with water (3 mL), then dried with MgSO₄. After filtering, basic alumina (~2 g) was added to the filtrate. The mixture was concentrated by rotatory evaporation to a powder, which was used as a dry-load for silica chromatography (**FIGURE 7.16**). Fractions 12-25 were combined and concentrated by rotatory evaporation to an oil (0.6987 g, 54.2% yield).

¹H-NMR δ (ppm)(DMSO-d₆): 7.34-7.40 (2 H, m), 7.10-7.17 (2 H, m), 6.86 (1 H, d, J = 8.88 Hz), 6.83 (1 H, d, J = 2.96 Hz), 6.70 (1 H, dd, J = 8.92, 3.00 Hz), 6.11 (1 H, t, J = 6.12 Hz), 4.21 (2 H, d, J = 6.04 Hz), 4.15 (2 H, t, J = 6.48 Hz), 3.84 (2 H, t, J = 6.44 Hz), 1.58-1.68 (4 H, m), 1.33-1.43 (4 H, m), 1.23-1.33 (8 H, m), 0.84-0.90 (6 H, m).

¹³C-NMR δ (ppm)(DMSO-d₆): 166.6, 161.0 (1 C, d, J = 241.76 Hz), 148.6 (1 C, d, J = 44.51 Hz), 142.3, 136.2 (1 C, d, J = 2.89 Hz), 129.0 (1 C, d, J = 8.03 Hz), 121.6, 116.7, 115.9, 115.0, 114.8, 113.9, 69.3, 64.2, 46.2, 31.0, 30.9, 28.9, 28.2, 25.2 (2 C), 22.1, 22.0, 13.9 (2 C).

Synthetic Methods

FIGURE 7.16: Chromatographic purification of **G5-050s7**.

Sample: grndy5-050s7

Rf 200 : OHSU COHEN RF200#1

Thursday 16 August 2012 03:51PM

RediSep Column: Silica 24g

Peak Tube Volume: Max.

SN: E041039E8A1DA Lot: 1920177010W

Non-Peak Tube Volume: Max.

Flow Rate: 35 ml/min

Loading Type: Solid

Equilibration Volume: 5.0 CV

Wavelength 1 (red): 254nm

Initial Waste: 0.0 CV

Peak Width: 1 min

Air Purge: 1.0 min

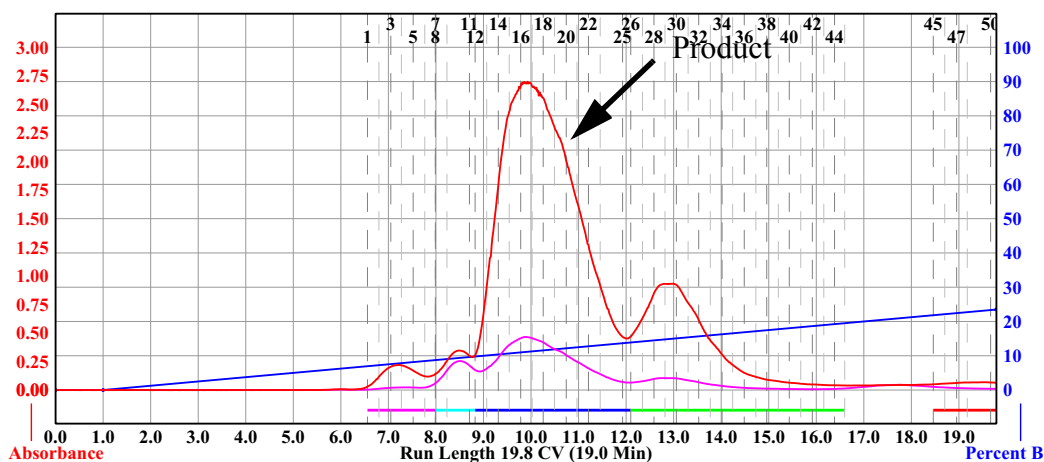
Threshold: 0.05 AU

Solvent: A2 hexane

Wavelength 2 (purple): 280nm

Solvent: B2 ethyl acetate

Run Notes:



Rack A												Peak #	Start Tube	End Tube
108	107	106	105	104	103							1	A:1	A:7
97	98	99	100	101	102							2	A:8	A:11
96	95	94	93	92	91							3	A:12	A:25
85	86	87	88	89	90							4	A:26	A:44
84	83	82	81	80	79							5	A:45	A:50
73	72	71	70	69	68									
72	71	70	69	68	67									
61	62	63	64	65	66									
60	59	58	57	56	55									
49	48	47	46	45	44									
48	47	46	45	44	43									
37	36	35	34	33	32									
36	35	34	33	32	31									
25	24	23	22	21	20									
24	23	22	21	20	19									
13	12	11	10	9	8									
12	11	10	9	8	7									
1	2	3	4	5	6									

13 mm x 100 mm Tubes

Duration	%B	Solvent A	Solvent B
0.0	0.0	A2 hexane	B2 ethyl acetate
1.0	0.0	A2 hexane	B2 ethyl acetate
18.8	23.5	A2 hexane	B2 ethyl acetate

Synthetic Methods

7.1.2.21 Hexyl 2-(hexyloxy)-5-((pyridin-2-ylmethyl)amino)benzoate: G5-051s10

In a 20 mL vial, **hexyl 5-amino-2-(hexyloxy)benzoate (G5-047s9, 82.95 mass% w/EtOAc, 3 mmol, 1.1627 g)**, and picolinaldehyde (3 mmol, 0.3213 g, 0.2854 mL) were dissolved in methanol (10 mL). The solution was stirred for 15 minutes, then NaBH_3CN (3.3 mmol, 0.2215 g) was slowly added, and the reaction stirred for another 18 hours. The reaction was worked-up by adding 1 M NaOH (3 mL), then extracting with hexanes (2 x 3 mL). The combined hexane phases were washed with water (3 mL), then dried with MgSO_4 . After filtering, silica (~2 g) was added to the filtrate. The mixture was concentrated by rotatory evaporation to a powder, which was used as a dry-load for silica chromatography (**FIGURE 7.17**). Fractions 31-54 were combined and concentrated by rotatory evaporation to an oil (0.68 g, 55.0% yield).

$^1\text{H-NMR}$ δ (ppm)(DMSO- d_6): 8.50-8.54 (1 H, m), 7.73 (1 H, td, $J = 7.67, 1.82$ Hz), 7.35 (1 H, d, $J = 7.86$ Hz), 7.22-7.27 (1 H, m), 6.87 (1 H, d, $J = 8.92$ Hz), 6.85 (1 H, d, $J = 3.00$ Hz), 6.71 (1 H, dd, $J = 8.87, 3.02$ Hz), 6.21 (1 H, t, $J = 6.16$ Hz), 4.32 (2 H, d, $J = 6.11$ Hz), 4.15 (2 H, d, $J = 6.48$ Hz), 3.84 (2 H, t, $J = 6.38$ Hz), 1.59-1.68 (4 H, m), 1.33-1.43 (4 H, m), 1.24-1.33 (8 H, m), 0.84-0.90 (6 H, m).

$^{13}\text{C-NMR}$ δ (ppm)(DMSO- d_6): 166.6, 159.7, 148.9, 142.3, 136.6, 122.0, 121.7, 121.0, 116.7, 115.9, 113.8, 69.3, 64.2, 49.0, 31.0, 30.9, 28.9, 28.2, 25.2, 25.1, 22.1, 22.0, 13.9 (2 C).

Synthetic Methods

FIGURE 7.17: Chromatographic purification of **G5-051s7**.

Sample: grandy5-051s7

Rf 200 : OHSU COHEN RF200#1

Friday 17 August 2012 02:18PM

RediSep Column: Silica 40g

Peak Tube Volume: Max.

SN: E04103BADFD88 Lot: 1922189010X

Non-Peak Tube Volume: Max.

Flow Rate: 40 ml/min

Loading Type: Solid

Equilibration Volume: 5.0 CV

Wavelength 1 (red): 254nm

Initial Waste: 0.0 CV

Peak Width: 2 min

Air Purge: 1.0 min

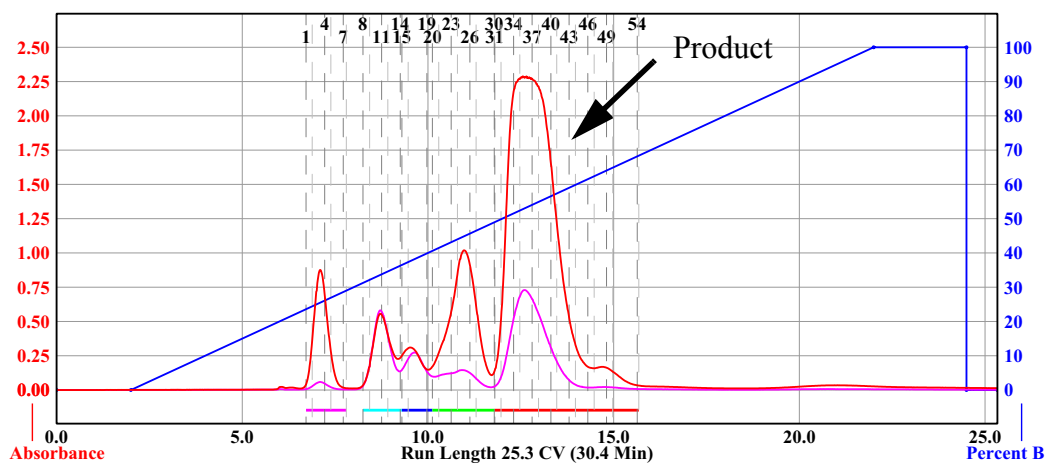
Threshold: 0.05 AU

Solvent: A2 hexane

Wavelength 2 (purple): 280nm

Solvent: B2 ethyl acetate

Run Notes:



Rack A						Peak #	Start Tube	End Tube	
108	107	106	105	104	103	1	A:1	A:7	
97	98	99	100	101	102	2	A:8	A:14	
96	95	94	93	92	91	3	A:15	A:19	
85	86	87	88	89	90	4	A:20	A:30	
84	83	82	81	80	79	5	A:31	A:54	
73	72	71	70	69	68				
72	71	70	69	68	67				
61	62	63	64	65	66				
60	59	58	57	56	55				
49	48	47	46	45	44				
48	47	46	45	44	43				
37	36	35	34	33	32				
26	25	24	23	22	21				
15	14	13	12	11	10				
4	3	2	1	0	0				
1	2	3	4	5	6				
13 mm x 100 mm Tubes						Duration	%B	Solvent A	Solvent B
						0.0	0.0	A2 hexane	B2 ethyl acetate
						2.0	0.0	A2 hexane	B2 ethyl acetate
						20.0	100.0	A2 hexane	B2 ethyl acetate
						2.5	100.0	A2 hexane	B2 ethyl acetate
						0.0	0.0	A2 hexane	B2 ethyl acetate
						0.8	0.0	A2 hexane	B2 ethyl acetate

Synthetic Methods

7.1.2.22 Hexyl 5-((2-fluorobenzyl)amino)-2-(hexyloxy)benzoate: G5-052s10

In a 20 mL vial, **hexyl 5-amino-2-(hexyloxy)benzoate (G5-047s9**, 82.95 mass% w/EtOAc, 3 mmol, 1.1617 g), and 2-fluorobenzaldehyde (3 mmol, 0.3723 g, 0.316 mL) were dissolved in methanol (10 mL). The solution was stirred for 15 minutes, then NaBH₃CN (3.3 mmol, 0.2070 g) was slowly added, and the reaction stirred for another 18 hours. The reaction was worked-up by adding 1 M NaOH (3 mL), then extracting with hexanes (2 x 3 mL). The combined hexane phases were washed with water (3 mL), then dried with MgSO₄. After filtering, basic alumina (~2 g) was added to the filtrate. The mixture was concentrated by rotatory evaporation to a powder, which was used as a dry-load for silica chromatography (**FIGURE 7.18**). Fractions 13-31 were combined and concentrated by rotatory evaporation to an oil (0.7858 g, 61.0% yield).

¹H-NMR δ (ppm)(DMSO-d₆): 7.39 (1 H, t, J = 7.72 Hz), 7.25-7.33 (1 H, m), 7.11-7.21 (2 H, m), 6.88 (1H, d, J = 8.92 Hz), 6.87 (1 H, d, J = 3.00 Hz), 6.73 (1 H, dd, J = 8.88, 3.04 Hz), 6.07 (1 H, t, J = 6.18 Hz), 4.27 (2 H, d, J = 6.12 Hz), 4.15 (2 H, t, J = 6.52 Hz), 3.85 (2 H, t, J = 6.34 Hz), 1.58-1.69 (4 H, m), 1.33-1.44 (4 H, m), 1.22-1.33 (8 H, m), 0.81-0.93 (6 H, m).

¹³C-NMR δ (ppm)(DMSO-d₆): 166.6, 160.3 (1 C, d, J = 243.65 Hz), 148.9, 142.2, 129.3 (1 C, d, J = 4.55 Hz), 128.6 (1 C, d, J = 8.16 Hz), 126.6 (1 C, d, J = 14.64 Hz), 124.3 (1 C, d, J = 3.20 Hz), 121.6, 116.6, 115.9, 115.0 (1 C, d, J = 21.31

Synthetic Methods

Hz), 113.7, 69.3, 64.2, 40.4 (1 C, d, $J = 3.88$ Hz), 31.0, 30.9, 28.9, 28.2, 25.2 (2 C),
22.1, 22.0, 13.9 (2 C).

Synthetic Methods

FIGURE 7.18: Chromatographic purification of **G5-052s7**.

Sample: grandy5-052s7

Rf 200 : OHSU COHEN RF200#1

Thursday 16 August 2012 03:11PM

RediSep Column: Silica 24g

Peak Tube Volume: Max.

SN: E041039E8CEB1 Lot: 1920177010W

Non-Peak Tube Volume: Max.

Flow Rate: 35 ml/min

Loading Type: Solid (Pause)

Equilibration Volume: 5.0 CV

Wavelength 1 (red): 254nm

Initial Waste: 0.0 CV

Peak Width: 1 min

Air Purge: 1.0 min

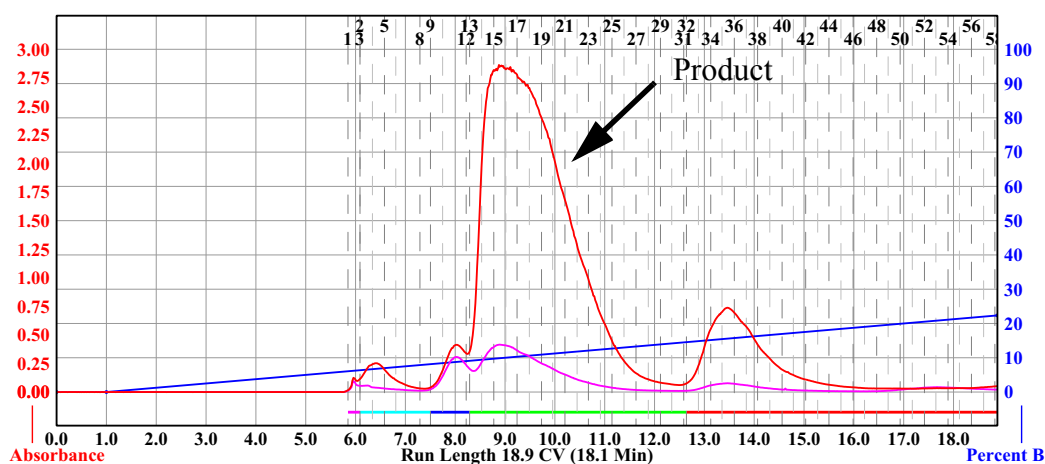
Threshold: 0.05 AU

Solvent: A2 hexane

Wavelength 2 (purple): 280nm

Solvent: B2 ethyl acetate

Run Notes:



Rack A						Peak #	Start Tube	End Tube
108	107	106	105	104	103	1	A:1	A:2
97	98	99	100	101	102	2	A:3	A:8
96	95	94	93	92	91	3	A:9	A:12
85	86	87	88	89	90	4	A:13	A:31
84	83	82	81	80	79	5	A:32	A:58
73	72	71	70	69	68			
72	71	70	69	68	67			
61	62	63	64	65	66			
60	59	58	57	56	55			
49	48	47	46	45	44			
48	47	46	45	44	43			
37	36	35	34	33	32			
36	35	34	33	32	31			
25	24	23	22	21	20			
24	23	22	21	20	19			
13	12	11	10	9	8			
12	11	10	9	8	7			
1	2	3	4	5	6			

Duration	%B	Solvent A	Solvent B
0.0	0.0	A2 hexane	B2 ethyl acetate
1.0	0.0	A2 hexane	B2 ethyl acetate
17.9	22.4	A2 hexane	B2 ethyl acetate

13 mm x 100 mm Tubes

Page 1 of 1

Synthetic Methods

7.1.2.23 Hexyl 5-((3-fluorobenzyl)amino)-2-(hexyloxy)benzoate: G5-053s10

In a 20 mL vial, **hexyl 5-amino-2-(hexyloxy)benzoate (G5-047s9, 82.95 mass% w/EtOAc, 3 mmol, 1.1658 g)**, and 3-fluorobenzaldehyde (3 mmol, 0.3723 g, 0.3182 mL) were dissolved in methanol (10 mL). The solution was stirred for 15 minutes, then NaBH_3CN (3.3 mmol, 0.20 g) was slowly added, and the reaction stirred for another 18 hours. The reaction was worked-up by adding 1 M NaOH (3 mL), then extracting with hexanes (2 x 3 mL). The combined hexane phases were washed with water (3 mL), then dried with MgSO_4 . After filtering, basic alumina (~2 g) was added to the filtrate. The mixture was concentrated by rotatory evaporation to a powder, which was used as a dry-load for silica chromatography (**FIGURE 7.19**). Fractions 11-26 were combined and concentrated by rotatory evaporation to an oil (0.7699 g, 59.7% yield).

$^1\text{H-NMR}$ δ (ppm)(DMSO-d_6): 7.32-7.40 (1 H, m), 7.19 (1 H, d, $J = 7.68$ Hz), 7.11-7.17 (1 H, m), 7.04 (1 H, td, $J = 8.61, 2.57$ Hz), 6.87 (1 H, d, $J = 8.86$ Hz), 6.84 (1 H, d, $J = 2.96$ Hz), 6.70 (1 H, dd, $J = 8.87, 2.98$ Hz), 6.17 (1 H, t, $J = 6.21$ Hz), 4.26 (2 H, d, $J = 6.16$ Hz), 4.15 (2 H, t, $J = 6.49$ Hz), 3.84 (2 H, t, $J = 6.37$ Hz), 1.58-1.68 (4 H, m), 1.33-1.43 (4 H, m), 1.24-1.33 (8 H, m), 0.83-0.90 (6 H, m).

$^{13}\text{C-NMR}$ δ (ppm)(DMSO-d_6): 166.6, 162.3 (1 C, d, $J = 243.38$ Hz), 148.9, 143.5 (1 C, d, $J = 6.75$ Hz), 142.2, 130.1 (1 C, d, $J = 8.24$ Hz), 123.0 (1 C, d, $J = 2.34$ Hz), 121.6, 116.3 (1 C, d, $J = 88.03$ Hz), 113.9, 113.7, 113.5 (1 C, d, $J = 8.78$

Synthetic Methods

Hz), 113.2, 69.3, 64.2, 46.4, 31.0, 30.9, 28.9, 28.2, 25.2, 25.1, 22.1, 22.0, 13.9 (2

C).

Synthetic Methods

FIGURE 7.19: Chromatographic purification of **G5-053s7**.

Sample: grandy5-053s7

Rf 200 : OHSU COHEN RF200#1

Thursday 16 August 2012 02:33PM

RediSep Column: Silica 24g

Peak Tube Volume: Max.

SN: E041037FE8E71 Lot: 1916333010W

Non-Peak Tube Volume: Max.

Flow Rate: 35 ml/min

Loading Type: Solid

Equilibration Volume: 5.0 CV

Wavelength 1 (red): 254nm

Initial Waste: 0.0 CV

Peak Width: 1 min

Air Purge: 1.0 min

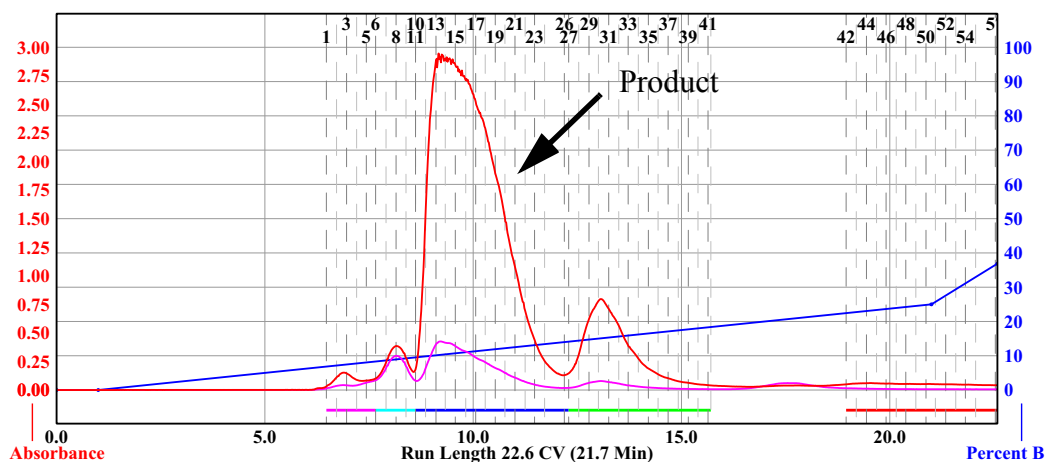
Threshold: 0.05 AU

Solvent: A2 hexane

Wavelength 2 (purple): 280nm

Solvent: B2 ethyl acetate

Run Notes:



Rack A						Peak #	Start Tube	End Tube	
108	107	106	105	104	103	1	A:1	A:5	
97	98	99	100	101	102	2	A:6	A:10	
96	95	94	93	92	91	3	A:11	A:26	
85	86	87	88	89	90	4	A:27	A:41	
84	83	82	81	80	79	5	A:42	A:57	
73	72	75	76	77	78				
72	71	70	69	68	67				
61	62	63	64	65	66				
60	59	58	57	56	55				
49	48	47	46	45	44				
48	47	46	45	44	43				
37	36	35	34	33	32				
36	35	34	33	32	31				
25	24	23	22	21	20				
24	23	22	21	20	19				
13	12	11	10	9	8				
12	11	10	9	8	7				
1	2	3	4	5	6				
13 mm x 100 mm Tubes						Duration	%B	Solvent A	Solvent B
						0.0	0.0	A2 hexane	B2 ethyl acetate
						1.0	0.0	A2 hexane	B2 ethyl acetate
						20.0	25.0	A2 hexane	B2 ethyl acetate
						1.6	36.9	A2 hexane	B2 ethyl acetate

Page 1 of 1

Synthetic Methods

7.1.2.24 (5-(benzylamino)-2-(hexyloxy)phenyl)(pyrrolidin-1-yl)methanone: G5-103s10

In a 20 mL vial, **(5-amino-2-(hexyloxy)phenyl)(pyrrolidin-1-yl)methanone (G5-101s5)**, 1 mmol, 0.290 g), and benzaldehyde (1 mmol, 0.1061 g, 0.102 mL) were dissolved in methanol (10 mL). The solution was stirred for 15 minutes, then NaBH₃CN (1.1 mmol, 0.0691 g) was added, and the reaction stirred for another 18 hours. The reaction was worked-up by adding 1 M NaOH (3 mL), then extracted with hexanes (5 x 3 mL). The combined hexane phases were washed with water (3 mL), then dried with MgSO₄. The hexane extractions were not effective, so the aqueous phase was diluted with water (15 mL), then extracted with ethyl acetate (EtOAc, 3 x 10 mL), and finally dried with MgSO₄. After filtering, the hexane and EtOAc solutions were combined, and concentrated by rotatory evaporation to a yellow oil, which was purified by silica chromatography (**FIGURE 7.20**). Fractions 15-30 were combined and concentrated by rotatory evaporation.

¹H-NMR δ (ppm)(DMSO-d₆): 7.29-7.38 (4 H, m), 7.19-7.25 (1 H, m), 6.79 (1 H, d, J = 8.83 Hz), 6.54 (1 H, dd, J = 8.83, 2.88 Hz), 6.40 (1 H, d, J = 2.86 Hz), 5.95 (1 H, t, J = 6.06 Hz), 4.21 (2 H, d, J = 6.01 Hz), 3.82 (2 H, t, J = 6.22 Hz), 3.38 (2 H, t, J = 6.82 Hz), 3.06 (2 H, m), 1.70-1.87 (4 H, m), 1.54-1.63 (2 H, m), 1.32-1.39 (2 H, m), 1.23-1.32 (4 H, m), 0.84-0.90 (3 H, t, J = 6.66 Hz).

Synthetic Methods

FIGURE 7.20: Chromatographic purification of G5-103s8.

Sample: grandy5-103s8

Rf 200 : PDX-PEYTON RF200#1

Monday 01 October 2012 11:13AM

RediSep Column: Silica 40g

Peak Tube Volume: Max.

SN: E0410597A508F Lot: 2112259020X

Non-Peak Tube Volume: Max.

Flow Rate: 40 ml/min

Loading Type: Solid (Pause)

Equilibration Volume: 5.0 CV

Wavelength 1 (red): 254nm

Initial Waste: 0.0 CV

Peak Width: 2 min

Air Purge: 1.0 min

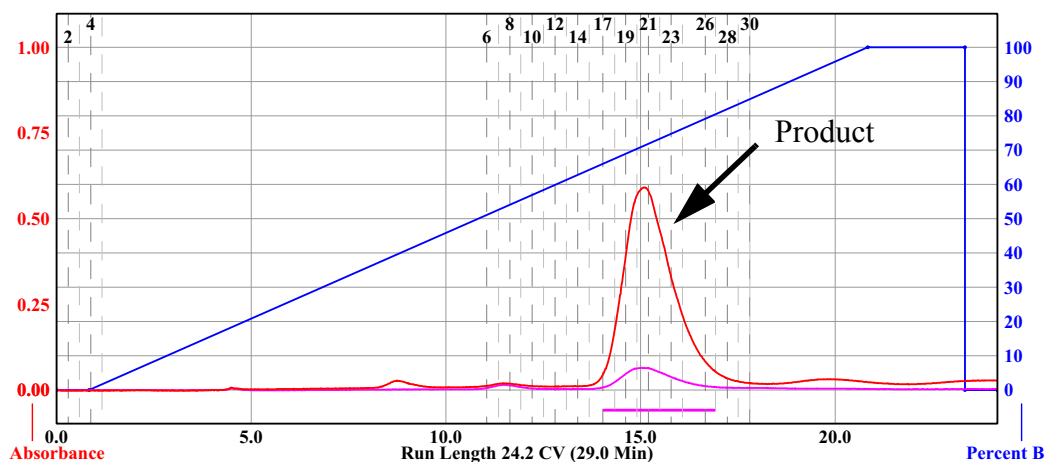
Threshold: 0.05 AU

Solvent: A1 hexane

Wavelength 2 (purple): 280nm

Solvent: B1 ethyl acetate

Run Notes:



Rack A					Peak #	Start Tube	End Tube	
71	72	73	74	75	1	A:17	A:26	
70	69	68	67	66				
61	62	63	64	65				
60	59	58	57	56				
51	52	53	54	55				
50	49	48	47	46				
41	42	43	44	45				
40	39	38	37	36				
31	32	33	34	35				
30	29	28	27	26				
21	22	23	24	25	Duration	%B	Solvent A	Solvent B
20	19	18	17	16				
11	12	13	14	15				
10	9	8	7	6				
1	2	3	4	5				
16 mm x 150 mm Tubes								
					0.0	0.0	A1 hexane	B1 ethyl acetate
					0.8	0.0	A1 hexane	B1 ethyl acetate
					20.0	100.0	A1 hexane	B1 ethyl acetate
					2.5	100.0	A1 hexane	B1 ethyl acetate
					0.0	0.0	A1 hexane	B1 ethyl acetate
					0.8	0.0	A1 hexane	B1 ethyl acetate

Synthetic Methods

7.1.2.25 (5-((4-fluorobenzyl)amino)-2-(hexyloxy)phenyl)(pyrrolidin-1-yl)methanone: G5-108s10

In a 20 mL vial, **(5-amino-2-(hexyloxy)phenyl)(pyrrolidin-1-yl)methanone (G5-106s7)**, 1 mmol, 0.2889 g, and 4-fluorobenzaldehyde (1 mmol, 0.1241 g, 0.1073 mL) were dissolved in methanol (10 mL). The solution was stirred for 15 minutes, then NaBH₃CN (1.59 mmol, 0.10 g) was added, and the reaction stirred for another 18 hours. The reaction was worked-up by adding 1 M NaOH (3 mL), then extracted with ethyl acetate (EtOAc, 2 x 5 mL), and finally dried with MgSO₄. After filtering, silica gel (~2 g) was added to the filtrate. The mixture was concentrated by rotatory evaporation to a powder, which was used as a dry-load for by silica chromatography (**FIGURE 7.21**). Fractions 1-27 were combined, using dichloromethane to aid the transfer, and concentrated by rotatory evaporation (0.4902 g gross, 42.9 mol% w/EtOAc by NMR, 77.23 mass%, ~ 0.3786 g net, ~95% yield).

¹H-NMR δ (ppm)(DMSO-d₆): 7.35-7.41 (2 H, m), 7.10-7.17 (2 H, m), 6.79 (1 H, d, J = 8.83 Hz), 6.53 (1 H, d, J = 8.86, 2.90 Hz), 6.39 (1 H, d, J = 2.86 Hz), 5.96 (1 H, t, J = 6.12 Hz), 4.20 (2 H, d, J = 6.14 Hz), 3.82 (2 H, t, J = 6.26 Hz), 3.37 (2 H, t, J = 6.78 Hz), 3.00-3.13 (2 H, m), 1.70-1.83 (4 H, m), 1.54-1.65 (2 H, m), 1.30-1.39 (2 H, m), 1.22-1.30 (4 H, m), 0.87 (3 H, t, J = 6.73 Hz).

Synthetic Methods

FIGURE 7.21: Chromatographic purification of **G5-108s7**.

Sample: grandy5-108s7

Rf 200 : OHSU COHEN RF200#1

Wednesday 10 October 2012 02:52PM

RediSep Column: Silica 40g

Peak Tube Volume: Max.

Flow Rate: 40 ml/min

Non-Peak Tube Volume: Max.

Equilibration Volume: 240.0 ml

Loading Type: Solid

Initial Waste: 0.0 ml

Wavelength 1 (red): 254nm

Air Purge: 1.0 min

Peak Width: 2 min

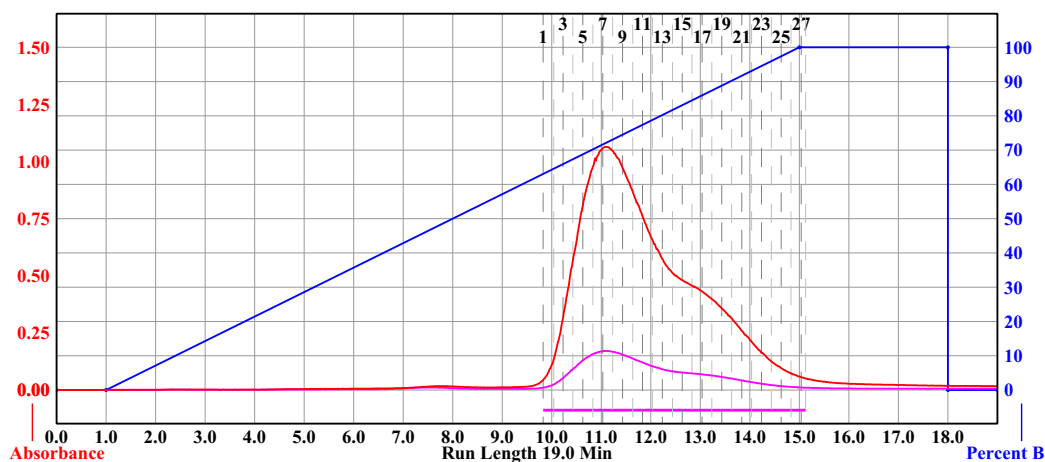
Solvent: A2 hexane

Threshold: 0.05 AU

Solvent: B2 ethyl acetate

Wavelength 2 (purple): 280nm

Run Notes:



Rack A							Peak #	Start Tube	End Tube
108	107	106	105	104	103		1	A:1	A:27
97	98	99	100	101	102				
96	95	94	93	92	91				
85	86	87	88	89	90				
84	83	82	81	80	79				
73	74	75	76	77	78				
72	71	70	69	68	67				
61	62	63	64	65	66				
60	59	58	57	56	55				
49	50	51	52	53	54				
48	47	46	45	44	43				
37	38	39	40	41	42				
36	35	34	33	32	31				
25	26	27	28	29	30				
24	23	22	21	20	19				
13	14	15	16	17	18				
12	11	10	9	8	7				
1	2	3	4	5	6				

13 mm x 100 mm Tubes

Page 1 of 1

Synthetic Methods

7.1.2.26 (5-((3-fluorobenzyl)amino)-2-(hexyloxy)phenyl)(pyrrolidin-1-yl)methanone: G5-109s8

In a 20 mL vial, **(5-amino-2-(hexyloxy)phenyl)(pyrrolidin-1-yl)methanone (G5-106s7)**, 1 mmol, 0.2990 g), and 3-fluorobenzaldehyde (1 mmol, 0.1241 g, 0.1061 mL) were dissolved in methanol (10 mL). The solution was stirred for 15 minutes, then NaBH₃CN (1.59 mmol, 0.10 g) was added, and the reaction stirred for another 18 hours. The reaction was worked-up by adding 1 M NaOH (3 mL), then extracted with ethyl acetate (EtOAc, 2 x 5 mL), and finally dried with MgSO₄. After filtering, silica gel (~2 g) was added to the filtrate. The mixture was concentrated by rotatory evaporation to a powder, which was used as a dry-load for silica chromatography (**FIGURE 7.22**). Fractions 1-18 were combined, using dichloromethane to aid the transfer, and concentrated by rotatory evaporation.

¹H-NMR δ (ppm)(DMSO-d₆): 7.31-7.40 (1 H, m), 7.17-7.21 (1 H, m), 7.12-7.17 (1 H, m), 7.00-7.07 (1 H, m), 6.80 (1 H, d, J = 8.84 Hz), 6.53 (1 H, dd, J = 8.83, 2.89 Hz), 6.39 (1 H, d, J = 2.86 Hz), 6.02 (1 H, t, J = 6.23 Hz), 4.24 (2 H, d, J = 6.18 Hz), 3.82 (2 H, t, J = 6.22 Hz), 3.38 (2 H, t, J = 6.80 Hz), 3.06 (2 H, m), 1.71-1.87 (4 H, m), 1.54-1.64 (2 H, m), 1.31-1.39 (2 H, m), 1.23-1.31 (4 H, m), 0.87 (3 H, t, J = 6.72 Hz).

Synthetic Methods

FIGURE 7.22: Chromatographic purification of G5-109s7.

Sample: grandy5-109s7

Rf 200 : OHSU COHEN RF200#1

Wednesday 10 October 2012 03:27PM

RediSep Column: Silica 40g

Peak Tube Volume: Max.

Flow Rate: 40 ml/min

Non-Peak Tube Volume: Max.

Equilibration Volume: 240.0 ml

Loading Type: Solid

Initial Waste: 0.0 ml

Wavelength 1 (red): 254nm

Air Purge: 1.0 min

Peak Width: 2 min

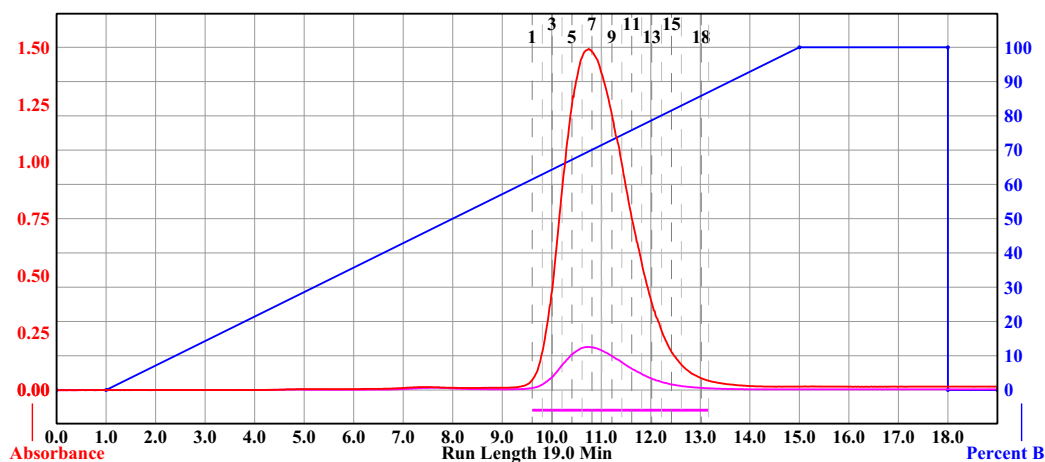
Solvent: A2 hexane

Threshold: 0.05 AU

Solvent: B2 ethyl acetate

Wavelength 2 (purple): 280nm

Run Notes:



Rack A							Peak #	Start Tube	End Tube
108	107	106	105	104	103		1	A:1	A:18
97	98	99	100	101	102				
86	85	84	83	82	81				
85	86	87	88	89	90				
84	83	82	81	80	79				
73	74	75	76	77	78				
72	71	70	69	68	67				
61	62	63	64	65	66				
60	59	58	57	56	55				
49	50	51	52	53	54				
48	47	46	45	44	43				
37	38	39	40	41	42				
36	35	34	33	32	31				
25	26	27	28	29	30				
24	23	22	21	20	19				
13	14	15	16	17	18				
12	11	10	9	8	7				
1	2	3	4	5	6				

13 mm x 100 mm Tubes

Page 1 of 1

Synthetic Methods

7.1.2.27 (5-((2-fluorobenzyl)amino)-2-(hexyloxy)phenyl)(pyrrolidin-1-yl)methanone: G5-110s8

In a 20 mL vial, **(5-amino-2-(hexyloxy)phenyl)(pyrrolidin-1-yl)methanone (G5-106s7)**, 1 mmol, 0.2857 g, and 2-fluorobenzaldehyde (1 mmol, 0.1241 g, 0.1053 mL) were dissolved in methanol (10 mL). The solution was stirred for 15 minutes, then NaBH₃CN (1.59 mmol, 0.10 g) was added, and the reaction stirred for another 18 hours. The reaction was worked-up by adding 1 M NaOH (3 mL), then extracted with ethyl acetate (EtOAc, 2 x 5 mL), and finally dried with MgSO₄. After filtering, silica gel (~2 g) was added to the filtrate. The mixture was concentrated by rotatory evaporation to a powder, which was used as a dry-load for silica chromatography (**FIGURE 7.23**). Fractions 1-19 were combined, using dichloromethane to aid the transfer, and concentrated by rotatory evaporation.

¹H-NMR δ (ppm)(DMSO-d₆): 7.37-7.43 (1 H, m), 7.25-7.33 (1 H, m), 7.12-7.21 (2 H, m), 6.81 (1 H, d, J = 8.82 Hz), 6.56 (1 H, dd, J = 8.82, 2.89 Hz), 6.42 (1 H, d, J = 2.85 Hz), 5.91 (1 H, t, J = 6.15 Hz), 4.25 (2 H, d, J = 6.08 Hz), 3.83 (2 H, t, J = 6.20 Hz), 3.38 (2 H, t, J = 6.74 Hz), 3.03-3.12 (2 H, m), 1.71-1.88 (4 H, m), 1.54-1.64 (2 H, m), 1.31-1.40 (2 H, m), 1.23-1.31 (4 H, m), 0.87 (3 H, t, J = 6.53 Hz).

Synthetic Methods

FIGURE 7.23: Chromatographic purification of **G5-110s7**.

Sample: grandy5-110s7

RediSep Column: Silica 40g

Flow Rate: 40 ml/min

Equilibration Volume: 240.0 ml

Initial Waste: 0.0 ml

Air Purge: 1.0 min

Solvent: A2 hexane

Solvent: B2 ethyl acetate

Rf 200 : OHSU COHEN RF200#1

Wednesday 07 November 2012 02:28PM

Peak Tube Volume: Max.

Non-Peak Tube Volume: Max.

Loading Type: Solid

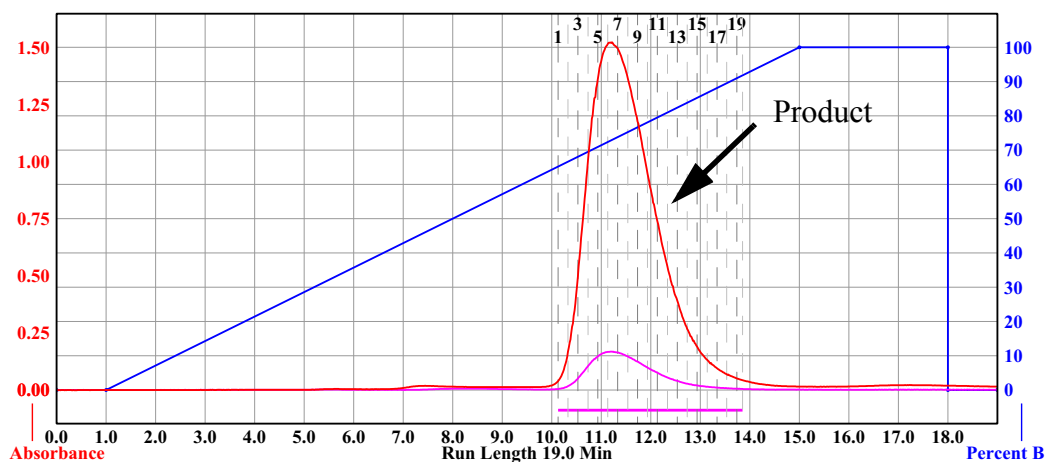
Wavelength 1 (red): 254nm

Peak Width: 2 min

Threshold: 0.05 AU

Wavelength 2 (purple): 280nm

Run Notes:



Rack A							Peak #	Start Tube	End Tube
108	107	106	105	104	103		1	A:1	A:19
97	98	99	100	101	102				
86	85	84	83	82	81				
75	76	77	78	79	80				
64	65	66	67	68	69				
53	54	55	56	57	58				
42	43	44	45	46	47				
31	32	33	34	35	36				
20	21	22	23	24	25				
9	10	11	12	13	14				
1	2	3	4	5	6				

13 mm x 100 mm Tubes

Page 1 of 1

Synthetic Methods

7.1.2.28 (2-(hexyloxy)-5-((pyridin-2-ylmethyl)amino)phenyl)(pyrrolidin-1-yl)methanone: G5-111s8

In a 20 mL vial, **(5-amino-2-(hexyloxy)phenyl)(pyrrolidin-1-yl)methanone (G5-106s7)**, 1 mmol, 0.2919 g), and picolinaldehyde (1 mmol, 0.1071 g, 0.0951 mL) were dissolved in methanol (10 mL). The solution was stirred for 15 minutes, then NaBH_3CN (1.59 mmol, 0.10 g) was added, and the reaction stirred for another 18 hours. The reaction was worked-up by adding 1 M NaOH (3 mL), then extracted with ethyl acetate (EtOAc, 2 x 5 mL), and finally dried with MgSO_4 . After filtering, silica gel (~2 g) was added to the filtrate. The mixture was concentrated by rotatory evaporation to a powder, which was used as a dry-load for silica chromatography (**FIGURE 7.23**). Fractions 14-45 were combined, using dichloromethane to aid the transfer, and concentrated by rotatory evaporation.

$^1\text{H-NMR}$ δ (ppm)(DMSO-d_6): 8.52 (1 H, ddd, $J = 4.82, 1.72, 0.90$ Hz), 7.73 (1 H, td, $J = 7.66, 1.83$ Hz), 7.36 (1 H, d, $J = 7.86$ Hz), 7.22-7.27 (1 H, m), 6.80 (1 H, d, $J = 8.82$ Hz), 6.54 (1 H, dd, $J = 8.80, 2.95$ Hz), 6.40 (1 H, d, $J = 2.89$ Hz), 6.08 (1 H, t, $J = 6.16$ Hz), 4.31 (2 H, d, $J = 6.12$ Hz), 3.82 (2 H, t, $J = 6.23$ Hz), 3.03-3.09 (2 H, m), 1.70-1.87 (4 H, m), 1.54-1.63 (2 H, m), 1.29-1.38 (2 H, m), 1.22-1.29 (4 H, m), 0.87 (3 H, t, $J = 6.67$ Hz).

$^{13}\text{C-NMR}$ δ (ppm)(DMSO-d_6): 166.7, 159.8, 148.8, 145.4, 142.7, 136.6, 128.6, 121.9, 121.1, 114.5, 113.2, 111.3, 68.7, 49.1, 46.8, 45.0, 30.9, 28.9, 25.4, 25.2, 24.1, 22.1, 13.8.

Synthetic Methods

FIGURE 7.24: Chromatographic purification of **G5-111s7**.

Sample: grandy5-111s7

RediSep Column: Silica 40g

Flow Rate: 40 ml/min

Equilibration Volume: 5.0 CV

Initial Waste: 0.0 CV

Air Purge: 1.0 min

Solvent: A1 ethyl acetate

Solvent: B1 methanol

Rf 200 : OHSU COHEN RF200#1

Peak Tube Volume: Max.

Non-Peak Tube Volume: Max.

Loading Type: Solid

Wavelength 1 (red): 254nm

Peak Width: 2 min

Threshold: 0.05 AU

Wavelength 2 (purple): 280nm

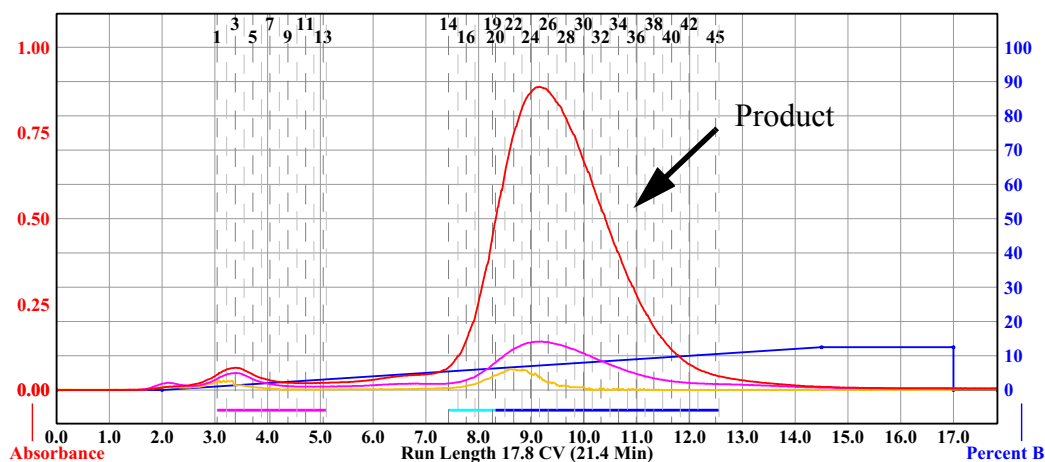
Friday 09 November 2012 12:41PM

All Wavelength (orange): 200nm - 360nm

Peak Width: 2 min

Threshold: 0.20 AU

Run Notes: self-packed column



Rack A							Peak #	Start Tube	End Tube
108	107	106	105	104	103		1	A:1	A:13
97	98	99	100	101	102		2	A:14	A:19
96	95	94	93	92	91		3	A:20	A:45
85	86	87	88	89	90				
84	83	82	81	80	79				
73	74	75	76	77	78				
72	71	70	69	68	67				
61	62	63	64	65	66				
60	59	58	57	56	55				
49	50	51	52	53	54				
48	47	46	45	44	43				
32	33	34	35	36	37				
31	30	29	28	27	26				
20	21	22	23	24	25				
19	18	17	16	15	14				
8	9	10	11	12	13				
7	6	5	4	3	2				

13 mm x 100 mm Tubes

Page 1 of 1

Synthetic Methods

7.1.2.29 Hexyl 5-amino-2-(hexyloxy)benzoate: G5-048s10

In a 75 mL #25 bushing pressure vessel (ChemGlass: CG-1880-43 with CG-364-62) connected to a Parr hydrogenator, a solution of ethyl acetate (EtOAc, 30 mL) and glacial acetic acid (60 mmol, 3.603 g, 3.43 mL) was added to **hexyl 2-(hexyloxy)-5-nitrobenzoate** (G5-047s10, 29.1 mmol, 10.23 g) and 10% Pd/C (0.25 g). The vessel was sealed, then evacuated and filled with H₂ to 55 PSI three times. The reaction mixture was stirred until the pressure ceased to drop. The mixture was filtered through a packed plug of celite (~5 cm thick), and the plug washed with EtOAc (~30 mL) and water (~20 mL). Water (200 mL) was added to the filtrate, and the pH was adjusted with NaHCO₃ until the pH = 8. After mixing thoroughly, the phases were separated, and the aqueous phase was extracted with EtOAc (2 x 50 mL). The combined EtOAc phases were washed with brine (100 mL), then dried with MgSO₄. After filtering, the filtrate was concentrated by rotary evaporation to an oil. A ¹H-NMR spectrum of the oil revealed that it was 82.95 mass% product with the remainder EtOAc.

Note: Later experiments revealed that the use of acid was unnecessary.

¹H-NMR δ (ppm)(DMSO-d₆): 6.85 (1 H, d, J = 2.88 Hz), 6.83 (1 H, d, J = 8.76 Hz), 6.70 (1 H, dd, J = 8.73, 2.89 Hz), 4.86 (2 H, s), 4.16 (2 H, t, J = 6.52 Hz), 3.84 (2 H, t, J = 6.34 Hz), 1.59-1.70 (4 H, m), 1.34-1.45 (4 H, m), 1.22-1.34 (8 H, m), 0.82-0.93 (6 H, m).

Synthetic Methods

7.1.2.30 (5-amino-2-(hexyloxy)phenyl)(pyrrolidin-1-yl)methanone : G5-106s7

In a 75 mL #25 bushing pressure vessel (ChemGlass: CG-1880-43 with CG-364-62) connected to a Parr hydrogenator, ethanol (30 mL) was added to **(2-(hexyloxy)-5-nitrophenyl)(pyrrolidin-1-yl)methanone (G5-099s8, 7.27 mmol, 2.3298 g)** and 10% Pd/C (0.2387 g). The vessel was sealed, then evacuated and filled with H₂ to 55 PSI three times. The reaction mixture was stirred until the pressure ceased to drop. The mixture was filtered through a packed plug of celite (~2 cm thick), and the plug washed with ethanol (~10 mL). The filtrate was concentrated by rotatory evaporation to an oil. The oil was dissolved in ethyl acetate (EtOAc, 10 mL), and the solution was extracted with water (2 x 5 mL). The EtOAc phase was dried with MgSO₄. After filtering, the filtrate was concentrated by rotatory evaporation to an oil. A ¹H-NMR spectrum of the oil revealed that it was 86.83 mass% product with the remainder EtOAc (2.1567 g gross, 1.8727 g net product, 88.7% yield).

¹H-NMR δ (ppm)(DMSO-d₆): 6.75 (1 H, d, J = 8.70 Hz), 6.54 (1 H, dd, J = 8.68, 2.80 Hz), 6.38 (1 H, d, J = 2.78 Hz), 4.74 (2 H, s), 3.82 (2 H, t, J = 6.23 Hz), 3.39 (2 H, t, J = 6.88 Hz), 3.08-3.17 (2 H, m), 1.73-1.88 (4 H, m), 1.55-1.65 (2 H, m), 1.31-1.40 (2 H, m), 1.24-1.31 (4 H, m), 0.87 (3 H, t, J = 6.72 Hz).

7.1.2.31 3-(1,3-dioxolan-2-yl)-4-(hexyloxy)aniline: G5-124s5

In a 75 mL #25 bushing pressure vessel (ChemGlass: CG-1880-43 with CG-364-62) connected to a Parr hydrogenator, a solution of ethyl acetate (EtOAc, 20 mL) and ethanol (5 mL) was added to **2-(2-(hexyloxy)-5-nitrophenyl)-1,3-dioxol-**

Synthetic Methods

ane (**G5-122s6**, 5.73 g, 19.4 mmol) and 10% Pd/C (0.8 g). The vessel was sealed, then evacuated and filled with H₂ to 55 PSI three times. The reaction mixture was stirred until the pressure ceased to drop. The mixture was filtered through a packed plug of celite (~5 cm thick), and the plug washed with EtOAc (~20 mL). The filtrate was concentrated by rotatory evaporation to an oil. A ¹H-NMR spectrum of the oil revealed that it was 90.0 mass% product with the remainder EtOAc (5.28 g gross, 4.752 g net product, 92.3%).

¹H-NMR δ (ppm)(DMSO-d₆): 6.72(1 H, d, J = 8.64 Hz), 6.69 (1 H, d, J = 2.84 Hz), 6.52 (1 H, dd, J = 8.60, 2.89 Hz), 5.89 (1 H, s), 4.68 (2 H, s), 3.86-4.07 (4 H, m), 3.83 (2 H, m), 1.60-1.69 (2 H, m), 1.33-1.44 (2 H, m), 1.26-1.33 (4 H, m), 0.88 (3 H, t, J = 6.58 Hz).

¹³C-NMR δ (ppm)(DMSO-d₆): 148.2, 142.2, 126.6, 115.4, 114.4, 113.3, 112.7, 98.3, 69.1, 31.0, 30.9, 29.0, 28.9, 25.3, 25.2, 22.1, 16.0, 13.9 (2 C).

7.1.2.32 2-(5-bromo-2-(hexyloxy)phenyl)-2-phenylacetonitrile: G4-026s10

A 20 mL vial was charged with InBr₃ (0.0117 g, 0.033 mmol), evacuated and filled with N₂ followed by the addition of anhydrous dichloromethane (DCM, 2.5 mL) and trimethylsilyl cyanide (TMSCN, 0.069 mL, 54.5 mg, 0.550 mmol). In a round bottom flask, and under N₂ atmosphere, **(5-bromo-2-(hexyloxy)phenyl)(phenyl)methanol (G4-019s14**, 100 mg, 0.275 mmol) was dissolved in anhydrous DCM (2.5 mL). The solution containing **G4-019s14** was added dropwise to

Synthetic Methods

the $\text{InBr}_3/\text{TMSCN}$ solution at a rate of 2-3 drops per second to ensure no color change occurred, which is an indication of a side reaction that results in the transfer of the n-hexyl group from the phenolic oxygen to the methanolic oxygen. After the addition of **G4-019s14** was complete, the reaction was stirred for an additional 30 minutes. Basic alumina (~1 g) was added to the reaction mixture, then the solvent was removed by rotatory evaporation. The resulting powder was used as a dry load for basic alumina chromatography (**FIGURE 7.25**). Fraction 11 was concentrated by rotatory evaporation to a colorless oil that slowly crystallized to a white solid (0.0749 g, 73.2% yield).

Notes: Using silica, instead of basic alumina, as the stationary phase during chromatography results in an impure product. Also, the use of a gradient is required to remove residual TMSCN (UV inactive at 254 nm and 280 nm).

$^1\text{H-NMR}$ δ (ppm)(DMSO-d_6): 7.50-7.65 (2 H, m), 7.30-7.42 (5 H, m), 7.03 (1 H, d, $J = 8.41$ Hz), 5.77 (1 H, s), 3.90-4.00 (2 H, m), 1.59-1.68 (2 H, m), 1.21-1.36 (6 H, m), 0.84-0.90 (3 H, m).

$^{13}\text{C-NMR}$ δ (ppm)(DMSO-d_6): 155.0, 135.1, 132.5, 131.3, 128.8, 127.9, 127.4, 126.4, 119.4, 114.7, 111.6, 68.3, 36.4, 30.9, 28.3, 25.0, 22.0, 13.9.

HRMS (ESI) m/z for $\text{C}_{20}\text{H}_{22}\text{BrNNaO}^+ [\text{M} + \text{Na}]^+$: calcd, 394.07770; found, 394.07787.

Synthetic Methods

FIGURE 7.25: Chromatographic purification of **G4-026s8**.

Sample: grandy4-026s8

Rf 200 : OHSU COHEN RF200#1

Tuesday 14 February 2012 04:48PM

RediSep Column: Al2O3 pH=7 24g

Peak Tube Volume: Max.

SN: E0410597B6D1A Lot: 2115308090W

Non-Peak Tube Volume: Max.

Flow Rate: 30 ml/min

Loading Type: Liquid

Equilibration Volume: 3.0 CV

Wavelength 1 (red): 254nm

Initial Waste: 0.0 CV

Peak Width: 1 min

Air Purge: 0.5 min

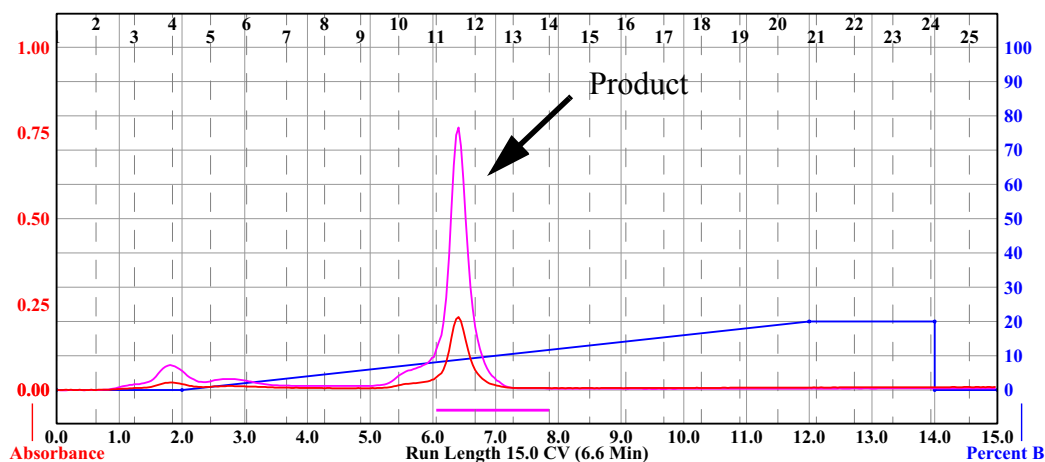
Threshold: 0.05 AU

Solvent: A1 hexane

Wavelength 2 (purple): 280nm

Solvent: B1 ethyl acetate

Run Notes: Basic Alumina was used.



Rack A							Peak #	Start Tube	End Tube
108	107	106	105	104	103		1	A:11	A:13
97	98	99	100	101	102				
96	95	94	93	92	91				
85	86	87	88	89	90				
84	83	82	81	80	79				
73	74	75	76	77	78				
72	71	70	69	68	67				
61	62	63	64	65	66				
60	59	58	57	56	55				
49	50	51	52	53	54				
48	47	46	45	44	43				
37	38	39	40	41	42				
36	35	34	33	32	31				
25	26	27	28	29	30				
24	23	22	21	20	19				
13	14	15	16	17	18				
12	11	10	9	8	7				
1	2	3	4	5	6				

13 mm x 100 mm Tubes

Page 1 of 1

Synthetic Methods

7.1.2.33 2-(5-(4-fluorophenoxy)-2-(hexyloxy)phenyl)-2-phenylacetonitrile: G4-079s9

A round bottom flask was charged with InBr_3 (0.1496 g, 0.422 mmol), evacuated and filled with N_2 , followed by the addition of anhydrous dichloromethane (DCM, 35 mL) and trimethylsilylcyanide (TMSCN, 1.056 mL, 0.837 g, 8.44 mmol). In a separate round bottom flask, and under N_2 atmosphere, **(5-(4-fluorophenoxy)-2-(hexyloxy)phenyl)(phenyl)methanol (G4-074s14)**, 1.6659 g, 4.22 mmol) was dissolved in anhydrous DCM (35 mL). The solution containing **G4-074s14**, was added dropwise to the InBr_3 /TMSCN solution at a rate of 2-3 drops per second to ensure no color change occurred, which is an indication of a side reaction that results in the transfer of the n-Hexyl group from the phenolic oxygen to the methanolic oxygen. Towards the end of the reaction, additional TMSCN (0.5 mL, 0.3965 g, 4.00 mmol) was added because a color change was occurring despite the slow rate of addition of **G4-074s14**. After the addition of **G4-074s14** was complete, the reaction was stirred for an additional 30 minutes. Basic alumina (~5 g) was added to the reaction mixture, then the solvent was removed by rotatory evaporation. The resulting powder was used as a dry load for basic alumina chromatography (see **FIGURE 7.26**). Fractions 1-51 were combined and concentrated by rotatory evaporation to a pale yellow oil (1.7027 g, 88.5% yield).

Notes: Using silica, instead of basic alumina, as the stationary phase during chromatography results in an impure product (mixture of regenerated starting material (**G4-074s14**), the desired product and a side-product: 4-(4-fluorophenyl)-2-(hexyloxy)phenylmethanol).

Synthetic Methods

noxy)-2-((hexyloxy)(phenyl)methyl)phenol). Also, the use of a gradient is required to remove residual TMSCN (UV inactive at 254 nm and 280 nm).

$^1\text{H-NMR}$ δ (ppm)(DMSO- d_6): 7.30 - 7.41 (m, 5H), 7.19 - 7.24 (m, 2H), 7.094 (d, $J = 3.0$ Hz, 1H), 7.060 (d, $J = 9.0$ Hz, 1H), 7.04 - 7.005 (m, 2H), 6.994 (dd, $J = 9.0$ Hz, 3.0 Hz, 1H), 5.748 (s, 1H), 3.90 - 3.96 (m, 2H), 1.61-1.67 (m, 2H), 1.30 - 1.36 (m, 2H), 1.22-1.30 (m, 4H), 0.874 (t, $J = 7.5$ Hz, 3H).

$^{13}\text{C-NMR}$ δ (ppm)(DMSO- d_6): 157.88 (d, $J = 239.9$ Hz), 153.47 (d, $J = 1.5$ Hz), 151.86, 149.74, 135.37, 128.76, 127.75, 127.41, 125.37, 119.79, 119.76, 119.62, 119.53 (d, $J = 7.5$ Hz), 116.47 (d, $J = 22.6$ Hz), 113.67, 68.33, 36.61, 30.94, 28.50, 25.04, 21.99, 13.86.

$^{19}\text{F-NMR}$ δ (ppm)(DMSO- d_6 , with C_6F_6 as reference at -164.9 ppm): -122.84 to -122.94.

HRMS (ESI) m/z for $\text{C}_{26}\text{H}_{26}\text{FNNaO}_2^+ [\text{M} + \text{Na}]^+$: calcd, 426.18398; found, 426.18435.

Synthetic Methods

FIGURE 7.26: Chromatographic purification of **G4-079s8**.

Sample: grandy4-079s8

RediSep Column: Al2O3 pH=7 160g

Flow Rate: 60 ml/min

Equilibration Volume: 3.0 CV

Initial Waste: 0.0 CV

Air Purge: 1.0 min

Solvent: A1 hexane

Solvent: B1 ethyl acetate

Rf 200 : OHSU COHEN RF200#1

Peak Tube Volume: Max.

Non-Peak Tube Volume: Max.

Loading Type: Solid

Wavelength 1 (red): 254nm

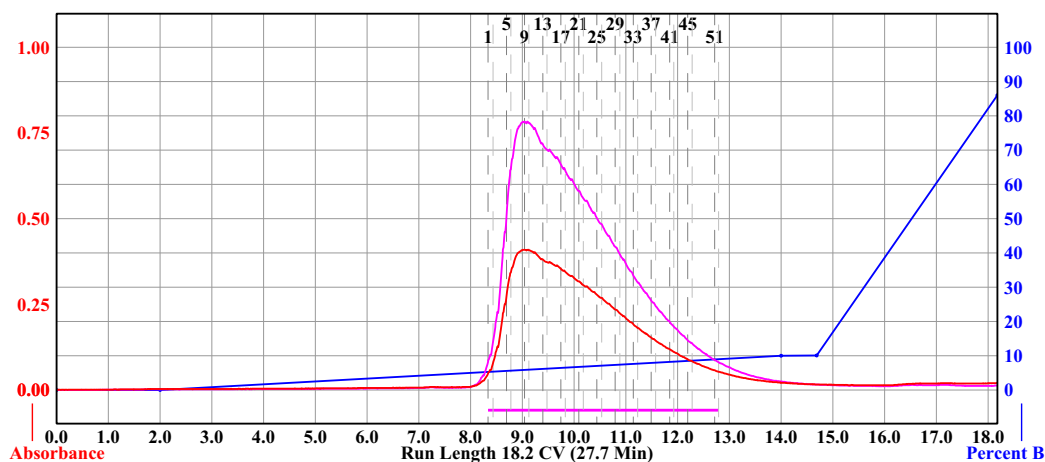
Peak Width: 2 min

Threshold: 0.05 AU

Wavelength 2 (purple): 280nm

Thursday 19 April 2012 01:55PM

Run Notes: Basic Alumina was used.



Rack A						Peak #	Start Tube	End Tube	
108	107	106	105	104	103	1	A:1	A:51	
97	98	99	100	101	102				
96	95	94	93	92	91				
88	86	87	88	89	90				
89	83	82	81	80	79				
73	72	75	76	77	78				
72	71	70	69	68	67				
61	62	63	64	65	66				
60	59	58	57	56	55				
49	50	51	52	53	54				
48	47	46	45	44	43				
37	38	39	40	41	42				
36	35	34	33	32	31				
25	26	27	28	29	30				
23	23	22	21	20	19				
13	14	15	16	17	18				
12	11	10	9	8	7				
1	2	3	4	5	6				
13 mm x 100 mm Tubes						Duration	%B	Solvent A	Solvent B
						0.0	0.0	A1 hexane	B1 ethyl acetate
						2.0	0.0	A1 hexane	B1 ethyl acetate
						12.0	10.0	A1 hexane	B1 ethyl acetate
						0.7	10.1	A1 hexane	B1 ethyl acetate
						3.5	86.0	A1 hexane	B1 ethyl acetate

Synthetic Methods

7.1.2.34 2-(5-bromo-2-(hexyloxy)phenyl)-1,3-dioxolane: G1-130s5

In a round bottom flask, equipped with a Dean-Stark trap and a reflux condenser, 5-bromo-2-(hexyloxy)benzaldehyde (25 mmol, 7.130 g), ethylene glycol (50 mmol, 3.105 g, 2.790 mL) and p-toluenesulfonic acid monohydrate (0.25 mmol, 0.0475 g) were dissolved in toluene (100 mL). The reaction mixture was refluxed at 150 °C (pot temperature) for 18 hours. The reaction mixture was extracted with 0.1 M Na₂CO₃ (3 x 100 mL), and the toluene phase was dried with MgSO₄. After filtering, the filtrate was concentrated by rotatory evaporation to an oil that smelled of toluene (8.3989 g).

¹H-NMR δ (ppm)(CH₂Cl₂-d₂): 7.64 (1 H, d, J = 2.62 Hz), 7.44 (1 H, dd, J = 8.76, 2.63 Hz), 6.83 (1 H, d, J = 8.78 Hz), 6.11 (1 H, s), 3.98-4.18 (6 H, m), 1.78-1.87 (2 H, m), 1.45-1.55 (2 H, m), 1.35-1.44 (4 H, m), 0.96 (3 H, t, J = 6.66 Hz).

7.1.2.35 2-(2-(hexyloxy)-5-nitrophenyl)-1,3-dioxolane: G5-122s6

In a round bottom flask, equipped with a Dean-Stark trap and a reflux condenser, **2-(hexyloxy)-5-nitrobenzaldehyde (G5-120s11)**, 8.00 g, 31.57 mmol, ethylene glycol (35 mmol, 2.1725 g, 1.95 mL) and p-toluenesulfonic acid monohydrate (0.0475 g) were dissolved in toluene (50 mL). The reaction mixture was refluxed at 150 °C (pot temperature) for 48 hours. Basic alumina (~5 g) was added to the reaction mixture, which was then concentrated by rotatory evaporation to a paste. The paste was used as a dry-load for basic alumina chromatography

Synthetic Methods

(**FIGURE 7.27**). Fractions 19-87 were combined, and concentrated by rotatory evaporation (5.73 g).

^1H -NMR δ (ppm)(DMSO- d_6): 8.27 (1 H, dd, $J = 9.08, 3.00$ Hz), 8.22 (1 H, d, $J = 2.92$ Hz), 7.28 (1 H, d, $J = 9.14$ Hz), 6.01 (1 H, s), 4.18 (2 H, t, $J = 6.41$ Hz), 3.93-4.15 (4 H, m), 1.71-1.80 (2 H, m), 1.38-1.49 (2 H, m), 1.26-1.38 (4 H, m), 0.88 (3 H, t, $J = 6.75$ Hz).

^{13}C -NMR δ (ppm)(DMSO- d_6): 162.0, 140.2, 127.0, 126.6, 122.4, 112.7, 97.4, 69.0, 64.9, 30.8, 28.2, 24.9, 22.0, 13.8.

Synthetic Methods

FIGURE 7.27: Chromatographic purification of G5-122s5.

Sample: grandy5-122s5

Rf 200 : OHSU COHEN RF200#1

Friday 19 October 2012 10:38AM

RediSep Column: Al2O3 pH 7.48g

Peak Tube Volume: Max.

All Wavelength (orange): 200nm - 360nm

Flow Rate: 50 ml/min

Non-Peak Tube Volume: Max.

Peak Width: 1 min

Equilibration Volume: 5.0 CV

Loading Type: Solid

Threshold: 0.20 AU

Initial Waste: 0.0 CV

Wavelength 1 (red): 254nm

Air Purge: 1.0 min

Peak Width: 1 min

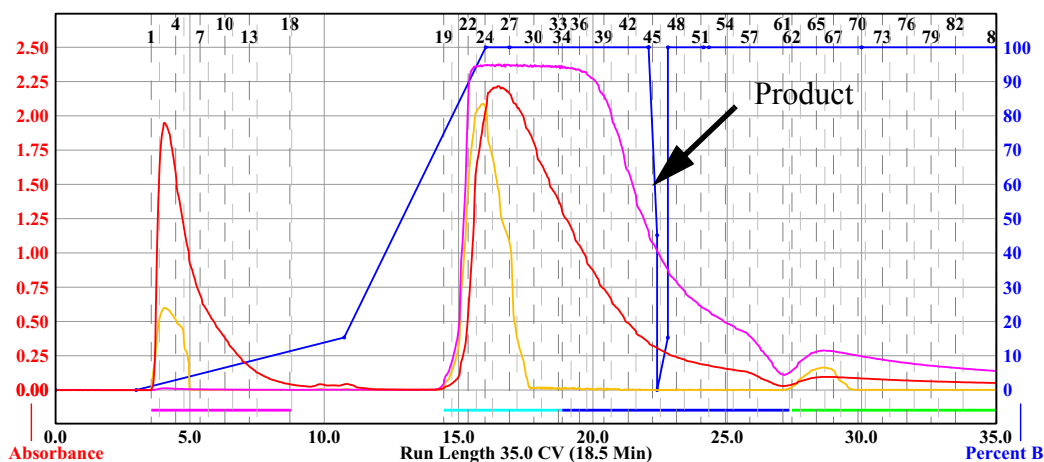
Solvent: A2 hexane

Threshold: 0.05 AU

Solvent: B2 dichloromethane

Wavelength 2 (purple): 280nm

Run Notes: self-packed basic alumina



Rack A

108	107	106	105	104	103
97	98	99	100	101	102
96	95	94	93	92	91
88	87	86	85	84	83
82	81	80	79	78	77
76	75	74	73	72	71
70	69	68	67	66	65
64	63	62	61	60	59
58	57	56	55	54	53
52	51	50	49	48	47
46	45	44	43	42	41
40	39	38	37	36	35
34	33	32	31	30	29
28	27	26	25	24	23
22	21	20	19	18	17
16	15	14	13	12	11
10	9	8	7	6	5
4	3	2	1	0	0

13 mm x 100 mm Tubes

Peak # Start Tube End Tube

1	A:1	A:18
2	A:19	A:33
3	A:34	A:61
4	A:62	A:87

Duration	%B	Solvent A	Solvent B
0.0	0.0	A2 hexane	B2 dichloromethane
3.0	0.0	A2 hexane	B2 dichloromethane
7.7	15.3	A2 hexane	B2 dichloromethane
5.3	100.0	A2 hexane	B2 dichloromethane
0.9	100.0	A2 hexane	B2 dichloromethane
5.2	100.0	A2 hexane	B2 dichloromethane
0.0	100.0	A2 hexane	B2 dichloromethane
0.3	45.2	A2 hexane	B2 dichloromethane
0.0	0.0	A2 hexane	B2 dichloromethane
0.4	15.3	A2 hexane	B2 dichloromethane
...

Synthetic Methods

7.1.2.36 2-(5-(4-fluorophenoxy)-2-(hexyloxy)phenyl)-2-phenylethanamine hydrochloride: ET-92 (G4-091s14 and G5-002s12)

In a round bottom flask equipped with a reflux condenser, **2-(5-(4-fluorophenoxy)-2-(hexyloxy)phenyl)-2-phenylacetonitrile (G4-079s9**, 0.0574 g, 0.142 mmol) was dissolved in anhydrous tetrahydrofuran (THF, 5 mL). The reaction vessel was evacuated and filled with N₂, then 1 M BH₃·DMS in THF (0.145 mL, 0.145 mmol) was slowly added by syringe. The reaction was refluxed for 2.5 hours, and then cooled to room temperature. Methanol (MeOH, 0.25 mL, 6.17 mmol) was slowly added by syringe. After H₂ evolution stopped, 3.0 M HCl in EtOAc (0.05 mL, 0.15 mmol) was added, and the mixture was heated to 40 °C for 15 minutes. The mixture was then concentrate by rotatory evaporation, chasing with MeOH (3 x 5 mL) and ethyl acetate (1 x 2 mL). Next, diethyl ether (2 mL) was added, and the solution was then cool to -68 °C. After a precipitate form, the mixture was centrifuged, and the supernatant was decanted off. The white solid was dried under vacuum for 12 hours (0.0246 g, 38.9% yield).

¹H-NMR δ (ppm)(DMSO-d₆): 7.895 (bs, 3H), 7.30 - 7.33 (m, 4H), 7.224 (d, J = 3.0, 1H), 7.23 - 7.25 (m, 1H), 7.16 - 7.21 (m, 2H), 6.96 - 7.00 (m, 2H), 6.960 (d, J = 9.0 Hz, 1H), 6.841 (dd, J = 9.0 Hz, 3.0 Hz, 1H), 4.619 (t, J = 8.1 Hz, 1H), 3.83 - 3.94 (m, 2H), 3.46 - 3.54 (m, 2H), 1.66-1.72 (m, 2H), 1.35 - 1.42 (m, 2H), 1.26-1.35 (m, 4H), 0.891 (t, J = 6.9 Hz, 3H).

Synthetic Methods

^{13}C -NMR δ (ppm)(DMSO- d_6): 157.61 (d, $J = 238.4$ Hz), 154.04 (d, $J = 22.2$ Hz), 152.46, 149.56, 140.32, 130.33, 128.48, 128.03, 126.90, 119.36, 118.92 (d, $J = 9.1$ Hz), 118.38, 116.29 (d, $J = 24.1$ Hz), 113.12, 68.07, 41.63, 42.08, 31.00, 28.74, 25.21, 22.04, 13.91.

^{19}F -NMR δ (ppm)(DMSO- d_6 , with C_6F_6 as reference at -164.9 ppm): -123.54 to -123.65.

HRMS (ESI) m/z for $\text{C}_{26}\text{H}_{31}\text{FNO}_2^+ [\text{M} + \text{H}]^+$: calcd, 408.23333; found, 408.23287.

7.1.2.37 (2-hydroxy-5-nitrophenyl)(pyrrolidin-1-yl)methanone: G5-098s6 and G5-088s8

In a round bottom flask, 2-hydroxy-5-nitrobenzoic acid (30 mmol, 5.4956 g), and 1-ethyl-3-(3-dimethylaminopropyl)carbodiimide hydrochloride (5.751 g, 30 mmol) were dissolved in anhydrous dichloromethane (DCM, 100mL). The solution was stirred for 5 minutes, then pyrrolidine (120 mmol, 8.5544 g, 10 mL) was added. The reaction was stirred for 2 hours, then extracted with 0.72 M HCl (2 x 56 mL) then the DCM phase was dried with MgSO_4 . After filtering, the filtrate was concentrated by rotatory evaporator.

^1H -NMR δ (ppm)(DMSO- d_6): 11.56 (1 H, s), 8.16 (1 H, dd, $J = 9.06, 2.91$ Hz), 8.06 (1 H, d, $J = 2.88$ Hz), 7.07 (1 H, d, $J = 9.07$ Hz), 3.46 (2 H, t, $J = 6.74$ Hz), 3.23 (2 H, t, $J = 6.74$ Hz), 1.79-1.89 (4 H, m).

Synthetic Methods

^{13}C -NMR δ (ppm)(DMSO- d_6): 164.5, 159.7, 139.3, 126.3, 125.9, 124.3, 116.5, 47.0, 45.4, 25.4, 23.9.

7.1.2.38 5-(4-fluorophenoxy)-2-(hexyloxy)benzaldehyde: G4-068s20 and G4-70s6

CuI (6.3595 g, 35.01 mmol), 1,10-phenanthroline (6.3102 g, 35.02 mmol), KI (0.292 g, 1.757 mmol) and K_2CO_3 (9.6753 g, 70.00 mmol) were combined in a round bottom flask equipped with a reflux condenser, Dean-Stark trap, addition funnel and gas inlet valve. The apparatus was then purged and filled with N_2 . Anhydrous dimethylformamide (DMF, 70 mL) and toluene (20 mL) were added. The resulting mixture was stirred for 30 minutes. **5-bromo-2-(hexyloxy)benzaldehyde (G4-012s16**, 5.0038 g, 17.55 mmol) was dissolved in anhydrous DMF (10 mL), then added to the reaction vessel. Next, 4-fluorophenol (7.8464 g, 69.99 mmol) was dissolved in anhydrous DMF (20 mL), then transferred to the addition funnel, whereupon one quarter of the solution was added to the reaction. The reaction was heated to 120 °C for 2 hours. The remaining 4-fluorophenol solution was added dropwise, and heating was continued for a total of 19 hours. The reaction was cooled to room temperature, then water (500 mL) and hexanes (250 mL) were added. After mixing and breaking-up the solids, the mixture was filtered through a medium sintered glass funnel. The residue was washed with hexanes (200 mL) then discarded. The phases of the filtrate were separated. The aqueous phase was extracted with hexanes (3 x 250 mL). The combined hexane layers were washed

Synthetic Methods

with 0.05 M NaOH (2 x 500 mL), then dried over MgSO_4 . After filtering, the filtrate was concentrated by rotatory evaporator to an oil (5.0759 g).

The crude product was dissolved in dichloromethane and silica gel (~20 g) was added. The mixture was concentrated by rotatory evaporator to a powder. The powder was used as a dry load for silica chromatography (**FIGURE 7.28**). Fractions A1-B73 were combined, then concentrated by rotatory evaporator to an oil (3.9806 g, ~75% desired product by NMR).

Synthetic Methods

The final purification was done by 7 reverse phase HPLC (**TABLE 7.4**) runs, were a solution of the crude oil dissolved in methanol (15 mL) was used to load the HPLC column. The product was the last major peak observed at ~44 minute mark. The HPLC product fractions were combined, then concentrated by rotatory evaporator to an orange oil (2.47 g, 44.5% yield).

Notes: The toluene was an attempt to azeotropically remove any water in the reaction, however the vapor condensed before reaching the Dean-Stark trap, leaving water droplets on the glassware. The toluene definitely doesn't hurt the reaction but it is unclear if it helps. Also, with a larger batch, it may be possible to distill the product under high vacuum.

TABLE 7.4: HPLC Conditions used to purify **G4-068s16**

Column	Supelco Discovery 18 (C18, 25 cm x 21.2mm, 5µm (cat#:569226- U))	Gradient (min.)	% B
Flow	20 mL/min	0	50
λ_1	254 nm	5	50
λ_2	280 nm	55	100
Solvent A:	water	60	100
Solvent B:	acetonitrile	-	-

$^1\text{H-NMR}$ δ (ppm)(DMSO- d_6): 10.337 (s, 1H), δ 7.380 (dd, J = 9.0 Hz, 3.0 Hz, 1H), 7.189 (d, J = 3.0 Hz, 1H), 7.289 (d, J = 9.0 Hz, 1H), 7.210-7.26 (m, 2H), 7.03-7.08 (m, 2H), 4.132 (t, J = 6.6 Hz, 2H), 1.75-1.81 (m, 2H), 1.42-1.49 (m, 2H), 1.28-1.36 (m, 4H), 0.885 (t, J = 6.9 Hz, 3H).

Biological Assays: TEVC Methods

^{13}C -NMR δ (ppm)(DMSO- d_6): 188.54, 158.93, 157.36, 152.99, 150.35, 126.94, 124.83, 120.16, 116.61, 115.96, 115.77, 68.90, 30.90, 28.43, 25.09, 22.00, 13.86.

^{19}F -NMR δ (ppm)(DMSO- d_6 , with C_6F_6 as reference at -164.9 ppm): -122.17 to -122.26.

TABLE 7.5: High resolution MS (ESI) of 5-(4-fluorophenoxy)-2-(hexyloxy)benzaldehyde (**G4-068s20**)

Species	Chemical Formula	Calculated m/z	Observed m/z
$[\text{M} + \text{H}]^+$	$\text{C}_{19}\text{H}_{22}\text{FO}_3^+$	317.15475	371.16291
$[\text{M} + \text{Na}]^+$	$\text{C}_{19}\text{H}_{21}\text{FNaO}_3^+$	339.13669	339.13728
$[\text{M} + \text{MeOH} + \text{Na}]^{+a}$	$\text{C}_{20}\text{H}_{25}\text{FNaO}_4^+$	371.16291	371.16289

a. This is the sodium cation form of the hemiacetal with MeOH.

7.2 Biological Assays: TEVC Methods

7.2.1 In Vitro Transcription (used with permission from Dr. Yohei Norimatsu)

Human CFTR cDNA was used in a modified pBluescript vector (Agilent Technologies, Santa Clara, CA) containing T7 promoter and the 5' untranslated region of the *Xenopus* β -globin gene upstream from the coding sequence of CFTR.

Human TAAR1 cDNA was used in the pcDNA3.1 vector (Life Technologies, Carlsbad, CA). The DNA sequences were confirmed by direct DNA sequencing. The cRNAs for *Xenopus* oocyte injection were synthesized using the mMessage mMachine T7-UltraTM *in vitro* transcription kit from Life Technologies (Carlsbad, CA). After transcription, poly(A) tails were added to the transcripts using *E. coli*

Biological Assays: TEVC Methods

Poly(A) polymerase as described in the mMessage mMachine T7 Ultra transcription kit.

7.2.2 Preparation and Microinjection of Oocytes (used with permission from Dr. Yohei Norimatsu)

Female *Xenopus Laevis* frogs were anesthetized by immersion in cold water containing Tricaine, 3mg/ml (Sigma Chemical Co., St. Louis, MO). The oocytes were removed through a small abdominal incision which was then closed by 4.0 nylon suture. The follicular membranes were removed by mechanical agitation (1–2 h) in a Ca^{2+} -free solution containing 82.5 mM NaCl, 2 mM KCl, 1 mM MgCl_2 , 5 mM HEPES (pH 7.5), and 0.2 Wünsch units/mL Liberase Blendzyme™ (Roche Molecular Biochemicals, Indianapolis, IN). We selected Stage V and VI defolliculated oocytes, which were then washed and incubated at 18 °C in a modified Barth's solution (MBSH) containing 88 mM NaCl, 1 mM KCl, 0.82 mM MgSO_4 , 0.33 mM $\text{Ca}(\text{NO}_3)_2$, 0.41 mM CaCl_2 , 2.4 mM NaHCO_3 , 10 mM HEPES-Hemi-Na, and 250 mg/L Amikacin with 150 mg/L Gentamicin (pH 7.5) until injection the next day. Each oocyte was injected with 50 nl of RNA solution containing 100 ng/ μl hTAAR1 and 10 ng/ μl hCFTR cRNA. Injected oocytes were incubated at 18 °C in 12-well plates containing MBSH. Injection pipettes were pulled from filamented glass capillary tubes (Sutter Instrument, Novato CA) on a P-97 Flaming – Brown micropipette puller (Sutter Instrument, Novato CA). Typically, the oocytes were used 3 to 7 days after injection.

Biological Assays: TEVC Methods

7.2.3 Whole Cell Recordings (used with permission from Dr. Yohei Norimatsu)

Individual oocytes were placed in a 500 μ L RC-1Z recording chamber (Warner Instruments, Hamden CT) and continuously perfused with Frog Ringer's solution (~5 mL/min) via a siphon. The Ringer's solution contained 98 mM NaCl, 2 mM KCl, 1 mM MgCl₂, 1.8 mM CaCl₂, and 5 mM HEPES (hemi-Na) (pH 7.4).

Oocytes were initially maintained in the experimental chamber under open circuit conditions and experiments began when the transmembrane voltage was between -25mV and -40 mV. The membrane potential was ramped from -120 mV to +60 mV in 1.8 s.

Membrane currents were recorded from oocytes with a two-electrode voltage clamp using an amplifier (TEV-200; Dagan, Minneapolis, MN) at a room temperature of ~ 22°C. Current-injecting and potential-measuring electrodes had resistances of ~1.0–3.0 M Ω , when filled with 3 M KCl. The bath solution was connected to the ground via a low-resistance agarose bridge containing 2% agarose in 3 M KCl. Current measurements were low-pass filtered at 0.5 kHz. Data acquisition was performed on a Pentium-based microcomputer using pCLAMP software and an analog-to-digital converter (Axon Instruments, Foster City, CA).

7.2.3.1 Compound Assays

A 100 mM stock solution of each test compound, in DMSO, was made, and then used to make the test solutions.

Biological Assays: TEVC Methods

With the exception of the first and last compound assay (**FIGURE 7.4** and **7.6(1)**, respectfully), all assays followed a head-to-head competition assay paradigm where a 1.5 minute pulse of 10 μ M Meth in Frog Ringer's solution (FR) was perfused over an oocyte, injected with hTAAR1 and hCFTR encoding RNA, followed by a wash-out period with FR. After the initial Meth pulse and wash-out, a series of 1.5 minute pulse of 10 μ M Meth and test compound (1 nM to 10 μ M) in FR followed by FR wash-out cycles were preformed. At the end of each experiment, a 1.5 minute pulse of 10 μ M forskolin and 10 μ M of the test compound in FR followed by a FR wash-out period. The wash-out periods lasted between 15 and 25 minutes (long enough for the conductance to stabilize).

The assay shown in **FIGURE 4.4** used an oocyte injected with hTAAR1 and hCFTR encoding RNA. The Meth pulses were 1.5 minutes long and at 100 μ M concentration in FR. Each Meth pulse was followed by a 15 minute FR wash-out period. After the second pulse of Meth, 20 μ M **G5-109s8** in FR was applied immediately followed by a Meth pulse. No forskolin control was done in this experiment.

The assay shown in **FIGURE 4.6(1)** used an oocyte injected with hCFTR encoding RNA. Between each pulse of testing solution, the oocyte was washed with FR. The 1.5 minute pulses used were: 5 μ M forskolin, 10 μ M **G5-109s8**, 10

Biological Assays: TEVC Methods

μM Meth, and a combination of 5 μM forskolin and 10 μM **G5-109s8**. All of these solutions were made using FR.

References & Notes

1. Katzung, B.G. *Basic and Clinical Pharmacology*, 11th ed.; Lange Medical Books/McGraw Hill: New York, 2007; pp 557 and 565.
2. *Ibid.*, p 556.
3. Wikipedia: *Dopamine* (accessed Feb. 6, 2013), <http://en.wikipedia.org/wiki/Dopamine>
4. Bunzow, J. R.; et al.; Amphetamine, 3,4-methylenedioxymethamphetamine, lysergic acid diethylamide, and metabolites of the catecholamine neurotransmitters are agonists of a rat trace amine receptor. *Mol. Pharmacol.* **2001**, *60*(6), 1181-1188.
5. Achat-Mendes, C., et al., *Augmentation of methamphetamine-induced behaviors in transgenic mice lacking the trace amine-associated receptor 1*. *Pharmacol. Biochem. Behav.* **2012**, *101*(2), 201-207.
6. Miller, G. M. The emerging role of trace amine-associated receptor 1 in the functional regulation of monoamine transporters and dopaminergic activity. *J. Neurochem.* **2011**, *116*(2), 164-176.
7. Borowsky, B.; et al.; Trace amines: identification of a family of mammalian G protein-coupled receptors. *Proc. Natl. Acad. Sci. U.S.A.* **2001**, *98*(16), 8966-8971.
8. Revel, F. G.; et al.; A new perspective for schizophrenia: TAAR1 agonists reveal antipsychotic- and antidepressant-like activity, improve cognition and control body weight. *Mol. Psychiatry*, DOI: 10.1038/mp.2012.57, Published online May 30, 2012, <http://www.ncbi.nlm.nih.gov/pubmed/22641180>.
9. Revel, F. G.; et al.; Trace amine-associated receptor 1 partial agonism reveals novel paradigm for neuropsychiatric therapeutics. *Biol. Psychiatry*, **2012**, *72*(11), 934-942.
10. Miller, G. M. Avenues for the development of therapeutics that target trace amine associated receptor 1 (TAAR1). *J. Med. Chem.* **2012**, *55*(5), 1809-1814.
11. Bradaia, A.; et al.; The selective antagonist EPPTB reveals TAAR1-mediated regulatory mechanisms in dopaminergic neurons of the mesolimbic system. *Proc. Natl. Acad. Sci. U.S.A.*, **2009**, *106*(47), 20081-20086.
12. Smith, S. B.; et al.; Large candidate gene association study reveals genetic risk factors and therapeutic targets for fibromyalgia. *Arthritis Rheum.* **2012**, *64*(2), 584-593.

13. Wasik, A. M.; et al.; Evidence for functional trace amine associated receptor-1 in normal and malignant B cells. *Leuk. Res.* **2012**, *36*(2), 245-249.
14. Salahpour, A.; et al.; BRET biosensors to study GPCR biology, pharmacology, and signal transduction. *Front. Endocrinol. (Lausanne)*, **2012**, *3*, 105 and references therein.
15. A survey of the literature revealed a paucity of information on what happens to the GDP after it is released from the TAAR1-G α_s /G β/γ complex.
16. Wettschureck, N.; Offermanns, S. Mammalian G proteins and their cell type specific functions. *Physiol. Rev.* **2005**, *85*(4), 1159-1204.
17. Tan, E.S. Understanding the molecular basis of trace amine-associated receptor 1 activation by thyronamines and related analogs. Ph.D. Dissertation, University of California, San Francisco, CA, 2007.
18. (a) Piehl, S.; et al.; Thyronamines-past, present, and future. *Endocr. Rev.* **2011**, *32*(1), 64-80 and references therein. (b) Scanlan, T. S.; et al.; 3-Iodothyronamine is an endogenous and rapid-acting derivative of thyroid hormone. *Nat. Med.* **2004**, *10*, 638 – 642
19. Panas, H. N.; et al.; Normal thermoregulatory responses to 3-iodothyronamine, trace amines and amphetamine-like psychostimulants in trace amine associated receptor 1 knockout mice. *J. Neurosci. Res.* **2010**, *88*(9), 1962-1969.
20. Simmler, L.; et al.; Pharmacological characterization of designer cathinones in vitro. *Br. J. Pharmacol.* **2013**, *168*(2), 458-470.
21. Katzung, B. G. *Basic and Clinical Pharmacology*, 11th ed.; Lange Medical Books/McGraw Hill: New York, 2007; pp 134, 141, 144-145, and 553-568.
22. Benjamin, J.; et al.; Population and familial association between the D4 dopamine receptor gene and measures of Novelty Seeking. *Nat. Genet.* **1996**, *12*(1), 81-84.
23. Ebstein, R. P.; et al.; Dopamine D4 receptor (D4DR) exon III polymorphism associated with the human personality trait of Novelty Seeking. *Nat. Genet.* **1996**, *12*(1), 78-80.
24. Ikemoto, S.; Panksepp, J. The role of nucleus accumbens dopamine in motivated behavior: a unifying interpretation with special reference to reward-seeking. *Brain Res. Rev.* **1999**, *31*(1), 6-41.
25. Pessiglione, M.; et al.; Dopamine-dependent prediction errors underpin reward-seeking behaviour in humans. *Nature*, **2006**, *442*(7106), 1042-1045.
26. Roitman, M. F.; et al.; Dopamine operates as a subsecond modulator of food seeking. *J. Neurosci.* **2004**, *24*(6), 1265-1271.
27. Suhara, T.; et al.; Dopamine D2 receptors in the insular cortex and the personality trait of novelty seeking. *Neuroimage*, **2001**, *13*(5), 891-895.

-
28. Wikipedia: *Methylphenidate* (accessed May 5, 2013), http://en.wikipedia.org/wiki/Methylphenidate#ADHD_and_stimulant_dynamics_in_general.
 29. Wikipedia: *Anxiety* (accessed May 5, 2013), <http://en.wikipedia.org/wiki/Anxiety>.
 30. Wikipedia: *Norepinephrine* (accessed May 6, 2013), <http://en.wikipedia.org/wiki/Norepinephrine>.
 31. Wikipedia: *Atomoxetine* (accessed May 7, 2013), <http://en.wikipedia.org/wiki/Atomoxetine>.
 32. Wikipedia: *Serotonin* (accessed May 6, 2013), <http://en.wikipedia.org/wiki/Serotonin>.
 33. Wikipedia: *Serotonin Syndrome* (accessed May 6, 2013), http://en.wikipedia.org/wiki/Serotonin_syndrome.
 34. Galley, G.; et al.; *Preparation of substituted benzamide derivatives for use as CNS agents*, WO 2009016088 A1, 2009.
 35. Wikipedia: *Cystic fibrosis transmembrane conductance regulatory* (accessed May 15, 2013), http://en.wikipedia.org/wiki/Cystic_fibrosis_transmembrane_conductance_regulator.
 36. Tallman, K.; et al.; *Pharmacologic and Genetic Manipulation of Trace Amine-Associated Receptor 1 Signaling In Mice Demonstrates its Role in Methamphetamine-Stimulated Activity*, to be submitted for publication, 2012.
 37. Galley, G.; et al.; *Optimisation of imidazole compounds as selective TAAR1 agonists: discovery of RO5073012*. *Bioorg Med Chem Lett*, 2012, **22**(16), 5244-5248.
 38. Galley, G.; Norcross, R.; Polara, A.; *Preparation of aminooxazoline derivatives for use as TAAR1 ligands*. US 20110112080 A1, 2011.
 39. Galley, G.; et al.; *4,5-Dihydrooxazol-2-yl derivatives as TAAR gene expression agents and their preparation, pharmaceutical compositions and use in the treatment of diseases*. US 20100029589 A1, 2010.
 40. Galley, G.; et al.; *Preparation of 4,5-dihydro-oxazol-2-yl derivatives with selectivity for trace amine associated receptors (TAAR) for treatment of diseases*, WO 2010010014 A1, 2010.
 41. Decoret, G.; et al.; *Preparation of 2-aminooxazolines as trace amine associated receptor 1 (TAAR1) ligands*, WO 2010139707 A1, 2010.
 42. Galley, G.; et al.; *Preparation of nicotinamide derivatives as TAAR1 ligands for the treatment of CNS disorders*, US 20090036452 A1, 2009.
 43. Galley, G.; et al.; *Preparation of 2-imidazolines as trace amine associated receptors modulators*, WO 2009003868 A2, 2009.
 44. Galley, G.; et al.; *Preparation of 2-imidazolines as antidepressants*, WO 2009003867 A1, 2009.
-

-
45. Galley, G.; et al.; *Preparation of 2-azetidinemethaneamines and 2-pyrrolidinemethaneamines as TAAR ligands*, US 20090029962 A1, 2009.
 46. Galley, G.; et al.; *Imidazole derivatives as TAAR modulators and their preparation and pharmaceutical compositions*, US 20080146523 A1, 2008.
 47. Galley, G.; et al.; *Preparation of aminooxazoline derivatives for use as TAAR1 ligands*, WO 2008098857 A1, 2008.
 48. Galley, G.; et al.; *Preparation of aminooxazoline derivatives for use as central nervous system agents*, WO 2008092785 A1, 2008.
 49. Galley, G.; et al.; *Preparation of novel substituted 2-imidazoles as ligands for trace amine associated receptors (TAAR)*, WO 2008071574 A1, 2008.
 50. Galley, G.; et al.; *Preparation of substituted 4-imidazoles having good affinity to the trace amine associated receptors (TAARs)*, WO 2008058867 A2, 2008.
 51. Galley, G.; et al.; *Preparation of substituted 2-imidazoles as modulators of the trace amine associated receptors*, WO 2008052907 A1, 2008.
 52. Galley, G.; et al.; *Aminomethyl-2-imidazoles with affinity with the trace amine associated receptors and their preparation, pharmaceutical compositions and use in the treatment of diseases*, WO 2008046756 A1, 2008.
 53. Galley, G.; et al.; *Aminomethyl-4-imidazoles and their preparation, pharmaceutical compositions and use in the treatment of diseases*, WO 2008046757 A1, 2008.
 54. Galley, G.; et al.; *Preparation of 2-imidazoles for the treatment of CNS disorders*, WO 2007085558 A1, 2007.
 55. Galley, G.; et al.; *Preparation of aralkylimidazoles as ligands of trace amine associated receptors, especially TAAR1*, WO 2007085556 A2, 2007.
 56. Galley, G.; et al.; *Preparation of substituted 2-imidazole imidazoline derivatives for the treatment of diseases related to trace amine associated receptors*, WO 2007085557 A2, 2007.
 57. Scanlan, T.S.; et al.; *Thyronamine derivatives and analogs and methods of use thereof*, US 20050096485 A1, 2005.
 58. Naganathan, S., Exelixis Inc., South San Francisco, CA, Personal communication, c. 2002.
 59. Imanishi, M.; et al.; *Discovery of a Novel Series of Benzoic Acid Derivatives as Potent and Selective Human β_3 Adrenergic Receptor Agonists with Good Oral Bioavailability. Phenylethanolaminotetraline (PEAT) Skeleton Containing Biphenyl or Biphenyl Ether Moiety*. J. Med. Chem. **2008**, *51*, 4804-4822.
-

-
60. Tipparaju, S. K.; et al.; Design and synthesis of aryl ether inhibitors of the *Bacillus anthracis* enoyl-ACP reductase. *ChemMedChem*, **2008**, *3*, 1250-1268.
 61. Zhu, L.; Duquette, J.; Zhang, M.; An Improved Preparation of Arylboronates: Application in One-Pot Suzuki Biaryl Synthesis. *J. Org. Chem.* **2003**, *68*, 3729-3732.
 62. Chen, Z.; et al.; A New Multidentate Hexacarboxylic Acid for the Construction of Porous Metal-Organic Frameworks of Diverse Structures and Porosities. *Cryst. Growth Des.* **2010**, *10*, 2775-2779.
 63. Esumi, T.; et al.; Efficient synthesis and structure-activity relationship of honokiol, a neurotrophic biphenyl-type neolignan. *Bioorg. Med. Chem. Lett.* **2004**, *14*, 2621-2625.
 64. Inglis, S. R.; et al.; Synthesis and Evaluation of 3-(Dihydroxyboryl)benzoic Acids as D,D-Carboxypeptidase R39 Inhibitors. *J. Med. Chem.* **2009**, *52*, 6097-6106.
 65. Ishiyama, T.; Murata, M.; Miyaura, N. Palladium(0)-Catalyzed Cross-Coupling Reaction of Alkoxydiboron with Haloarenes: A Direct Procedure for Arylboronic Esters. *J. Org. Chem.* **1995**, *60*, 7508-10.
 66. Jin, S.; et al.; Synthesis, evaluation, and computational studies of naphthalimide-based long-wavelength fluorescent boronic acid reporters. *Chem.-Eur. J.* **2008**, *14*, 2795-2804.
 67. McKiernan, G. J.; Hartley, R. C. Boronate titanium alkylidene reagents for diversity-based synthesis of benzofurans. *Org. Lett.* **2003**, *5*(23), 4389-92.
 68. DiMauro, E. F.; Vitullo, J. R. Microwave-Assisted Preparation of Fused Bicyclic Heteroaryl Boronates: Application in One-Pot Suzuki Couplings. *J. Org. Chem.* **2006**, *71*, 3959-3962.
 69. Ley, S.V.; Thomas, A. W. Modern synthetic methods for copper-mediated C(aryl)-O, C(aryl)-N, and C(aryl)-S bond formation. *Angew. Chem., Int. Ed.* **2003**, *42*, 5400-5449.
 70. Kürti, L.S.; Czakó, B. *Strategic applications of named reactions in organic synthesis: background and detailed mechanisms*; Elsevier Academic Press I: Amsterdam; Boston, 2005; pp 464-467.
 71. Sigma-Aldrich: *Falling-film distillation heads* (accessed June 1, 2012), <http://www.sigmaaldrich.com/catalog/search?interface=All&term=falling-film%20&lang=en®ion=US&focus=product&N=0+220003048+219853269+219853286> p.
 72. Van Allen, D. Methodology and Mechanism: Reinvestigating the Ullmann Reaction, Ph.D. Dissertation, University of Massachusetts, Amherst, MA, 2004
-

-
73. Fan, X. Y.; et al.; AlCl₃ and BDMAEE: A Pair of Potent Reactive Regulators of Aryl Grignard Reagents and Highly Catalytic Asymmetric Arylation of Aldehydes. *Chem.-Eur. J.* **2010**, *16*, 7988-7991.
74. Chen, G.; et al.; Facile Preparation of α -Aryl Nitriles by Direct Cyanation of Alcohols with TMSCN Under the Catalysis of InX₃. *Org. Lett.* **2008**, *10*, 4573-4576.
75. Beignet, J. LinkedIn.com: *Can some one suggest ways to reduce an 2-(2-alkoxyphenyl)-2-phenylacetone nitrile to a 2-(2-alkoxyphenyl)-2-phenylethanolamine?*, 2012, http://www.linkedin.com/groups/Can-some-one-suggest-ways-923867.S.111649468?qid=c9e503d9-2127-4a41-87bb-31e2304-da5c6&trk=group_items_see_more-0-b-ttl p.
76. Rannug, U.; et al.; International Commission for Protection against Environmental Mutagens and Carcinogens. An evaluation of the genetic toxicity of paracetamol. *Mutat. Res.* **1995**, *327*(1-2), 179-200.
77. McGregor, D. Hydroquinone: an evaluation of the human risks from its carcinogenic and mutagenic properties. *Crit. Rev. Toxicol.* **2007**, *37*(10), 887-914.
78. Cha, J. S.; Kwon, S. S. Exceptionally facile reduction of carboxylic esters to aldehydes by lithium aluminum hydride in the presence of diethylamine. *J. Org. Chem.* **1987**, *52*, 5486-5487.
79. Wikipedia: *Forskolin* (accessed May 15, 2013), <http://en.wikipedia.org/wiki/Forskolin>
80. Connors, K.A. *Chemical Kinetics: The Study of Reaction Rates in Solution*; John Wiley & Sons: New York, 1990; p 179.
81. ALA Scientific: *OctaFlow II Multi-function Multi-valve Perfusion System* (accessed May 10, 2013), http://www.alascience.com/products/index.php?main_page=product_info&cPath=1_6&products_id=57
82. Suchland, K. Oregon Health & Science University, Portland, OR, Unpublished work, 2007.
83. *By reason of similarity*: a logical argument stating that if **A** is similar to **B**, then **A** will have similar properties to **B**. In Euclidean geometry, two triangles are similar if their corresponding interior angles are equivalent. By similarity, the length of the sides of one triangle will be proportional to the length of the corresponding sides of the other triangle.
84. Compounds can be designated as agonists, neutral antagonists (does not block basal activity) or inverse agonists (an antagonist that blocks basal activity) when dealing with enzymes and receptors that have basal activity. Depending on how strongly they effect their target proteins, compounds may get the modifier of either “full” or “partial” and sometimes “super.” The author dislikes the conventional names, as they can easily lead to confusion,
-

and prefers “activator” instead of “agonist” and “inhibitor” instead of “antagonist,” with inhibitors being further broken down into “access inhibitors” which prevent other ligands from binding to the protein, “active-site inhibitors” an inhibitor that binds to the active site, “conformational inhibitors” taking the place of “inverse agonist” and which prevent the protein from spontaneously changing into the active form, finally “allosteric inhibitors” which prevent allosteric activation.

85. Connors, K. A. *Chemical Kinetics: The Study of Reaction Rates in Solution*; John Wiley & Sons: New York, 1990.
86. Revel, F. G.; et al.; Brain-specific overexpression of trace amine-associated receptor 1 alters monoaminergic neurotransmission and decreases sensitivity to amphetamine. *Neuropsychopharmacology*. **2012**, 37(12), 2580-2592.

A.1 5-bromo-2-(hexyloxy)benzaldehyde: G4-012s16

FIGURE A.1: Structure of G4-012s16.

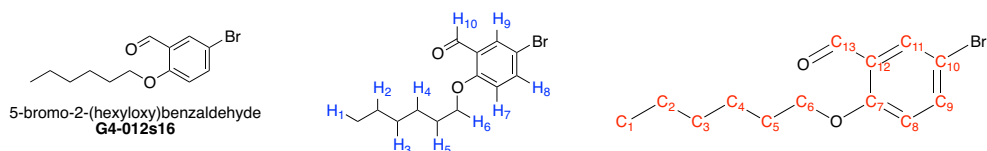


TABLE A.1: ^1H -NMR assignments for G4-012s16, 600 MHz in DMSO (2.50 ppm)

Proton	ppm ^a	Number	Type	J_a	J_b
H ₁	0.870	3	t	6.9	
H ₂ & H ₃	1.309	4	m		
H ₄	1.435	2	m		
H ₅	1.763	2	m		
H ₆	4.126	2	t	6.6	
H ₇	7.225	1	d	9.0	
H ₈	7.79	1	dd	9.0	3.0
H ₉	7.724	1	d	3.0	
H ₁₀	10.286	1	s		

a. Taken at the center of the peak.

TABLE A.2: ^{13}C -NMR assignments for G4-012s16, 600 MHz in DMSO (39.50 ppm)

Carbon	ppm
C ₁	13.84
C ₂	21.98
C ₃	30.87
C ₄	25.02
C ₅	28.28
C ₆	68.82
C ₇	160.08
C ₈	116.33
C ₉	138.45
C ₁₀	112.23
C ₁₁	129.69
C ₁₂	125.7
C ₁₃	187.99

5-bromo-2-(hexyloxy)benzaldehyde: G4-012s16

FIGURE A.2: ^1H -NMR of G4-012s16.

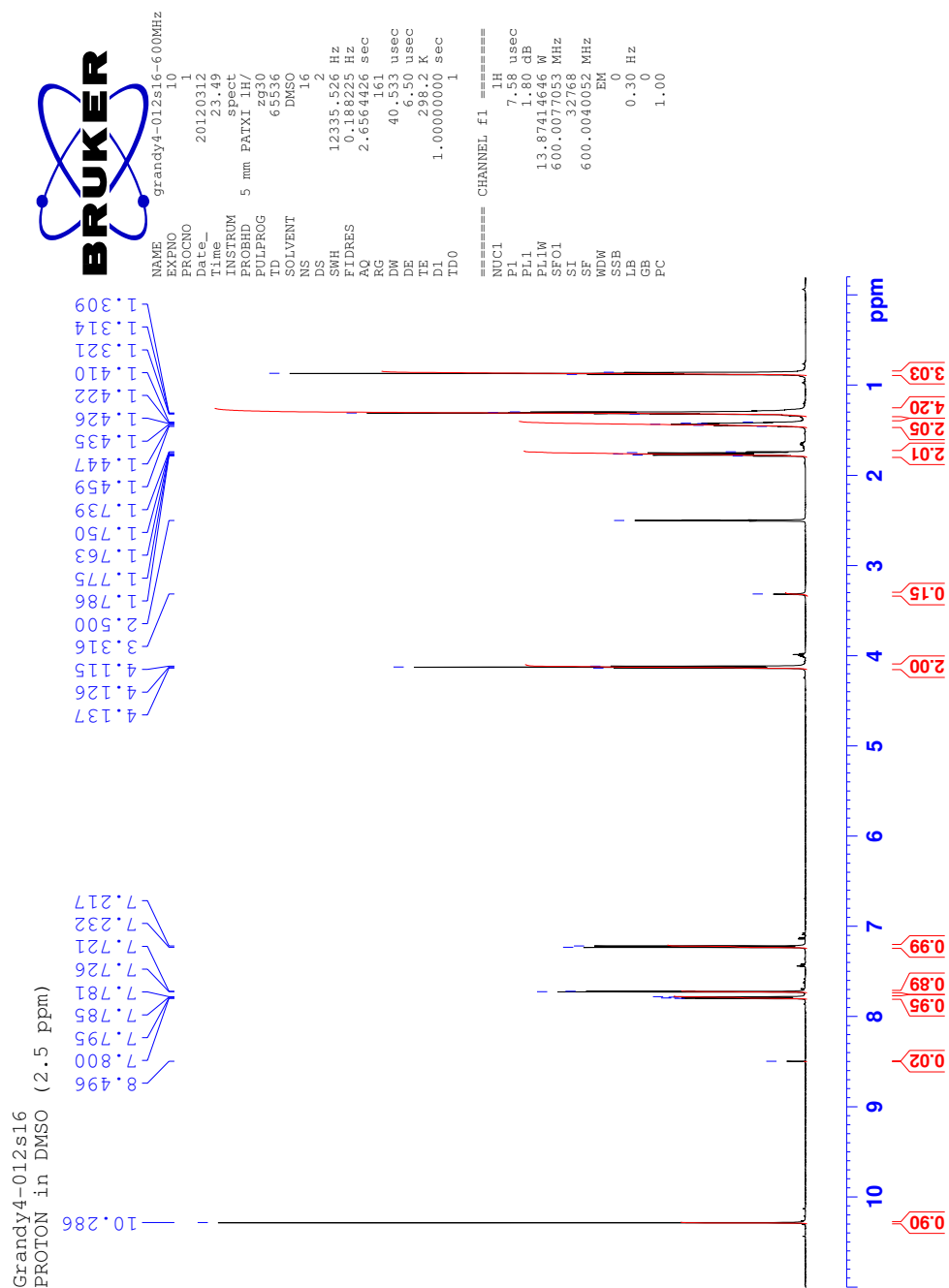
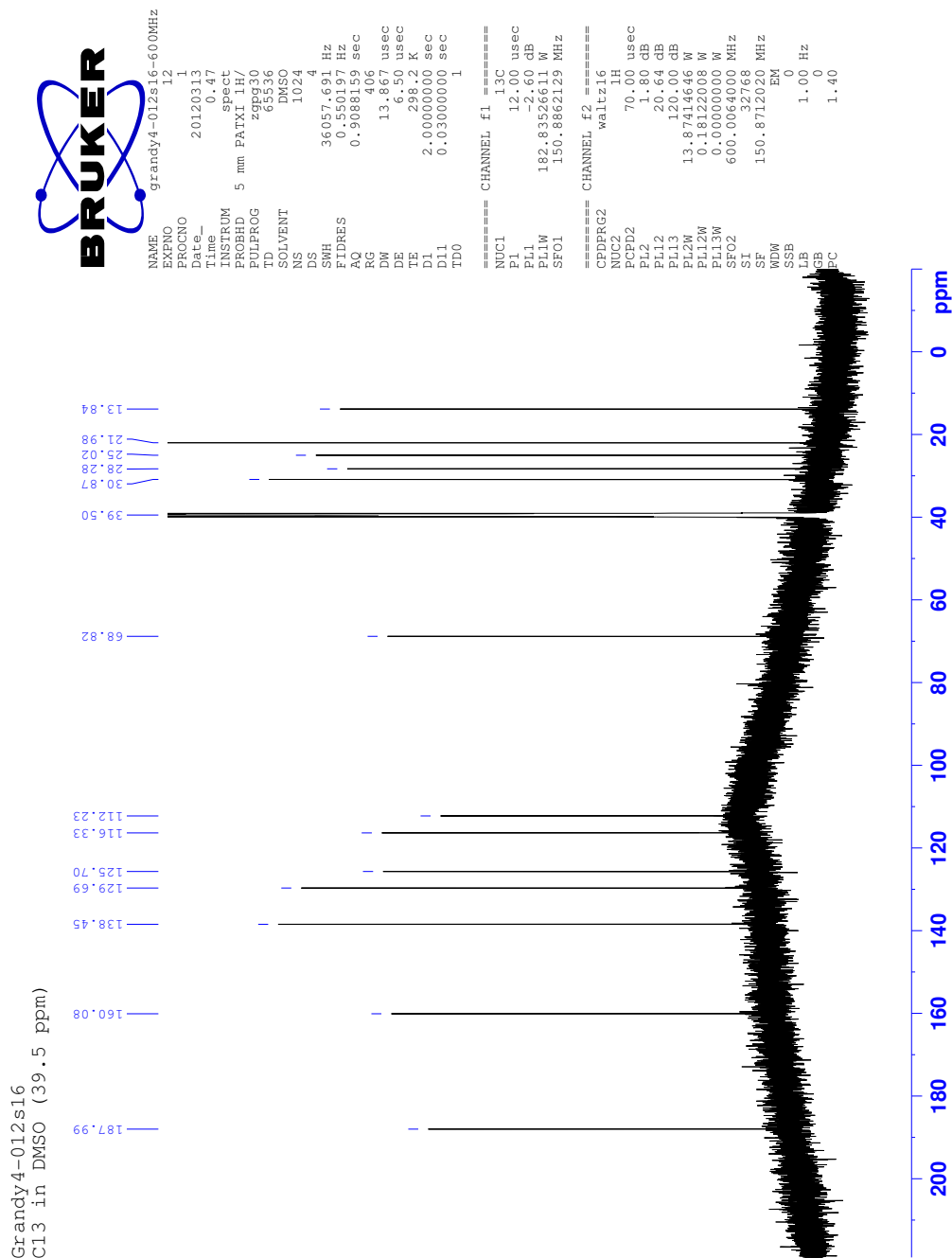


FIGURE A.3: COSY-NMR of G4-012s16.



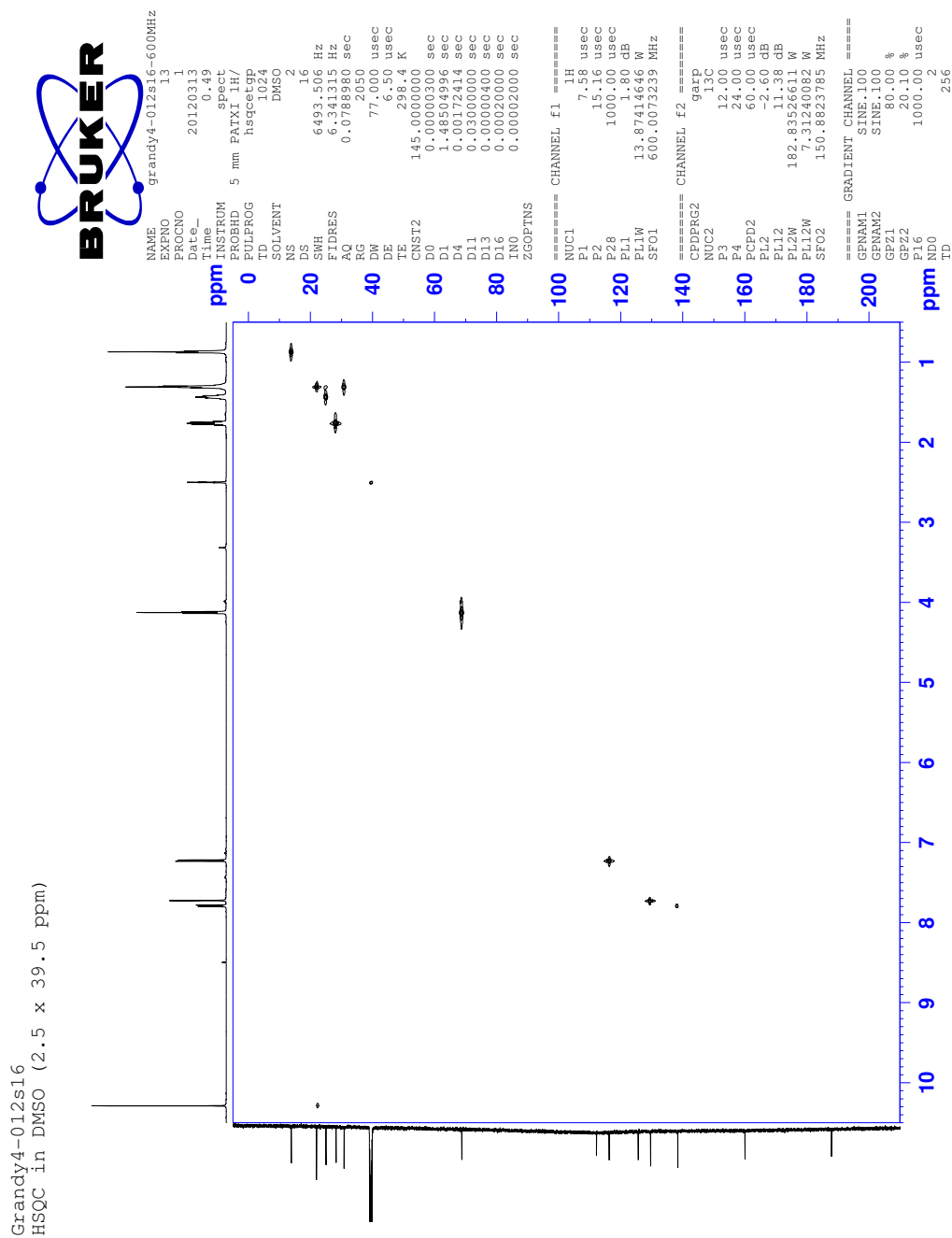
5-bromo-2-(hexyloxy)benzaldehyde: G4-012s16

FIGURE A.4: ^{13}C -NMR of G4-012s16.



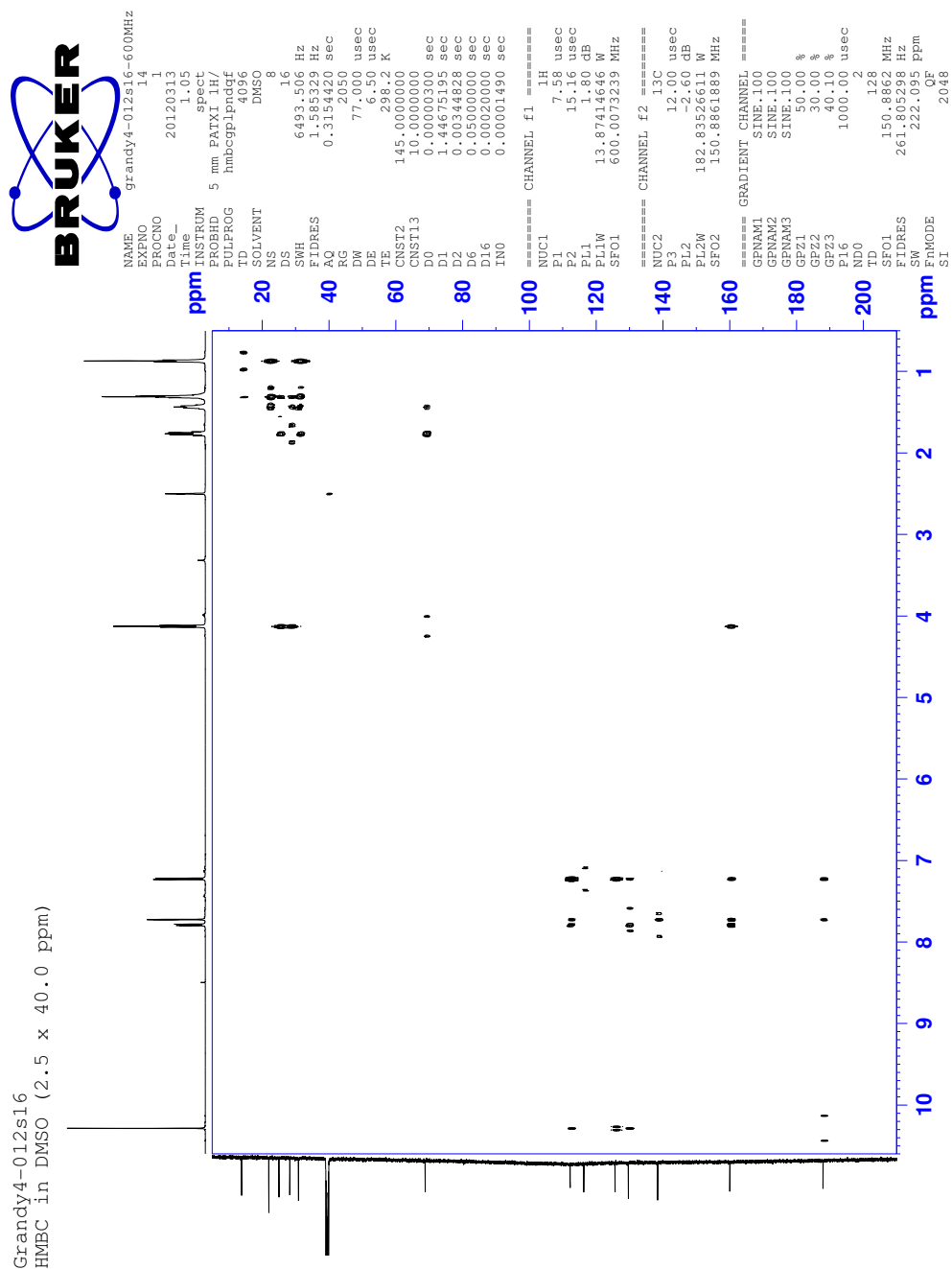
5-bromo-2-(hexyloxy)benzaldehyde: G4-012s16

FIGURE A.5: HSQC-NMR of G4-012s16.



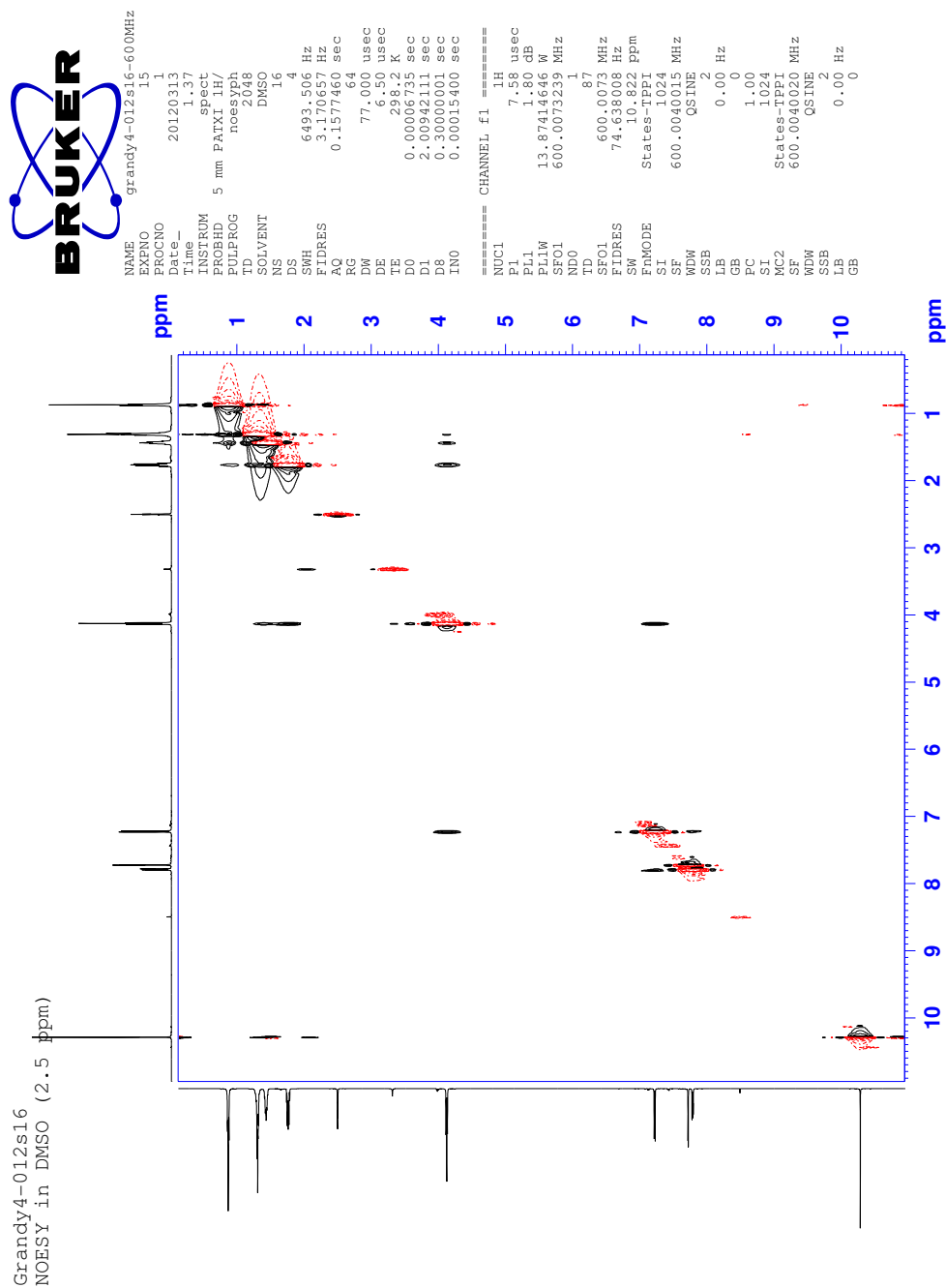
5-bromo-2-(hexyloxy)benzaldehyde: G4-012s16

FIGURE A.6: HMBC-NMR of G4-012s16.



5-bromo-2-(hexyloxy)benzaldehyde: G4-012s16

FIGURE A.7: NOESY-NMR of G4-012s16.



5-(4-fluorophenoxy)-2-(hexyloxy)benzaldehyde: G4-068s20 & G4-070s6

A.2 5-(4-fluorophenoxy)-2-(hexyloxy)benzaldehyde: G4-068s20 & G4-070s6

FIGURE A.8: Structure of G4-070s6.

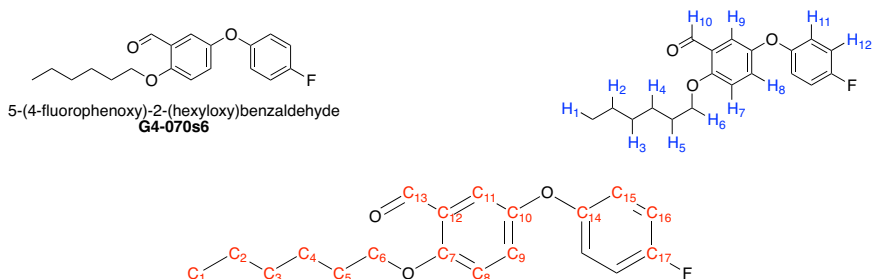


TABLE A.3: ^1H -NMR assignments for G4-070s6, 600 MHz in DMSO (2.50 ppm)

Proton	ppm ^a	Number	Type	J_a	J_b
H ₁	0.885	3	t	6.9	
H ₂ & H ₃	1.328	4	m		
H ₄	1.456	2	m		
H ₅	1.779	2	m		
H ₆	4.132	2	t	6.6	
H ₇	7.289	1	d	9.0	
H ₈	7.380	1	dd	9.0	3.0
H ₉	7.189	1	d	3.0	
H ₁₀	10.337	1	s		
H ₁₁	7.231	2	m		
H ₁₂	7.054	2	m		

a. Taken at the center of the peak.

TABLE A.4: ^{13}C -NMR assignments for G4-070s6, 600 MHz in DMSO (39.50 ppm)

Carbon	ppm
C ₁	13.86
C ₂	22.00
C ₃	30.90
C ₄	25.09
C ₅	28.43
C ₆	68.90
C ₇	157.36
C ₈	115.77
C ₉	126.94
C ₁₀	150.35
C ₁₁	115.96
C ₁₂	124.83
C ₁₃	188.54
C ₁₄	152.99
C ₁₅	116.61
C ₁₆	120.16
C ₁₇	158.93

5-(4-fluorophenoxy)-2-(hexyloxy)benzaldehyde: G4-068s20 & G4-070s6

FIGURE A.9: ^1H -NMR of G4-070s6.

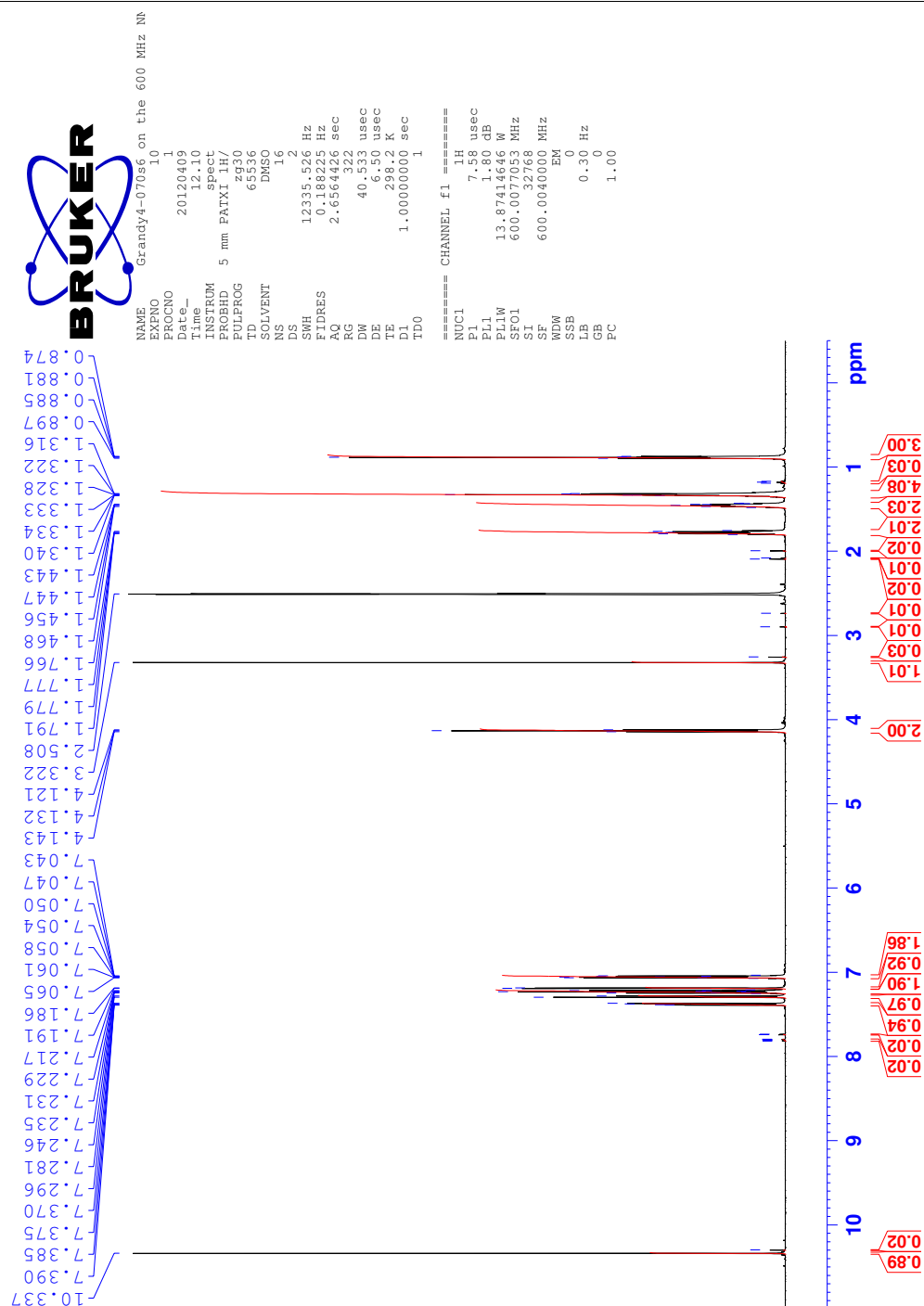
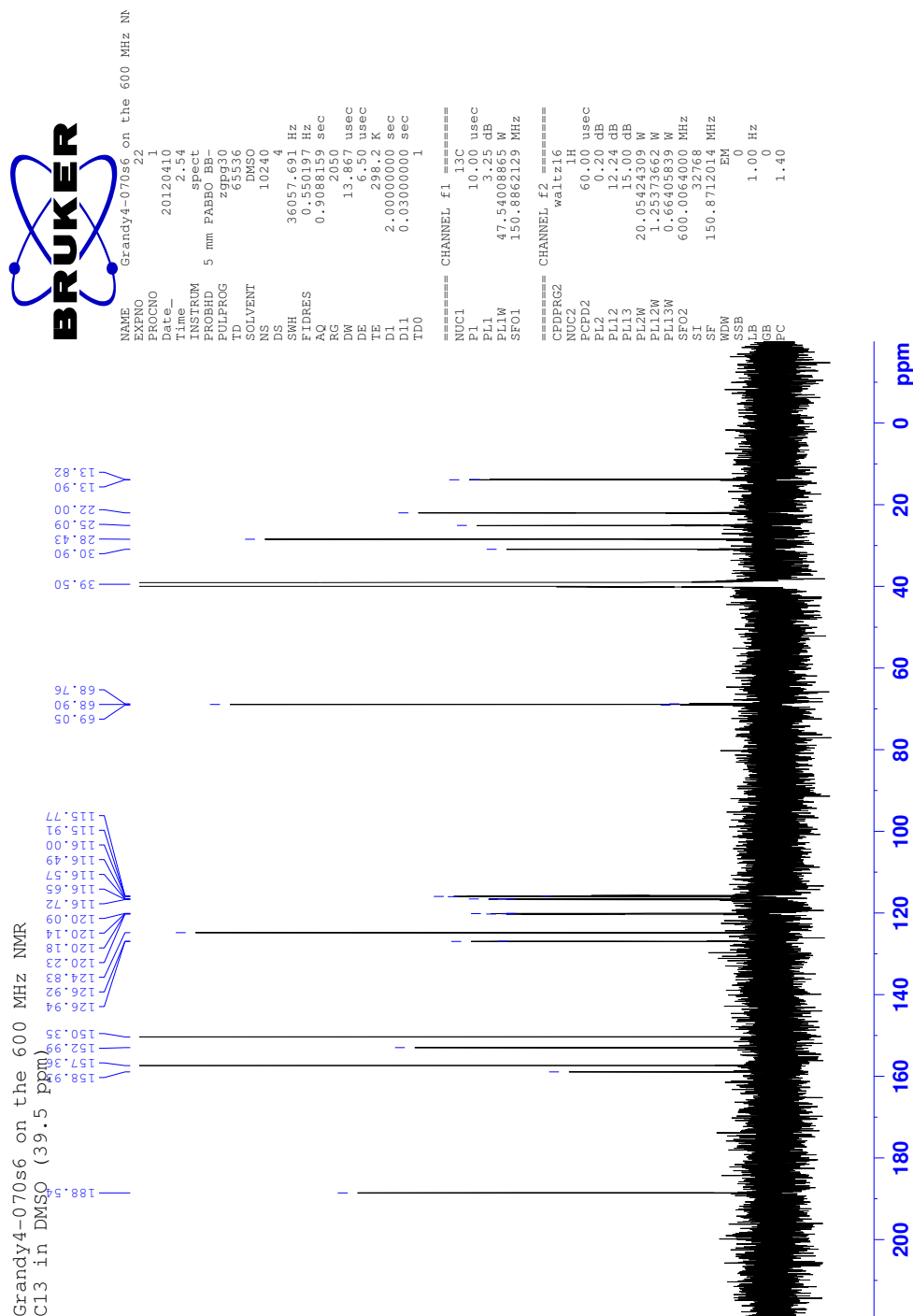


FIGURE A.10: COSY-NMR of G4-070s6.



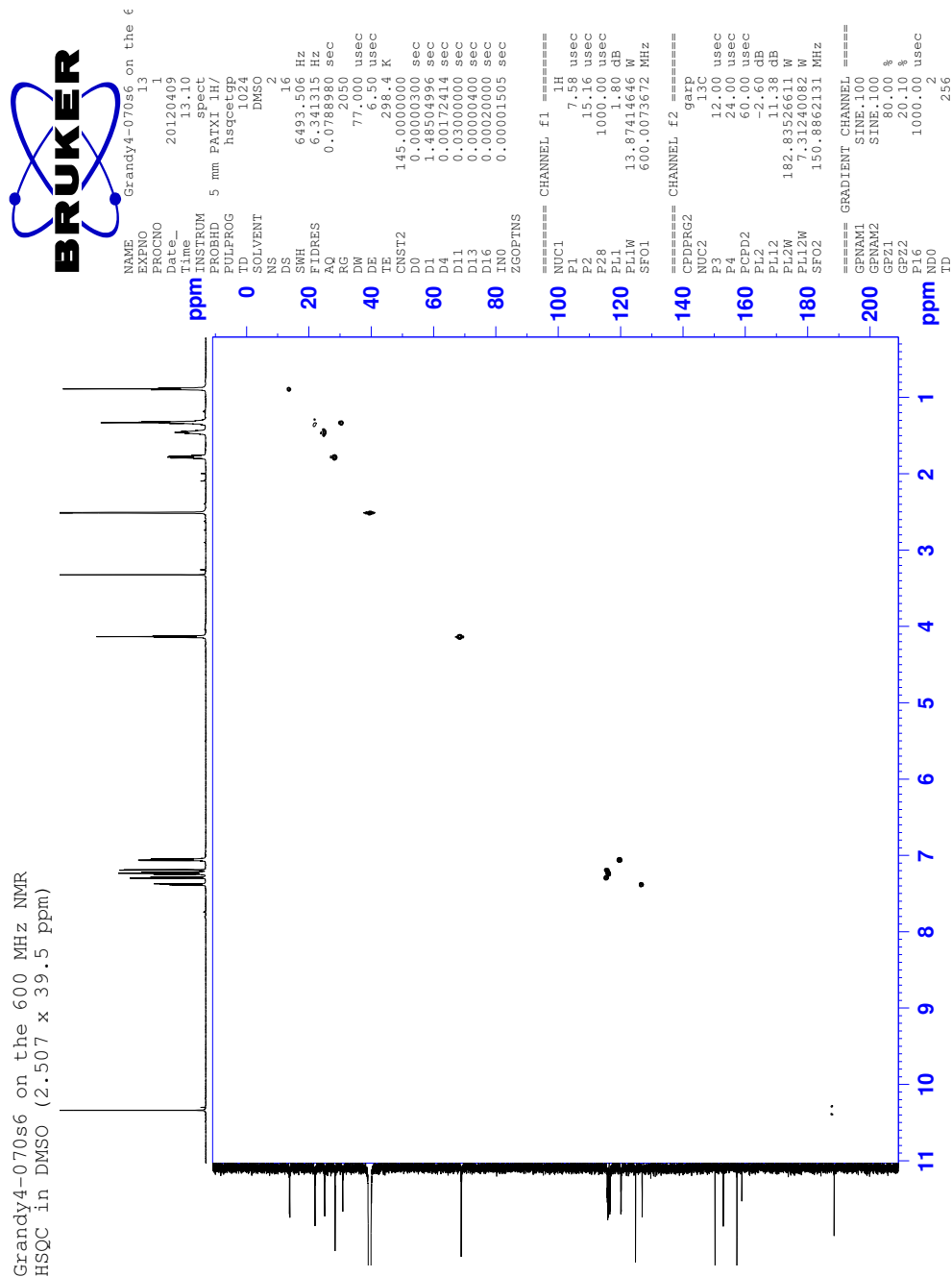
5-(4-fluorophenoxy)-2-(hexyloxy)benzaldehyde: G4-068s20 & G4-070s6

FIGURE A.11: ^{13}C -NMR of G4-070s6.



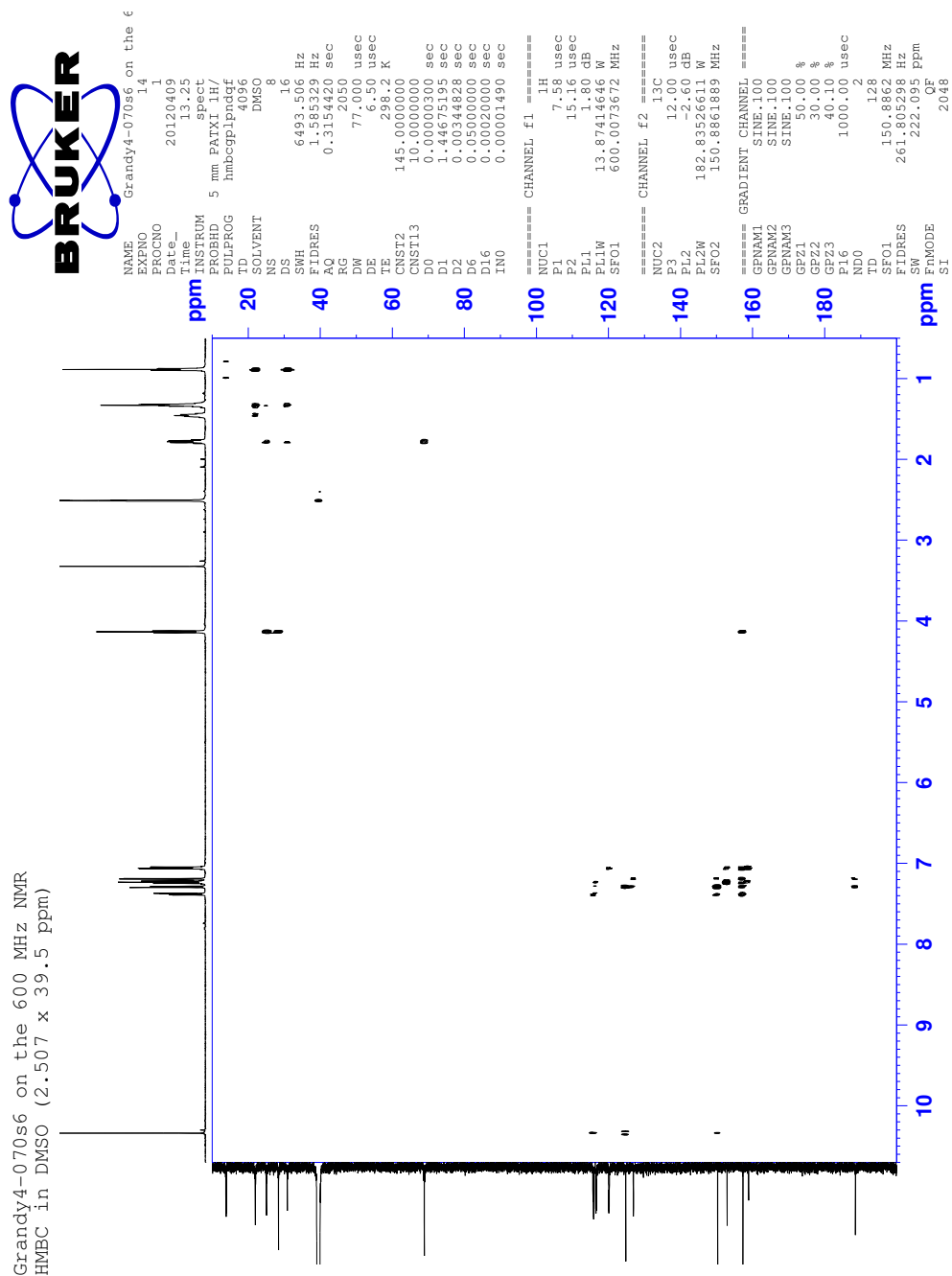
5-(4-fluorophenoxy)-2-(hexyloxy)benzaldehyde: G4-068s20 & G4-070s6

FIGURE A.12: HSQC-NMR of G4-070s6.



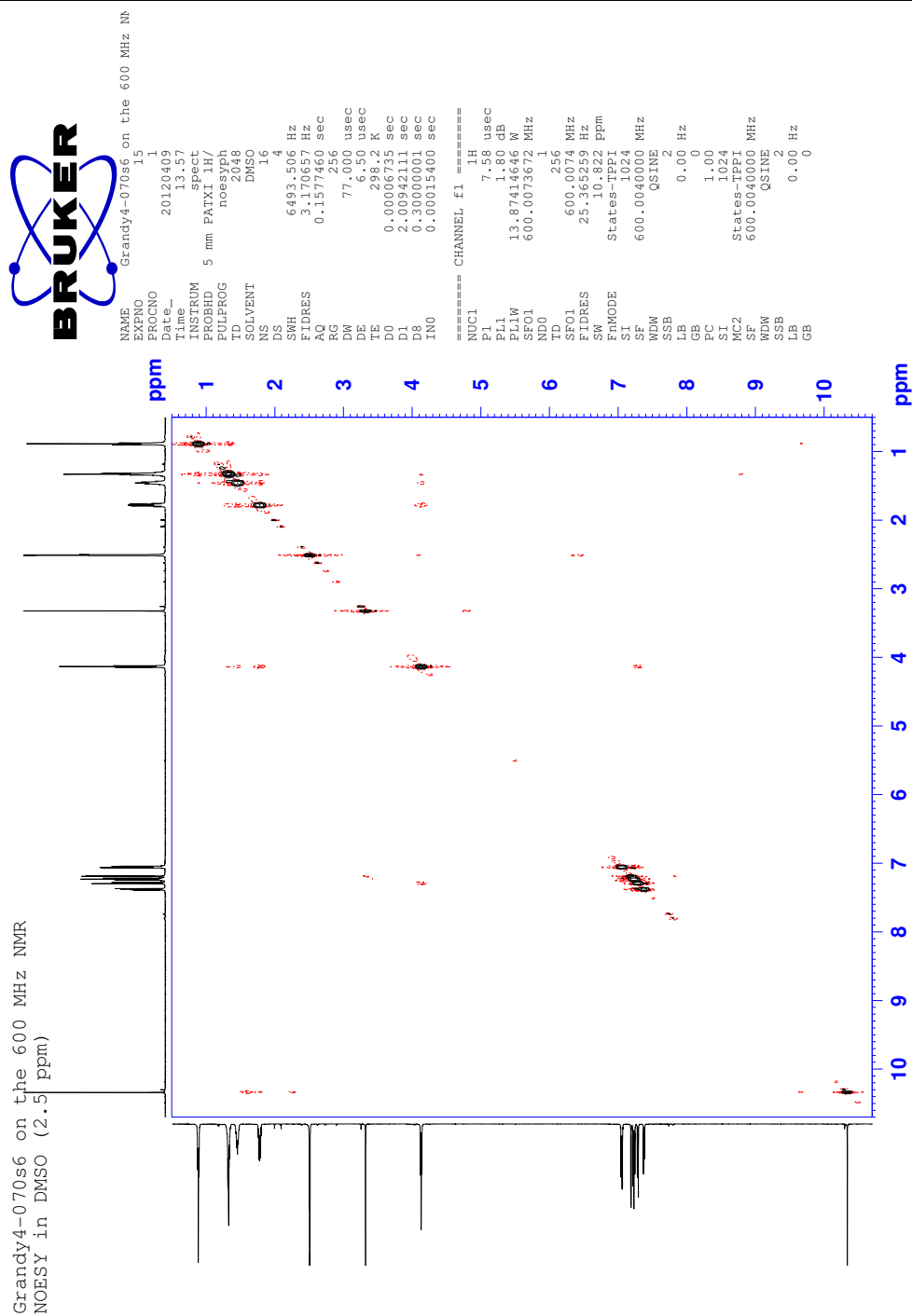
5-(4-fluorophenoxy)-2-(hexyloxy)benzaldehyde: G4-068s20 & G4-070s6

FIGURE A.13: HMBC-NMR of G4-070s6.



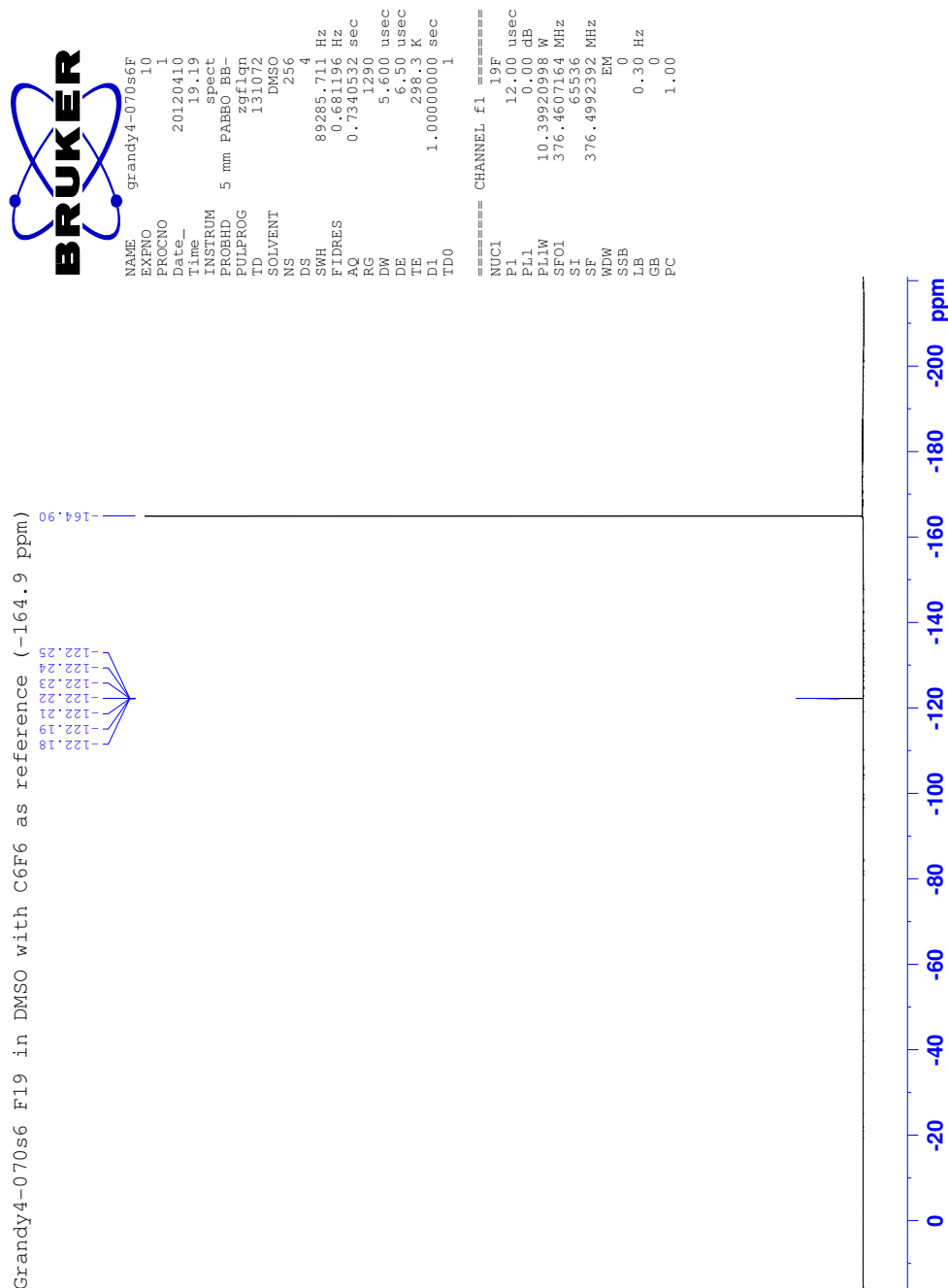
5-(4-fluorophenoxy)-2-(hexyloxy)benzaldehyde: G4-068s20 & G4-070s6

FIGURE A.14: NOESY-NMR of G4-070s6.

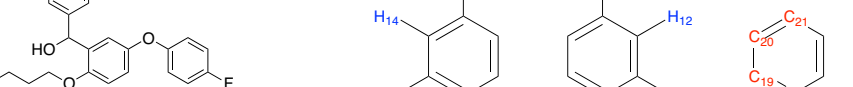


5-(4-fluorophenoxy)-2-(hexyloxy)benzaldehyde: G4-068s20 & G4-070s6

FIGURE A.15: ^{19}F -NMR of G4-070s6, 400 MHz with C_6F_6 (-164.0 ppm).



A.3 (5-(4-fluorophenoxy)-2-(hexyloxy)phenyl)(phenyl)methanol: G4-074s14



 (5-(4-fluorophenoxy)-2-((hexyloxy)phenyl)(phenyl)methanol
G4-074s14

Proton	ppm ^a	Number	Type	J _a	J _b
H ₁	0.881	3	t	7.2	
H ₂ & H ₃	1.289	4	m		
H ₄	1.354	2	m		
H ₅	1.660	2	m		
H ₆	3.888	2	m		
H ₇	6.922	1	d	9.0	
H ₈	6.848	1	dd	9.0	3.0
H ₉	7.228	1	d	3.0	
H ₁₀	5.912	1	d	9.3	
H ₁₁	7.197	2	m		
H ₁₂	6.974	2	m		
H ₁₃	7.186	2	m		
H ₁₄	7.287	2	m		
H ₁₅	7.265	2	m		
H ₁₆	5.730	1	d		

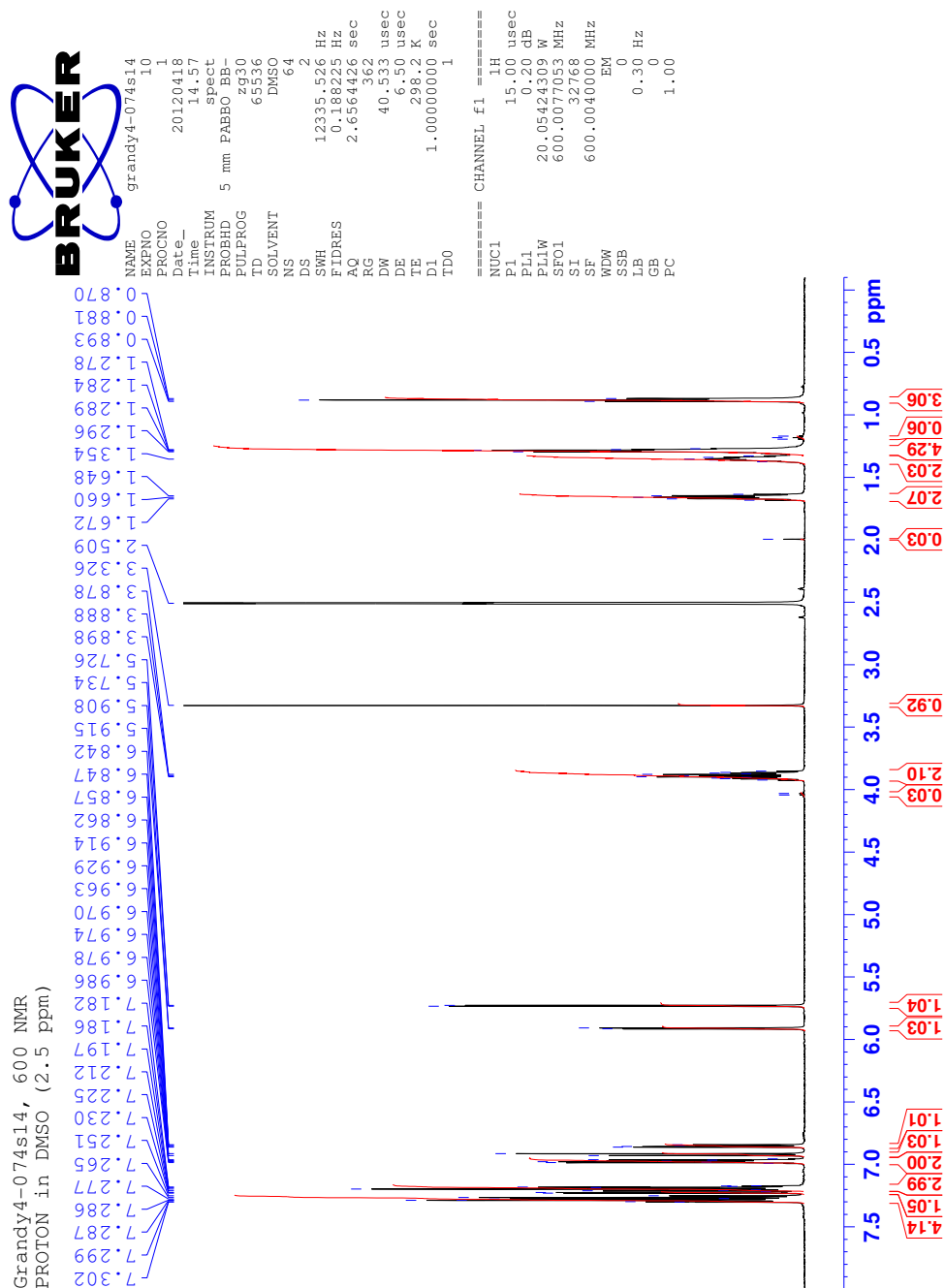
Carbon	ppm ^a	Carbon	ppm ^a	Type ^b	J
C ₁	13.87	C ₁₂	135.38		
C ₂	22.03	C ₁₃	68.22		
C ₃	30.93	C ₁₄	153.94		
C ₄	25.22	C ₁₅	119.20	d	7.5
C ₅	28.69	C ₁₆	116.33	d	22.6
C ₆	67.90	C ₁₇	157.64	d	239.9
C ₇	151.09	C ₁₈	144.80		
C ₈	112.58	C ₁₉	126.65		
C ₉	117.92	C ₂₀	127.82		
C ₁₀	149.73	C ₂₁	126.54		
C ₁₁	117.16				

b. Singlet unless noted otherwise.

181

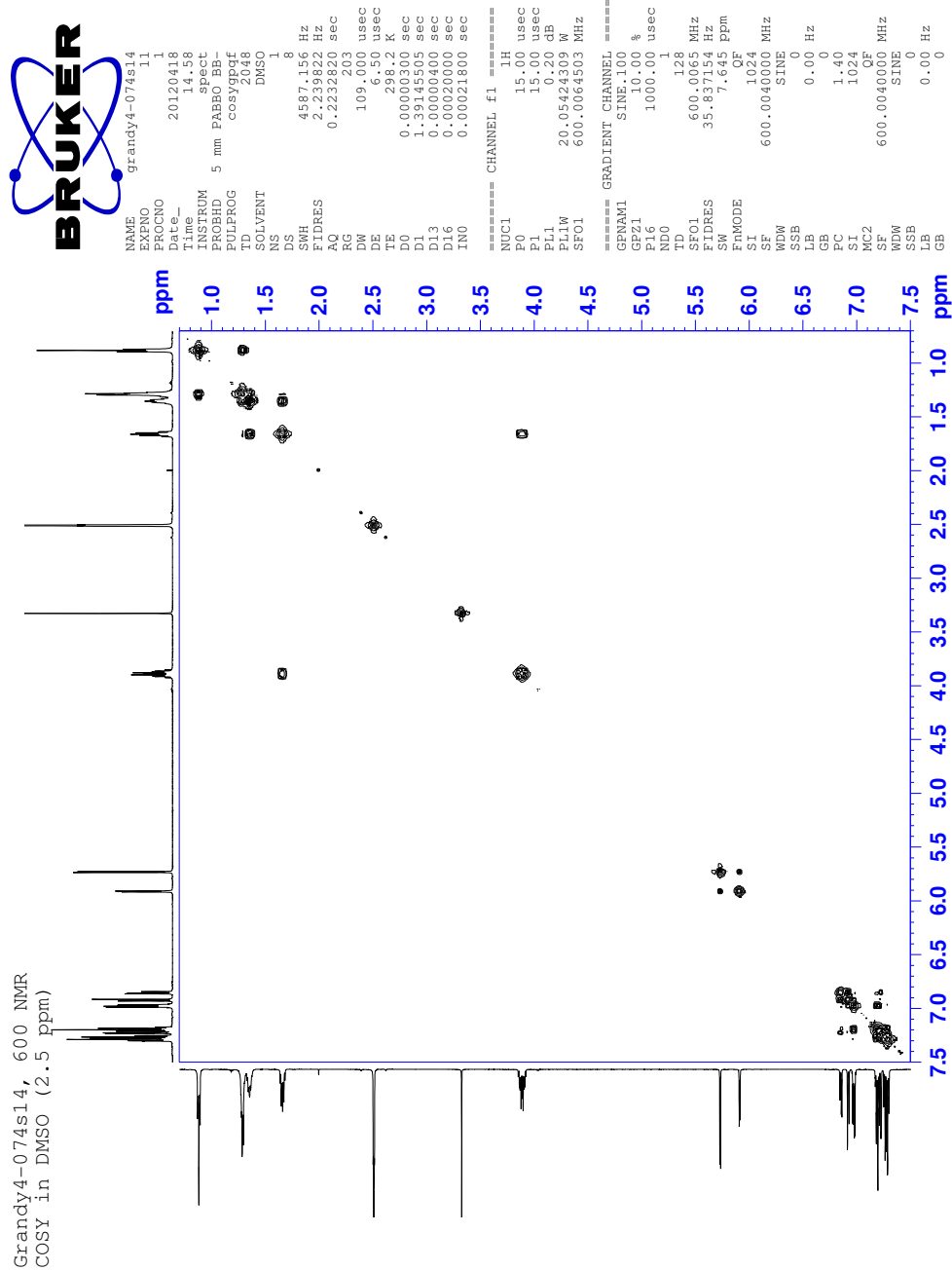
(5-(4-fluorophenoxy)-2-(hexyloxy)phenyl)(phenyl)methanol: G4-074s14

FIGURE A.17: ^1H -NMR of G4-074s14.



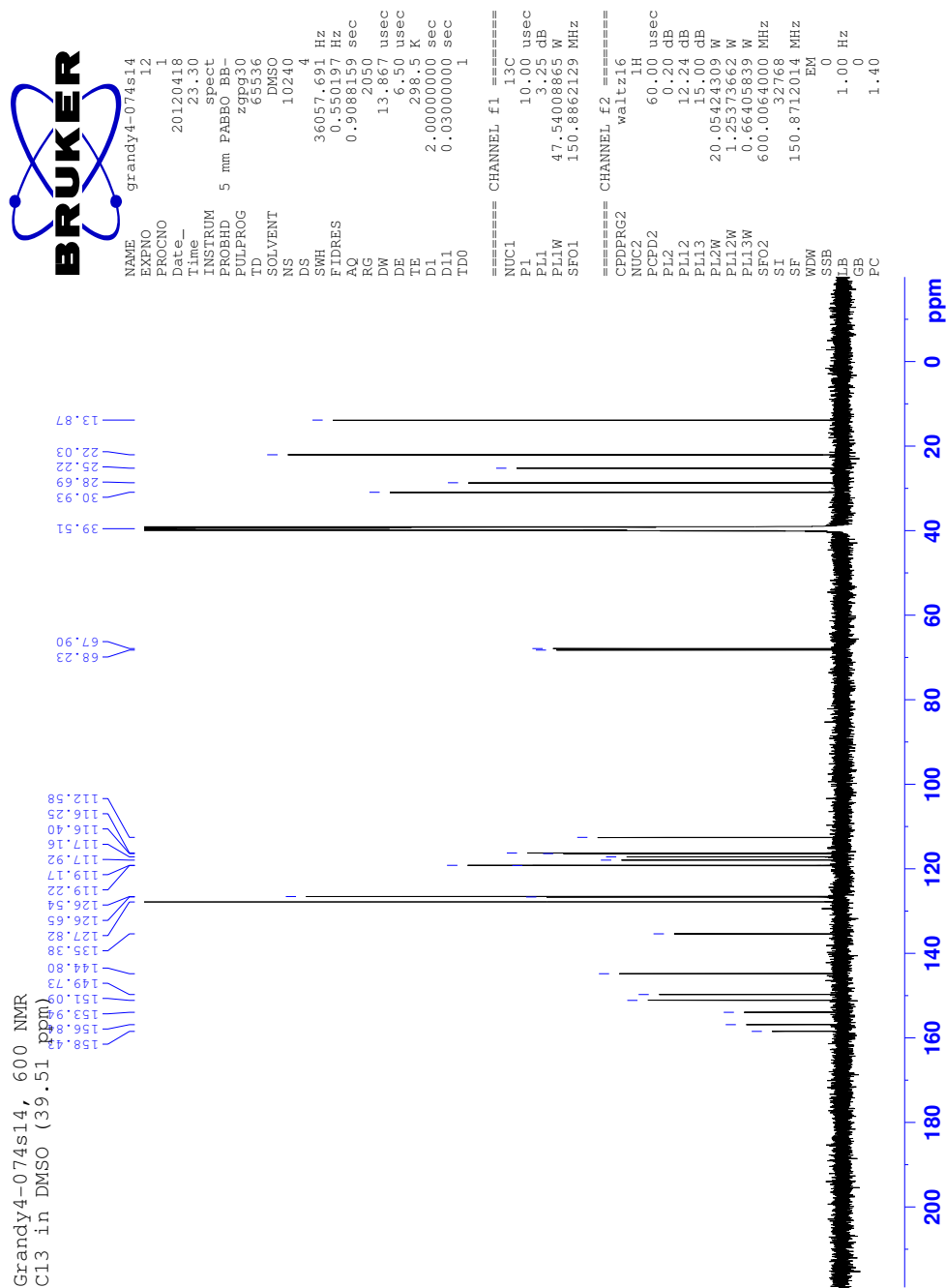
(5-(4-fluorophenoxy)-2-(hexyloxy)phenyl)(phenyl)methanol: G4-074s14

FIGURE A.18: COSY-NMR of G4-074s14.



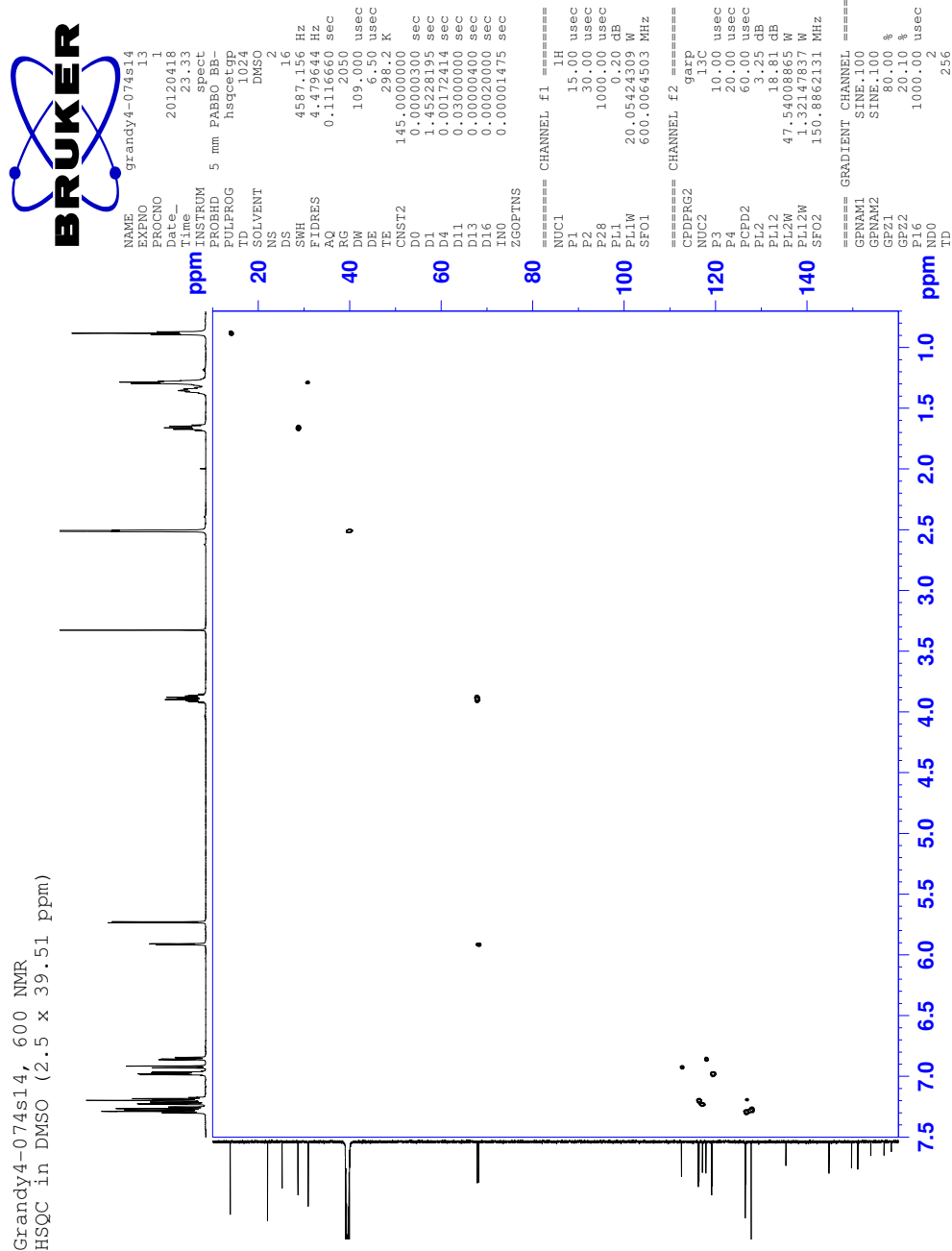
(5-(4-fluorophenoxy)-2-(hexyloxy)phenyl)(phenyl)methanol: G4-074s14

FIGURE A.19: ^{13}C -NMR of G4-074s14.



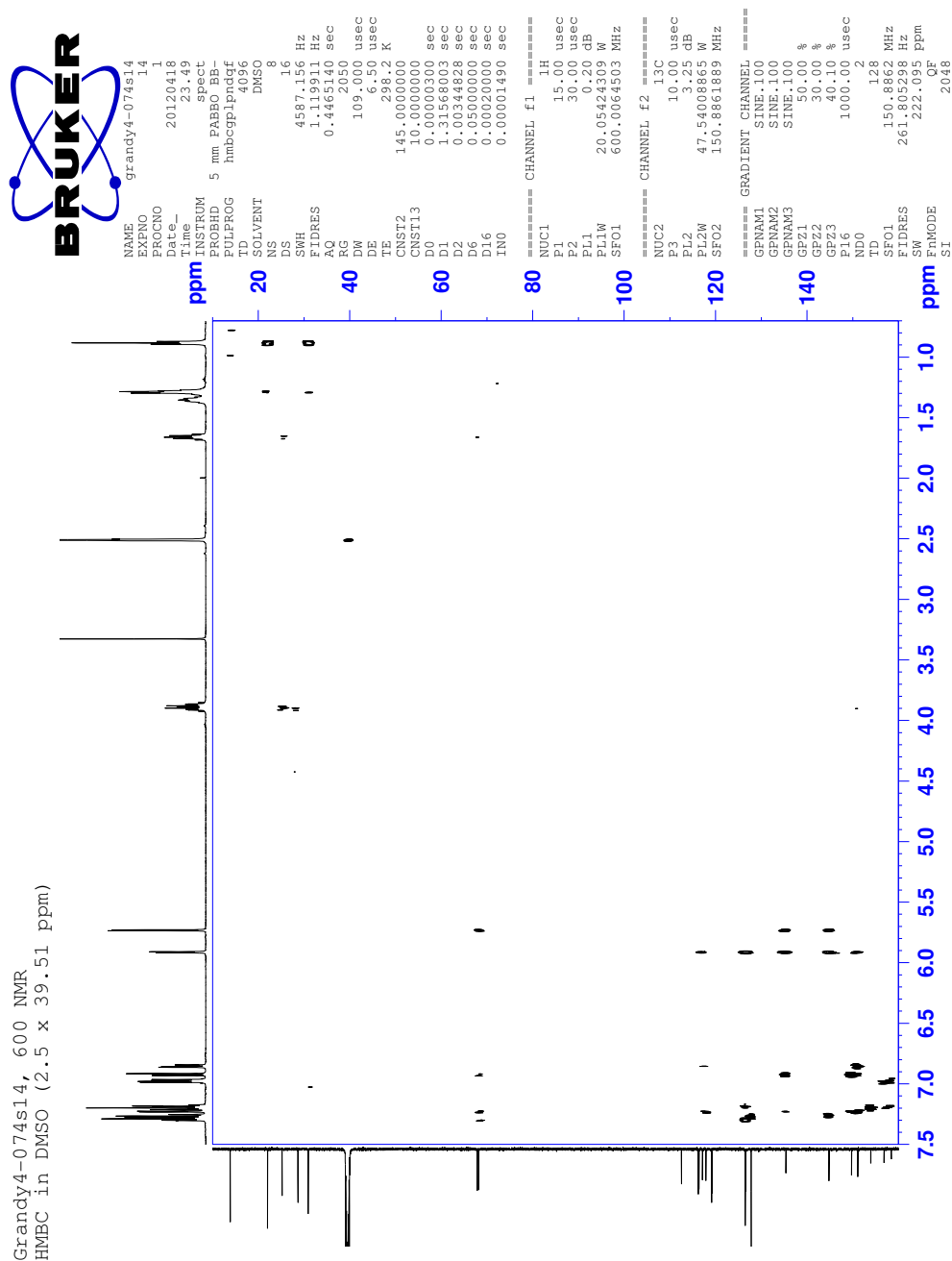
(5-(4-fluorophenoxy)-2-(hexyloxy)phenyl)(phenyl)methanol: G4-074s14

FIGURE A.20: HSQC-NMR of G4-074s14.



(5-(4-fluorophenoxy)-2-(hexyloxy)phenyl)(phenyl)methanol: G4-074s14

FIGURE A.21: HMBC-NMR of G4-074s14.



(5-(4-fluorophenoxy)-2-(hexyloxy)phenyl)(phenyl)methanol: G4-074s14

FIGURE A.22: NOESY-NMR of G4-074s14.

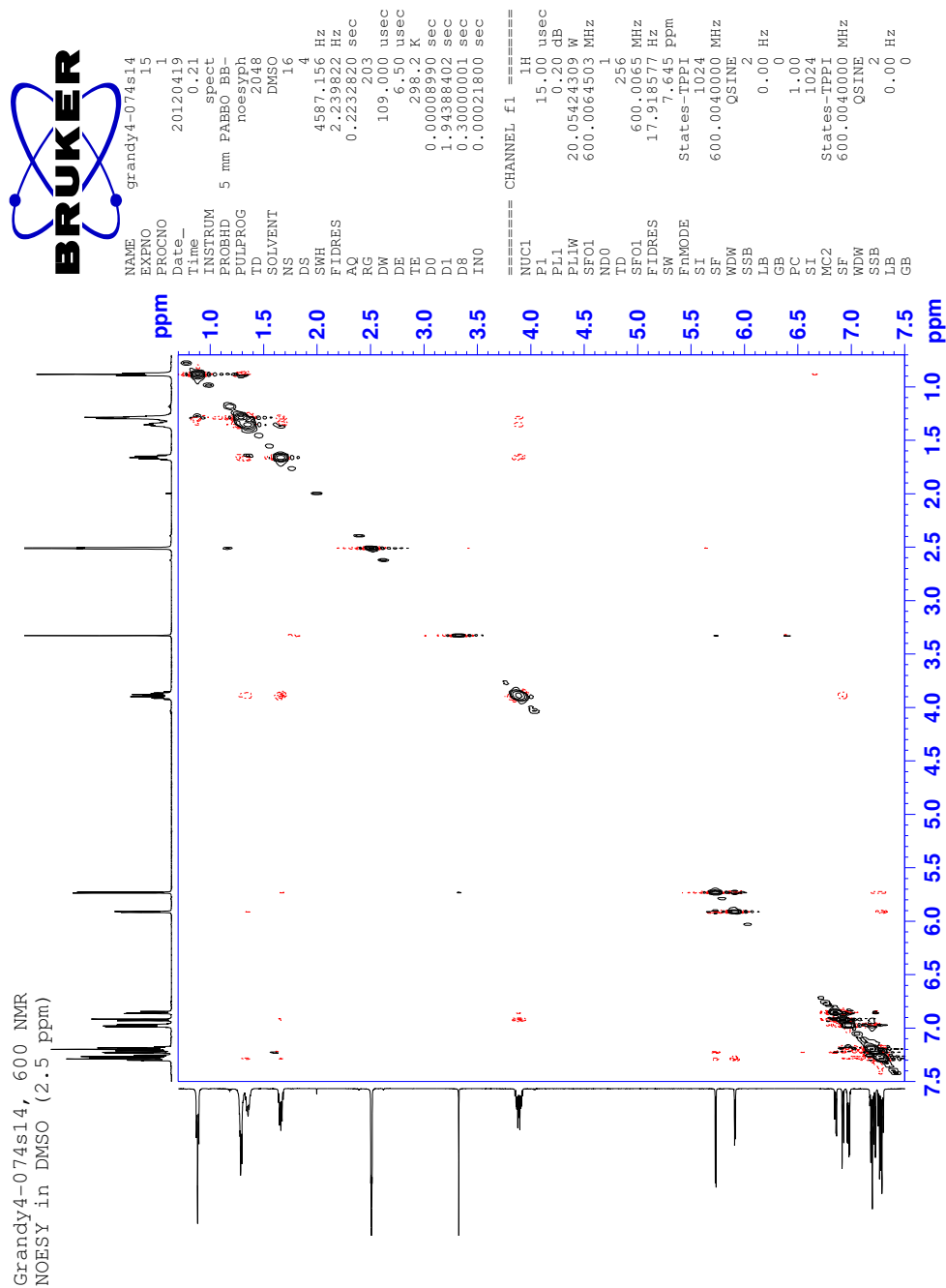
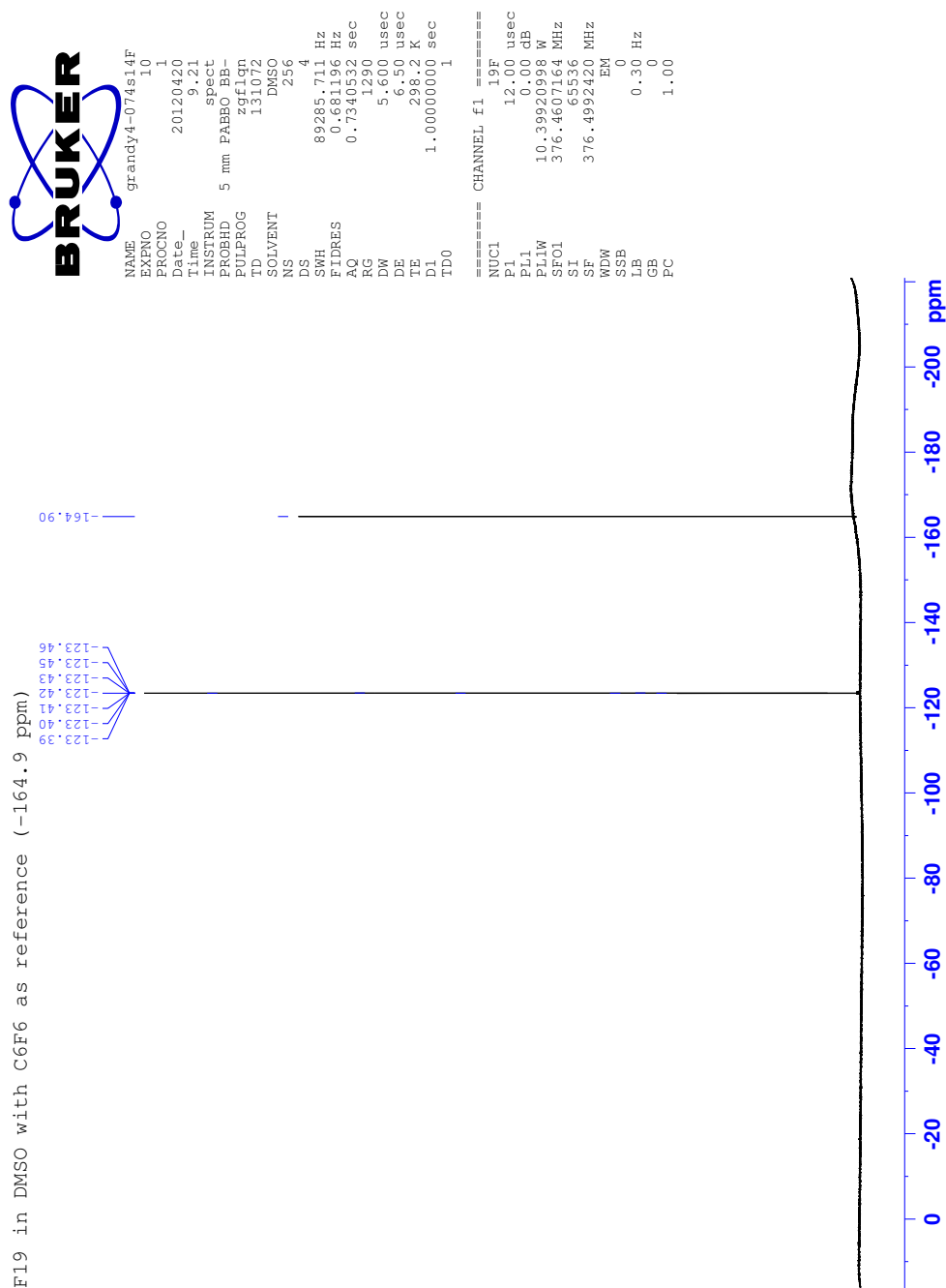


FIGURE A.23: ^{19}F -NMR of **G4-074s14**, 400 MHz with C_6F_6 (-164.0 ppm).



2-(5-(4-fluorophenoxy)-2-(hexyloxy)phenyl)-2-phenylacetonitrile: G4-079s9

A.4 2-(5-(4-fluorophenoxy)-2-(hexyloxy)phenyl)-2-phenylacetonitrile: G4-079s9

FIGURE A.24: Structure of G4-079s9.

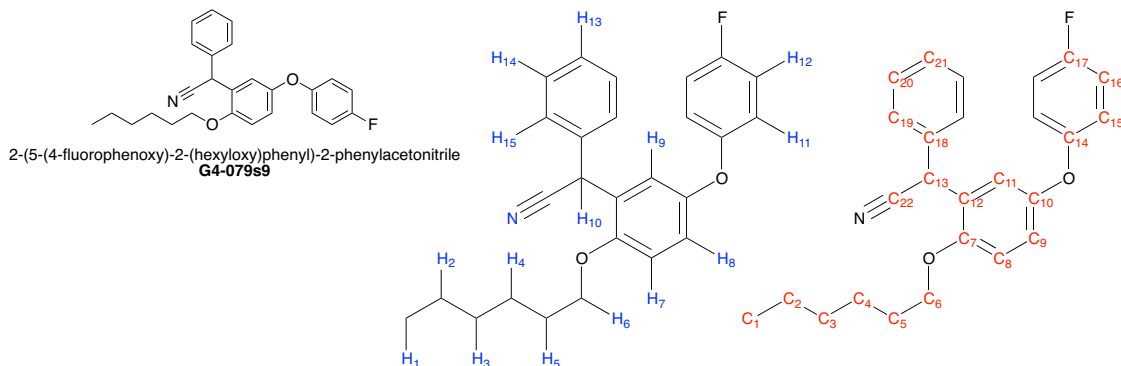


TABLE A.7: ^1H -NMR assignments for G4-079s9, 600 MHz in DMSO (2.51 ppm)

Proton	ppm ^a	Number	Type	J_a	J_b
H ₁	0.874	3	t	7.5	
H ₂ & H ₃	1.269	4	m		
H ₄	1.331	2	m		
H ₅	1.644	2	m		
H ₆	3.929	2	m		
H ₇	7.060	1	d	9.0	
H ₈	6.994	1	dd	9.0	3.0
H ₉	7.094	1	d	3.0	
H ₁₀	5.748	1	s		
H ₁₁	7.210	2	m		
H ₁₂	7.015	2	m		
H ₁₃	7.320	2	m		
H ₁₄	7.385	2	m		
H ₁₅	7.357	2	m		

a. Taken at the center of the peak.

TABLE A.8: ^{13}C -NMR assignments for G4-079s9, 600 MHz in DMSO (39.52 ppm)

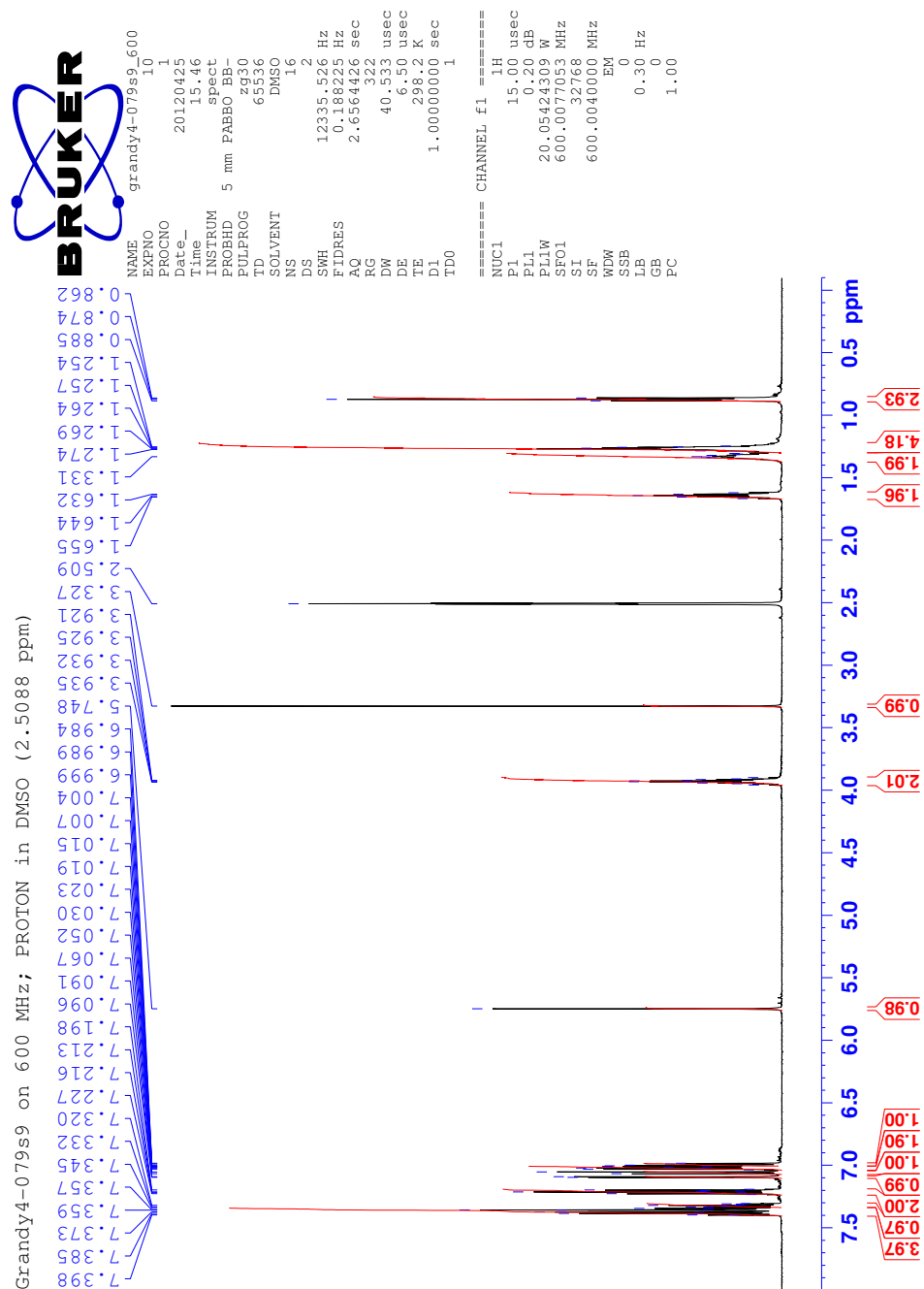
Carbon	ppm ^a	Carbon	ppm ^a	Type ^b	J
C ₁	13.86	C ₁₂	125.37		
C ₂	21.99	C ₁₃	36.61		
C ₃	30.94	C ₁₄	153.47	d	1.5
C ₄	25.04	C ₁₅	119.53	d	7.5
C ₅	28.50	C ₁₆	116.47	d	22.6
C ₆	68.33	C ₁₇	157.88	d	239.9
C ₇	151.86	C ₁₈	135.37		
C ₈	113.67	C ₁₉	127.41		
C ₉	119.76	C ₂₀	128.76		
C ₁₀	149.74	C ₂₁	127.75		
C ₁₁	119.79	C ₂₂	119.62		

a. Taken at the center of the peak.

b. Singlet unless noted otherwise.

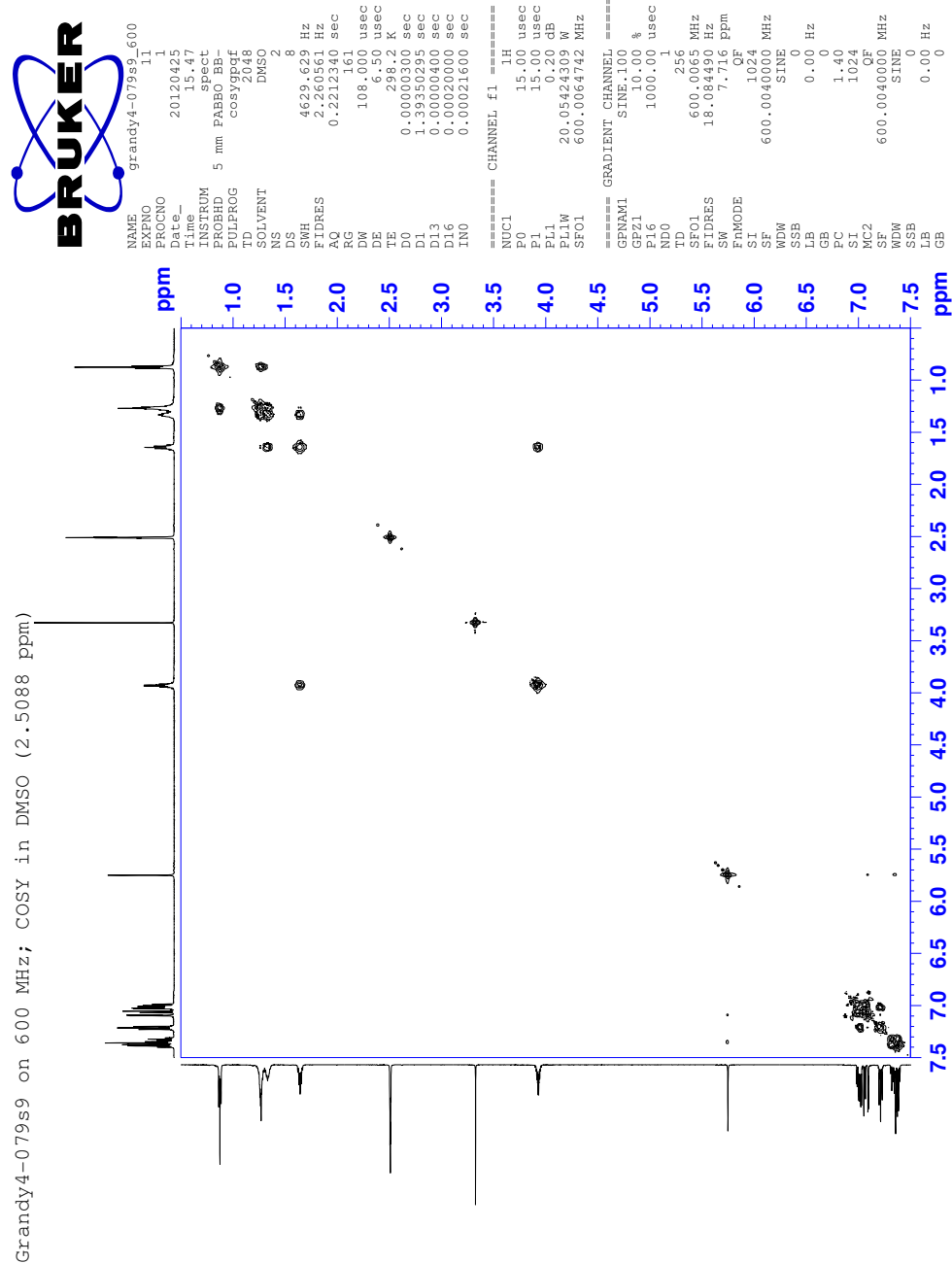
2-(5-(4-fluorophenoxy)-2-(hexyloxy)phenyl)-2-phenylacetonitrile: G4-079s9

FIGURE A.25: ^1H -NMR of G4-079s9.



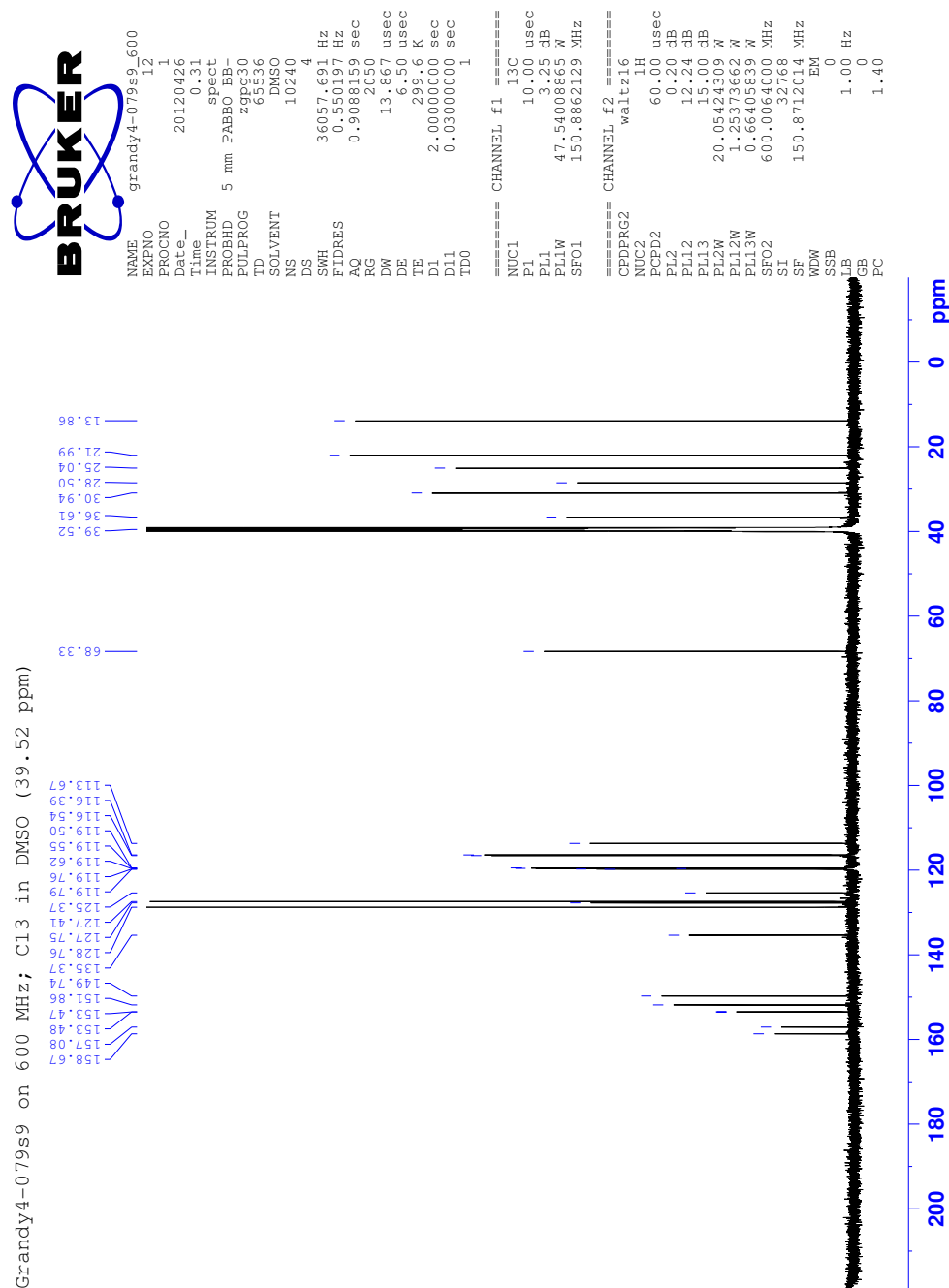
2-(5-(4-fluorophenoxy)-2-(hexyloxy)phenyl)-2-phenylacetonitrile: G4-079s9

FIGURE A.26: COSY-NMR of G4-079s9.



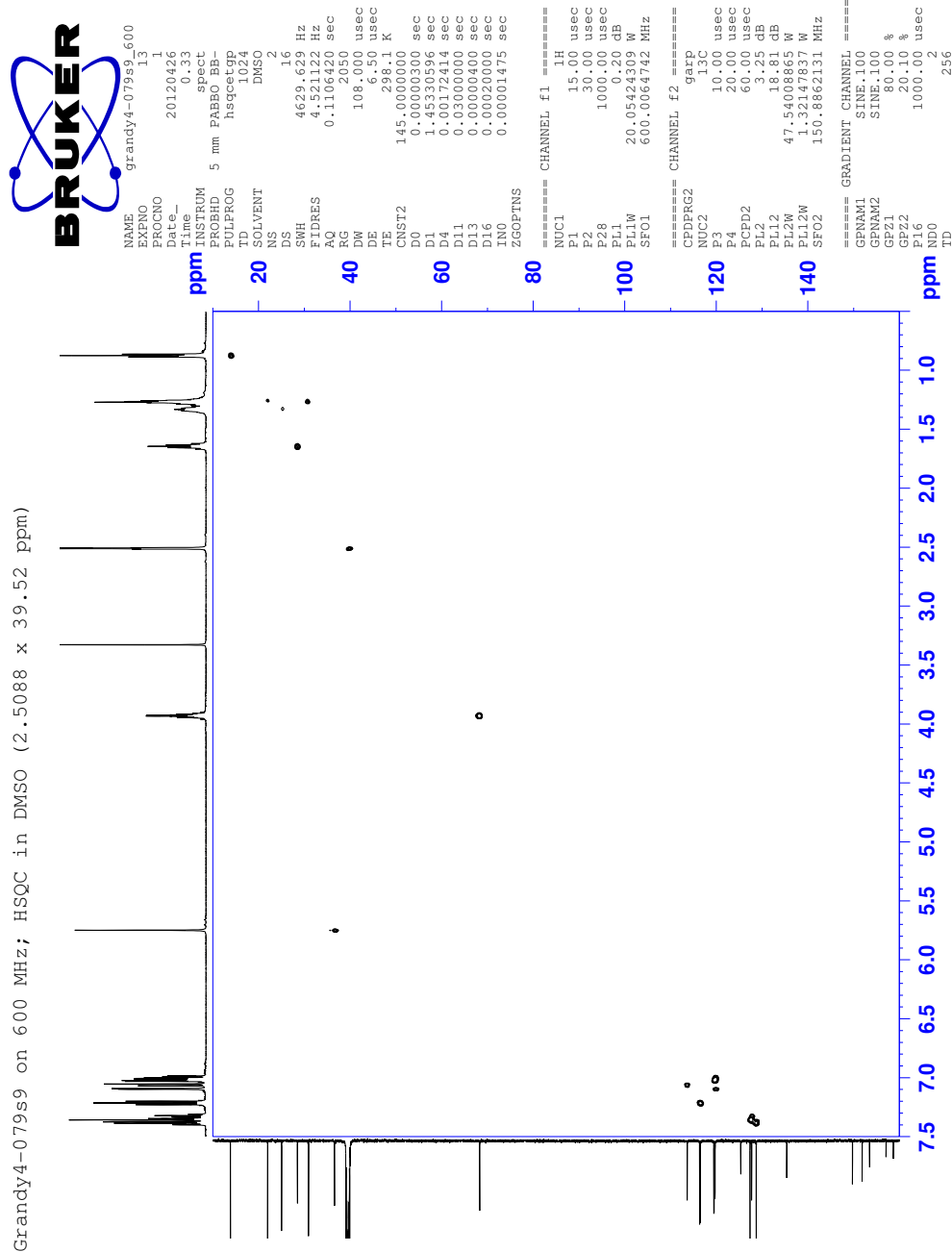
2-(5-(4-fluorophenoxy)-2-(hexyloxy)phenyl)-2-phenylacetonitrile: G4-079s9

FIGURE A.27: ^{13}C -NMR of G4-079s9.



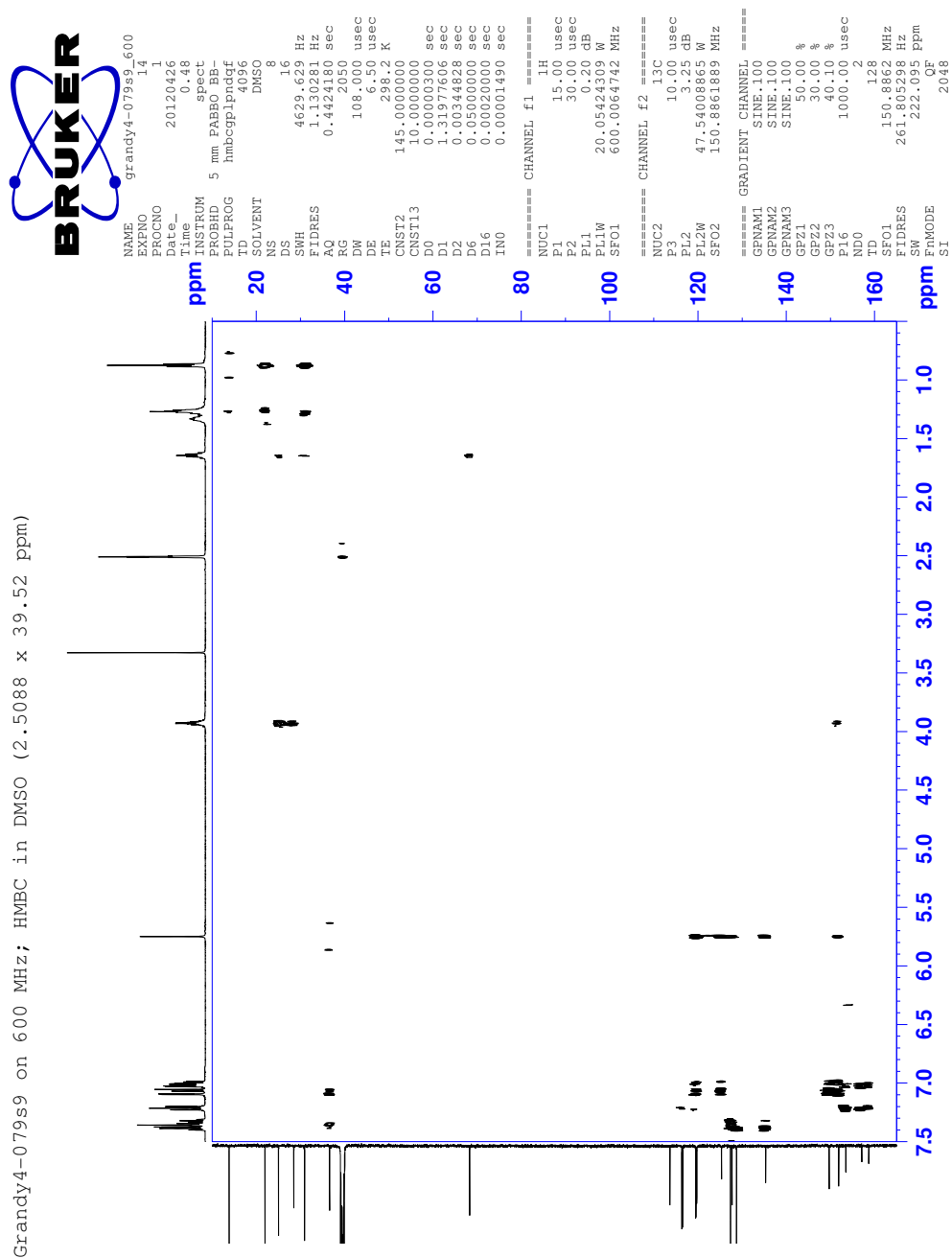
2-(5-(4-fluorophenoxy)-2-(hexyloxy)phenyl)-2-phenylacetonitrile: G4-079s9

FIGURE A.28: HSQC-NMR of G4-079s9.



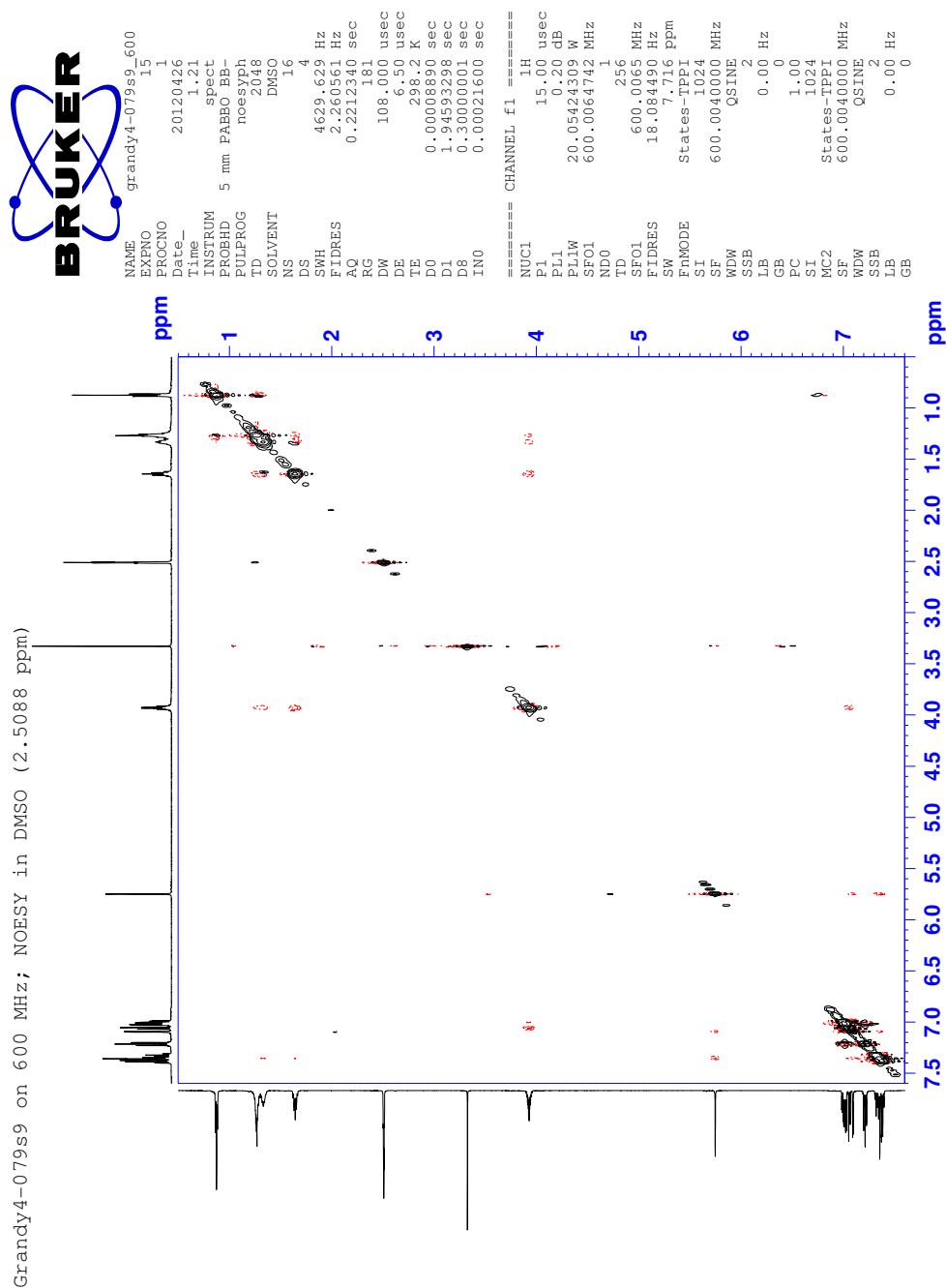
2-(5-(4-fluorophenoxy)-2-(hexyloxy)phenyl)-2-phenylacetonitrile: G4-079s9

FIGURE A.29: HMBC-NMR of G4-079s9.



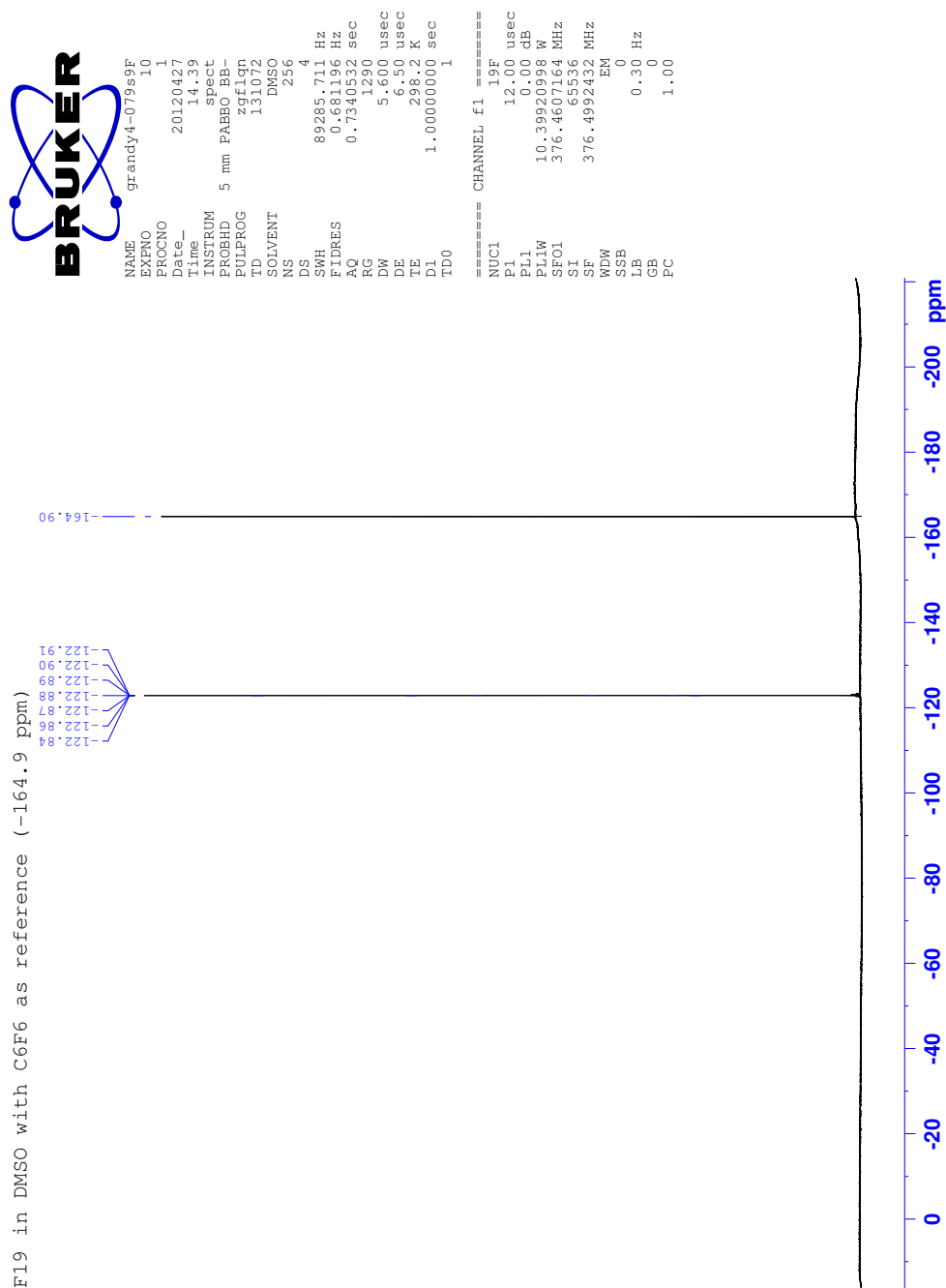
2-(5-(4-fluorophenoxy)-2-(hexyloxy)phenyl)-2-phenylacetonitrile: G4-079s9

FIGURE A.30: NOESY-NMR of G4-079s9.



2-(5-(4-fluorophenoxy)-2-(hexyloxy)phenyl)-2-phenylacetonitrile: G4-079s9

FIGURE A.31: ^{19}F -NMR of G4-079s9, 400 MHz with C_6F_6 (-164.0 ppm).



ET-92: 2-(5-(4-fluorophenoxy)-2-(hexyloxy)phenyl)-2-phenylethanamine hydrochloride

A.5 ET-92: 2-(5-(4-fluorophenoxy)-2-(hexyloxy)phenyl)-2-phenylethanamine hydrochloride: G4-091s14

FIGURE A.32: Structure of ET-92 (G4-090s14).

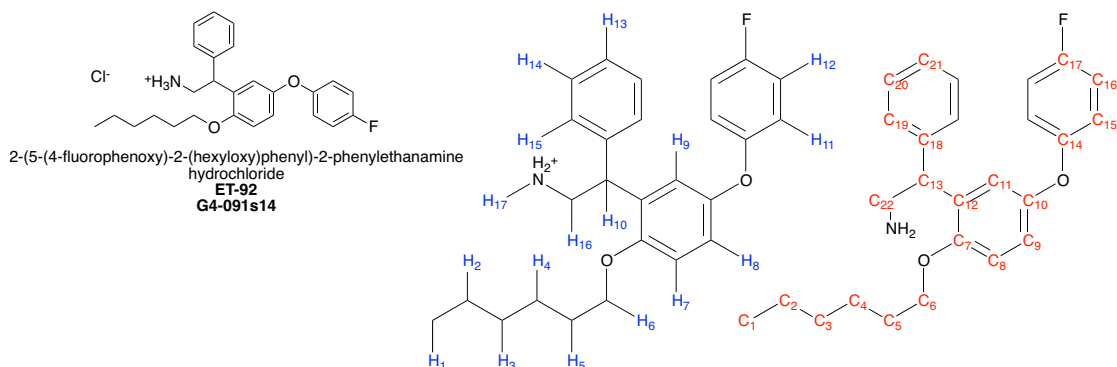


TABLE A.9: ^1H -NMR assignments for G4-090s14, 600 MHz in DMSO (2.50 ppm)

Proton	ppm ^a	Number	Type	J_a	J_b
H ₁	0.891	3	t	6.9	
H ₂ & H ₃	1.303	4	m		
H ₄	1.384	2	m		
H ₅	1.690	2	m		
H ₆	3.887	2	m		
H ₇	6.690	1	d	9.0	
H ₈	6.841	1	dd	9.0	3.0
H ₉	7.224	1	d	3.0	
H ₁₀	4.619	1	t	8.1	
H ₁₁	7.183	2	m		
H ₁₂	6.975	2	m		
H ₁₃	7.239	2	m		
H ₁₄ & H ₁₅	7.314	4	m		
H ₁₆	3.500	2	m		
H ₁₇	7.895	3	b.s.		

a. Taken at the center of the peak.

TABLE A.10: ^{13}C -NMR assignments for G4-090s14, 600 MHz in DMSO (39.52 ppm)

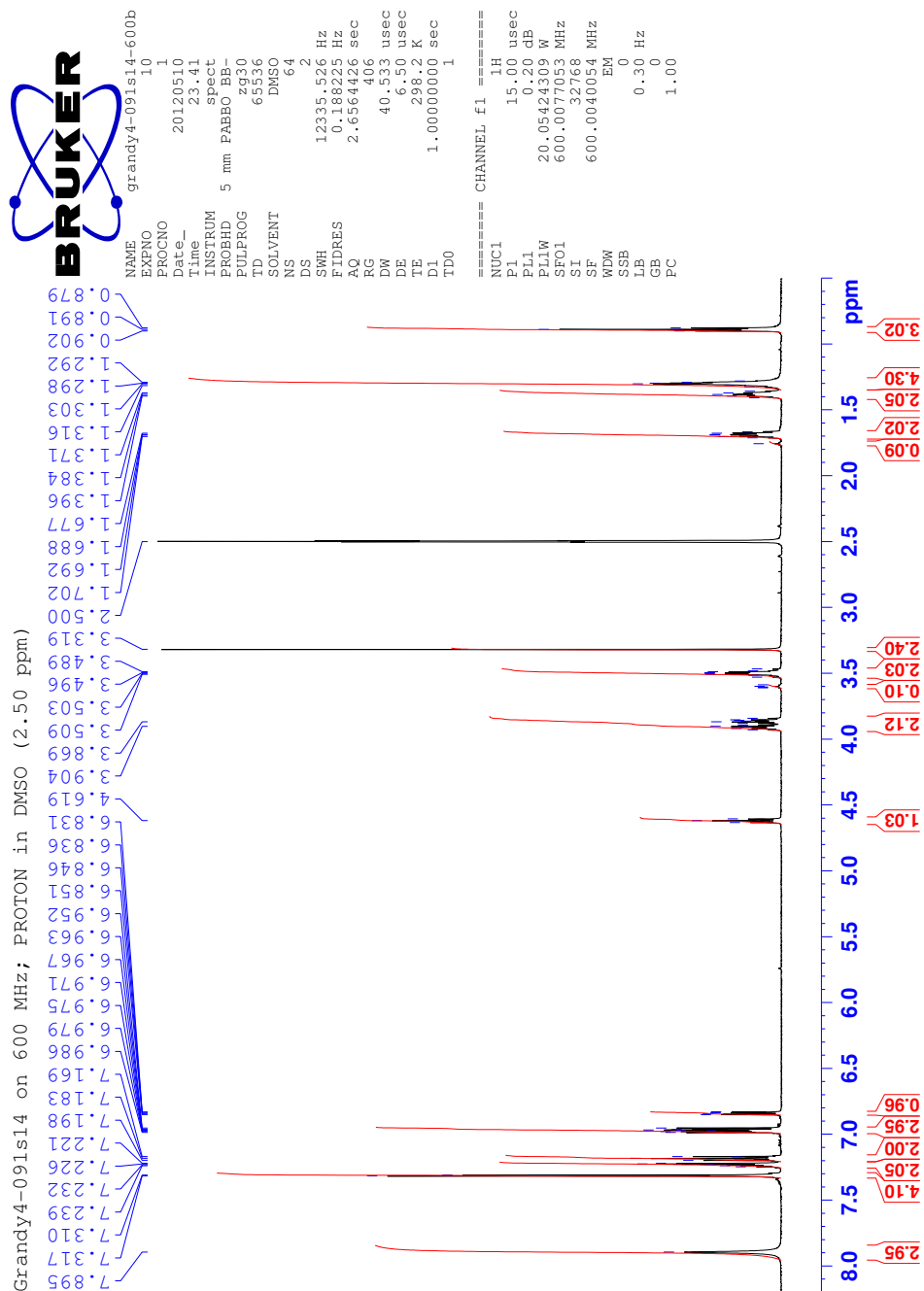
Carbon	ppm ^a	Carbon	ppm ^a	Type ^b	J
C ₁	13.91	C ₁₂	130.33		
C ₂	22.04	C ₁₃	42.08		
C ₃	31.00	C ₁₄	154.04	d	2.2
C ₄	25.21	C ₁₅	118.92	d	9.1
C ₅	28.74	C ₁₆	116.29	d	24.1
C ₆	68.07	C ₁₇	157.61	d	238.4
C ₇	149.56	C ₁₈	140.32		
C ₈	113.12	C ₁₉	128.03		
C ₉	118.38	C ₂₀	128.48		
C ₁₀	152.46	C ₂₁	126.90		
C ₁₁	119.36	C ₂₂	41.63		

a. Taken at the center of the peak.

b. Singlet unless noted otherwise.

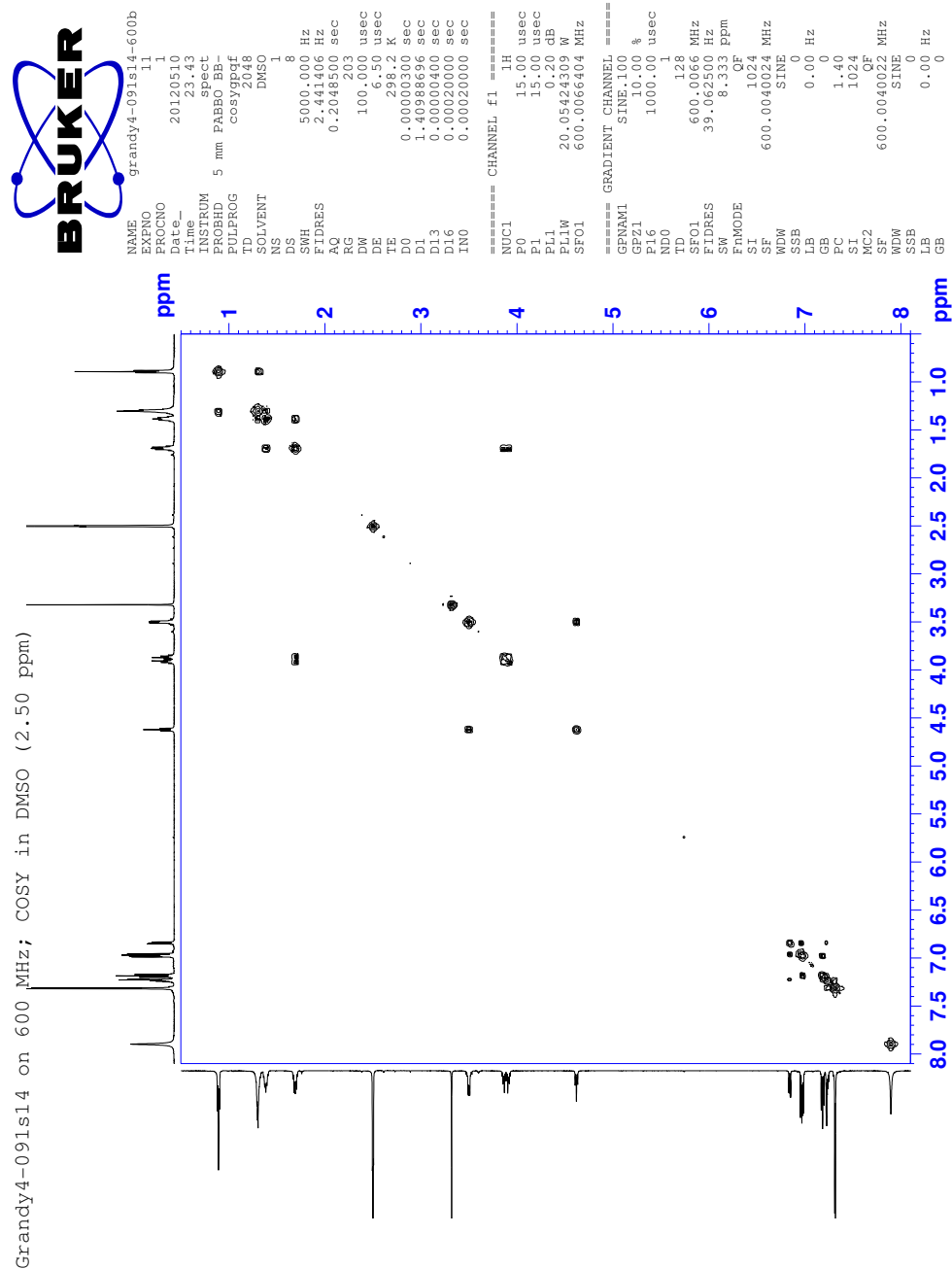
ET-92: 2-(5-(4-fluorophenoxy)-2-(hexyloxy)phenyl)-2-phenylethanamine hydrochloro-

FIGURE A.33: ^1H -NMR of ET-92 (G4-090s14).



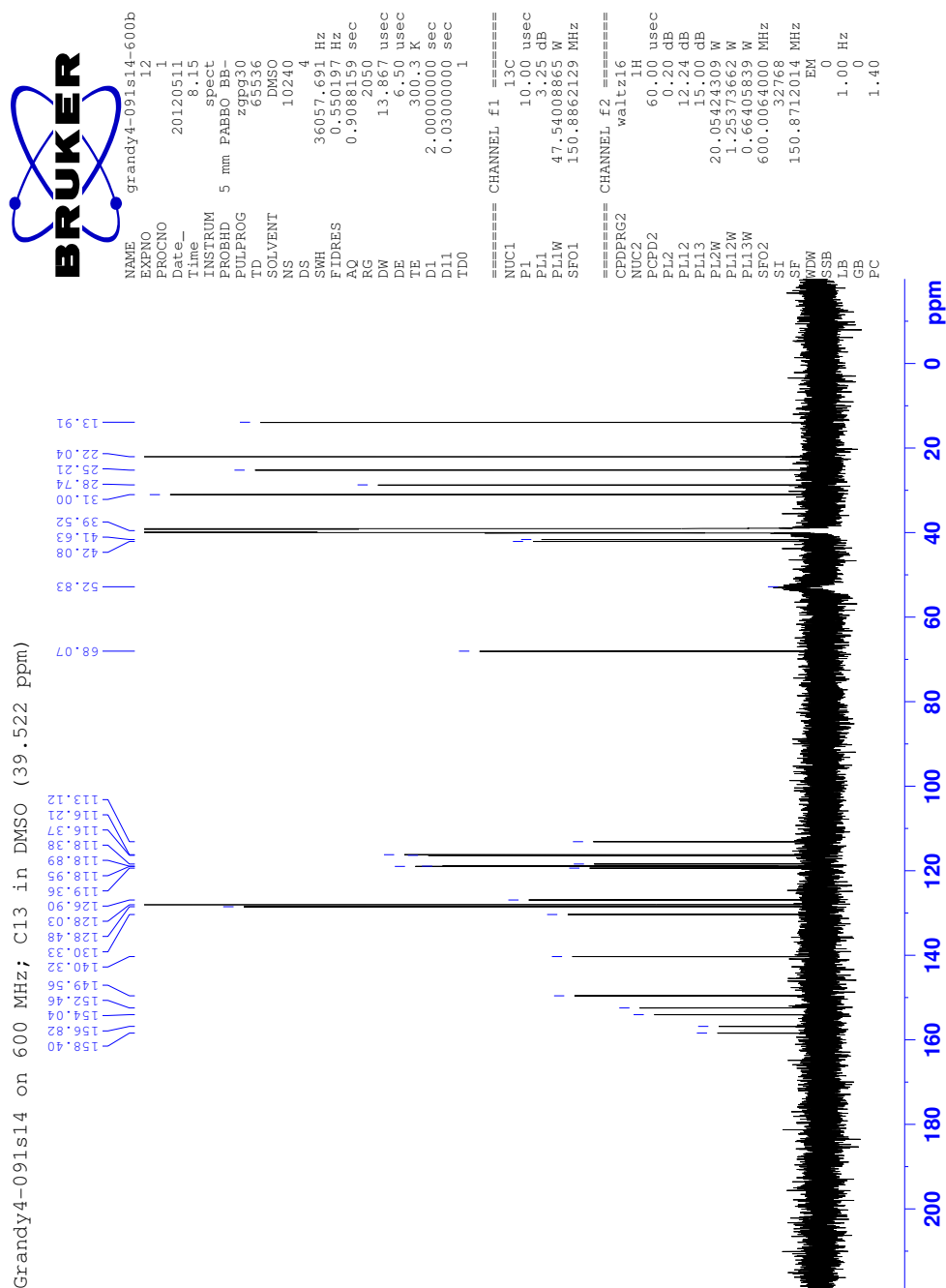
ET-92: 2-(5-(4-fluorophenoxy)-2-(hexyloxy)phenyl)-2-phenylethanamine hydrochloride

FIGURE A.34: COSY-NMR of ET-92 (G4-090s14).



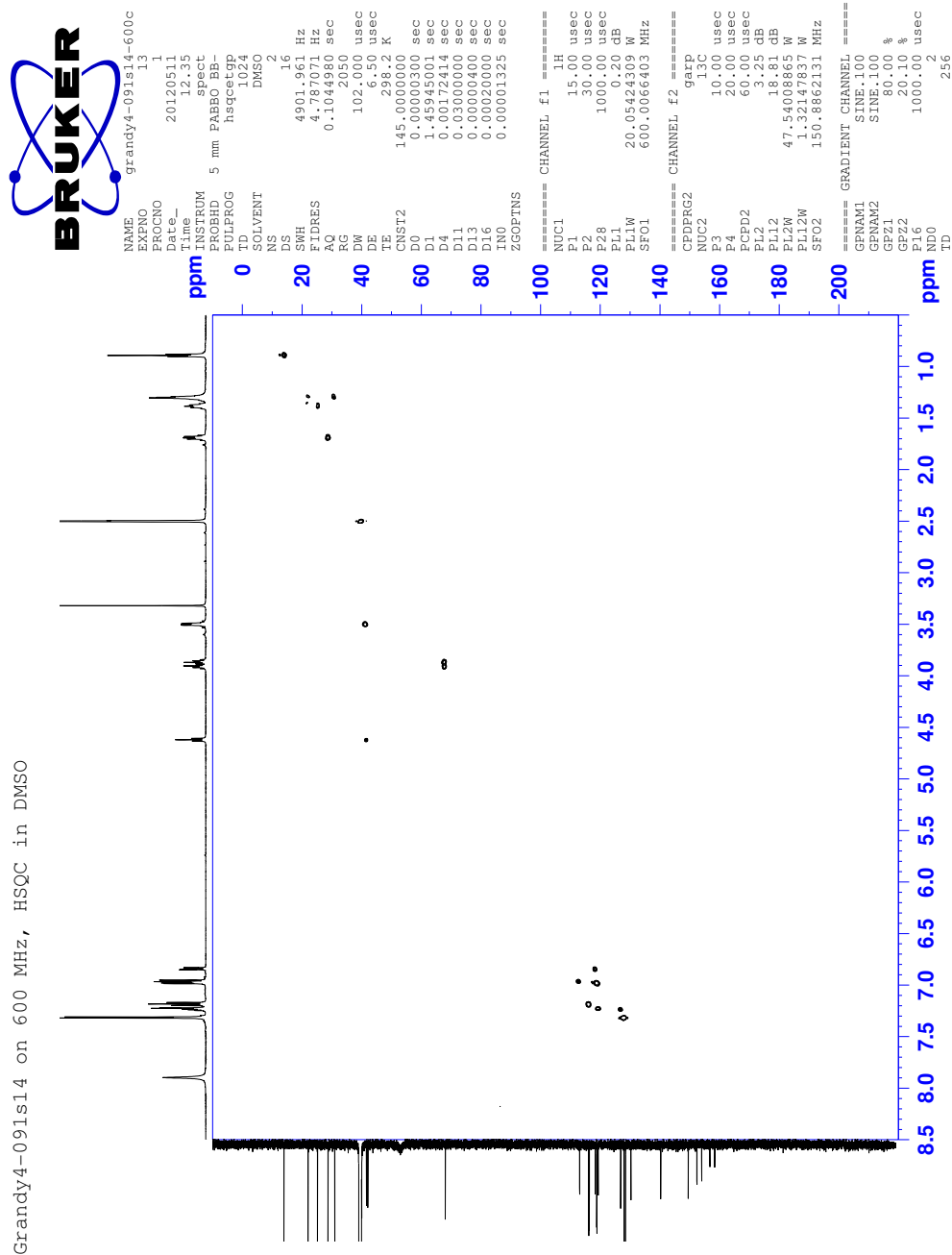
ET-92: 2-(5-(4-fluorophenoxy)-2-(hexyloxy)phenyl)-2-phenylethanamine hydrochloride

FIGURE A.35: ^{13}C -NMR of ET-92 (G4-090s14).



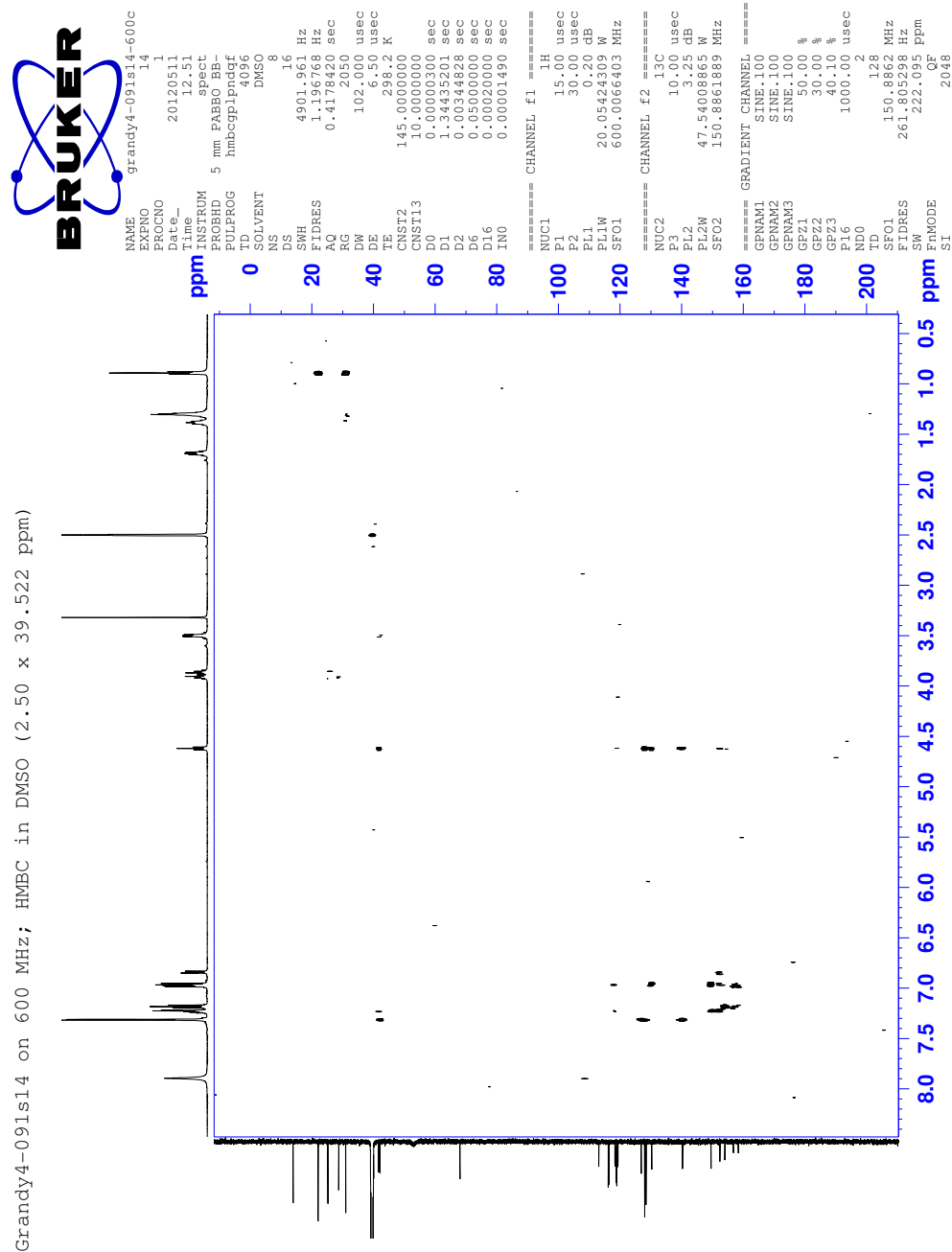
ET-92: 2-(5-(4-fluorophenoxy)-2-(hexyloxy)phenyl)-2-phenylethanamine hydrochloride

FIGURE A.36: HSQC-NMR of ET-92 (G4-090s14).



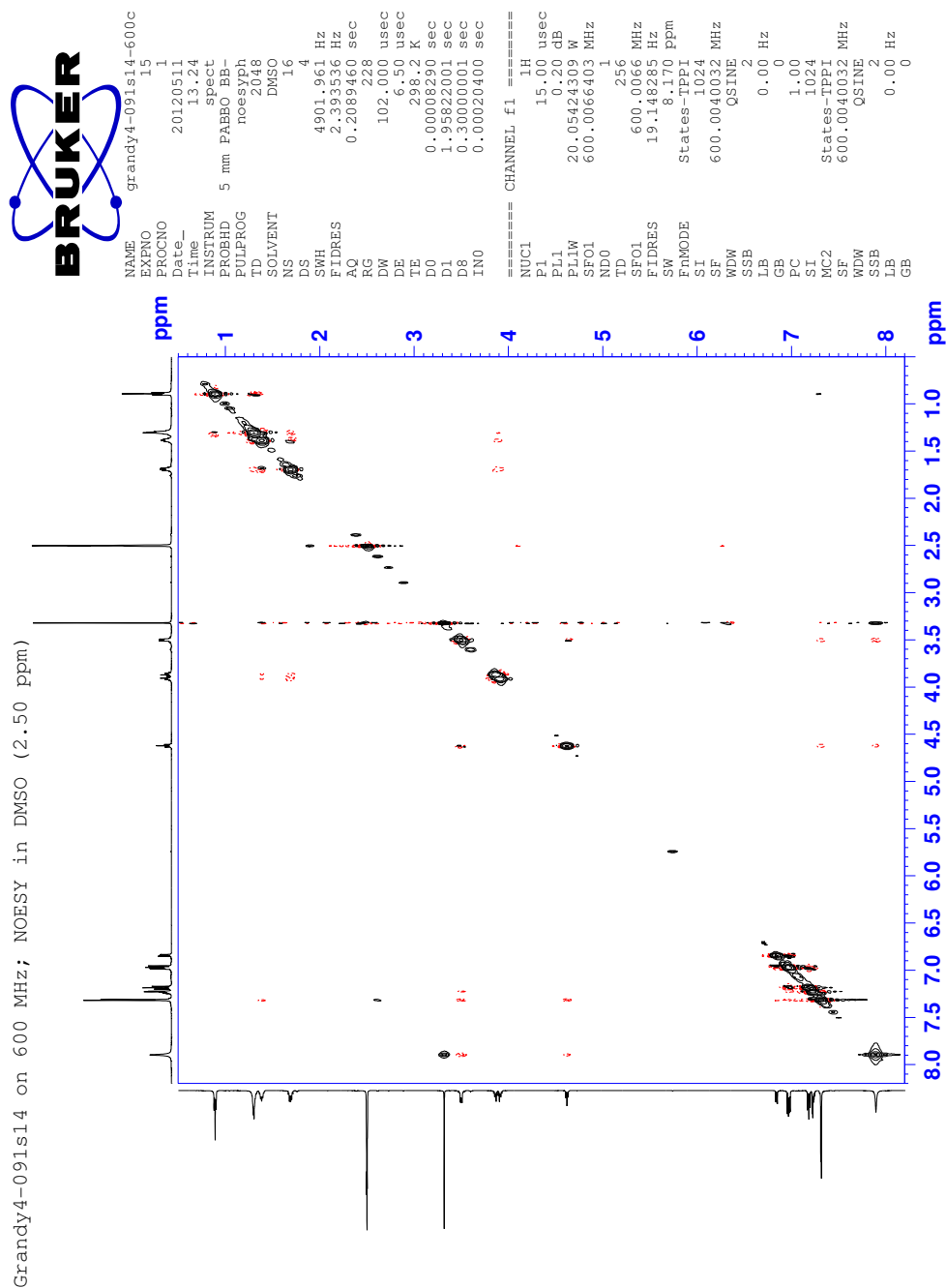
ET-92: 2-(5-(4-fluorophenoxy)-2-(hexyloxy)phenyl)-2-phenylethanamine hydrochloride

FIGURE A.37: HMBC-NMR of ET-92 (G4-090s14).



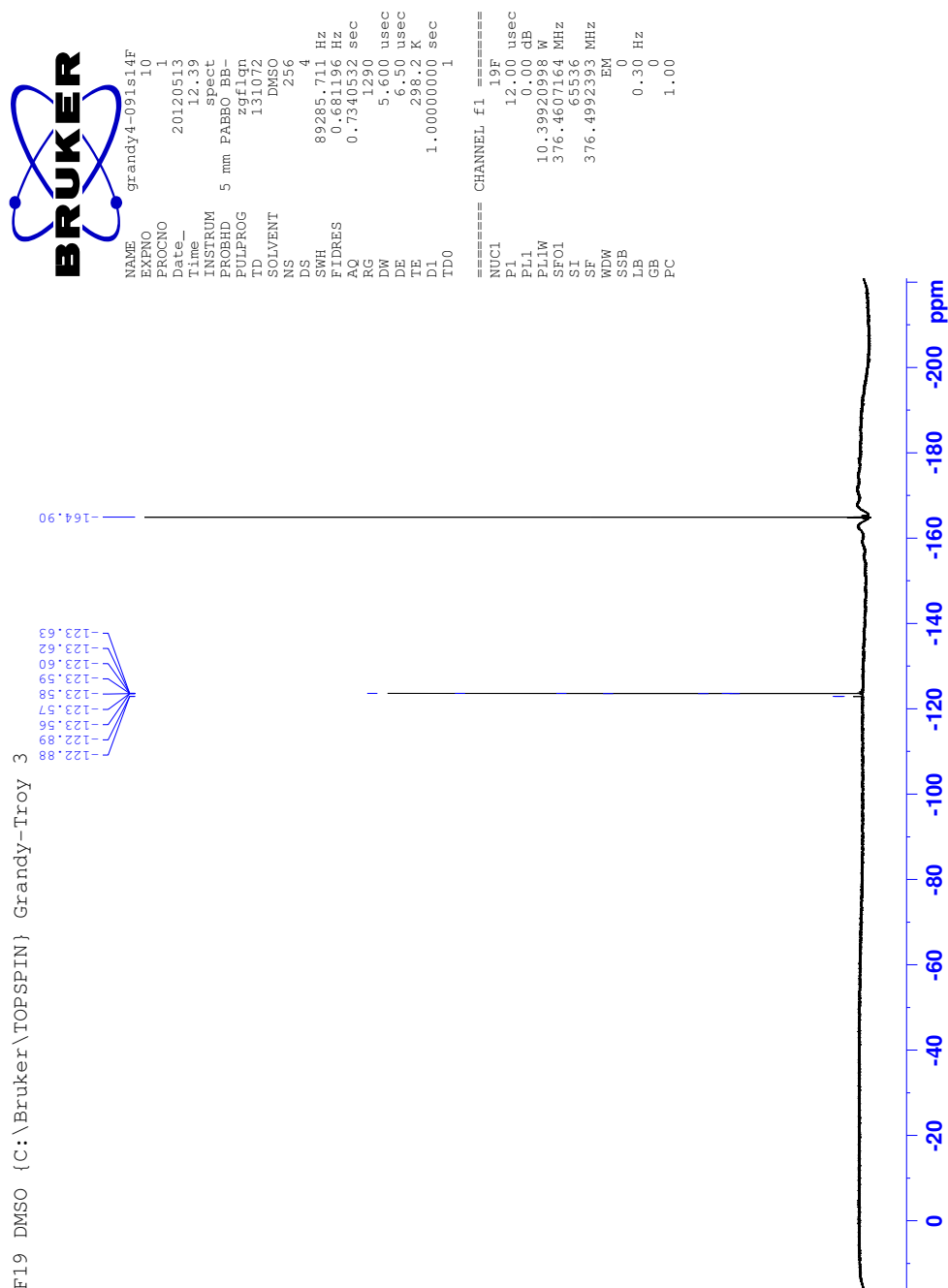
ET-92: 2-(5-(4-fluorophenoxy)-2-(hexyloxy)phenyl)-2-phenylethanamine hydrochloride

FIGURE A.38: NOESY-NMR of ET-92 (G4-090s14).



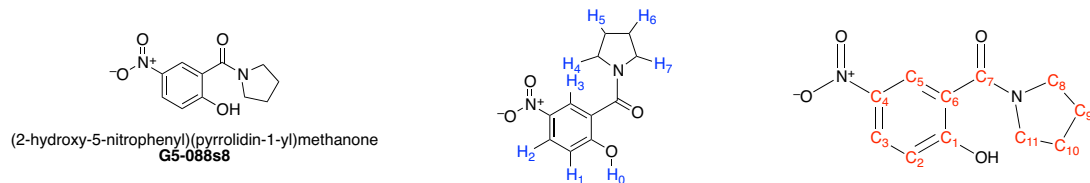
ET-92: 2-(5-(4-fluorophenoxy)-2-(hexyloxy)phenyl)-2-phenylethanamine hydrochloride

FIGURE A.39: ^{19}F -NMR of ET-92 (G4-090s14), 400 MHz with C_6F_6 (-164.0 ppm).



(2-hydroxy-5-nitrophenyl)(pyrrolidin-1-yl)methone: G5-088s8

A.6 *(2-hydroxy-5-nitrophenyl)(pyrrolidin-1-yl)methone: G5-088s8*

FIGURE A.40: Structure of G5-088s8.**TABLE A.11:** ¹H-NMR assignments for G5-088s8, 400 MHz in DMSO (2.50 ppm)

Proton	ppm ^a	Number	Type	J _a	J _b
H ₀	11.56	1	s		
H ₁	7.07	1	d	9.07	
H ₂	8.16	1	dd	9.06	2.91
H ₃	8.06	1	d	2.88	
H ₄	3.23	2	t	6.74	
H ₅ & H ₆	1.84	4	m		
H ₇	3.46	2	t	6.74	

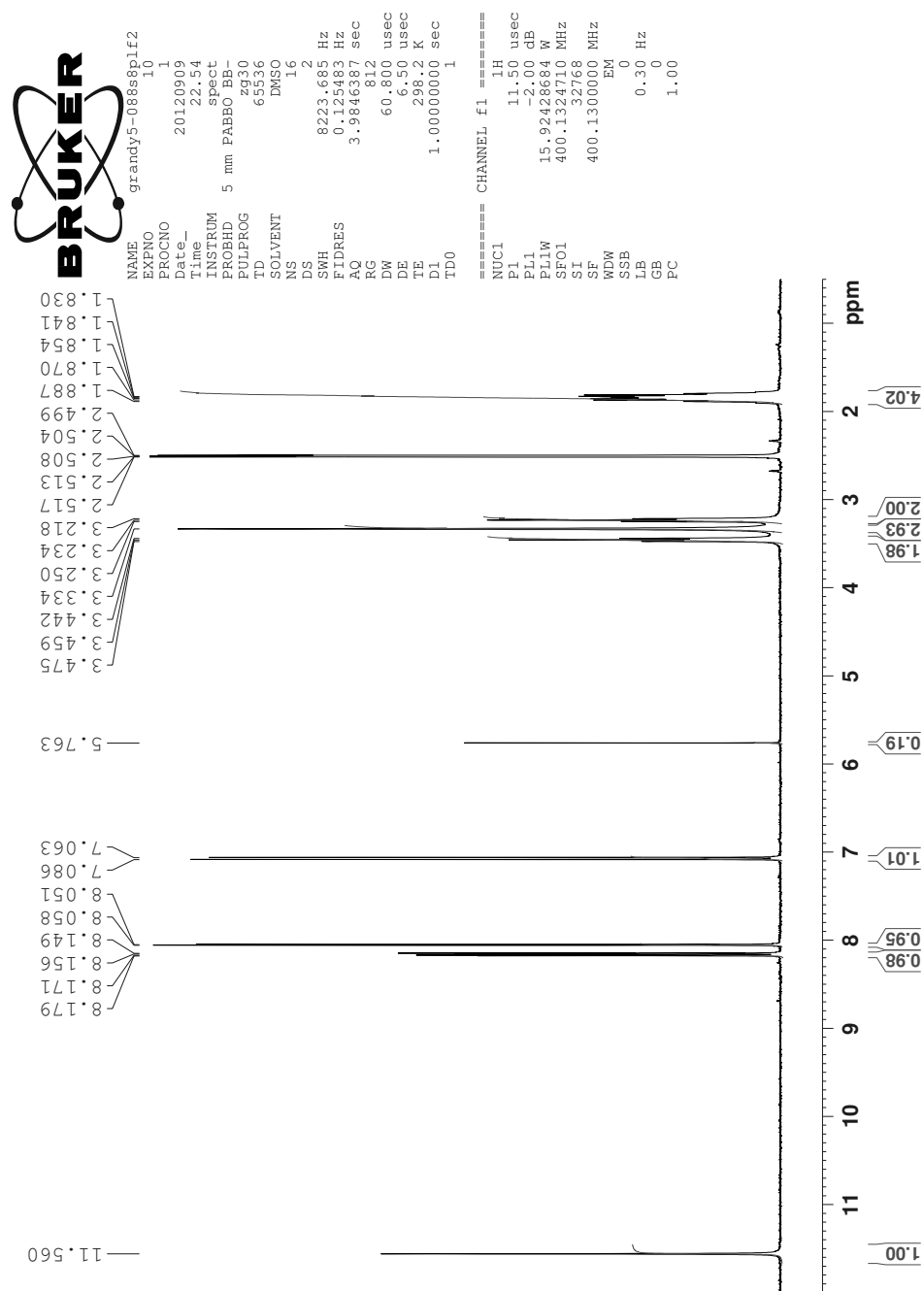
a. Taken at the center of the peak.

TABLE A.12: ¹³C-NMR assignments for G5-088s8, 400 MHz in DMSO (39.52 ppm)

Carbon	ppm
C ₁	159.74
C ₂	116.50
C ₃	126.26
C ₄	139.33
C ₅	125.91
C ₆	124.29
C ₇	164.47
C ₈	45.43
C ₉	23.94
C ₁₀	25.38
C ₁₁	46.95

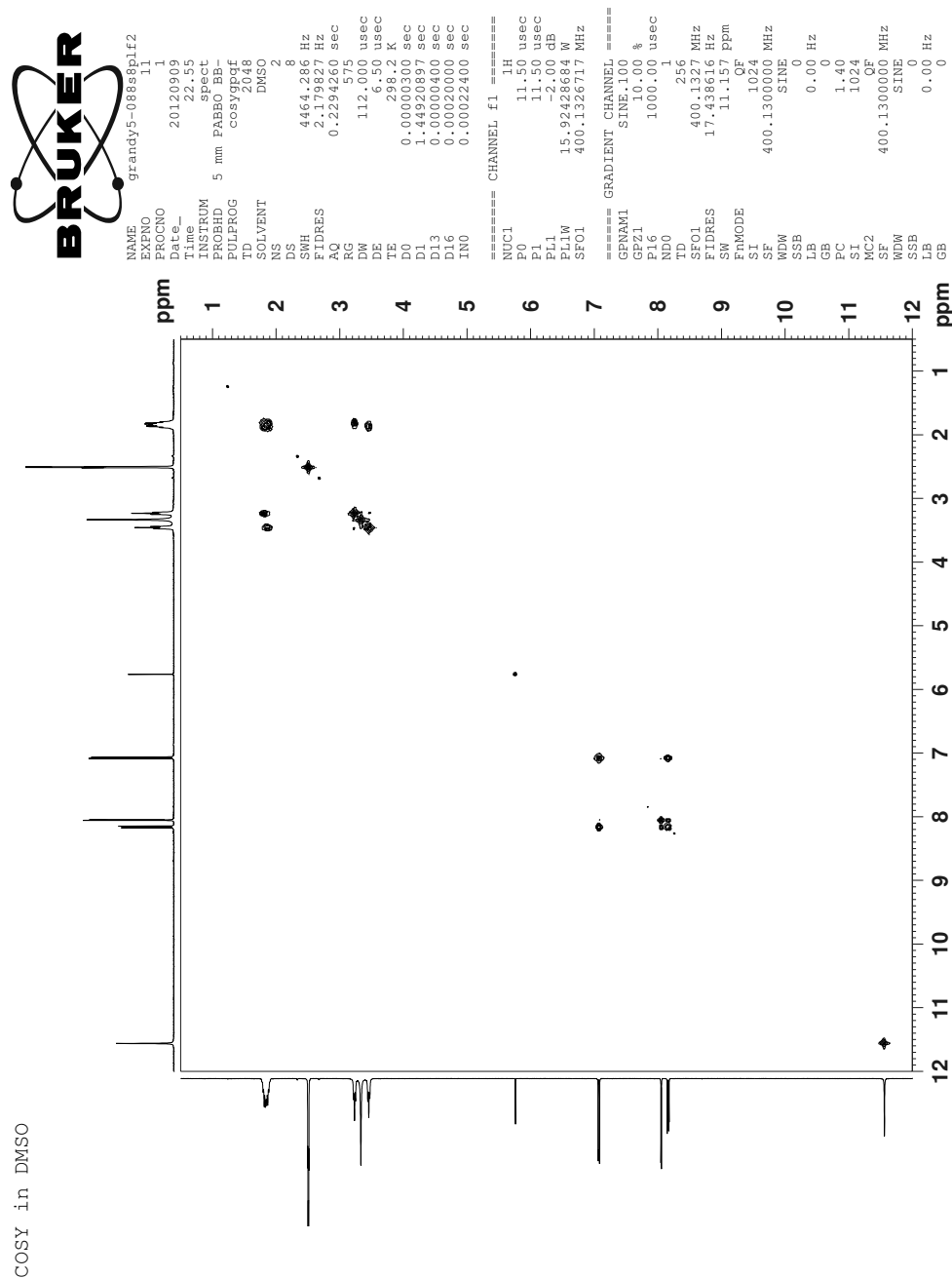
(2-hydroxy-5-nitrophenyl)(pyrrolidin-1-yl)methone: G5-088s8

FIGURE A.41: ^1H -NMR of G5-088s8.



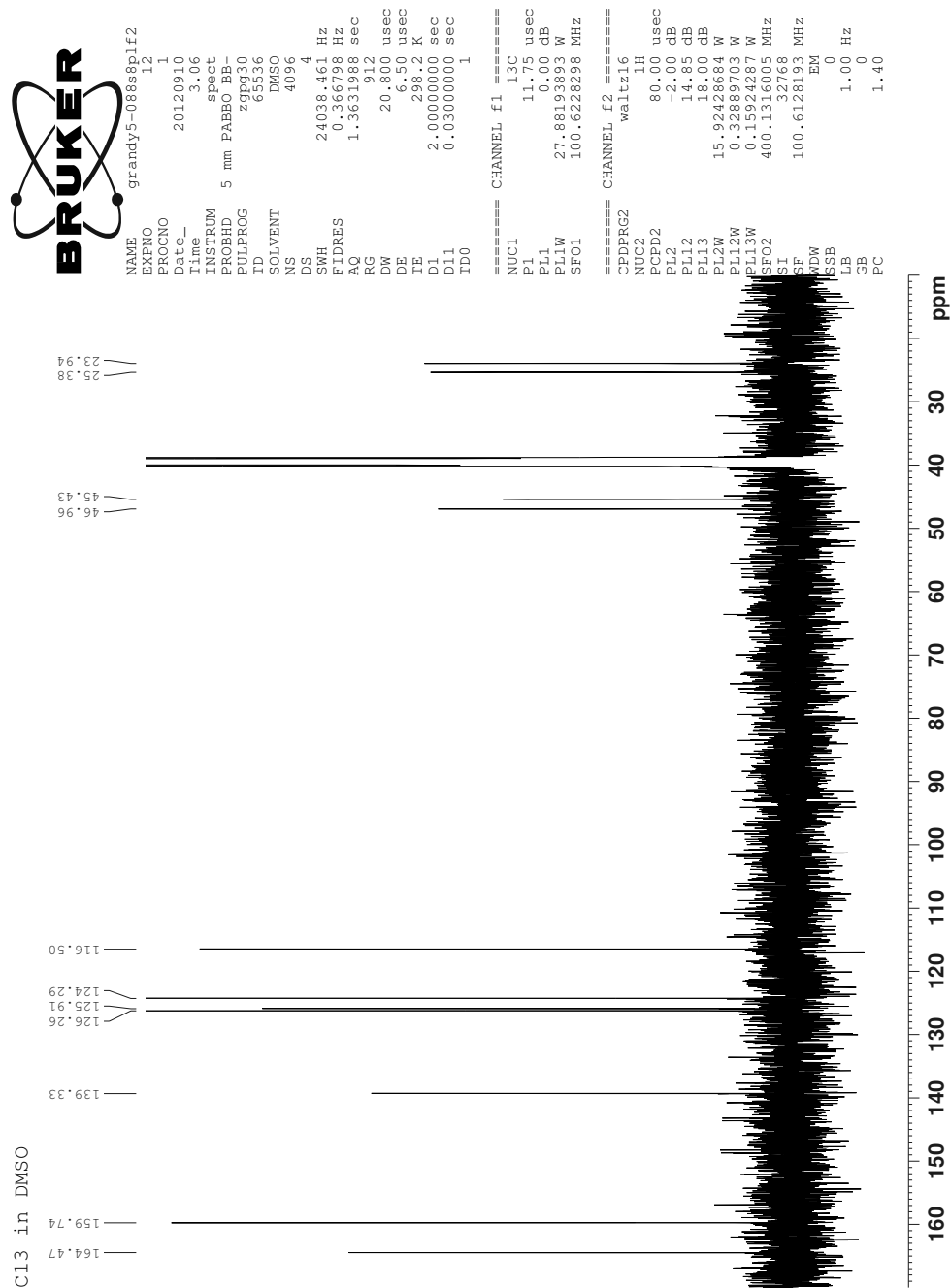
(2-hydroxy-5-nitrophenyl)(pyrrolidin-1-yl)methone: G5-088s8

FIGURE A.42: COSY-NMR of G5-088s8.



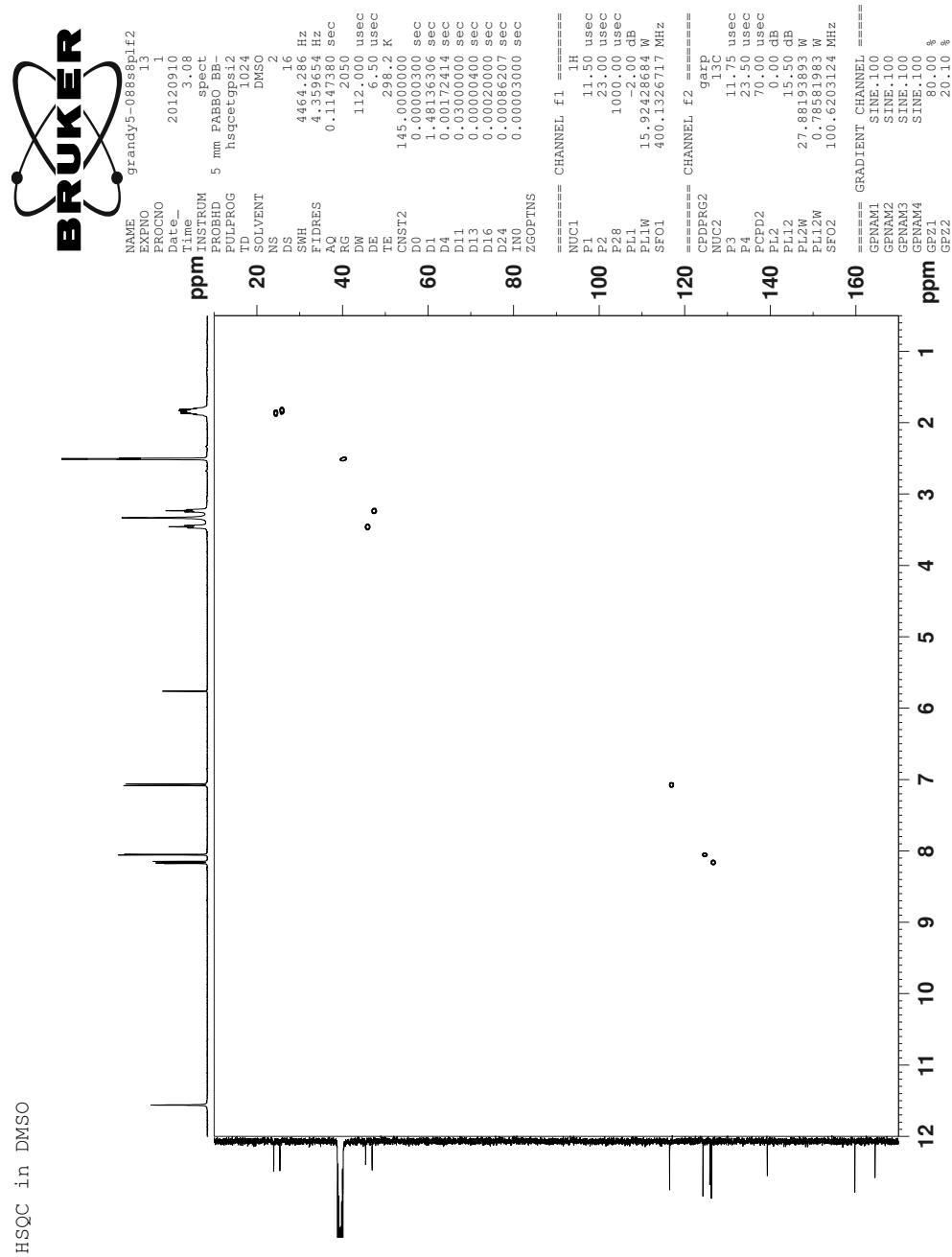
(2-hydroxy-5-nitrophenyl)(pyrrolidin-1-yl)methone: G5-088s8

FIGURE A.43: ^{13}C -NMR of G5-088s8.



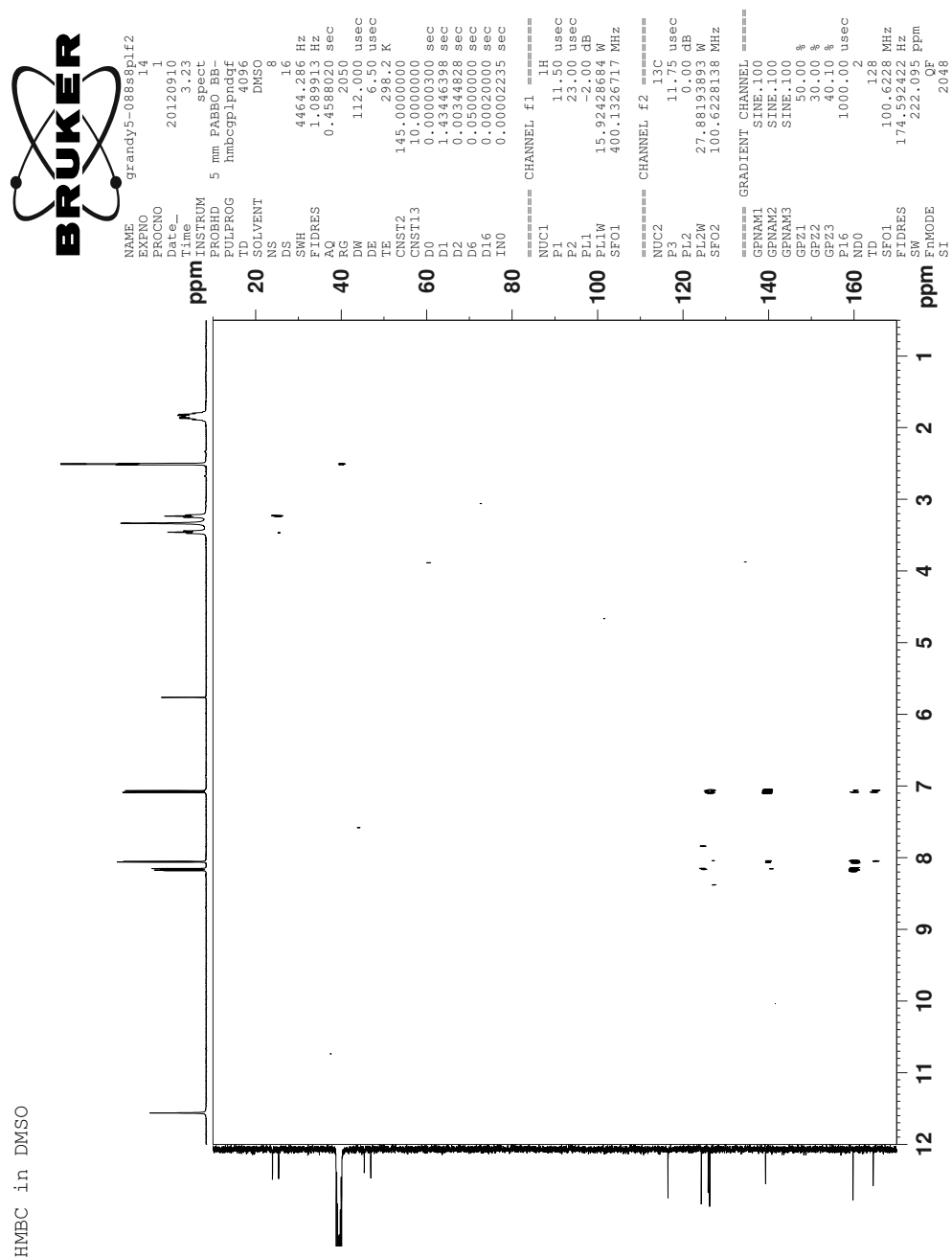
(2-hydroxy-5-nitrophenyl)(pyrrolidin-1-yl)methone: G5-088s8

FIGURE A.44: HSQC-NMR of G5-088s8.



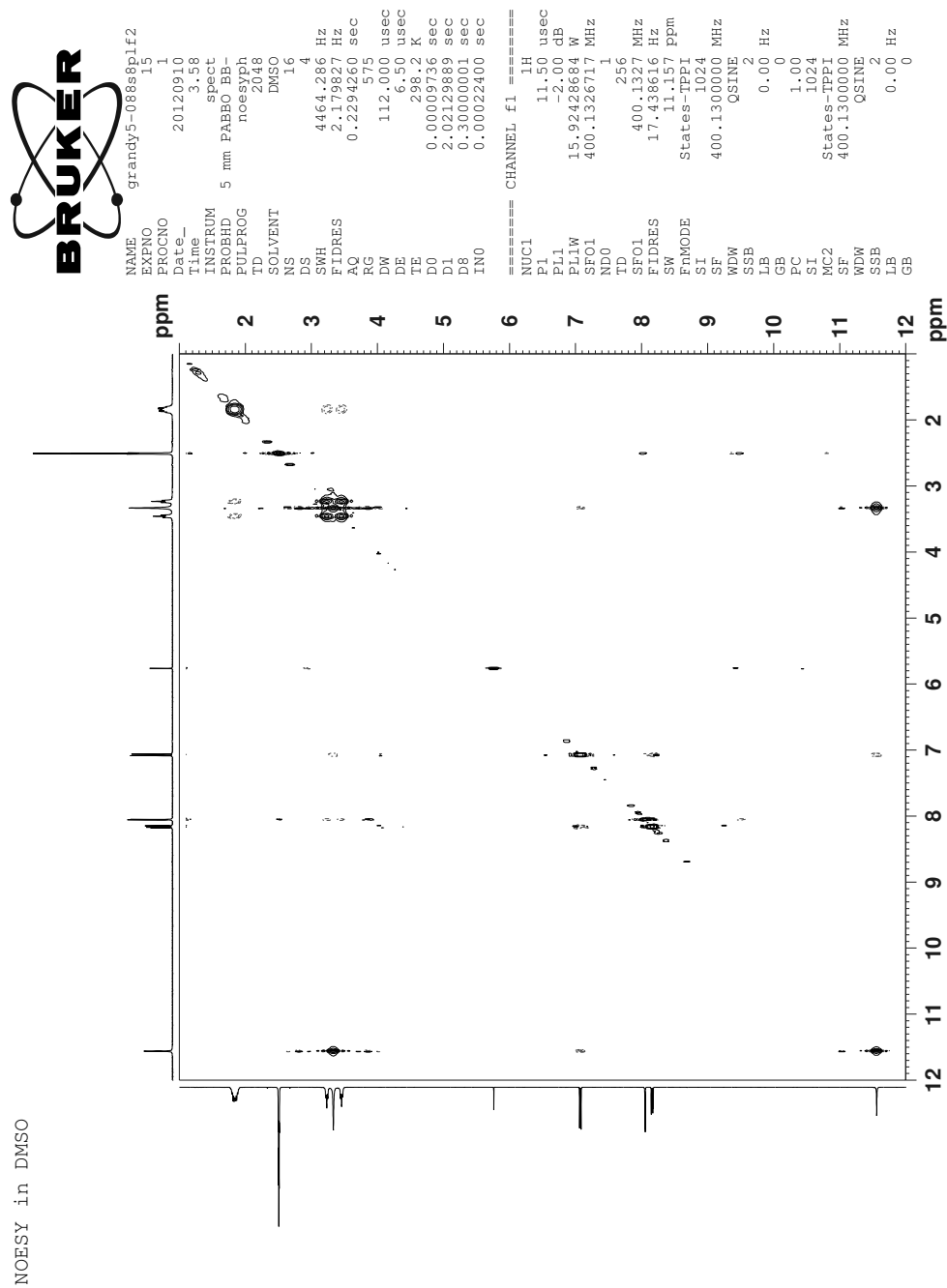
(2-hydroxy-5-nitrophenyl)(pyrrolidin-1-yl)methone: G5-088s8

FIGURE A.45: HMBC-NMR of G5-088s8.



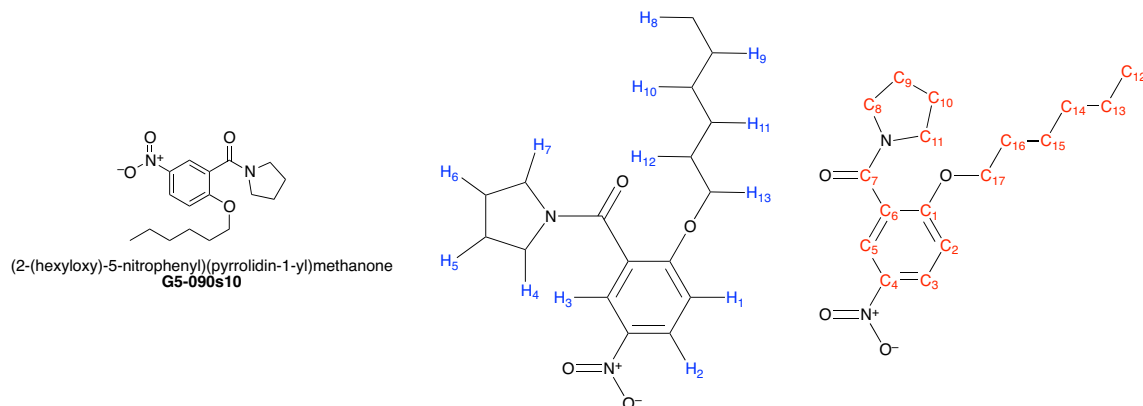
(2-hydroxy-5-nitrophenyl)(pyrrolidin-1-yl)methone: G5-088s8

FIGURE A.46: NOESY-NMR of G5-088s8.



(2-(hexyloxy)-5-nitrophenyl)(pyrrolidin-1-yl)methone: G5-090s10

A.7 (2-(hexyloxy)-5-nitrophenyl)(pyrrolidin-1-yl)methone: G5-090s10

FIGURE A.47: Structure of G5-090s10.**TABLE A.13:** ^1H -NMR assignments for G5-090s10, 400 MHz in DMSO (2.50 ppm)

Proton	ppm ^a	Number	Type	J_a	J_b
H ₁	7.31	1	d	9.24	
H ₂	8.28	1	dd	9.19	2.90
H ₃	8.06	1	d	2.89	
H ₄	3.13	2	t	6.55	
H ₅ & H ₆	1.84	4	m		
H ₇	3.46	2	t	6.55	
H ₈	0.88	3	t	6.83	
H ₉ & H ₁₀	1.30	4	m		
H ₁₁	1.39	2	m		
H ₁₂	1.71	2	m		
H ₁₃	4.18	2	t	6.27	

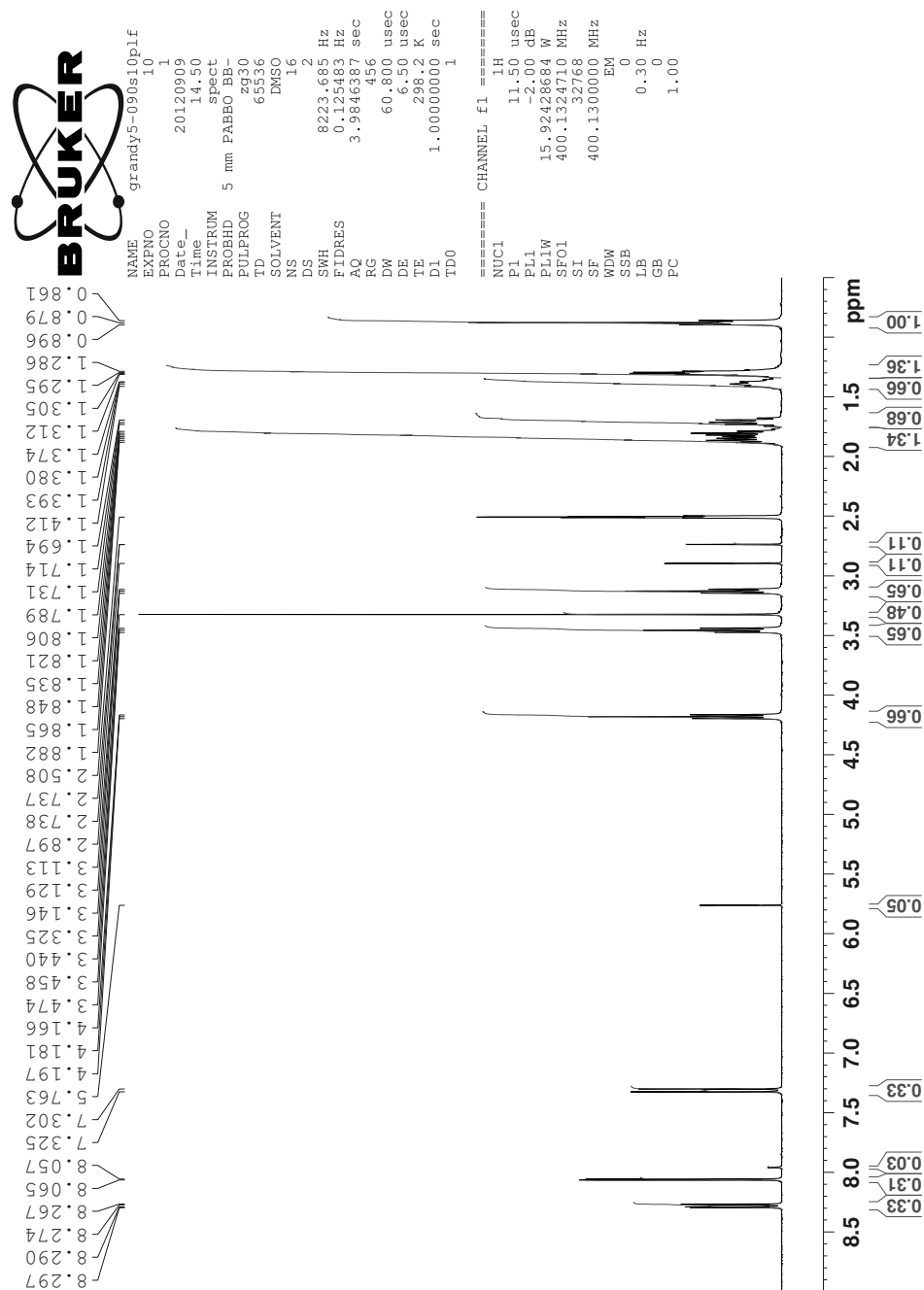
a. Taken at the center of the peak.

TABLE A.14: ^{13}C -NMR assignments for G5-090s10, 400 MHz in DMSO (39.52 ppm)

Carbon	ppm	Carbon	ppm
C ₁	159.38	C ₁₀	25.36
C ₂	112.81	C ₁₁	46.85
C ₃	126.30	C ₁₂	13.79
C ₄	140.42	C ₁₃	22.02
C ₅	123.28	C ₁₄	30.77
C ₆	128.11	C ₁₅	24.93
C ₇	163.89	C ₁₆	28.25
C ₈	45.28	C ₁₇	68.99
C ₉	24.06	-	-

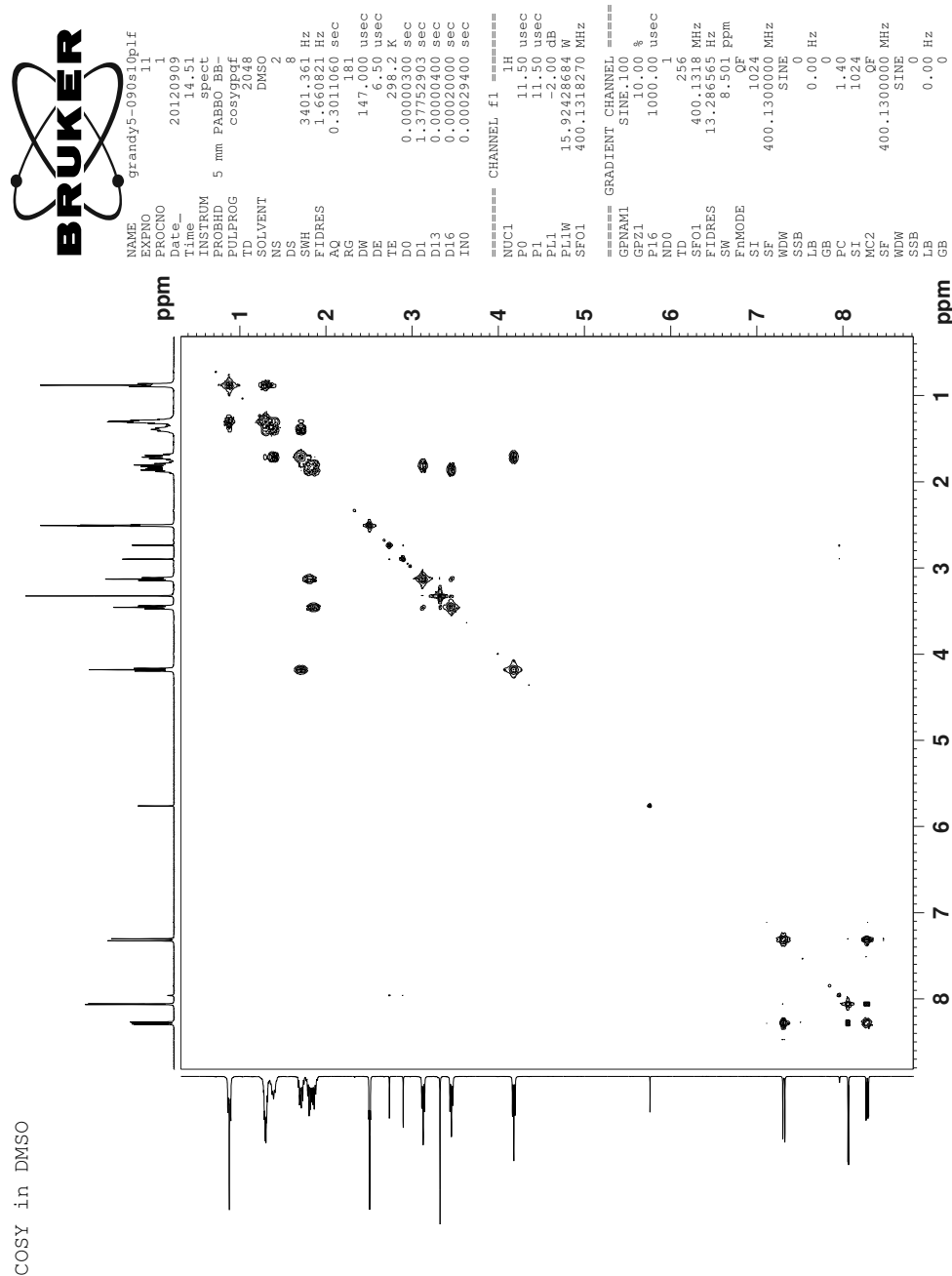
(2-(hexyloxy)-5-nitrophenyl)(pyrrolidin-1-yl)methone: G5-090s10

FIGURE A.48: ^1H -NMR of G5-090s10.



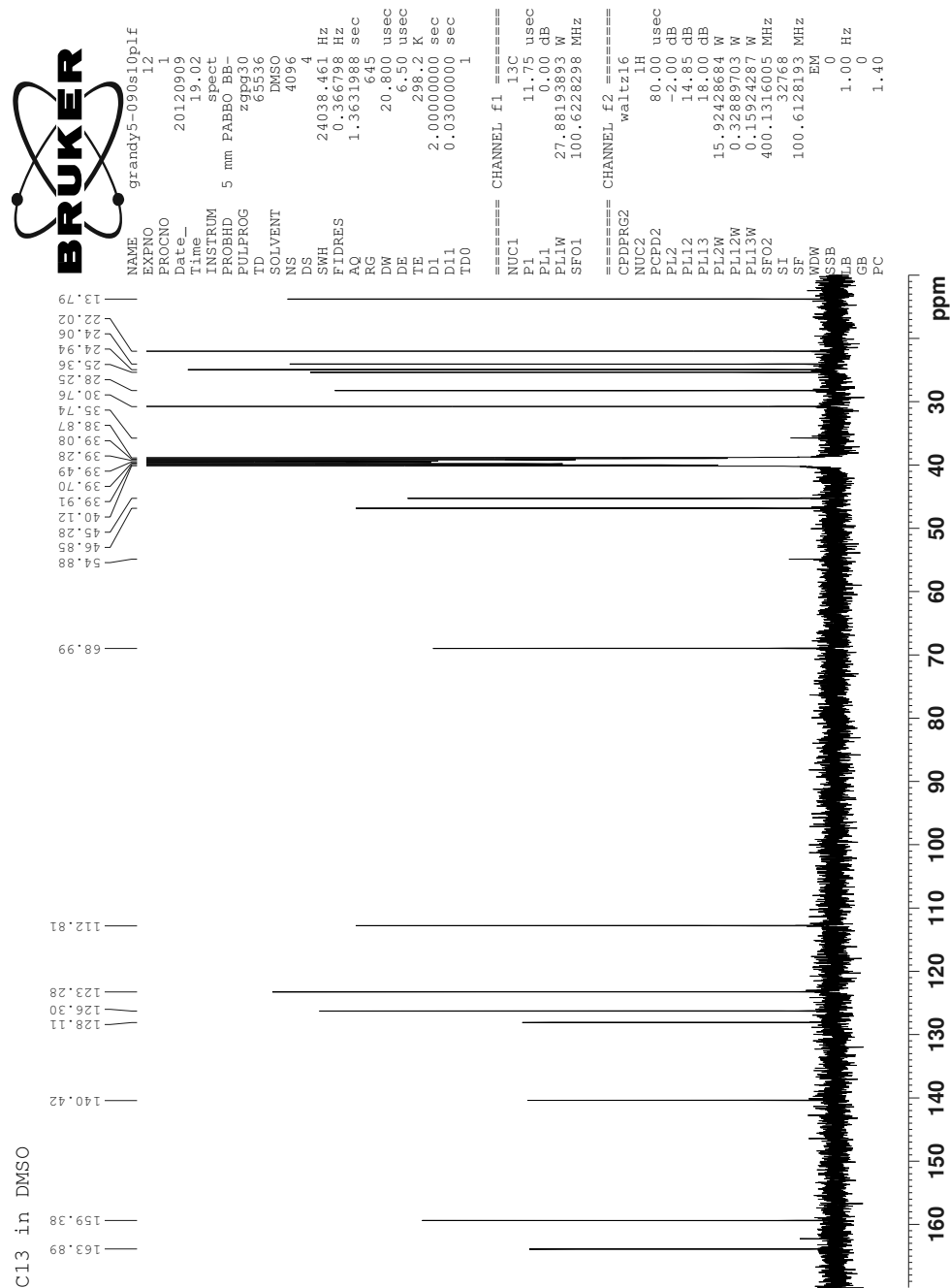
(2-(hexyloxy)-5-nitrophenyl)(pyrrolidin-1-yl)methone: G5-090s10

FIGURE A.49: COSY-NMR of G5-090s10.



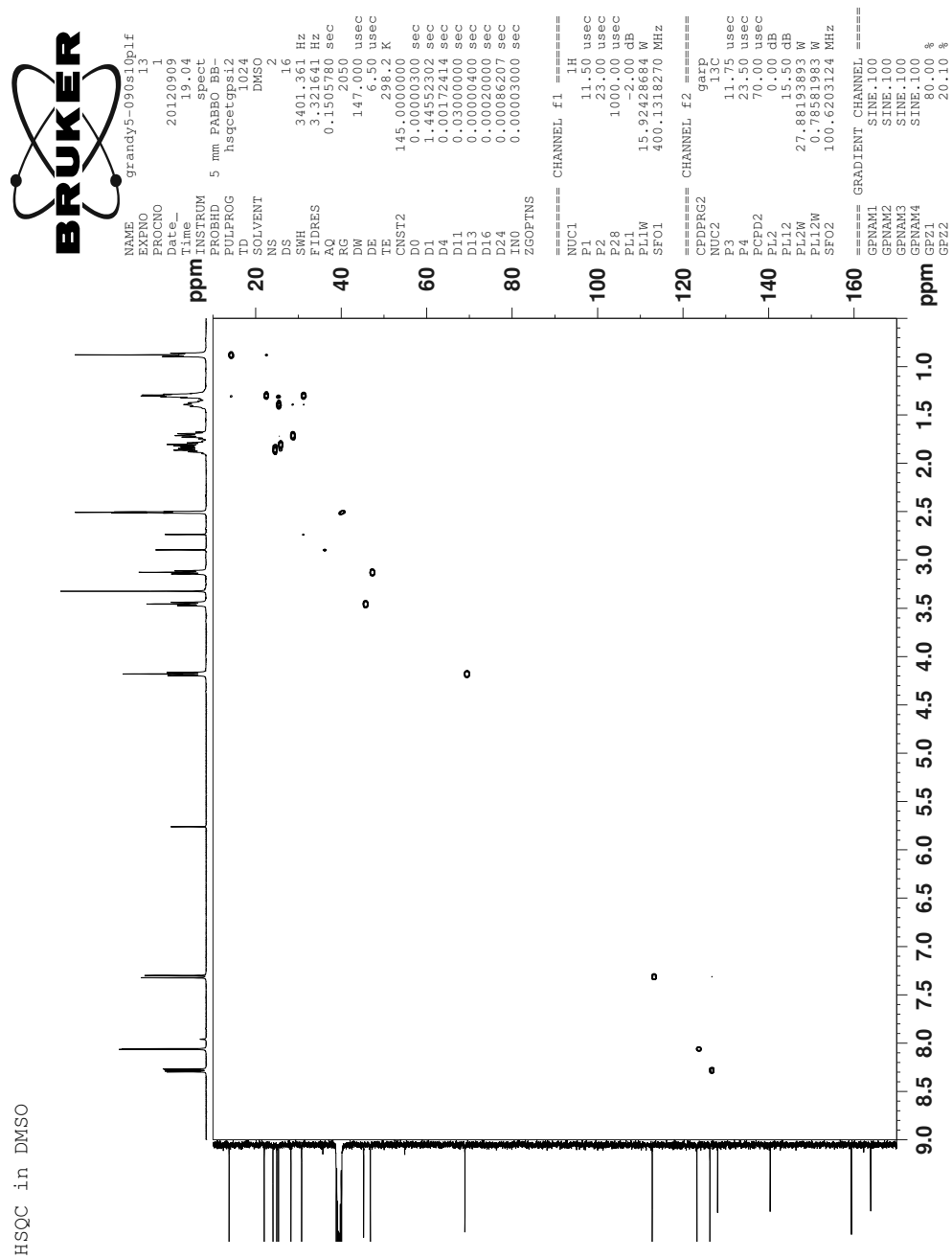
(2-(hexyloxy)-5-nitrophenyl)(pyrrolidin-1-yl)methone: G5-090s10

FIGURE A.50: ^{13}C -NMR of G5-090s10.



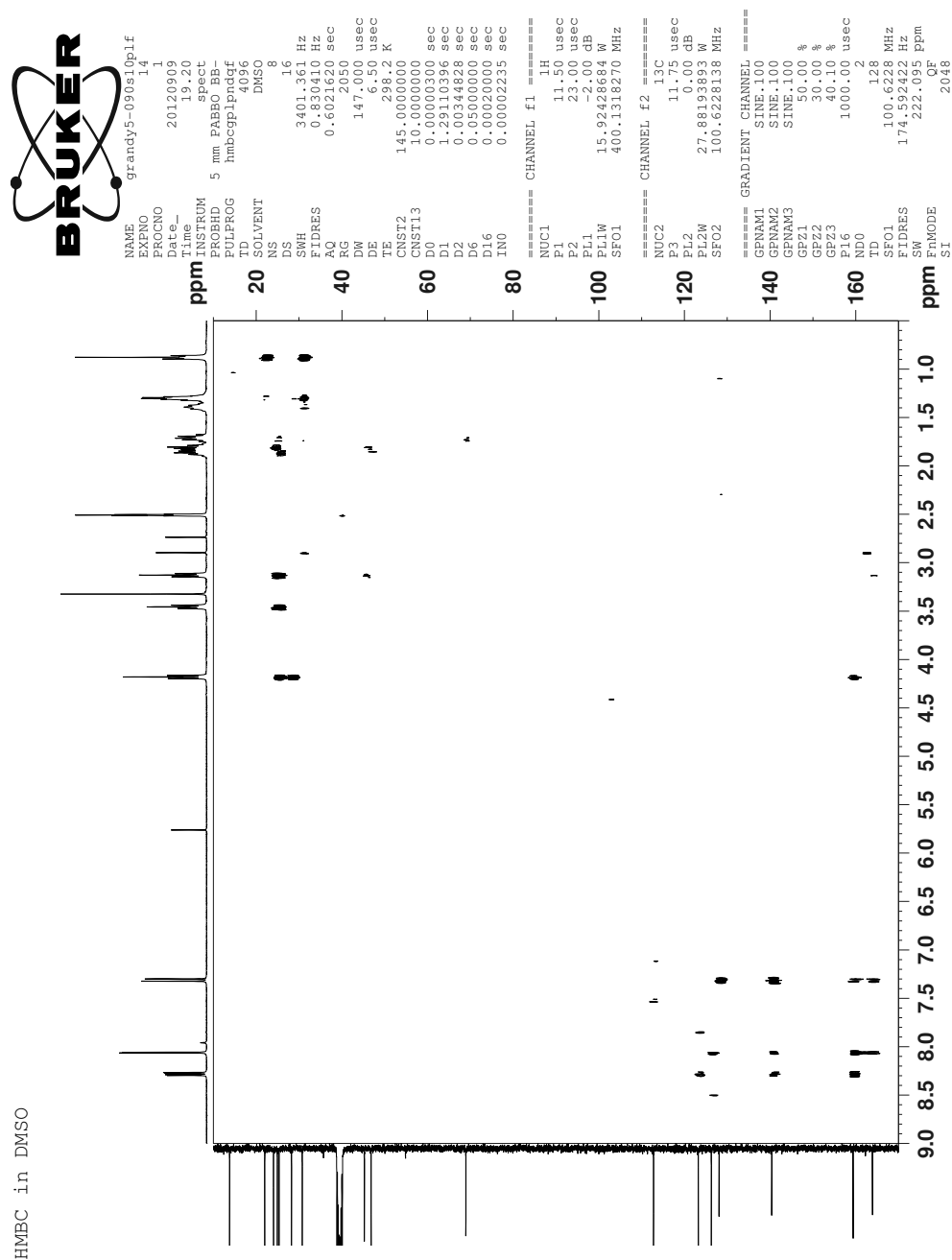
(2-(hexyloxy)-5-nitrophenyl)(pyrrolidin-1-yl)methone: G5-090s10

FIGURE A.51: HSQC-NMR of G5-090s10.



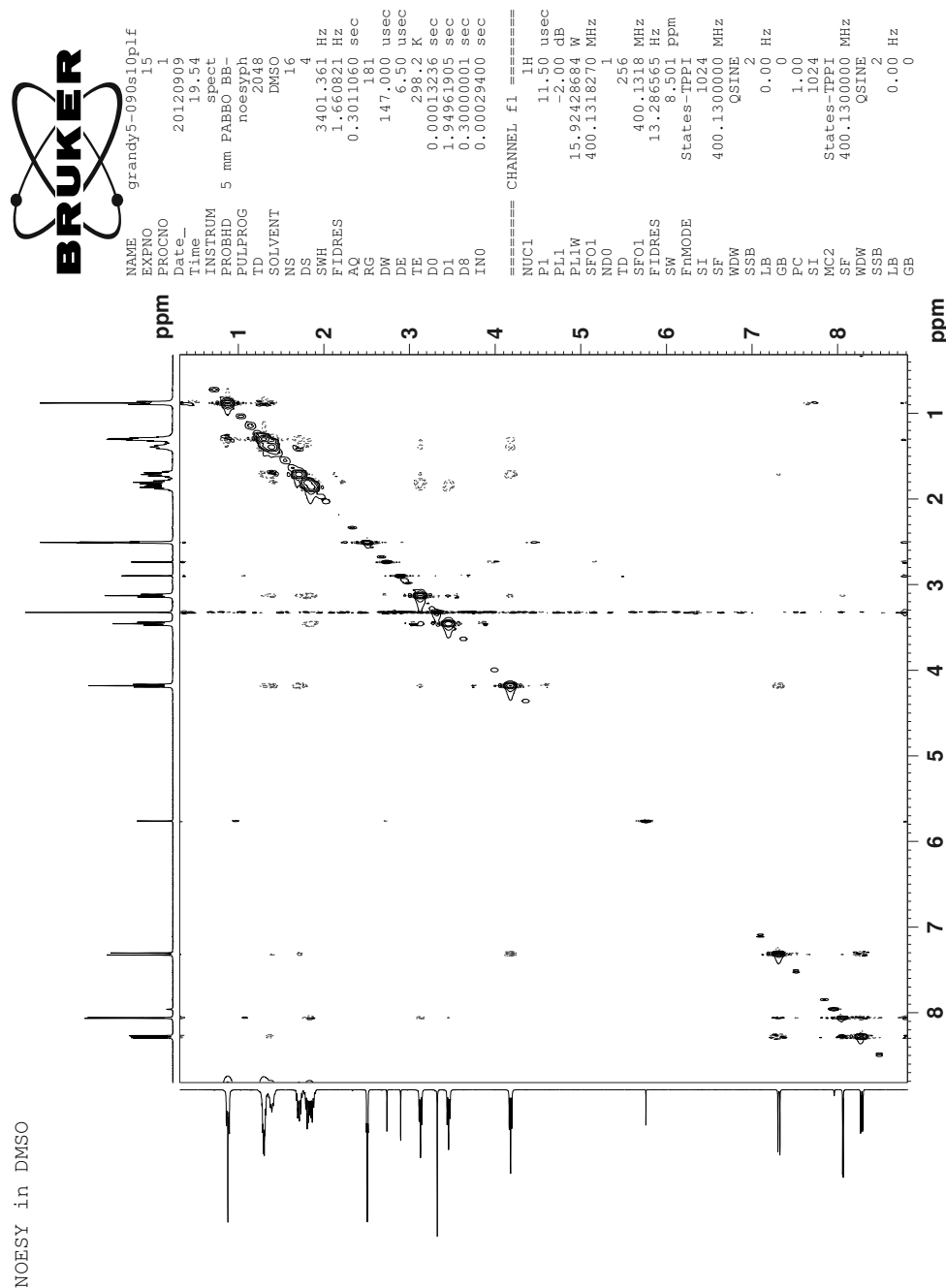
(2-(hexyloxy)-5-nitrophenyl)(pyrrolidin-1-yl)methone: G5-090s10

FIGURE A.52: HMBC-NMR of G5-090s10.



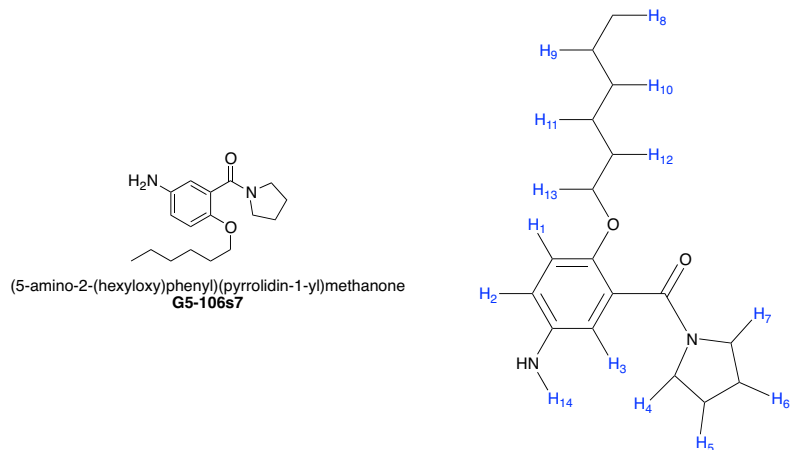
(2-(hexyloxy)-5-nitrophenyl)(pyrrolidin-1-yl)methone: G5-090s10

FIGURE A.53: NOESY-NMR of G5-090s10.



(5-amino-2-(hexyloxy)phenyl)(pyrrolidin-1-yl)methone: G5-106s7

A.8 (5-amino-2-(hexyloxy)phenyl)(pyrrolidin-1-yl)methone: G5-106s7

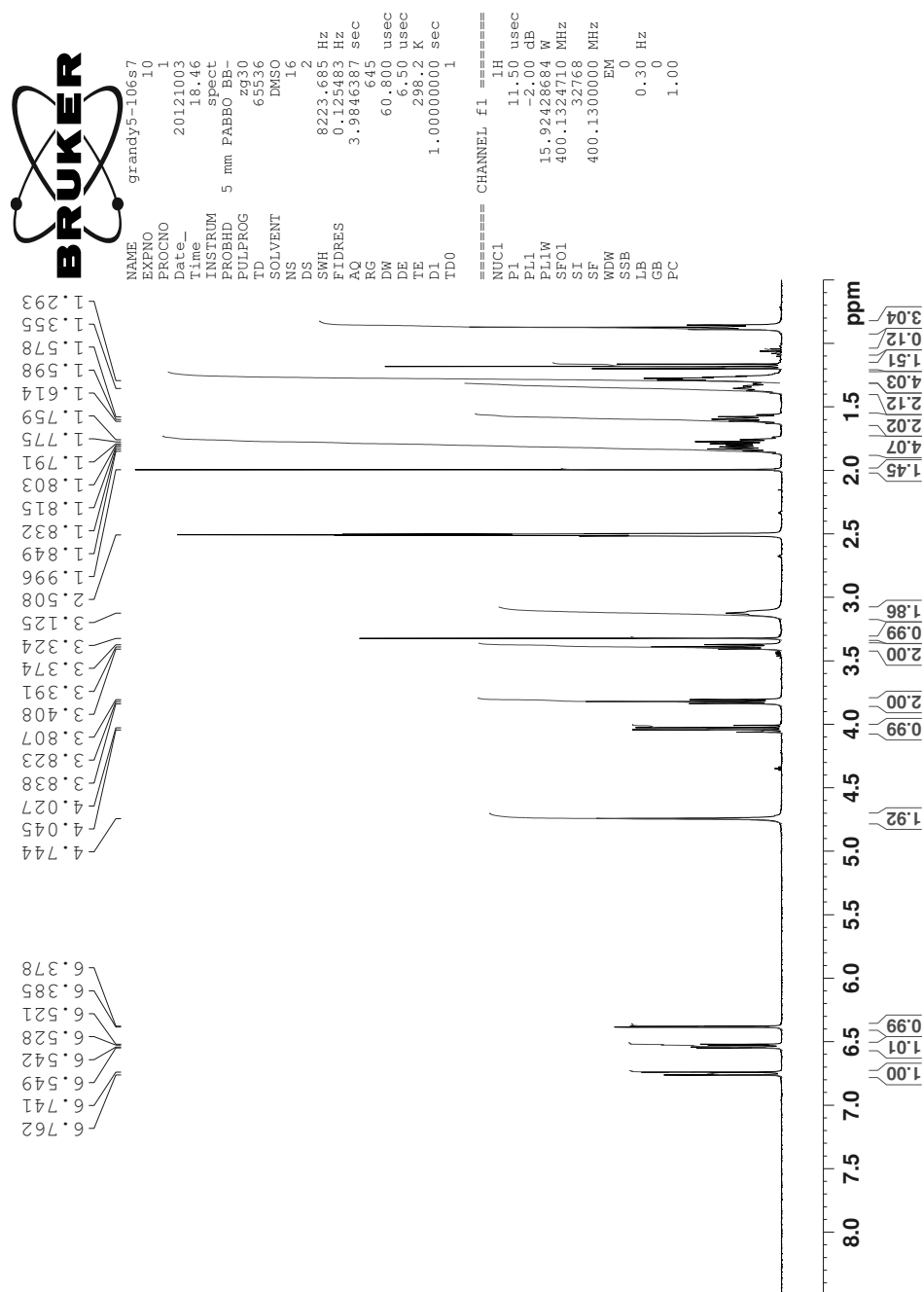
FIGURE A.54: Structure of G5-106s7.**TABLE A.15:** ¹H-NMR assignments for G5-106s7, 400 MHz in DMSO (2.50 ppm)

Proton	ppm ^a	Number	Type	J _a	J _b
H ₁	6.75	1	d	8.70	
H ₂	6.54	1	dd	8.68	2.80
H ₃	6.38	1	d	2.78	
H ₄	3.13	2	m		
H ₅ & H ₆	1.81	4	m		
H ₇	3.39	2	t	6.88	
H ₈	0.87	3	t	6.72	
H ₉ & H ₁₀	2.89	4	m		
H ₁₁	1.36	2	m		
H ₁₂	1.60	2	m		
H ₁₃	3.82	2	t	6.23	
H ₁₄		2	s		

a. Taken at the center of the peak.

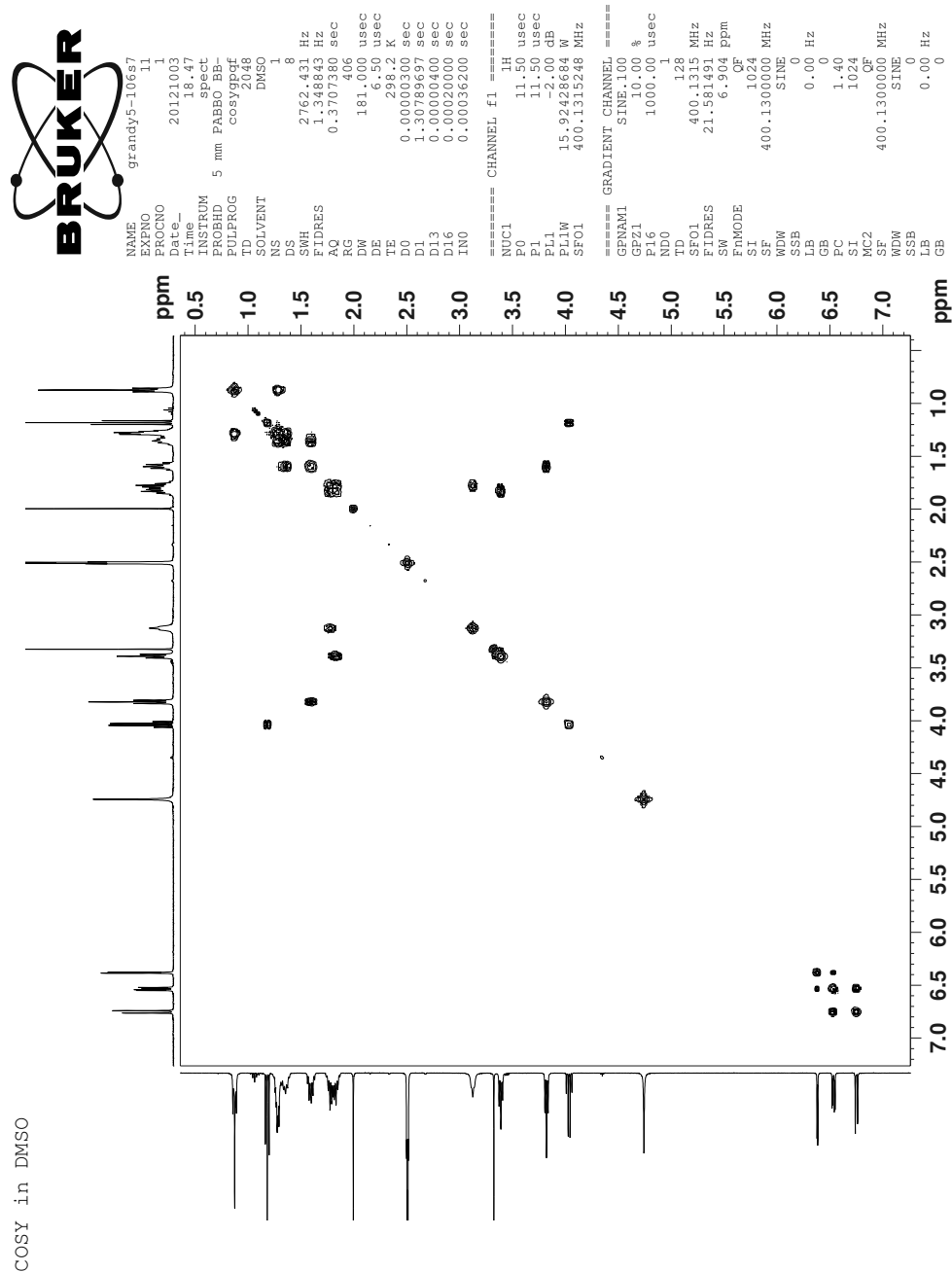
(5-amino-2-(hexyloxy)phenyl)(pyrrolidin-1-yl)methone: G5-106s7

FIGURE A.55: ^1H -NMR of G5-106s7.



(5-amino-2-(hexyloxy)phenyl)(pyrrolidin-1-yl)methone: G5-106s7

FIGURE A.56: COSY-NMR of G5-106s7.



(5-((3-fluorobenzyl)amino)-2-(hexyloxy)phenyl)(pyrrolidin-1-yl)methone: G5-109s8

**A.9 (5-((3-fluorobenzyl)amino)-2-(hexyloxy)phenyl)(pyrrolidin-1-yl)methone:
G5-109s8**

FIGURE A.57: Structure of G5-109s8.

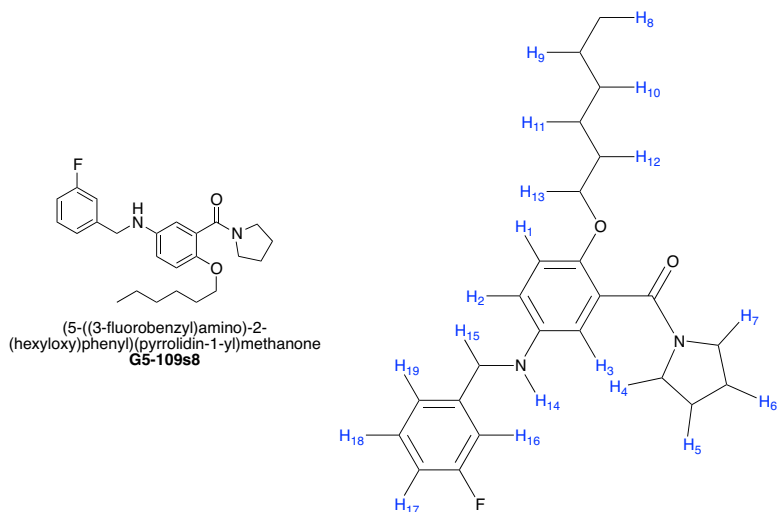


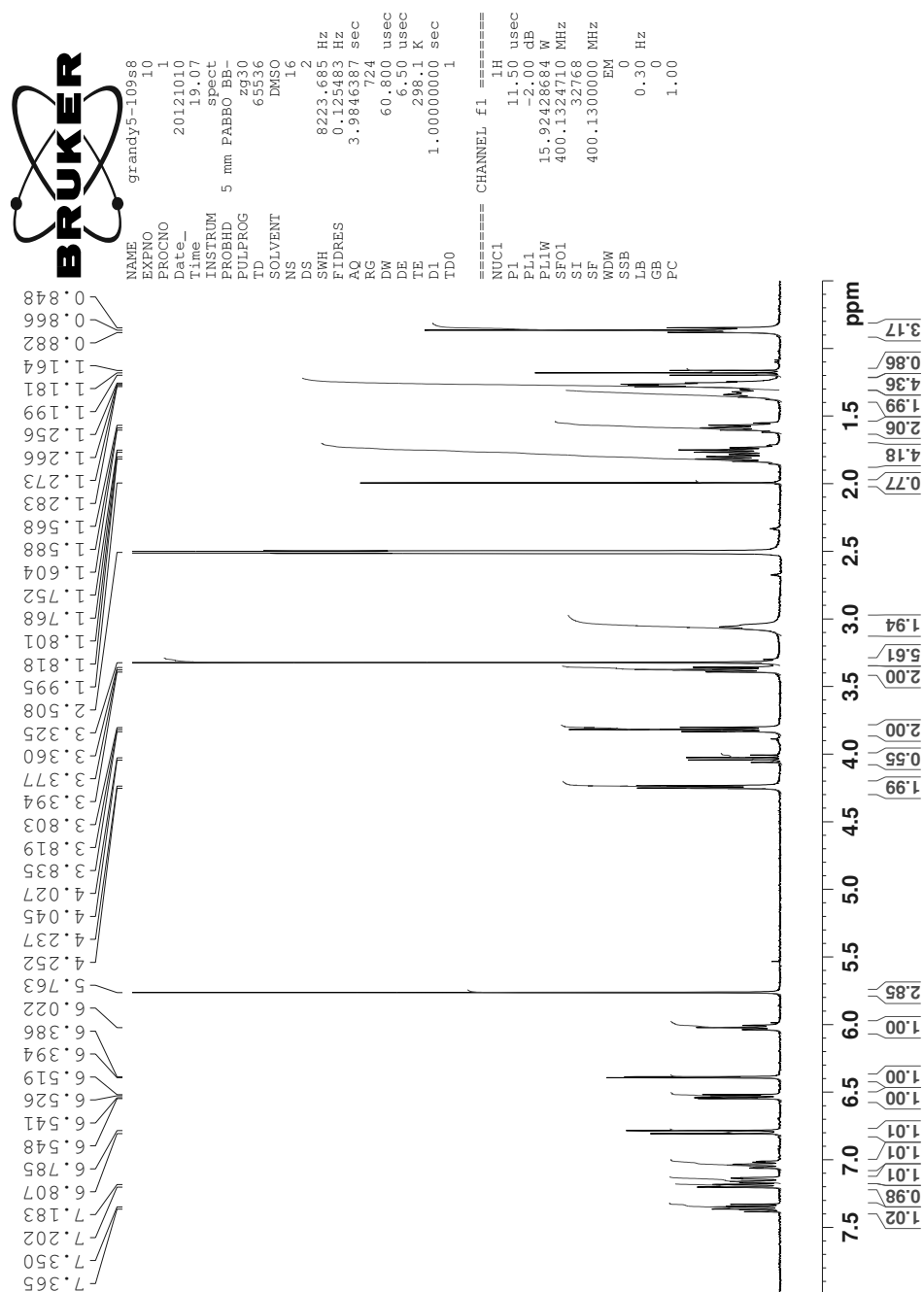
TABLE A.16: ¹H-NMR assignments for G5-109s8, 400 MHz in DMSO (2.50 ppm)

Proton	ppm ^a	Number	Type	J _a	J _b	Proton	ppm ^a	Number	Type	J _a	J _b
H ₁	6.80	1	d	8.84		H ₁₂	1.60	2	m		
H ₂	6.53	1	dd	8.83	2.89	H ₁₃	3.82	2	t	6.22	
H ₃	6.39	1	d	2.86		H ₁₄	6.02	1	t	6.23	
H ₄	3.06	2	m			H ₁₅	4.24	2	d	6.18	
H ₅ & H ₆	1.78	4	m			H ₁₆	7.15	1	m		
H ₇	3.38	2	t	6.80		H ₁₇	7.04	1	m		
H ₈	0.87	3	m	6.72		H ₁₈	7.36	1	m		
H ₉ & H ₁₀	1.27	4	m			H ₁₉	7.20	1	m		
H ₁₁	1.35	2	m			-	-	-	-	-	-

a. Taken at the center of the peak.

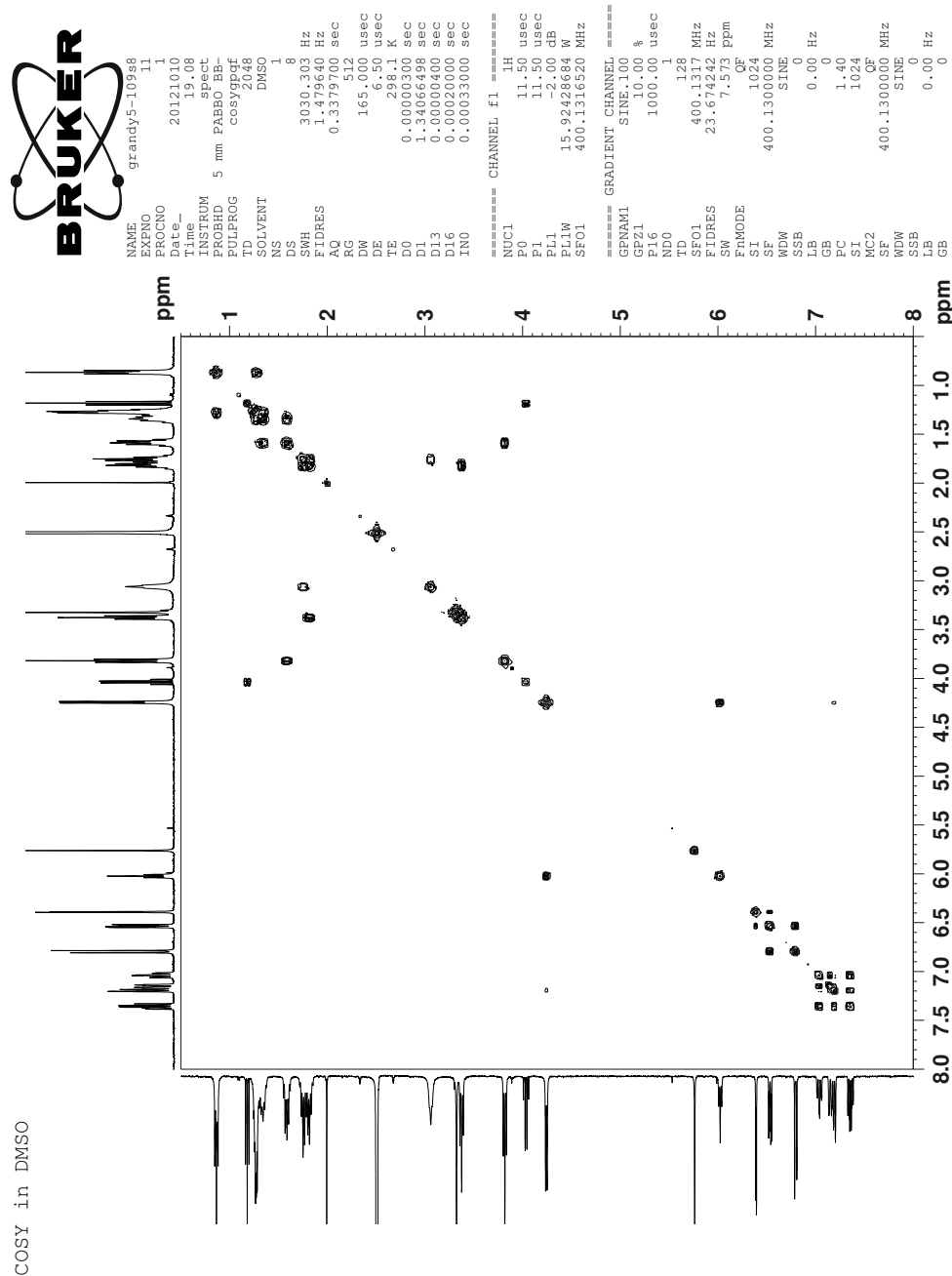
(5-((3-fluorobenzyl)amino)-2-(hexyloxy)phenyl)(pyrrolidin-1-yl)methone: G5-109s8

FIGURE A.58: ^1H -NMR of G5-109s9.

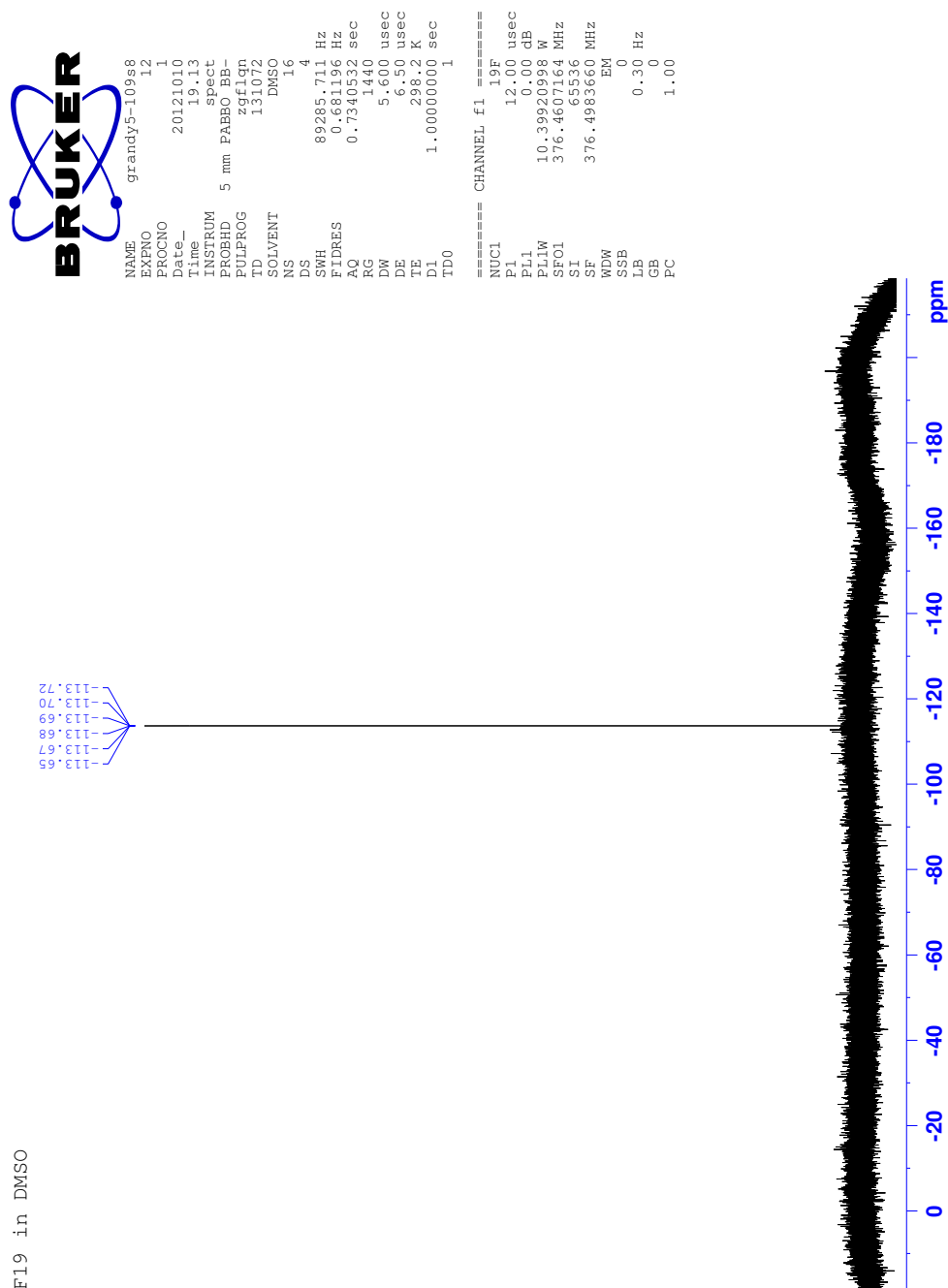


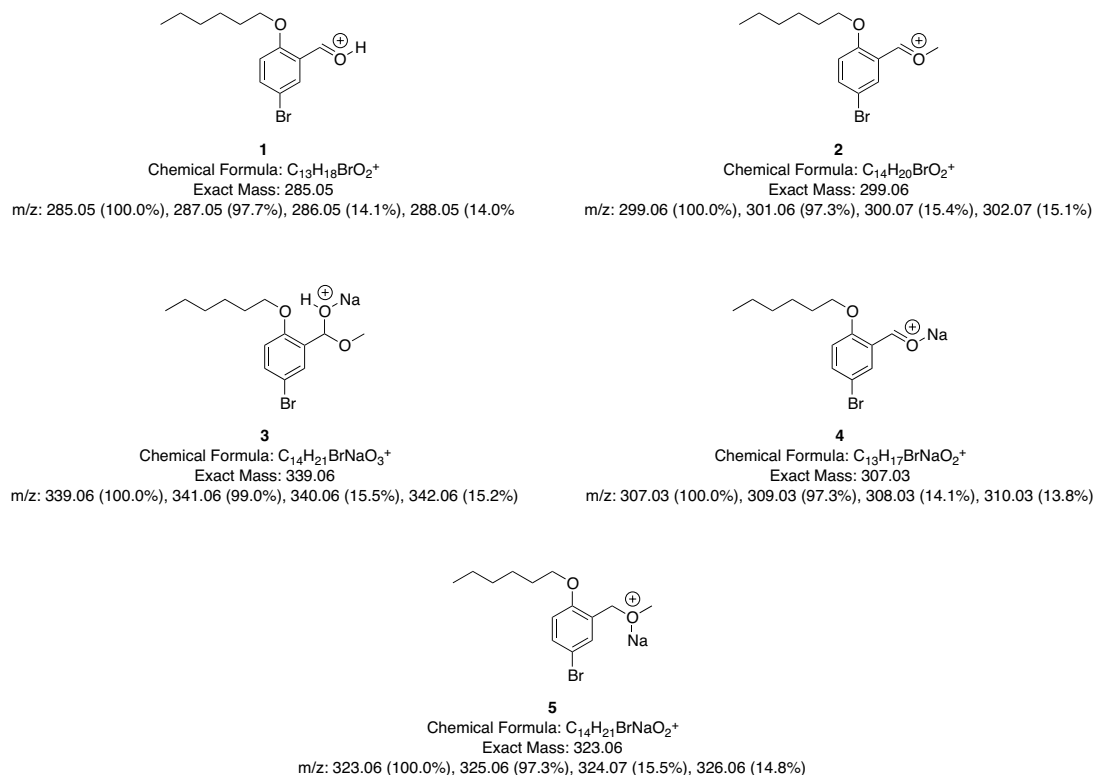
(5-((3-fluorobenzyl)amino)-2-(hexyloxy)phenyl)(pyrrolidin-1-yl)methone: G5-109s8

FIGURE A.59: COSY-NMR of G5-109s9.



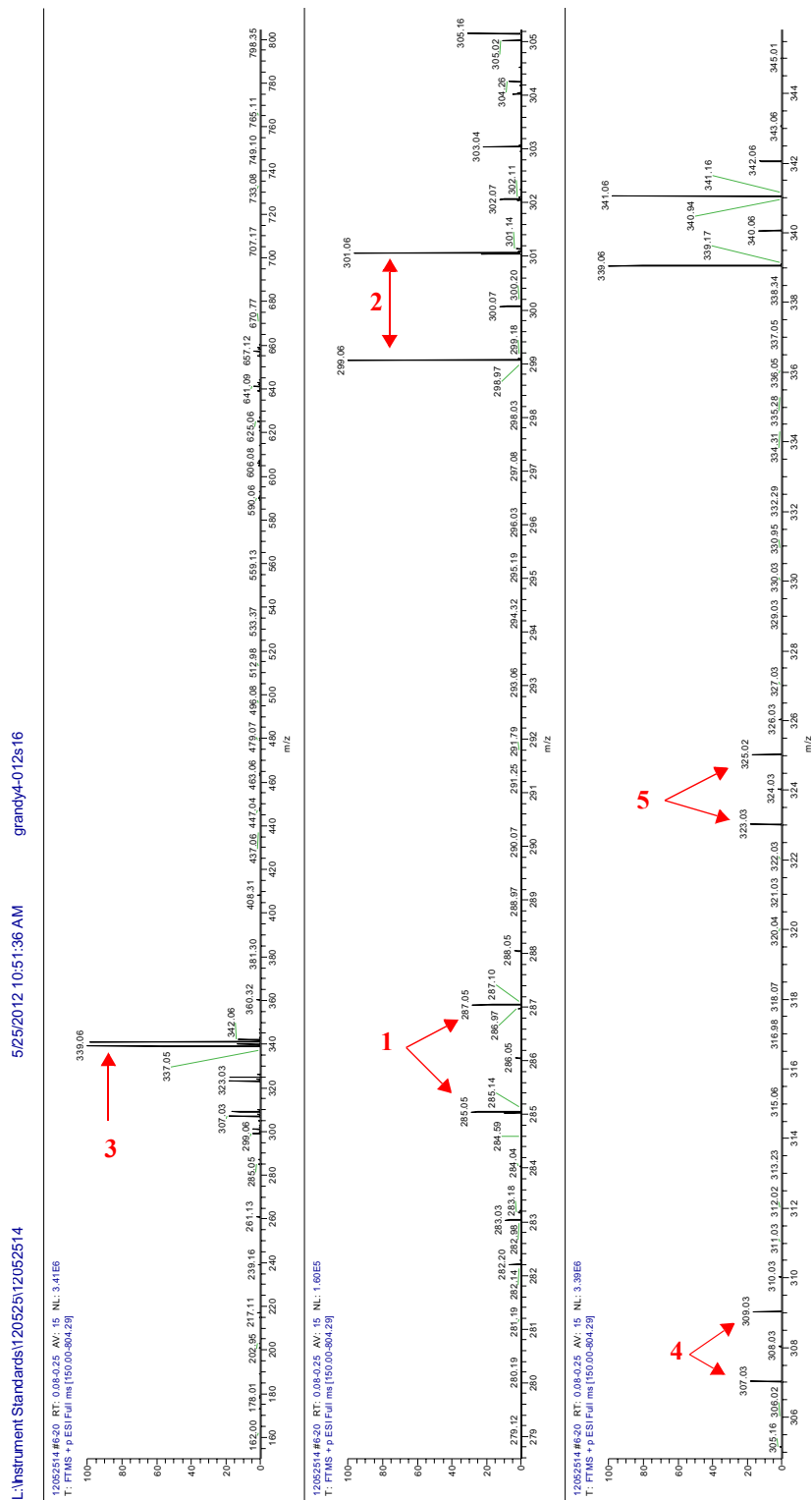
(5-((3-fluorobenzyl)amino)-2-(hexyloxy)phenyl)(pyrrolidin-1-yl)methone: G5-109s8



B.1 5-bromo-2-(hexyloxy)benzaldehyde: G4-012s16**FIGURE B.1:** Ionic forms of G4-012s16.

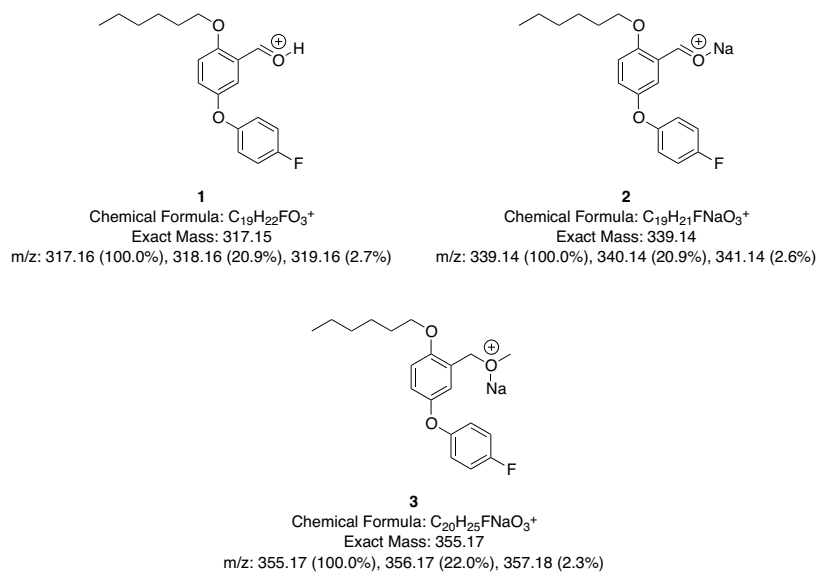
5-bromo-2-(hexyloxy)benzaldehyde: G4-012s16

FIGURE B.2: Mass spectrum of G4-012s16. The red numbers refer to the ionic forms in FIGURE B.1.



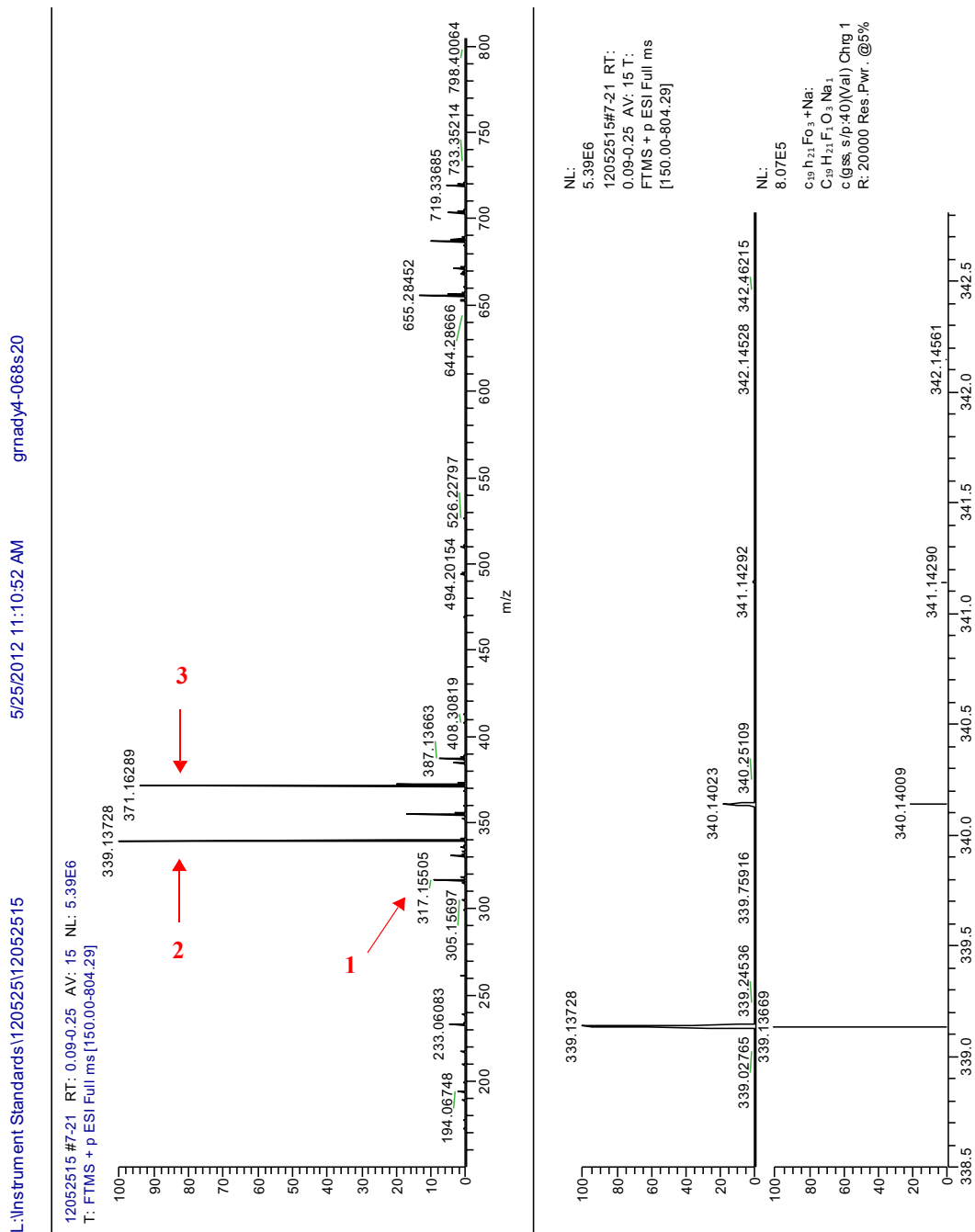
5-(4-fluorophenoxy)-2-(hexyloxy)benzaldehyde: G4-068s20 & G4-070s6

B.2 5-(4-fluorophenoxy)-2-(hexyloxy)benzaldehyde: G4-068s20 & G4-070s6

FIGURE B.3: Ionic forms of **G4-070s6**.

5-(4-fluorophenoxy)-2-(hexyloxy)benzaldehyde: G4-068s20 & G4-070s6

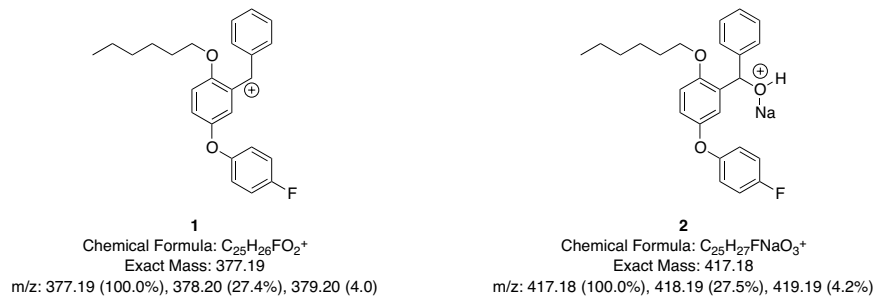
FIGURE B.4: Mass spectrum of **G4-068s20**. The red numbers refer to the ionic forms in **FIGURE B.3**.



(5-(4-fluorophenoxy)-2-(hexyloxy)phenyl)(phenyl)methanol: G4-074s14

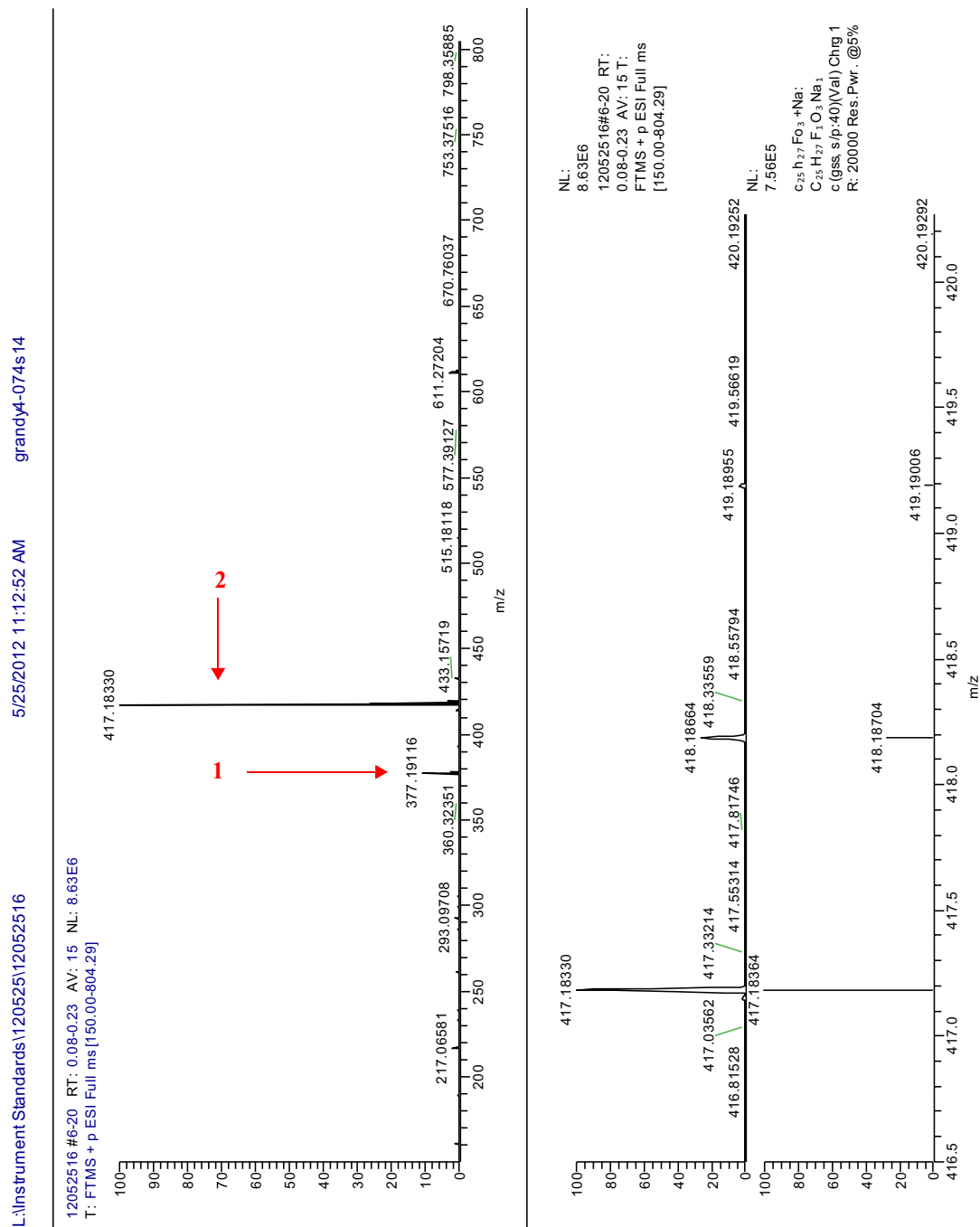
B.3 (5-(4-fluorophenoxy)-2-(hexyloxy)phenyl)(phenyl)methanol: G4-074s14

FIGURE B.5: Ionic forms of **G4-074s14**.



(5-(4-fluorophenoxy)-2-(hexyloxy)phenyl)(phenyl)methanol: G4-074s14

FIGURE B.6: Mass spectrum of **G4-074s14**. The red numbers refer to the ionic forms in **FIGURE B.5**.



2-(5-(4-fluorophenoxy)-2-(hexyloxy)phenyl)-2-phenylacetonitrile: G4-079s9

B.4 2-(5-(4-fluorophenoxy)-2-(hexyloxy)phenyl)-2-phenylacetonitrile: G4-079s9

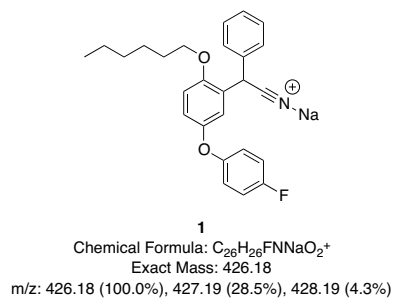
FIGURE B.7: Ionic form of G4-079s9.

FIGURE B.8: Mass spectrum of **G4-079s9**. The red number refers to the ionic form in **FIGURE B.7**.



ET-92: 2-(5-(4-fluorophenoxy)-2-(hexyloxy)phenyl)-2-phenylethanamine hydrochloride

B.5 *ET-92: 2-(5-(4-fluorophenoxy)-2-(hexyloxy)phenyl)-2-phenylethanamine hydrochloride: G4-091s14*

FIGURE B.9: Ionic form of ET-92 (G4-090s14).

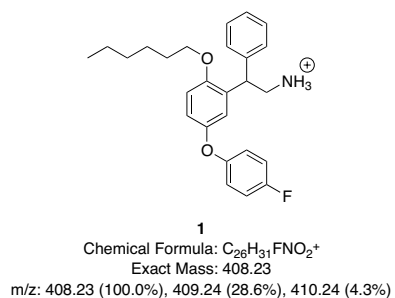


FIGURE B.10: Mass spectrum of **ET-92**. The red number refers to the ionic form in **FIGURE B.9**.

